Electrochemical pH-swing Extraction for Carboxylic Acid Purification

Elektrochemische pH-swing Extraktion zur Aufarbeitung von Carbonsäuren

Von der Fakultät für Maschinenwesen der Rheinisch-Westfälischen Technischen Hochschule Aachen zur Erlangung des akademischen Grades eines Doktors der Ingenieurwissenschaften genehmigte Dissertation

vorgelegt von

Marcel Gausmann

Berichter: Univ.-Prof. Dr.-Ing. Andreas Jupke
Univ.-Prof. Doctor Nick Wierckx

Tag der mündlichen Prüfung: 19.12.2023

Impressum

Titel:	Electrochemical pH-swing Extraction for Carboxylic Acid Purification Elektrochemische pH-swing Extraktion zur Aufarbeitung von Carbonsäuren
Autor:	Marcel Gausmann
Reihe:	Aachener Verfahrenstechnik - Fluidverfahrenstechnik Dissertationen, Band 9 (2024)
Herausgeber:	Aachener Verfahrenstechnik Forckenbeckstraße 51 52074 Aachen Tel.: +49 (0)241 80 95246 E-Mail: secretary.fvt@avt.rwth-aachen.de http://www.avt.rwth-aachen.de/AVT

Volltext verfügbar: https://doi.org/10.18154/RWTH-2024-00046

Danksagung

Diese Dissertationsschrift entstand während meiner Zeit als wissenschaftlicher Mitarbeiter und Promotionsstudent am Lehrstuhl für Fluidverfahrenstechnik der Aachner Verfahrenstechnik (AVT.FVT). Besonderer Dank gilt dabei meinem Doktorvater Prof. Dr.-Ing. Andreas Jupke. Die Freiheit Neues auszuprobieren und das sehr eigenverantwortliche Arbeiten am Lehrstuhl waren eine fordernde aber auch sehr bereichernde Erfahrung. Danke für das Vertrauen und die Chance ein neues Forschungsfeld am Lehrstuhl bereits in der Promotion selbst zu gestalten. Ein 1,5 mio € Projekt selbst vor dem Ministerium vorzustellen und erfolgreich zu verteidige, ist eine Erfahrung, die ich nicht so schnell vergessen werde. Ebenfalls vielen Dank an Prof. Dr. Nick Wierckx für die Übernahme des Ko-Referats und für die Entwicklung des säuretoleranten *Ustilago cynodontis* Stammes, der auch Verwendung in dieser Arbeit gefunden hat. Selbst zu sehen, welche Ergebnisse möglich sind, wenn Biotechnologie und Verfahrenstechnik Hand in Hand arbeiten, war beeindruckend. Ebenfalls danken, möchte ich den Projektpartnern im Kopernikus Projekt Synergie. Allen voran Prof. Alexander Mitsos und den Kollegen der AVT.SVT für die gewissenhafte Projektkoordination sowie Prof. Michael Helmut Kopf und Christian Riedele von der BASF für die intensiven fachlichen Diskussionen zur Elektrifizierung von Aufarbeitungsprozessen der industriellen Biotechnologie. Außerdem danke ich meinen Kolleginnen und Kollegen am Lehrstuhl. Vielen Dank Tim, Armin, Martin und Benedikt für die Aufnahme im Team der Fluidverfahrenstechnik und den fachlichen Input, der am Ende den Anstoß für die Forschungsidee gegeben hat, die nun zum Grundstein dieser Arbeit geworden ist. Ein großer Dank gilt auch den Teamkollegen der elektrochemischen Trennverfahren. Christian Kocks, Jonas, Robert, Chris-

tian Schröder, Jan, Janik und Niclas, wenn ich zurückblicke und überlege, dass wir vor fünf Jahren mit einer alten analogen Stromquelle und geliehenen Elektroden gestartet sind und mir ansehe, was wir in den letzten Jahren an Anlagen, Kompetenz und Know-How aufgebaut haben, macht es mich stolz euch als Teamkollegen zu haben. Ohne eure Unterstützung wäre alles das nicht möglich gewesen. Es freut mich sehr, dass wir mit unserer Arbeit nicht nur den Grundstein für unsere eigenen Promotionsarbeiten gelegt haben, sondern über die Jahre auch neue Kollegen dazu gestoßen sind und sich für ein Promotionsprojekt in den elektrochemischen Trennverfahren entschieden haben. Unser Team wachsen zu sehen und zu sehen, dass wir heute in wenigen Wochen komplette elektrochemische Aufarbeitungsverfahren vom Konzept zur Validierung im Labor bringen können, finde ich eine beeindruckende Teamleistung. Neben meinen Kolleginnen und Kollegen am Lehrstuhl möchte ich auch allen Studierenden danken, die entweder als HiWi oder im Rahmen einer Projekt-, Bachelor- oder Masterarbeit ein Teil zu dieser Arbeit beigetragen haben. Die Zusammenarbeit mit euch war eine der besten Erfahrungen meiner Promotionszeit. Jede Arbeit, die ich betreut habe, war einzigartig und es war großartig zu sehen, wie viele von euch sich durch exzellente Leistung tolle Abschlussnoten verdient haben. Ein absolutes Highlight meiner Promotion war die Auszeichnung von Franziska mit dem Christian Wandrey Preis für ihre herausragende Masterarbeit. Die Auszeichnung war eine tolle Bestätigung, dass wir an der Fluidverfahrenstechnik die Voraussetzungen schaffen konnten, die solche erfolgreichen Arbeiten ermöglichen. Außerdem freut es micht, dass mit Christian, Robert und Franziska drei meiner ehemaligen Studierenden neue Kolleginnen und Kollegen an der FVT geworden sind.

Abschließend möchte ich meiner Familie und allen Freunden danken, die mich auf dem Weg durch die harten Zeiten der Promotion begleitet haben und auf deren Unterstützung ich jederzeit zählen konnte. Danke für eure Geduld und Verständnis, wenn die Forschung mich wieder einmal (zu) lange am Schreibtisch gehalten hat.

Abstract

The value chains of the chemical industry face a transformation from linear business models built on the utilization of fossil resources towards circular economy approaches. In this pivot, biotechnological processes and bio-based resources play a central role to replace the carbon losses in the material cycle. Carboxylic acids like succinic acid play a central role in microbial metabolism and are regarded as the tier-one group of next-generation platform chemicals. The implementation of such processes requires technological advances that ensure sustainable production of these chemicals at a large scale. Electrochemical separation technologies overcome waste emissions and enable clean and sustainable processing of carboxylic acids. The mitigation of environmental footprints is a crucial requirement to develop the process technologies which make industrial biotechnology successful and sustainable at the industrial scale.

The electrochemical stability of mid-chain carboxylic acid enables cation recovery by direct pH swing electrolysis which introduces the driving force for subsequent separation by reactive extraction. The utilization of both electrode reactions makes closed-loop downstream process layouts viable. A proof of concept demonstrated the recovery of crystalline succinic acid with 94 w% from the electrolyte-containing solution.

The integration of electrochemical pH swing reactive extraction and high-yield succinic acid fermentation has the potential to enable low carbon and potentially carbon-negative production of an important base chemical that can become a central building block for a circular chemical industry and create synergies by the integration of sustainable chemical production with renewable energy generation.

Zusammenfassung

In der chemischen Industrie findet eine Transformation der Wertschöpfungsketten statt. Bei dem Wandel zu einer Kreislaufwirtschaft spielen biotechnologische Verfahren und Rohstoffe eine tragende Rolle, um Verluste im Materialkreislauf mit erneuerbaren Kohlenstoffressourcen zu ersetzen. Carbonsäuren wie Bernsteinsäure sind zentrale Zwischenstufen in mikrobiellen Stoffwechselprozessen und sind die vielversprechendste Gruppe zukünftiger Plattformchemikalien. Elektrochemische Trennverfahren sind in der Lage bisher anfallende Abfallströme in der Aufarbeitung von Carbonsäuren zu eliminieren und eine nachhaltige Herstellung im großen Maßstab zu ermöglichen. Die elektrochemische Stabilität von mittelkettigen Carbonsäuren erlaubt die Nutzung einer pH swing Elektrolyse zur Rückgewinnung der im Prozess zur pH Kontrolle eingesetzten Kationen. Der elektrochemisch erzeugte pH Gradient liefert die notwendige Triebkraft für die anschließende Abtrennung der Säure in einer Reaktivextraktion. Durch die Nutzung beider Elektrodenreaktionen können Aufarbeitungsprozesse mit geschlossenen Kreislaufströmen zur Rückführung der eingesetzten Hilfsstoffe entwickelt werden. Die Machbarkeit des Verfahren wurde gezeigt und kristalline Bernsteinsäure mit einer Reinheit von 94 % aus einer elektrolythaltigen Lösung gewonnen. Die Integration der elektrochemischen pH swing Reaktivextraktion mit einer prokaryotischen Fermentation hat das Potential, die Herstellung von Bernsteinsäure mit minimalem Prozessemissionen zu ermöglichen. Die Elektrifizierung von Aufarbeitungsverfahren liefert den Grundstein für die nachhaltige Produktion von erneuerbaren Plattformchemikalien und bietet durch intelligente Sektorenkopplung Synergieeffekte zwischen der Chemiekalienherstellung und der Nutzung erneuerbarer Energien.

Contents

List of Figures

List of Tables

Nomenclature

List of Abbreviations

H_2Suc Succinic acid

$HSuc^-$ Hydrogen succinate

Suc^{2-} Succinate

ANOVA Analysis of variance

ATP Adenosine triphosphate

bio-SA bio-based succinic acid

BPM Bipolar membrane

CAGR Compound Annual Growth Rate

CAPEX Capital expenditure

CDW Cell dry weight (biomass)

COM Cost of manufacturing

CV Cyclic voltammetry

DAE Differential algebraic equations

DeOH n-Decanol

Dodec 1-Dodecanol

DoE Design of Experiments

e-NRTL electrolyte non-random-two-liquid

ED	Electrodialysis
FTE	Full time equivalents
Glu	Glucose
Gly	Glycerol
HDA	Hexanediamine
HER	Hydrogen evolution reaction
INO	Inoculum
LCA	Life cycle assessment
Mal	Maltose
MIBK	Methyl isobutyl ketone
MSE	Membrane supported extraction
NADH	Nicotinamide adenine dinucleotide
nHex	n-Hexane
NPV	net present value
Oct	1-Octanol
OER	Oxygen evolution reaction
OPEX	Operational expenditure
PEM	Proton exchange membrane electrolysis
RHE	Reversible hydrogen electrode
SHE	Standard hydrogen electrode
SLE	Solid liquid equilibrium
STY	Space time yield

Sucr	Sucrose
TAM	Tertiary amine
TCA	Tricarboxylic acid cycle
TEA	Techno economic assessment
TEHA	Tris-ethylhexylamine
THA	Tri-hexylamine
TOA	Tri-octylamine
TOPO	Trioctylphosphine oxide

Index Directory

+	Anode
−	Cathode
α	Concentration at the inlet
ω	Concentration at the outlet
A	Southern boundary of the first control volume, representing the inflow
aq	Aqueous phase
B	Northern boundary of the last control volume, representing the outflow
b_N	boundary of the northern neighboring volume
b_S	boundary of the southern neighboring volume
N	Nodal grid point of the northern neighboring volume
S	Nodal grid point of the southern neighboring volume
sol	Solvent phase

0	Initial
aq	Aqueous phase
BE	Mass recovered in back-extraction
in	Inside the cell
org	Solvent phase
out	Outside the cell
P	Product
S	Substrate
tot	Total concentration

Symbol Directory

α	Degree of protonation	$[-]$
β	Fraction of the protonated amine	$[-]$
$\dot{F}$	Volumetric inflow of aqueous phase	$\left[\mathrm{L\,s^{-1}}\right]$
$\dot{K}$	Volumetric outflow of solvent	$\left[\mathrm{L\,s^{-1}}\right]$
$\dot{R}$	Volumetric outflow of aqueous phase	$\left[\mathrm{L\,s^{-1}}\right]$
$\dot{S}$	Volumetric inflow of solvent	$\left[\mathrm{L\,s^{-1}}\right]$
$\dot{n}$	Molar flow	$\left[mols^{-1}\right]$
$\dot{V}$	Volumetric flow	$\left[m^3 s^{-}1\right]$
η	Efficiency	$[-]$
$\eta_{ex,SA}$	Extraction efficiency	$[-]$
η_{prot}	Protonation efficiency	$[-]$

$\eta_{sel,SA}$	Protonation selectivity for succinic acid	$[-]$
κ	Ion specific conductivity	$\left[10^{-4}\mathrm{m}^2\mathrm{Smol}^{-1}\right]$
λ_i^0	Limiting ion conductivity	$\left[10^{-4}\mathrm{m}^2\mathrm{Smol}^{-1}\right]$
$\mathfrak{c}$	Individual component of manufacturing costs	$[EUR]$
$\mathfrak{I}$	Initial investment	$[EUR]$
$\mathfrak{L}$	Revenue from asset liquidation	$[EUR]$
$\mathfrak{p}^*$	New price level	$[EUR]$
$\mathfrak{p}_0$	Original price level	$[EUR]$
$\mathfrak{T}$	Plant lifetime	$[years]$
$\mathfrak{z}$	Discount rate	$[\%]$
$\mathrm{R_{ex}}$	IA recovery in the extraction	$[\%]$
ϕ	General flow variable, molar-related variable like mole fraction $[mol/mol]$	
$\rho \cdot \phi$	Molar concentration	$\left[mol/m^3\right]$
ρ	Molar density	$\left[mol/m^3\right]$
$\mathbf{x}$	State vector of concentrations in the aqueous phase	$\left[\mathrm{mol\,L}^{-1}\right]$
$\mathbf{y}$	State vector of concentrations in the solvent phase	$\left[\mathrm{mol\,L}^{-1}\right]$
θ	Dimensionless residence time	$[-]$
A	Cross section	$\left[m^2\right]$
A_{el}	Electrode area	$\left[m^2\right]$
c	Concentration	$\left[mol/m^3\right]$
c_0	Total feed concentration	$\left[molL^{-1}\right]$

D	Diffusion coefficient	$\left[m^2/s\right]$
d	Cell width	[mm]
D_a	Outer diameter	[mm]
d_i	Inner diameter	[mm]
d_p	Pore diameter	[µm]
E	Electrode potential	$[V]$
I	Electric current	$[\Omega]$
j	Electric flux	$\left[Am^{-2}\right]$
Ju_I	First proton flux unity number	$[-]$
k_{m}	Overall mass transport coefficient of the membrane	$\left[\mathrm{m\,s^{-1}}\right]$
K_n	Amine protonation constant	$[-]$
$K_{\mathrm{SO_{42}}^-}$	Sulfate extraction constant	$[-]$
K_{Ex}	Succinic acid extraction constant	$[-]$
K_{LA}	Equilibrium constant of lactic acid extraction	$[-]$
L	Conductance	$\left[\Omega^{-1}\right]$
l	Cell length	[mm]
n	Molar amount	$[mol]$
Pe	Peclet number	$[-]$
pK_{a1}	Logarithmic acid dissociation constant	$[-]$
R	Resistance	$[\Omega]$
s	Electrolyte gap	[mm]
S_ϕ	Source term	$\left[mol/(m^3 \cdot s)\right]$

t	Time	$[s]$
V	Volume	$\left[m^3\right]$
Y_{DSP}	Yield of the downstream process	[%]
Y_{P}	Process yield	[%]
K_n	Amine dissociation constant	[−]
K_{ex}	Extraction constant	[−]
A	Cross sectional electrolyte area	$\left[\mathrm{cm}^2\right]$
c	Concentration	$\left[g\ L^{-1}\right]$
c_i	Concentration	$\left[\mathrm{mol\AA m}^{-3}\right]$
c_{end}	Final concentration	$\left[\mathrm{molcm}^{-3}\right]$
c_{init}	Initial concentration	$\left[\mathrm{molcm}^{-3}\right]$
E	Extraction yield	[%]
F	Faraday constant	$\left[\mathrm{A\,s\,mol}^{-1}\right]$
I	Electric current	$[A]$
j	Molar flux	$\left[molm^{-2}s^{-1}\right]$
l	Electrolyte gap	[cm]
m	mass	$[g]$
n	Number of protons transported over the membrane	[−]
pmf	Proton motive force	[V]
R	Ideal gas constant	$\left[\mathrm{J\,mol}^{-1}\,\mathrm{K}\right]$
R	Ohmic resistance	$[\Omega]$

S	Selectivity	[%]
T	Temperature	[K]
t	Time	[s]
u	Velocity	$[m/s]$
V	Phase volume	$[L]$
Y	Yield	[%]
z	Number of electrons transferred per reaction	[−]
z_i	Charge number	[−]

1. Introduction

The course of the chemical industry has been determined by the available feedstock and energy resources. Although biomass feedstock has been used even before industrialization, modern chemical production is based on fossil carbon resources such as coal, oil and natural gas, and biomass-based products only fill niche or specialty applications [11]. Until today, large-volume chemicals are sourced from fossil feedstock [12, 13].

1.1. The transformation of the Chemical Industry

In the early 2000s, the peak of crude oil prices raised the interest in alternatives to fossil-based platform chemicals fig. A.1. Studies like the U.S. Department of Energy report on chemicals from biomass-screened molecules and biotechnological production pathways to identify those that had the prospect of becoming the platform chemicals of a biobased chemical industry[1].

Of 300 initial candidates, 12 molecules were selected. Members of this tier one group are displayed in fig. 1.2. Of the 12 selected molecules, six are carboxylic acids. This highlights the extraordinary importance of carboxylic acids for industrial biotechnology. Together with the two amino acids aspartic acid and glutamic acid 75 % of the highlighted potential platform molecules exhibit a molecular structure that makes the compounds sensitive towards the pH value of its surrounding.

Compared to fossil-sourced products, biobased chemicals provide the advantage that they are in principle carbon neutral toward the atmosphere, and any carbon emission caused by the incineration of a product at the end of its life is bound by the biosphere during the growth phase of

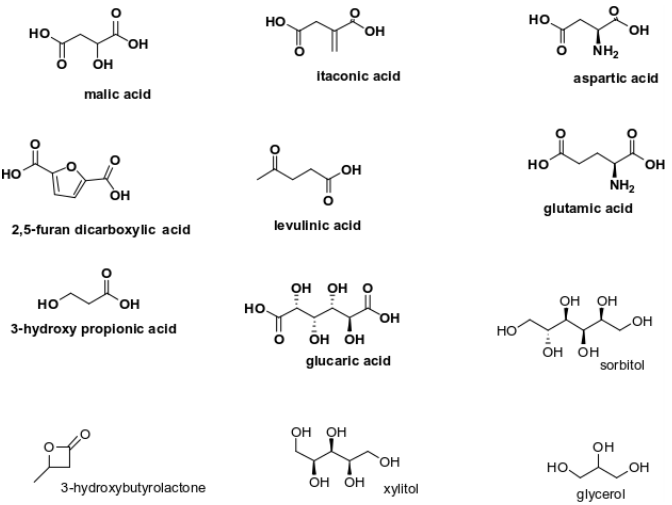

Figure 1.1.: Top 12 value added chemicals from biomass [1]

the plants. In addition to this ecological advantage, prices for biobased raw materials were historically less volatile compared to crude oil. That makes biobased chemicals an interesting option from both the ecological and economic point of view [14].

Some of the biobased platform chemicals are the same molecules that are currently produced from petroleum. Exemplary biobased succinic acid (bio-SA) can replace succinic acid produced by partial oxidation of butane to maleic anhydride followed by hydrogenation and hydrolysis to succinic acid [15]. This makes succinic acid a highly attractive candidate, as it enables the development of new purely biobased production networks but also provides linking points to connect biobased production with existing processes [16].

The biobased production of carboxylic acids such as succinic acid has made great progress in the past 20 years. Genomics and other high-throughput technologies developed in the field of industrial biotechnology enabled the rapid identification and optimization of microbial biocatalysts [17, 18, 14]. Despite the progress achieved with upstream de-

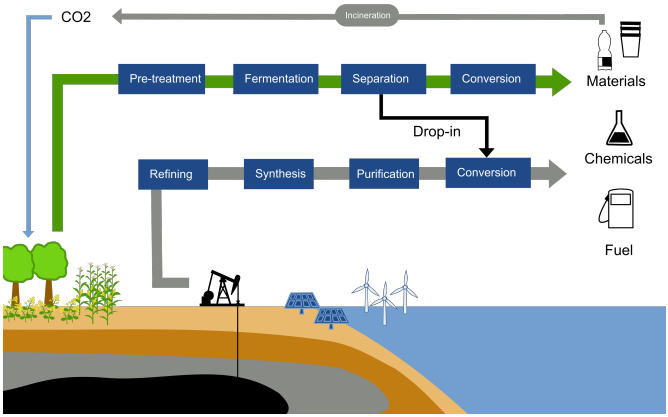

Figure 1.2.: Fossil-based chemical production and biobased route for chemicals and drop-in intermediates.

velopment, downstream processing, and product recovery after fermentation, it was found that it was cumbersome and eventually prevented a large-scale application of bio-SA. The extensive use of additives for pH control produced equimolar amounts of waste with succinic acid [19]. An equimolar waste production makes the sustainability claim of bio-SA production questionable and also compromises the economic perspective of such a process, especially if waste disposal becomes a cost issue or is limited by legislation [20].

The industrial standard for carboxylic acid purification is the calcium precipitation process. A detailed introduction and discussion will be given in chapter 9. However, new technologies have been researched to overcome the issue of waste production. Crystallization, ion exchange, reactive extraction, and membrane processes were tested for succinic acid separation [21, 22, 23, 24, 25]. The following shortcomings and development needs were identified:

- *In-situ* product removal enables continuous fermentation and alleviates performance losses caused by inhibition of the product. But extraction from fermentations operating at a neutral pH value is

limited in its yield.

- Reactive extraction with tertiary amines is a promising recovery technology for succinic acid from low-pH solutions.
- The conversion of carboxylates to carboxylic acid requires a cation recovery technology in order to avoid salt waste production.
- Electrochemical separation technologies can overcome salt waste production, but in order to achieve good operational practice, sources of inefficiencies and bottlenecks of current technologies must be addressed.

1.2. Electrification of Separation Technologies

Electrochemical separation technologies such as electrodialysis are known but are only applied on a small scale [26]. The reason for the limited application is likely found in the lack of low-priced electricity in the past combined with limited operational experience and high equipment costs. Electrodialysis was successfully applied to recover succinic and other short-chain carboxylic acids from diluted aqueous solutions [27]. The high costs of bipolar membranes have been identified as one obstacle for large-scale application [28]. In addition, low current efficiencies[27] and effects such as "proton poisoning"[29] reduce the effectiveness of electrochemical separation and cause high electricity consumption.

Recently, the decrease in electricity generation costs from renewable sources such as wind and solar[30] opened a new perspective for the introduction of electrochemical technologies. Progress in renewable electricity generation has the potential to accelerate the electrification of the chemical industry. Furthermore, the reduction in electrolyzer costs expected with the commercialization of large-scale hydrogen production projects[31] will also provide a supply chain for the key equipment needed in electrochemical separation processes. In

the last few years, successful applications of electrochemical separation have been published. Nasrollahnejad et al. demonstrated the electrochemically induced crystallization of fumaric acid [32]. Extensive research on integrated bioelectrochemical processes was conducted [33, 34]. They demonstrated electrochemical recovery of ammonia from digestate[35, 36], recovery of carboxylate from biorefinery side streams [37], recovery of carboxylic acid from stillage fermentation[38, 39] and succinic acid fermentation with removal of the product by electrodialytic anion extraction [40]. These applications showed great potential but require anion exchange membranes, which are known to suffer from a low selectivity of carboxylates over OH^-, which limits the current efficiency [41].

1.3. Synopsis, development needs and Outline

The development of improved electrochemical separation technologies requires the identification of inefficiencies that limit the performance of existing technologies. A key challenge is the development of robust and cost-effective ion exchange membranes [42]. In addition, the following development needs are identified:

- Thorough understanding of the limiting operational conditions in the upstream fermentation and downstream process to enable effective integration of the electrochemical processing steps.
- Improvement of current efficiency and current density to enable economic operation.
- Models and engineering concepts to scale electrochemical separation from the lab-scale to the pilot and industrial scale.
- Adaption of electrochemical processes to the supply of intermittent renewable energy sources.

With the current status of electrochemical separation technologies in mind, the objective of this thesis is guided by the following research question: *Does the integration of electrochemical pH swing induced by water splitting combined with reactive extraction provide a feasible downstream technology to overcome salt waste production and enable sustainable succinic acid separation?*

To answer this question, chapter 2 introduces the fundamentals of the electrochemical pH swing created by water splitting and the reversible pH extraction mechanism that is applied for succinic acid extraction. It also discusses the electrochemical stability of selected biobased platform chemicals at the water-splitting catalysts. Chapter 3 presents a design of experimental assessment supported by experiments and identification of factors relevant to the yield and selectivity of succinic acid extraction from electrolyte-containing solutions. In chapter 4 the proof of concept for electrochemical pH swing extraction and purification of succinic acid is demonstrated. In order to assess the viability of electrochemical pH swing extraction and better understand the complex interaction of the dissociation equilibria, which constitute the pH value of the aqueous phase, with the electrolytic pH shift and the reactive extraction equilibrium of succinic acid, a dynamic model 0D of electrochemical pH swing extraction is developed in chapter 5. The model is also used to analyze operational limits and provide a better understanding of mechanisms that may result in operational inefficiencies. The validity of the model is evaluated by comparison with experimental data.

Based on this model, a spatially structured model is derived in chapter 6. The objective herein is to assess limiting conditions caused by inhomogeneous spatial concentration and gas holdup distribution inside an electrolysis cell. Transfer of electrochemical pH swing reactive extraction to other carboxylic acids is presented in chapter 7 for itaconic and in chapter 8. The work closes with a techno-economic assessment in chapter 9, which compares the electrochemical pH swing extraction with separation technologies established for succinic acid separation. The results of this thesis confirm the promising ecological and economic perspective and thus this work seeks to contribute to the progress of electrochemical

separation technologies to establish them as "a platform for sustainable recovery of carboxylic acids" [43].

1.4. Previous publication and contribution

This thesis is the result of the research performed by the author during his time as a full-time researcher and doctoral candidate at the Chair of Fluid Process Engineering (AVT.FVT) from November 2017 until September 2021.Throughout his doctoral studies, the author has worked in the Kopernikus Project Synergy and gratefully acknowledges the financial support of the Kopernikus project SynErgie (03SFK3L1-2 by the Federal Ministry of Education and Research (BMBF) and the project supervision by the project management organization (PtJ). Parts of the thesis have already been published in different journals. In particular, parts of the following publications are reused and integrated into the chapters of the thesis as stated below. Unless otherwise indicated, the journals consented to the use of the previously published content in this thesis.

- **Chapter 3** has been published in Gausmann et al. "Reliable Identification of Relevant Factors for the Reactive Extraction of Succinic Acid from Electrolyte Containing Solutions" 2023 SOLVENT EXTRACTION AND ION EXCHANGE

- **Chapter 4** was published in a slightly modified version as: Gausmann et al. "Recovery of succinic acid by integrated multi-phase electrochemical pH-shift extraction and crystallization" 2020, Separation and Purification Technology

- A previous version of the model described in **Chapter 5** has bee published in Gausmann & Jupke "Dynamic Modeling of Electrochemical pH-Swing Extraction" 2020, Chemie Ingenieur Technik. The content of this chapter is a revised version of the original model extended by a more rigorous modeling approach for the

dissociation equilibrium constituting the pH value of the aqueous solution. The revised model was published as: Gausmann, & Kiefel, & Jupke "Modeling of electrochemical pH swing extraction reveals economic potential for closed-loop bio-succinic acid production" 2022, Chemical Engineering Research and Design)

- The content of **Chapter 7** and parts of appendix G.2 have been published in a joint publication with Angelo Gössi as: Gausmann & Gössi et al. "Electrochemical membrane-assisted pH swing extraction and back-extraction of lactic acid" 2022, Separation and Purification Technology. Parts of this chapter are also used in the Dissertation of Angelo Gössi, " Membrane supported reactive extraction using membranes with enhanced stability".

- **Chapter 8** has been published in parts in: Gausmann & Kocks et al. "Electrochemical pH-T-Swing Separation of Itaconic Acid" 2021, ACS Sustainable Chemistry & Engineering

- **Chapter 9** is intended for publication as: Gausmann & et al. "Techno economic assessment of downstream technologies for CO2-negative biosuccinic acid production" (2023), (Manuscript in preparation)

During the time at AVT.FVT the author supervised or co-supervised student theses that contributed to this work and formed the basis of some chapters. In particular, Till Königs, Dominik Schaefer, and Daniel Skarplik diligently collected the experimental data presented in chapter 2. The master's theses of Robert Kiefel, Julius Hausmann, and Johannes Krings laid the foundation for chapter 5 by contributing significant parts of the presented modeling code and carrying out the validation experiments. The master's thesis of Kerstin Brökelmann provided the basis for Chapter 6. The master's thesis of Franziska Bertram co-supervised with Angelo Gössi formed the basis for chapter 7 and the corresponding publication. The experiments presented in chapter 8 were carried out as part of the VIT student project supervised by the author and Christian Kocks. The execution of the aforementioned student

projects was carried out under the author's guidance for good scientific practice and accompanied by intensive subject-specific supervision and data revision. Results from these student projects have been utilized in accordance with the student's consent for the present doctoral thesis. The aforementioned contributions are highly acknowledged.

2. Fundamentals of pH swing separations

This chapter compiles the fundamentals required for the development of electrochemical pH swing extraction processes. While a focus is set on succinic acid, the presented methodology is considered to be applicable to other carboxylic acids as well. Section 2.1 starts by introducing the weak acid equilibrium of carboxylic acids, followed by section 2.2 where the basics of the electrochemical pH swing are presented. Then, section 2.3 highlights the importance of the bulk pH value for microbial metabolism and discusses the thermodynamic limits for industrially feasible end concentration of the fermentation process. In section 2.4 the reactive extraction mechanism of amine-based extractants is introduced. The dependency of the extraction efficiency on the pH value of the aqueous phase is derived from the mass action law governing the extraction equilibrium. The binding mechanism of tertiary amines is found to be reversible with regard to the aqueous pH value. With the knowledge of the feasible operating conditions for fermentation and extraction, a miss match in the operating windows with regard to the pH value is found. In this chapter, the electrochemical pH swing process for the separation of succinic acid is conceptualized to overcome the need for pH-adjusting agents in the downstream process. When electrochemical processing steps are applied to adjust the pH value, the presence of background electrolytes is likely. However, coextraction of inorganic anions is a known phenomenon that compromises the yield and selectivity of reactive extraction [44]. Although the phenomena of anion coextraction are known, it is unclear whether the impact of aqueous pH or the coextraction of anions is more relevant to the overall performance. To quantify both effects while taking into account other operational

conditions, an experimental screening plan is developed by applying a design of experiments method combined with statistical analysis. The applied method allows the statistically verified identification of factors that have the most relevant impact on extraction performance with a minimal number of experiments. The fundamental part is completed by an extensive experimental assessment of the electrochemical stability of biobased products with cyclic voltammetry (CV) measurements in section 2.5

2.1. The pH equilibrium of weak acids

Carboxylic acids, such as succinic acid, dissociate in an aqueous solution into protons and carboxylate ions.

$$\mathrm{HA} \longleftrightarrow \mathrm{H^+} + \mathrm{A^-} \tag{2.1}$$

The equilibrium constant K_a of the dissociation reaction is calculated from the equilibrium concentrations and often tabulated as the negative logarithm of K_a [2].

$$K_a = \frac{[\mathrm{H^+}] \cdot [\mathrm{A^-}]}{[\mathrm{HA}]} \tag{2.2}$$

With the equilibrium constant, the degree of protonation α at a given pH value can be calculated.

$$\alpha = \frac{[\mathrm{HA}]}{[\mathrm{HA}]_{\mathrm{tot}}} \tag{2.3}$$

$$= \frac{[\mathrm{HA}]}{[\mathrm{HA}] + [\mathrm{A^-}]} \tag{2.4}$$

For a monoprotic acid like lactic acid, this results in the following expression for α:

$$\alpha = \frac{[\mathrm{H^+}]}{[\mathrm{H^+}] + K_a} \tag{2.5}$$

And for polyprotic acids like succinic acid or itaconic acid, this expression extends to:

$$\alpha = \frac{[H^+]^2}{[H^+]^2 + K_{a1}[H^+] + K_{a1}K_{a2}} \tag{2.6}$$

Applying eq. (2.6) yields the acid species distribution for a given pH value shown in fig. 2.1. Above a pH value of six, virtually all succinic

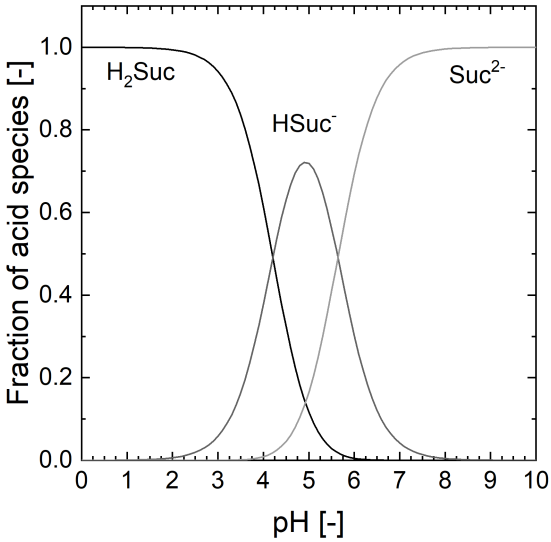

Figure 2.1.: Fractions of succinic acid species calculated for a pKa_1=4.21 and pKa_2=5.64 [2]

acid is present in ionic species of the succinic acid, either hydrogen succinate ($HSuc^-$) or succinate (Suc^{2-}). The same applies to itaconic acid fig. A.2 and lactic acid fig. A.3, which were investigated in this work in addition to succinic acid. As a consequence, the recovery of succinic acid with high yield is only viable below a pH value of three. If succinic acid is not produced at this pH, the addition of protons is required to

shift the pH value of the aqueous solution to conditions at which succinic acid is present.

2.2. Electrical generation of the driving force for pH swing separation

The concept of electrochemical water splitting by electrolysis is well known [45]. At pH=7 The overall reaction is constituted by the oxidative oxygen evolution reaction (OER)

$$4\,H_2O \longrightarrow O_2 + 4\,H^+ + 4\,e^- \qquad E_0 = 0.817\,V \tag{2.7}$$

and the reductive hydrogen evolution reaction (HER)

$$4\,H_2O + 4\,e \longrightarrow 2\,H_2 + 4\,OH^- \qquad E_0 = 0.413\,V \tag{2.8}$$

The sum of HER and OER yields the overall reaction for water electrolysis:

$$2\,H_2O \longrightarrow O_2 + 2\,H_2 \qquad E_0{=}1.23\,V \tag{2.9}$$

The reversible electrode potential of both reactions depends on the pH of the electrode. For conditions deviating from the reference state the electrode potential can be calculated with the Nernst equation [46]:

$$\Delta E = \Delta E^0 - \frac{R \cdot T}{z \cdot F} \ln \prod_{i=1}^{k} a^{\nu_i} \tag{2.10}$$

In electrochemical reactions, the reaction rates $\frac{dn}{dt}$ relate to the electric current according to Faraday's law of electrolysis. In addition to the differential formulation,

$$\frac{dn}{dt} = \frac{I}{z \cdot F} \tag{2.11}$$

the integral formulation

$$n = \frac{I \cdot t}{z \cdot F} \tag{2.12}$$

is also used frequently. With eq. (2.12) the number of protons (H^+), respectively, hydroxide ions (OH^-) can be calculated. If the electric circuit between the anodic OER and the cathodic HER is not closed by protons or hydroxide ions but by other ions, such as sodium or potassium, the OER and HER generate a pH swing between the anodic and the cathodic reactions.

2.3. The role of pH for succinic acid production

The feasible operational conditions for succinic acid fermentation are closely related to the microbial metabolism that produces the succinic acid. Therefore, the most important aspects of the production of microbial succinic acid and the export of cell products will be introduced in this section. Thermodynamic considerations for feasible operational conditions are based on the work of Taymaz-Nikerel et al. [47] which is extended by taking into account active product export.

Succinic acid is produced in the tricarboxylic acid (TCA) cycle. There are two paths in TCA that lead to succinic acid. One oxidative and one reductive route. To maintain a leveled reduction balance, both routes are used by microorganisms that produce succinic acid as the single major product [3]. A detailed overview of known succinic acid producing microorganisms and the substrate utilized is given in chapter 9.

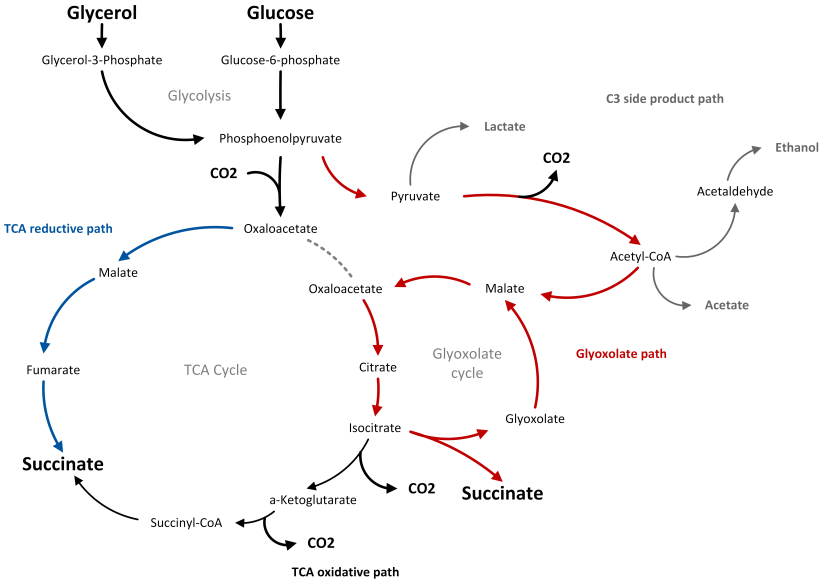

Figure 2.2.: Metabolic pathways for the production of succinic acid according to Dessie et al [3]. and Binns et al. [4].

Starting with a carbohydrate substrate (e.g. glucose), die C-source is converted to oxaloacetate and thereof converted via the reductive or oxidative path of the TCA to succinic acid. On the reductive path, two additional molecules of NADH and CO_2 are consumed for the production of two moles of succinic acid.

$$C_6H_{12}O_6 + 2\,NADH + 2\,CO_2 \longrightarrow 2\,Suc^{2-} + 4\,H^+ \tag{2.13}$$

The oxidative path yields additional reduction equivalents (NADH), CO_2 and also provides the microbial energy source ATP .

$$C_5H_{12}O_6 \longrightarrow 1\,Suc^{2-} + 2\,H^+ + 2\,ATP + 5\,NADH + 2\,CO_2 \tag{2.14}$$

Unless significant amounts of other side products are produced, the overall NADH balance of the succinic acid production must be leveled. As a consequence, the oxidative and the reductive paths are used, yielding the following overall reaction for selective microbial succinic acid production:

$$7\,C_6H_{12}O_6 + 6\,CO_2 \longrightarrow 12\,Suc^{2-} + 24\,H^+ + 4\,ATP \tag{2.15}$$

Meaning that with the production of each molecule of succinic acid, the microorganism receives $1/3$ mol of ATP for its maintenance metabolism. The amount of ATP produced by the product-forming pathway becomes especially important when product export is taken into account. Figure 2.3 shows the two export mechanisms available. Passive export is driven by a gradient in the electrochemical potential across the cell membrane, whereas the ABC transporter obtains the required energy for succinic acid export from ATP hydrolysis. The existence of the active export mechanism was not yet confirmed, but is considered likely because a succinate export-associated decrease in ATP yield was observed [48].

Inside the cell a constantly neutral pH is maintained [47]. Thus, succinic acid is present as anionic succinate inside the cell and in order to maintain the inner cell pH homeostasis protons must be exported with

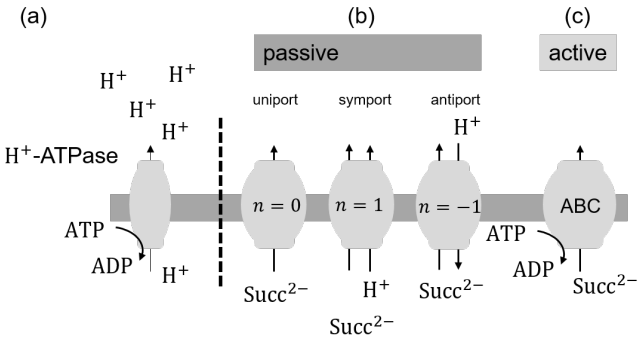

Figure 2.3.: (a) Proton export by H^+-ATPase and possible transport mechanisms for the export of succinic acid from the cell. (b) Passive transport is driven by a gradient in the electrochemical potential. (c) Active transport by ATP binding transport proteins like the ATP-Binding-Cassette (ABC). Adapted from [5]

the produced succinic acid as well. Depending on ratios of succinic acid concentration and pH between the outside and inside of the cell, succinic acid is either exported together with protons (symport) alone (uniport) or exchanged with protons (antiport). Considering the industrially desired succinic acid concentrations found in the range of $0.1\,\mathrm{mol\,L^{-1}}$ up to $2\,\mathrm{mol\,L^{-1}}$ and taking into account that the concentration of succinic acid within the cell will unlikely exceed $0.001\,\mathrm{mol\,L^{-1}}$ it becomes evident that an additional driving force is needed to transport succinic acid against the resulting concentration gradient.

The energy supply needed for the export of the product is found in the ATP available inside the cell or in the proton motive force (pmf) resulting from the proton gradient and the difference in the electric potential on the membrane that is shown in fig. 2.4. By balancing the energy, the microorganism obtains from the product formation and the energy required for product export the thermodynamic limits of microbial growth conditions are found. For a detailed discussion of the biological aspects of carboxylic acid export and the background of the thermodynamic

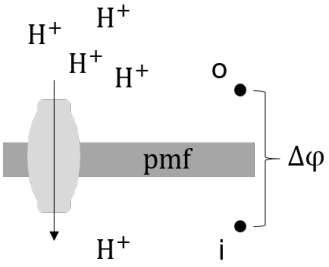

Figure 2.4.: The pmf is constituted by the concentration gradient of protons and the difference in the electric potential across the cell membrane

calculations, the reader is referred to [5] and [47]. The electrochemical potential E originating from the difference in the concentration of protons outside (pH_{out}) and inside (pH_{in}) the cell is calculated with the Nernst equation eq. (2.10) yielding

$$\Delta E = -\frac{RT}{zF} \ln\left(\frac{\mathrm{H}^+_{\mathrm{in}}}{\mathrm{H}^+_{\mathrm{out}}}\right), \tag{2.16}$$

$$\Longleftrightarrow \Delta E = -\frac{RT}{zF} \ln 10 \left(pH_{out} - pH_{in}\right). \tag{2.17}$$

The electrochemical potential of the proton gradient and the difference in the electrical potential φ constitute the pmf:

$$pmf = \Delta\varphi - \frac{RT}{zF} \ln 10 \left(pH_{out} - pH_{in}\right). \tag{2.18}$$

The microorganism maintains a constant pmf at a value between 120-150 mV while the electric potential changes with the outside pH. This affects the Gibbs energy available for product export. Including the electric potential, the balance of Gibbs energy for the product export of a dicarboxylic acid like succinic acid becomes:

$$\begin{aligned}\Delta G =& RT\left(\ln A_{out}^{-2} + \ln H_{out}^{+}\right) - RT\left(\ln A_{in}^{-2} + \ln H_{in}^{+}\right) - \\ & \Delta\varphi F(n-2) + m\Delta_R G_{ATP},\end{aligned} \tag{2.19}$$

with A^{2-} being the anion of the carboxylic acid and n the number of protons transported with the carboxylic acid. In the case of active transport m denotes the number of ATP molecules consumed per mole of succinic acid exported. The thermodynamic limit of product export is found when ΔG becomes zero. By inserting eq. (2.18) in eq. (2.19) and reformulating the equilibrium equation an expression for the feasible concentration difference (A_{out}^{-2}/A_{in}^{-2}) is found.

$$\log\left(\frac{A_{out}^{2-}}{A_{in}^{2-}}\right) = \frac{F\,(-pmf)\,(n-2)}{RT\ln 10} + 2\cdot(pH_{out} - pH_{in}) \tag{2.20}$$

$$- \frac{m\cdot\Delta_R G_{ATP}}{RT\ln 10} \tag{2.21}$$

By including the acid dissociation equilibrium, the anionic concentration ratio is translated to the total acid concentration ratio, which is of more practical interest.

$$\frac{A_{out}}{A_{in}} = 10^{\left(\frac{F(-pmf)(n-2)}{RT\ln 10} + 2\cdot(pH_{out}-pH_{in}) + \frac{m\cdot\Delta_R G_{ATP}}{RT\ln 10}\right)} \tag{2.22}$$

$$\cdot\left(\frac{10^{-2pH_{out}+pk_{a1}+pk_{a2}} + 10^{pk_{a2}-pH_{out}} + 1}{10^{-2pH_{in}+pk_{a1}+pk_{a2}} + 10^{pk_{a2}-pH_{in}} + 1}\right) \tag{2.23}$$

At a neutral pH, the export of succinic acid is possible by the $n = 1$ uniport mechanism leaving behind one proton with each molecule of succinic acid, which must be exported in addition to the succinic acid. Export of H^+-ATPase-driven proton requires approximately 1/3 mole additional ATP per mole H^+ in prokaryotic cells, causing the net ATP yield of product metabolism to decrease when approaching the $n = 1$

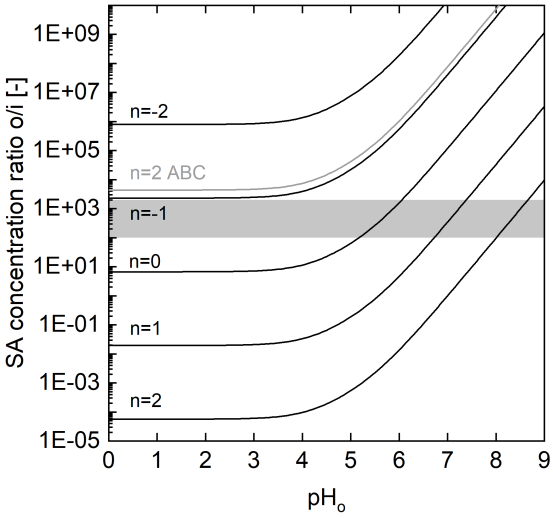

Figure 2.5.: Thermodynamic limits for succinic acid export mechanisms with regard to the concentration difference inside and outside the cell (A_{out}/A_{in}) and the pH outside the cell. The gray box indicates the industrially desirable concentration range of 0.1-2 $\mathrm{mol\,L^{-1}}$. Export of products is possible below the curve.

line [47].

Unless the microorganism can obtain the ATP required for product export from other metabolic activities, its ability to produce succinic acid is limited to neutral pH conditions for the industrially desired concentrations. This finding allows two conclusions:

1. Fermentation of succinic acid at low pH requires the utilization of additional ATP for product and proton export. This ATP must be provided either by ATP-generating coproduct formation or by aerobic respiration.

2. Metabolic engineering and inclusion of ABC transporters can enable fermentation at a low pH value at the expense of additional substrate consumption.

3. The highest substrate yield is expected for a fermentation run at neutral pH. This requires the addition of a base to maintain a constant pH during the fermentation and the conversion of succinate anions obtained in the fermentation to the free acid in the downstream processing.

The conclusions are underlined by experimental observations that succinic acid production at acidic conditions shows lower substrate yields than production at neutral pH [49].

As a consequence, acidic fermentation has the disadvantage that a lower extracellular pH is sustained at the expense of an increased energy demand for product export. Concentrations and pH values required for technical operations seem only feasible if additional metabolic energy is available, for example, from aerobic respiration or side product formation. In addition, the backdiffusion of protonated succinic acid becomes more severe at low extracellular pH and high concentrations of extracellular succinate [50, 51]. Hence, the development of low-pH-tolerant strains has the potential to reduce the separation effort, but the metabolic energy gain imposes operational limits which must be taken into account in order to not compromise the metabolic carbon yield.

Wahl et al. [50] reported that the recycling rate of succinic acid back to the cell of *Sacharomyces cerevisiae* at low pH (pH=3) was 46 times higher than the actual production rate. Taking into account the ATP demand for product export under these conditions the theoretical yield for glucose-based fermentation is limited to $0.40\,g_{Suc}/g_{Glu}$. This is consistent with the yields reported for succinic acid production with yeast hosts [49]. The costs for chemical pH-shift can be estimated by adding the costs of sulfuric acid ($0.06\,EUR/kg_{Suc}$), $Ca(OH)_2$ base addition ($0.10\,EUR/kg_{Suc}$), and the disposal costs of co-produced solid salt waste ($0.16\,EUR/kg_{Suc}$), which add up to ($0.32\,EUR/kg_{Suc}$). Assuming a glucose price of 330 EUR/t the acidic fermentation must achieve at least an overall yield of $0.54\,g_{Suc}/g_{Glu}$ to break even.

2.4. Reactive extraction of succinic acid

Reactive extraction of succinic acid is based on the formation of complexes between succinic acid and an extractant [52, 53]. The formed complex has a higher affinity for the solvent phase, and thus extracts succinic acid from the aqueous phase. Beyond succinic acid separation[54], reactive extraction was studied intensively for the separation of other carboxylic acids as well. The most prominent are citric acid[55], lactic acid[56], itaconic acid[57], and tartaric acid[58]. Therefore, extraction methods are considered the most popular methods for the primary recovery of carboxylic acids [23].

There are different types of extractants that can be used for the extraction of succinic acid. The most commonly used are aliphatic amines or phosphoric solvents [53, 59]. Amino acid extractants exhibit higher extraction capacity, while phosphoric extractants are considered less toxic to microorganisms [55].

In the case of aliphatic amines, two possible extraction mechanisms exist. Quaternary amines work as liquid anion exchangers and extract the acid by an ion exchange mechanism, as illustrated in fig. 2.6 [60]. This has the advantage that extraction is possible at high pH values.

However, the toxicity and difficult backextraction limit the usability of this extraction mechanism in practice [55, 54].

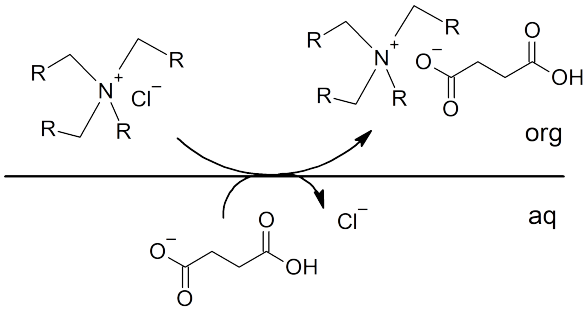

Figure 2.6.: Quaternary amines extract succinic acid by an ion exchange mechanism.

Figure 2.7 shows the second mechanism, which is based on the formation of hydrogen bonds between the nitrogen atom of the amine and the hydrogen atom of the carboxylic acid group [61, 62]. Depending on the diluent, different complexes are formed. In general, diluents are divided into two classes I) active diluents such as alcohols, ketones or halogenated hydrocarbons can interact with the acid-extractant complex and tend to stabilize the formation of 1:1 complexes, and II) inactive diluents such as alkanes or aromatic hydrocarbons that exhibit only little interaction and low solubility for the acid-extractant complex [53].

The complexation by a hydrogen-bond-mediated mechanism has the advantage of being reversible with respect to the aqueous pH. The addition of hydroxide ions cleaves the complex and the hydrogen succinate anion can be easily recovered in the aqueous phase as illustrated in fig. 2.8

The pH-dependent complexation mechanism enables a pH-swing extraction process. However, when acid and base are used to induce the pH swing concurrently, salt waste is formed. This production of salt waste is a major challenge and must be overcome by recycling acid and

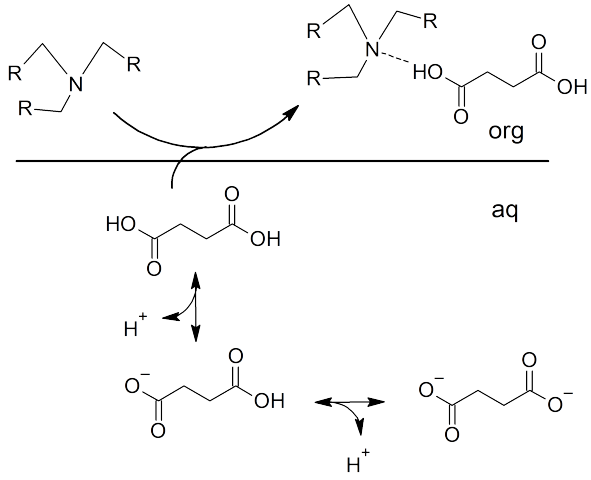

Figure 2.7.: Tertriary amines form complexes with succinic acid by hydrogen bonds or proton-transfer reactions.

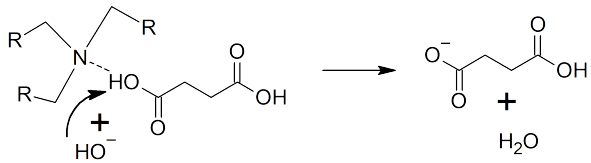

Figure 2.8.: Back-extraction of succinic acid by hydroxide ion addition

base [63].

The pH-dependent extraction behavior originates from the fact that in the case of tertiary amines only the protonated form of the carboxylic acid eg. H_2Suc acts on the extraction equilibrium:

$$H_2Suc + TAM \overset{K_{ex}}{\rightleftharpoons} [H_2Suc{-}TAM]. \tag{2.24}$$

This results in a mass-action-relationship governing the succinic acid

extraction by amine-based extractants[64, 65, 62]:

$$K_{ex} = \frac{[H_2Suc{-}TAM]}{H_2Suc \cdot TAM}, \tag{2.25}$$

which is coupled to the aqueous pH-equilibrium of the carboxylic acid:

$$H_2Suc \overset{pK_{a1}}{\rightleftharpoons} H^+ + HSuc^- \tag{2.26}$$

$$HSuc^- \overset{pK_{a2}}{\rightleftharpoons} H^+ + Suc^{2-}. \tag{2.27}$$

Another way of inducing the pH shift which results in the driving force for the succinic acid extraction is enabled by coupling the pH shift created by the water-splitting electrode reactions of water electrolysis with the reactive extraction. If the electric circuit is closed not by protons H^+ nor hydroxide ions OH^- but by other cations such as $Li^+, Na^+, K^+, Mg^+, Ca^+, NH_4{}^+$ or anions like $SO_4{}^{2-}, PO_4{}^{3-}, CL-, CO_3{}^{2-}$ the pH of the anolyte and catholyte changes with the progress of the water electrolysis. In order to differentiate this kind of electrolysis from proton exchange membrane electrolysis[66] or alkaline electrolysis[67, 68] this kind of electrolysis is denoted pH shift electrolysis in the following.

The pH gradient induced by the pH-shift electrolysis can be used to drive the extraction and back-extraction while the acid and base are produced and recycled internally. From a process perspective, this creates an internally closed loop and eliminates salt waste production. Compared to other electrochemical separation techniques used for the separation of carboxylic acids[42] the pH shift electrolysis requires fewer membranes, but the carboxylic acid must exhibit sufficient electrochemical stability to avoid product degradation at the electrodes. In a recent study investigating the electrochemical degradation of lignin carboxylic acids, the largest group of products was found, indicating a comparatively high resistance to electrochemical degradation [69].

2.5. Electrochemical stability of bio-based products

Electrochemical stability is a prerequisite for the application of pH shift electrolysis coupled with a pH swing extraction process for carboxylic acid recovery. Known electrochemical degradation reactions are oxidative C-C bond cleavage[70], decarboxylation *via* kolbe-electrolysis[6, 71] or electroreductive hydrogenation of unsaturated side chains[72].

In addition to carboxylic acids, other relevant bio-based products or components are sugars, alcohols, amines, and amino acids. Carbohydrates are essentially the most commonly used substrate in industrial biotechnology [1]. Glycerol is an abundant by-product of the biodiesel industry [73] and amines and amino acids are highly functional biobased products [18]. The molecules tested for their electrochemical stability are shown in fig. 2.9.

The electrochemical stability is examined by cyclic voltammetry (CV) measurements. During a cyclic voltammetry measurement the electrode potential E of the working electrode is linearly raised and then reversed. The electric current is recorded and plotted against the working electrode potential. Peaks in the cyclic voltammogram indicate electrochemical reactions. Symmetric peaks observed in both the forward and backward part of each cycle indicate a reversible reaction whereas a missing peak in either the forward or the backward part indicates an irreversible reaction [74, 75].

2.5.1. Materials and Methods

CV measurements were conducted in a corrosion test cell from Methrom, Germany. The working electrode potential was recorded against a mercury/mercurous Sulfate ($Hg/HgSO_4$) HgE10 reference electrode, Sensortechnik Meinsberg, Germany. A reference 3000 potentiostat, Gamry instruments, United States, was used to record CV data at a scan rate of 100 mV/s. The concentration, the initial pH value, and the supplier of each compound are stated in table B.1 and table B.2. All solutions

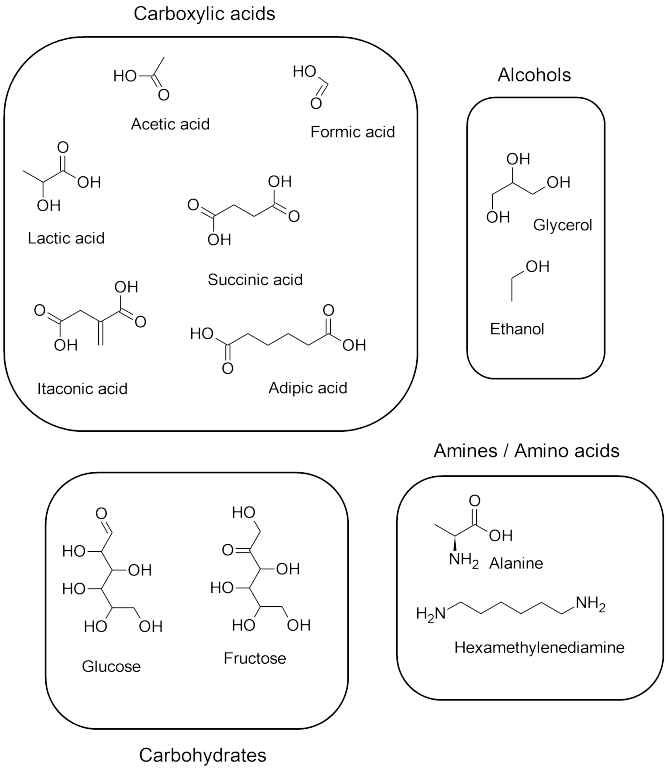

Figure 2.9.: Bio-based products or substrates

were prepared with 0.2 mol/L Na_2SO_4 as background electrolyte. The resolution of the CV scan was also tested with scan rates of 50 mV/s and 20 mV/s, which revealed results comparable to the scan rate of 100 mV/s. The potential measured in the CV experiments E_{exp} was recorded against the $Hg/HgSO_4$ reference electrode and converted first to the potential against the standard hydrogen electrode (SHE):

$$E_{SHE} = E_{exp} + E_{Hg/HgSO_4} \tag{2.28}$$

$$E_{SHE} = E_{exp} + 0.66V \tag{2.29}$$

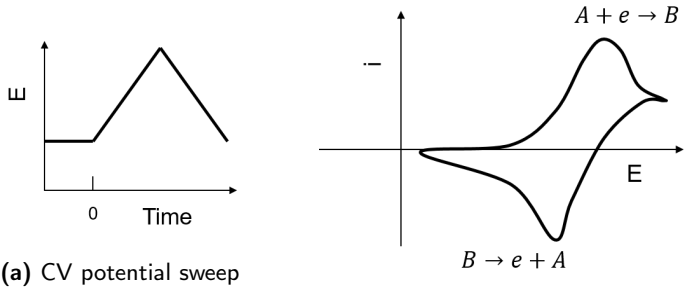

(a) CV potential sweep

(b) Resulting cyclic voltammogram

Figure 2.10.: Peaks in the current potential curve indicate electrochemical reactions.

In order to take the effect of the aqueous pH value into account the potential vs. SHE is converted to the reversible hydrogen electrode potential (RHE) that is displayed in the CV curves according to:

$$E_{\mathrm{RHE}} = E_{\mathrm{SHE}} + 0.059 \cdot pH \tag{2.30}$$

All potentials of the CV curves in the following section are stated in terms of RHE potential. In the context of this thesis, a component is considered "electrochemically stable" when the CV curves do not indicate additional peaks or significant deviations from the reference curves recorded with the electrode in the supporting electrolyte. It does not necessarily implicate that the tested component is electrochemically inert and does not participate in any electrolytic reaction. But electrochemical stability in terms of the targeted pH swing electrolysis means that the OER and HER are the dominant electrochemical reactions and that the respective compound does not undergo a significant degradation.

2.5.2. Results and Discussion

Figure 2.11 displays the CV curves of the respective electrode material in the 0.2 mol/L Na_2SO_4 supporting electrolyte.

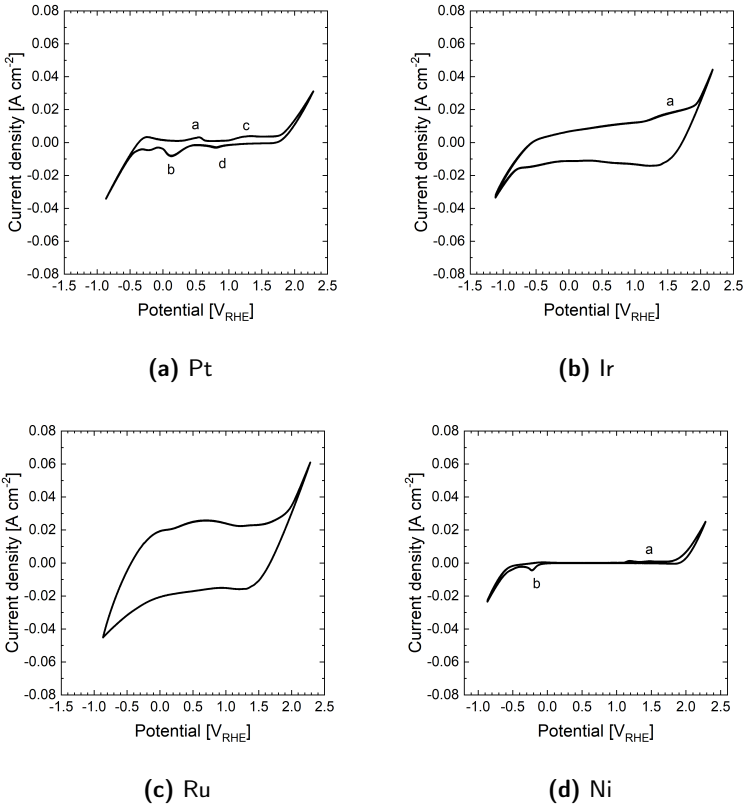

(a) Pt **(b)** Ir

(c) Ru **(d)** Ni

Figure 2.11.: CV scan of sodium sulfate at pH 5.5. Potential recorded vs. Hg/HgE and corrected for RHE

These curves reveal the features and peaks characteristic of each electrode material. All scans show the beginning of the HER at the negative potential as well as the (OER) at the anodic potential. The Pt curve also displays two distinct regions. The peaks close to zero potential (a,b) are attributed to the adsorption, respectively desorption of hydrogen atom on the platinum surface [76]. The other peak pair (c,d) indicates the ad- and desorption of oxygen at anodic potentials [77]. Ir has a small

shoulder (a) before the anodic OER likewise attributed to the formation of adsorbed oxygen species at the electrode surface [78]. Ruthenium has a multitude of redox equilibria[79] with its oxides and hydroxides that cause a significant current in the intermediate potential regions between HER and OER. Lastly, Ni shows small currents indicating the formation of nickel oxide and hydroxide species in the anodic potential range (a)[80] and a cathodic peak (b) characteristic for the reduction of the oxide/hydroxide layers [81].

The CV curves recorded for succinic acid show a pattern similar to that recorded for the electrodes in the supporting electrolyte. The shoulder indicating the formation of the oxide layer on the Ir electrode is more pronounced in the presence of succinic acid (fig. 2.12b) compared to the pure supporting electrolyte.

The formation of the nickel oxide/hydroxide layer seems to be affected by the pH value of the test solution. While it is likewise visible at neutral pH fig. 2.12d the peak vanishes under acidic conditions fig. 2.13d.

This observation corresponds to the stability diagram of nickel [80]. At pH values below 3 the formation of $NiO_x/Ni(OH)_y$ species is inhibited and Ni/Ni^{2+} becomes the active redox reaction competing with the reduction of proton to hydrogen, which is kinetically favored. In addition to these observations, no significant differences are visible between the neutral fig. 2.12 and acidic pH fig. 2.13 and the reference curves recorded in the supporting electrolyte alone. For that reason, succinic acid is considered to be electrochemically stable.

Like succinic acid, CV scans recorded with dicarboxylic acids itaconic acid figs. B.3 and B.4 and adipic acid figs. B.1 and B.2 show no strong indication of electrochemical degradation. (Di-)carboxylic acids potentially undergo electrochemical decarboxylation followed by kolbe and non-kolbe reactions [6, 82], electrochemical reduction of side chains [72] or the oxidative cleavage of C-C bonds [70].

Although the electrochemical conversion of carboxylic acids is known, the medium-chain length acids exhibit some degree of electrochemical stability. This finding is supported by reports that identified carboxylic acids as stable intermediates in the electrochemical decomposition of

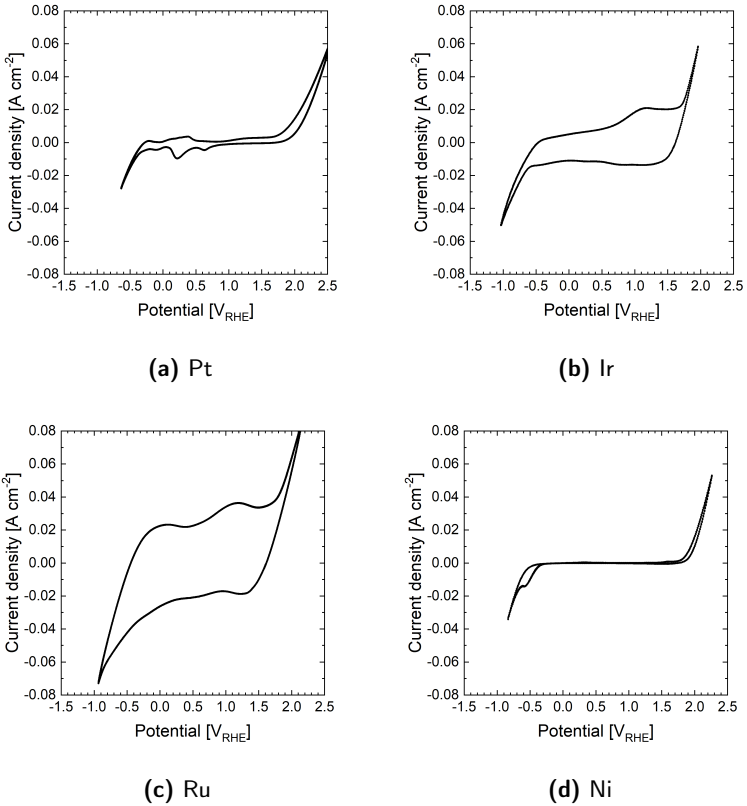

(a) Pt **(b)** Ir

(c) Ru **(d)** Ni

Figure 2.12.: CV scan of succinic acid at pH 6.85. Potential recorded vs. Hg/HgE and corrected for RHE

organic matter [69, 83].

Lactic acid (figs. 2.15 and 2.16), acetic acid (figs. B.7 and B.8) and formic acid (figs. B.5 and B.6) reveal less stability against electrochemical degradation than succinic, itaconic or adipic acid. The most distinct indications of electrochemical degradation are observed for lactic and formic acid at platinum and iridium. Formic acid is an active intermediate in electrochemical reduction CO_2 and is therefore prone to partici-

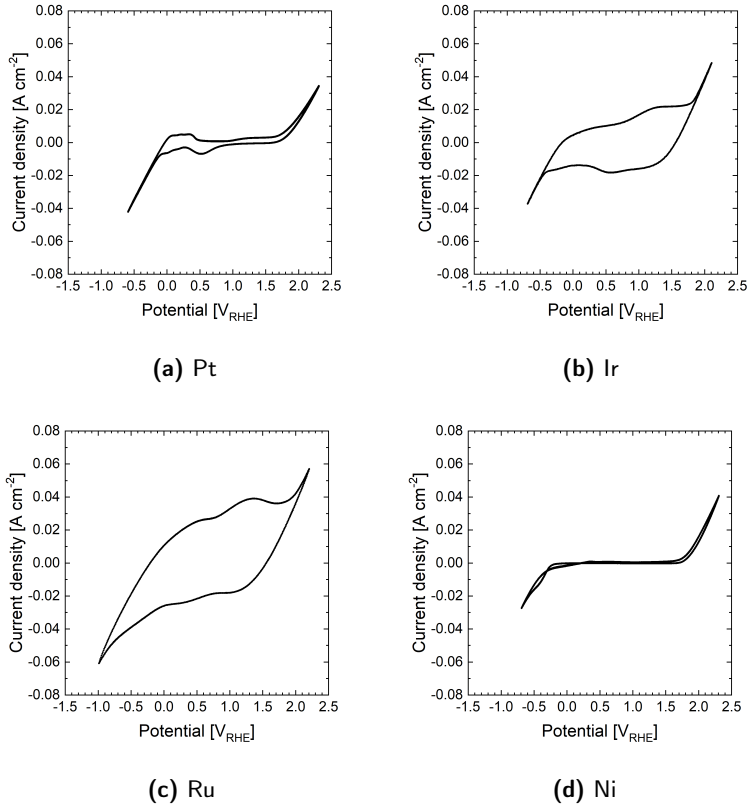

(a) Pt **(b)** Ir

(c) Ru **(d)** Ni

Figure 2.13.: CV scan of succinic acid at pH 2.52. Potential recorded vs. Hg/HgE and corrected for RHE

pate in electrochemical reactions [84, 85] and likewise, the mechanisms of electrochemical reactions for lactic acid were reported [86]. Among the short-chain carboxylic acids, acetic acid revealed the least signs of electrochemical decomposition. Furthermore, acetic acid was identified as an electrochemically stable intermediate in other studies[69] and could be considered stable under the conditions tested here.

The CV curves of ethanol fig. 2.17 and glycerol fig. B.9 show distinct

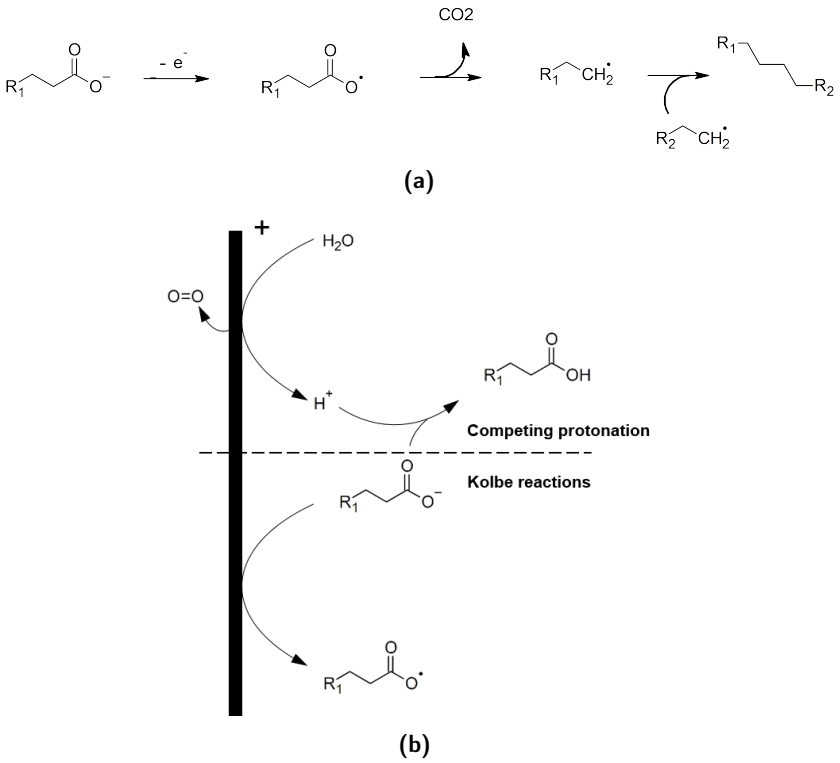

Figure 2.14.: Electrochemical decarboxylation of carboxylate anions (a) [6] and proposed mechanism for the inhibition of the carboxylate radical formation (b) (own work). In the active buffer range of the carboxylic acids protons from the OER lower the local pH at the anode surface and prevent carboxylate adsorption due to protonation.

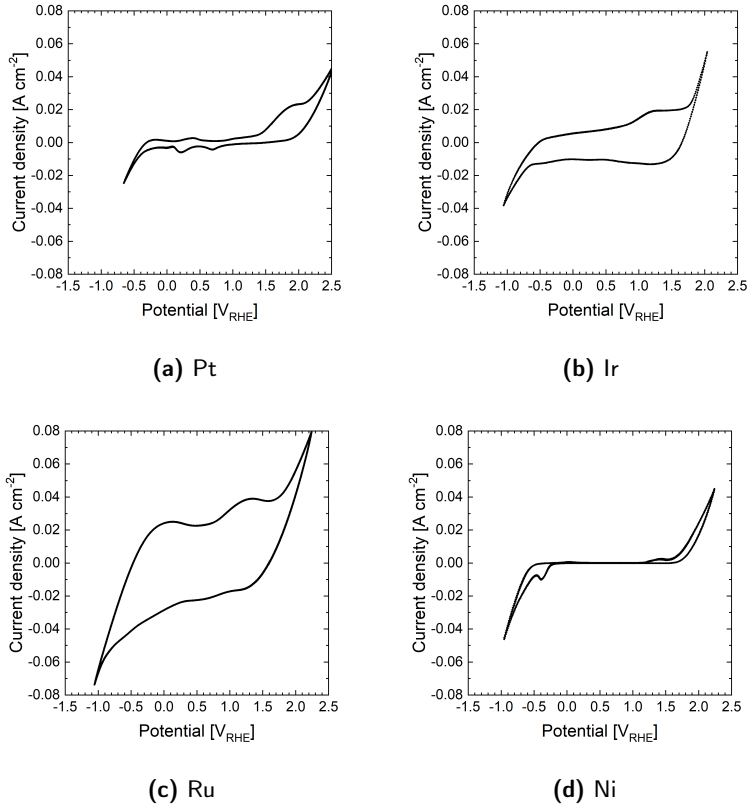

(a) Pt **(b)** Ir

(c) Ru **(d)** Ni

Figure 2.15.: CV scan of lactic acid at pH 6.5. Potential recorded vs. Hg/HgE and corrected for RHE

signs of electrocatalytic activity. Pt and Ni show a strong indication for reactions at anodic potentials. Ir and Ru do not show indications for reactions to the same extent, but it is possible that the reactions are masked by the large surface-associated current. The peaks visible in fig. 2.17a are similar to the potentials reported for ethanol oxidation [87]. Oxidation of higher alcohols, such as glycerol, is reported to be more difficult, but also possible, and is used, for example, in direct alcohol

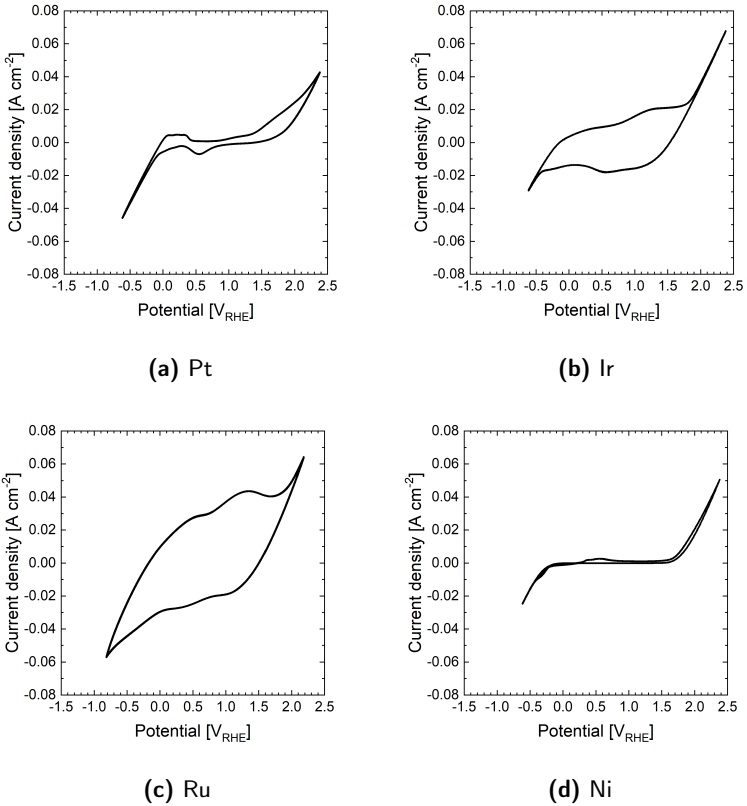

(a) Pt **(b)** Ir

(c) Ru **(d)** Ni

Figure 2.16.: CV scan of lactic acid at pH 2.12. Potential recorded vs. Hg/HgE and corrected for RHE

fuel cells [88].

The electrochemical oxidation of alcohols is affected by the pH value of the supporting electrolyte. A known mechanism that promotes the electrochemical reactivity of primary alcohols is the deprotonation of the $-OH$ group at alkaline pH values. The alcoholate anion formed readily reacts under anodic potentials and forms oxidation products such as aldehydes, ketones, or carboxylic acids [87].

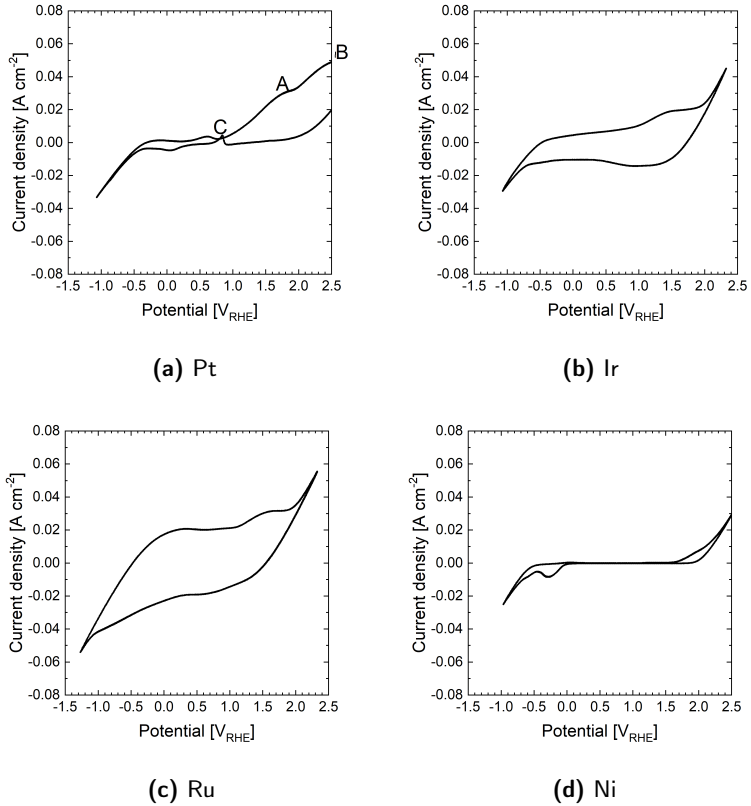

(a) Pt **(b)** Ir

(c) Ru **(d)** Ni

Figure 2.17.: CV scan of ethanol at pH 6.27. Potential recorded vs. Hg/HgE and corrected for RHE

Glucose and fructose are common carbon substrates of industrial biotechnology [1]. Electro-oxidation reactions of fructose and glucose are known and could compromise the carbon conversion efficiency of the overall process if significant fractions are degraded in the separation process. Reactions are exploited for the qualitative and quantitative analysis of sugers[89], which is a useful tool for determining the glucose level in blood samples [90]. With regard to electrochemical pH-swing

separations, a degradation of residual sugars is likely. This expectation is confirmed by the CV curves recorded for glucose fig. B.10 and fructose fig. B.11. The Pt and Ni curves reveal the characteristic features of oxidation reactions at anodic potentials of 1.2 V. With Ir and Ru the features are less distinguishable and potentially masked by the capacitive current. Electrochemical oxidation of sugars also produces carboxylic acids[83] and therefore is a potential source of side products that must be taken into account in the design of the separation process. Consequently, a low residual sugar level would be desirable for a selective electrochemical pH swing separation process. Otherwise, the contact of the sugars with the electrode must be prevented by measures such asmultichamber setups or careful control of the feed flow patterns in order to prevent sugar-containing broth from direct contact with the proton-producing anode.

Although the electro-oxidation of both fructose and glucose is known, fructose revealed more distinct peaks, which indicates a higher reactivity compared to glucose. This finding corresponds to the higher electrochemical sensitivity reported for fructose on electrochemical sensors [91, 89]. The higher electrochemical activity of fructose means that with regard to substrate stability, a glucose-based fermentation would be the preferred choice.

Whether the degradation of sugars is a relevant reaction, strongly depends on the fermentation efficiency. If no substrate is left after the fermentation, the electrochemical stability is not relevant. However, complex substrates often contain non-fermentable sugars that could potentially undergo similar reactions [92]. If electrochemical pH swing extraction is to be applied in the downstream processing of such fermentation processes, the electrochemical stability of the constituents in the fermentation broth should be assessed with representative samples.

In addition to carboxylic acids, Amino acids, and bio-based amines are other important bioproducts of industrial interest and possess pH-dependent solubility and extraction behavior [93, 94, 95]. For that reason, electrochemical pH swing separation could be applicable to these classes of molecules as well. Since the separation of amino acids or di-

amines is not in the scope of this work their results are discussed briefly in the appendix appendix B.2.

Table 2.1 summarizes the results of this chapter for the electrochemical stability of the investigated bio-products. The dicarboxylic acids showed no distinct signs of electrochemical degradation. Overall, the electrochemical stability of the carboxylic acids seems to depend on the length of the carbon chain. Short-chain acids are less stable than those with a longer carbon chain. Among the catalysts tested, Ir and Ni appeared to be the most promising anode materials, while Ni and Pt are considered suitable cathode materials.

The use of noble metal catalysts comes with the issue of high material costs. But the development of advanced non-noble metal catalysts currently in the development for water electrolysis may provide promising alternatives [96, 70]. Exemplary Ni and Ru-based catalysts could be an interesting alternative if the operational pH value of the pH shift electrolysis matches the stability region of the catalyst [80]. In contrast to PEM electrolysis, pH swing electrolysis does not require the acid stability of the catalyst normally needed with PEM electrolysis. Ni and Ru are generally not stable at acidic conditions with pH values of the electrolyte < 4, respectively < 2 [80, 97] but recently pH universal water splitting catalysts based on nickel and ruthenium nanostructures were reported [98].

Table 2.1.: Electrochemical stability of bioproducts. ●:stable, ○:partly stable, ∗: not stable

Component	**Pt**	**Ni**	**Ru**	**Ir**	**Pt**	**Ni**	**Ru**	**Ir**
anode(+)/cathode(-)	(+)				(-)			
Adipic acid	●	●	●	●	●	●	●	●
Itaconic acid	●	●	●	●	●	●	●	●
Succinic acid	●	●	●	●	●	●	●	●
Lactic acid	∗	●	○	○	●	●	●	●
Acetic acid	●	●	○	●	●	●	●	●
Formic acid	∗	○	○	○	○	∗	○	●
Ethanol	∗	∗	○	○	●	○	○	○
Glycerol	∗	∗	○	●	○	∗	○	○
Glucose	∗	○	●	○	○	○	○	○
Fructose	∗	○	●	○	○	○	○	○
L-Alanine	∗	∗	○	○	○	∗	○	○
Hexanediamine	∗	∗	○	○	∗	∗	○	○

2.6. Conclusion

This chapter introduced the fundamentals of the pH swing induced by electrolytic water splitting. It discussed the relevance of the aqueous pH for the reactive extraction equilibrium of tertiary carboxylic acids with the succinic acid example. The combination of both electrochemically induced pH swing and the pH value-responsive extraction equilibrium of carboxylic acids and tertiary amines constitutes the basis of the electrochemical pH swing extraction.

The electrochemical stability of the components targeted in the separation is a prerequisite for this concept to work. The electrochemical stability of twelve components common in bioprocesses was assessed by CV for four different electrode materials. Although sugars, alcohols, amino acids, and diamines showed signs of degradation, especially at anodic potentials, long-chain carboxylic acids did not reveal clear indications of degradation. Consequently, electrochemical pH swing extraction is considered a suitable method for succinic, itaconic, and, with potential limitations, lactic, and acetic acid separation.

The stability classification derived from CV curves provides a valuable and fast indication of whether a constituent is electrochemically stable under the tested conditions. However, it should not be interpreted as a rigorous assessment of electrochemical stability, since minor side reactions can be masked by high capacitive currents or occur at electrode potentials higher than those tested. However, the presented method is a valuable tool to quickly assess the processability of more complex mixtures, such as fermentation broth or product streams with high concentrations of impurities. The characteristic potentials at which peaks occur can help to resolve the side reaction and identify potentially critical impurities.

3. Factors affecting the reactive extraction of succinic acid

3.1. Motivation

In section 2.4 the basic principle of the reactive extraction of succinic acid with tertiary amines from aqueous solutions was introduced. Although the principle has been known for more than 30 years [62, 99, 100, 101]. The application for downstream processing of bio-based succinic acid appeared to be challenging. A severe reduction in extraction performance has been reported for electrolyte-containing solutions[44], the relevance of the initial aqueous pH value is often discussed [52, 65, 102] and much attention is paid to extractant and solvent selection[44, 61, 103].

On the basis of the knowledge about succinic acid extraction with tertiary amines, the aqueous pH should have extraordinary importance with regard to the overall extraction yield. However, a systematic analysis of the parameters affecting the reactive extraction of succinic acid from electrolyte-containing aqueous solutions in terms of yield and selectivity is currently missing.

This chapter aims to provide a systematic analysis, comparison, and identification of parameters that have a relevant influence on the reactive extraction of succinic acid from electrolyte-containing solutions. For this purpose, a statistically supported design of experiments method (DoE) is applied to minimize the necessary experimental effort while ensuring statistically quantified reliability of the results [104].

3.1.1. Design of Experiments

‡ Reactive liquid-liquid extraction is considered a key enabling technology for the sustainable separation of biobased carboxylic acids such as succinic acid [105, 106, 61]. It is based on the utilization of reactive extractants, which are able to form reversible complexes with succinic acid. These complexes exhibit a higher affinity for the solvent phase and thereby increase the extraction efficiency [107]. In the case of succinic acid extraction, tertiary aliphatic amines and phosphorous-based compounds like tri-n-ocytlamine (TOA) or tributylphosphate (TBP) are extractants studied intensively [55, 61, 53, 108]. Reactive extraction was successfully applied for the separation of various other carboxylic acids such as citric acid [55, 109] lactic acid [110, 111] and purivic acid[112], as well. However, reports on the successful large-scale applications of reactive extraction for succinic acid separation are still limited to a few cases[113], despite the promising economic potential identified in techno-economic evaluations [114, 115]. The studies conducted in the past focused mainly on the selection of extractants and diluents to obtain high yields or distribution coefficients for the extraction of succinic acid from artificial aqueous solutions [103, 116, 44]. It was observed that the extraction yield decreased significantly when extractants and diluents developed in artificial systems were applied for the recovery of succinic acid from aqueous solutions containing significant amounts of side components such as inorganic anions [44]. Although extraction yields up to 100% were achieved with artificial aqueous solutions[108], the maximum extraction yield reported for extraction of fermentation broth was 70-85% [117, 44]. Product losses of this magnitude are unacceptable, as they increase the substrate demand and simultaneously the raw material costs and make the process questionable with respect to sustainability standards. The presence of salts, respectively, anions was found to be responsible for the reduction of the extraction efficiency [118, 44, 102].

‡Parts of this chapter have been published in Gausmann et al. "Reliable Identification of Relevant Factors for the Reactive Extraction of Succinic Acid from Electrolyte Containing Solutions" SOLVENT EXTRACTION AND ION EXCHANGE (2023)

This is a significant drawback since many succinic acid-producing organisms require a neutral pH during fermentation.

As a consequence of the neutral pH required for fermentation, the fermentation broth must be acidified prior to extraction. If this is done by adding strong inorganic acids such as hydrochloric or sulfuric acid, equimolar amounts of inorganic anions such as SO_4^{2-} or Cl^- are added, limiting the feasible extraction efficiency. In addition, ions from the nutrient salts and metabolic coproducts may be present after fermentation. Typically, nutrients include NH_4^+, Na^+/K^+, Ca^{2+}/Mg^{2+}, HCO_3-,CO_3^{2-} and traces of sulfur and phosphorus [19, 119, 120]. Formic acid, acetic acid, lactic acid and ethanol are common side products found in succinic acid fermentation [105, 121]. Although the presence of coproducts can be reduced by means of microbial engineering, the presence of inorganic anions is inevitable and is a severe issue for reactive extraction with tertiary amines like TOA. The underlying effect is the competitive coextraction of anions by TOA [65]. This co-extraction is known to depend on concentration, aqueous pH, and the selection of the diluent. Depending on operational conditions, co-extraction can completely inhibit the extraction of carboxylic acid [44, 122]. Although the effect of anion coextraction is known to limit the extraction performance, it is rarely considered during the optimization and selection of suitable extractants and diluents.

3.1.2. Materials and Methods

Screening experiments have the objective of identifying the important factors with the highest relevance for the considered performance indicators. The straightforward approach of testing all possible combinations fails when multiple factors have to be studied. Even if only two states are tested for each factor, the number of possible combinations increases with a power of 2 for each additional factor. The reactive extraction of succinic acid is known to be affected by pH, temperature, succinic acid concentration, type and concentration of diluent, and obviously the choice of the extractant [123, 124, 125]. Adding the concentration and

type of anions amounts to a total of eight factors that could influence the yield and selectivity of succinic acid extraction. This results in 256 experiments required if all combinations are to be tested. Due to the multitude of possible extractants and diluents, testing only two of each would yield limited insights into the true impact and prone the experimental study to fail if the selected diluents and extractants are by chance unlucky choices. Furthermore, strong indications were reported that not only concentration but also type of anion were relevant for yield and selectivity [44]. Taking the additional factors into account would easily amount to many hundreds or thousands of experiments required. The total number of experiments is significantly reduced by applying the DoE approach. In the design of the experiment approach, the test points are systematically distributed in the factor space according to plans based on mathematical considerations. Depending on the type of experiment, different design plans are available. In the past quadratic design, plans were already applied to optimize the extraction of carboxylic acids using response surface methods [126, 127, 128, 56, 129, 130]. In contrast to the quadratic plans used for optimization, screening plans like fractional factorial designs or general orthogonal arrays focus on identifying the main effects. They are not able to cover the factor interaction, but they have the advantage of drastically reducing the amount of experiments required. The workflow applied in this study is presented in fig. 3.1 and is briefly described in the following.

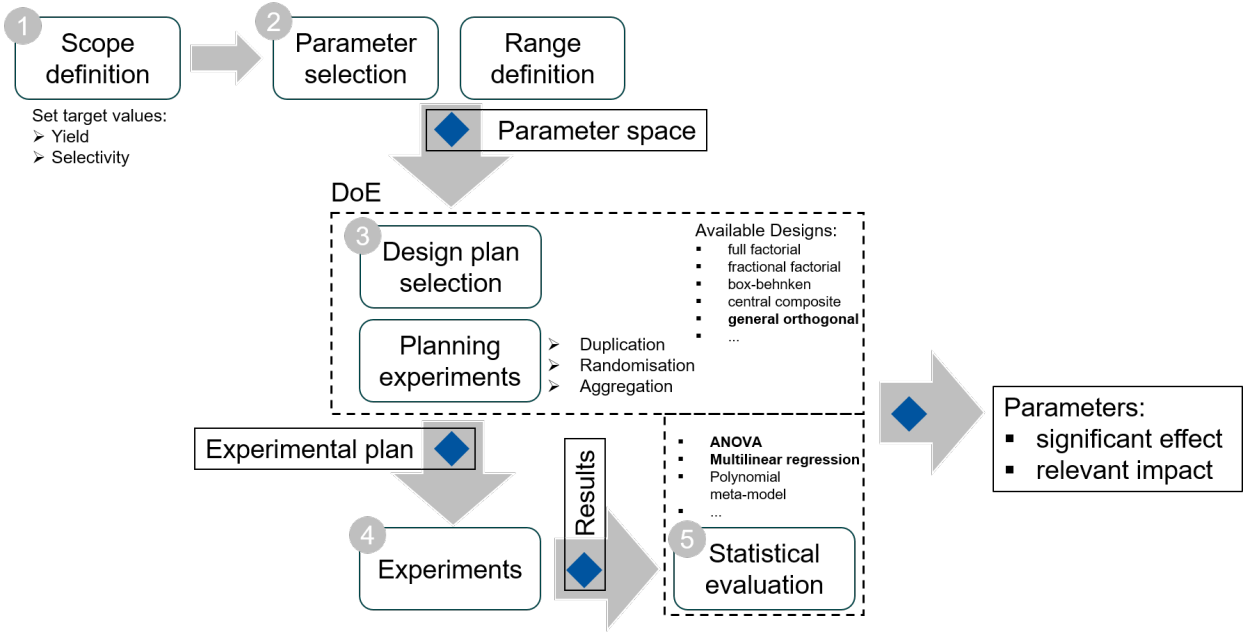

Figure 3.1.: Workflow of conducting the screening experiments with a DoE. 1) The scope and variables to be tested are defined. 2) Potentially relevant factors are selected on the basis of previous knowledge. The range for each factor is defined by constructing the factor space available. 3) A DoE plan is selected and used to plan the factor settings for the experiments. 4) Execution of the experiments according to the design plan. 5) The evaluation of the results by statistical methods identifies the factors that have a significant effect on the results.

1 Scope definition

The scope of this work is to identify operational factors that have an effect on the yield and selectivity of the reactive extraction of succinic acid in the presence of inorganic anions. The extraction yield E is defined as the fraction of succinic acid extracted from the solvent phase divided by the total amount of succinic acid present in the aqueous phase prior to extraction:

$$E = \frac{m_{org}}{m_{aq,0}} \cdot 100. \tag{3.1}$$

The selectivity of reactive extraction is calculated by the mass of succinic acid extracted divided by the sum of the components extracted. As the phase volume is constant, the formulation based on concentrations is equivalent:

$$S_x = \frac{m_{org,x}}{m_{org,x} + m_{org,y}} \cdot 100. \tag{3.2}$$

The mass of succinic acid, respectively, the anions extracted, was calculated by mass balance from the concentration measured in the aqueous phase:[131]

$$m_{org} = m_{aq,0} - m_{aq} \tag{3.3}$$

$$= V_{aq,0}c_{aq,0} - V_{aq}c_{aq}. \tag{3.4}$$

2 Factor selection

A total of eight influencing factors were chosen for the study. The selection is based on factors that were reportedly considered in similar studies, with the addition of the type of salt and electrolyte concentration. Inclusion of factors with known effects also enables quantification of practical relevance if a significant effect is observed. The factor ranges were chosen according to conditions that are practically feasible for succinic acid extraction. The temperature range is selected between

25 °C and 80 °C. 80 °C is a likely temperature if heat sterilization is used to inactivate the biocatalyst prior to extraction and 25 °C would be the minimal temperature obtainable by cooling with cooling water. The concentration of $60\,\mathrm{g\,L^{-1}}$ is taken as a reasonable upper limit, as a higher concentration would allow direct crystallization of succinic acid. $20\,\mathrm{g\,L^{-1}}$ is the lower limit expected, for example, in *in situ* product removal applications [132]. The extractants (Tri-octylamine (TOA), Tris-ethylhexylamine (TEHA) and Tri-hexylamine (THA) and solvents (1-Octanol (Oct) , Methyl isobutyl ketone (MIBK) , 1-Dodecanol (Dodec) and n-Hexane (nHex) are chosen as commonly used candidates. Alternatively, phosphorous-based extractants like trioctylphosphine oxide (TOPO) can also be used for succinic acid extraction [122]. However, in order to keep the chemical nature of the extraction mechanism comparable, the investigation is limited to the family of tertiary amine extractants. The pH is included with two stages at three and five, respectively, as its importance is well known and thus gives a benchmark for the highest effect expected. The anion effect is tested by the type of anion (chloride, sulfate, and phosphate) and the total salt concentration in the range of zero to 1 M covering the range between the absence of salt and the conditions equivalent to the equimolar acidification by a strong inorganic acid.

3 Design of experiments

Before conducting the experiments, a suitable design plan must be selected. Depending on the desired outcome and the experimental practicability, different options are available. Figure 3.2 illustrates the most popular options for design plans. Two-level fractional factorial or general orthogonal array designs are well suited for screening experiments. The quadratic design plans possess the advantage of accounting for interactions and nonlinear relations between the tested factors, which enables model-based optimization. However, they are impractical to employ with discrete factors such as the type of solvent, extractant, or anion. The last group of randomly selected design plans such as Monte Carlo

Table 3.1.: Factor settings for screening experiments

		-	+	⊖	⊕
Temperature	[°C]	25	80		
Concentration SA	$[gL^{-1}]$	20	60		
Extractant		TOA	TEHA	THA	
Concentration extractant	$[molL_{aq}^{-1}]$	0.5	1		
Diluent		Oct	MIBK	Dodec	nHex
pH	[-]	3	5		
Anion		SO_4	PO_4	Cl	
Concentration electrolyte	$[molL_{aq}^{-1}]$	0.0	0.5	1.0	

or space-filling designs requires more experiments to obtain a satisfying coverage and even distribution of test points in the factorial space. These designs are only practical for experiments with a high degree of automation [104]. In conclusion, a general orthogonal design is selected for the screening experiments.

The design was optimized and evaluated with the R-based DoE package RcmdrLugin.DoE [133]. With the selected design, the 1728 possible combinations of factor levels are reduced to a set of 72 experiments. The factor settings were randomized and aggregated in order to minimize the influence of systematic errors. Each factor setting was tested in duplicate in the equilibrium experiments. Table 3.2 shows a segment of the experimental plan for factor levels in experiments 47-56. The complete plan with the factor settings and results is given in table 3.2.

4 Execution ot experiments

Materials: Succinic acid (>99 %) 1-Dodecanole (98 %) and TOA (95 %) were obtained from Alfa Aesar, USA. 1-Octanol (>99 %), MIBK (>99 %), and TEA (>99 %) were purchased from Merck KGaA, Germany. n-Hexane (98 %) and Sulfuric acid (95 %) and Sodium sulfate (99.4 %) was purchased from VWR, Germany. Sodium chloride (>99.5 %), and Di-potassium phosphate were supplied by Carl Roth, Germany, while Sodium hydroxide (98 %) and TEHA (>97 %) were

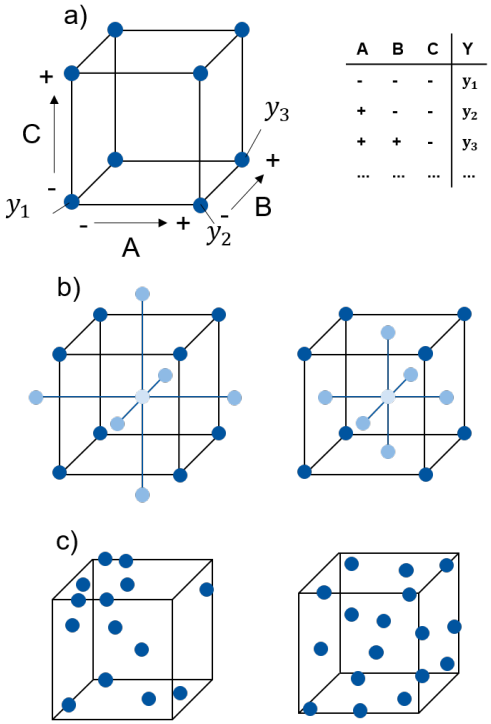

Figure 3.2.: Illustration of a design plan for three factors and the factor setting of each test point. a) Screening plan made up of orthogonal combinations of the minima and maxima of each factor. b) Quadratic design plans for polynomial optimization, central-composite design (left), and Box-Behnken design (right). c) Random approaches Monte Carlo (left) and space-filling design (right).

supplied by Sigma Aldrich, Germany.

Equilibrium measurements: Aqueous and organic stock solutions were prepared according to the settings in the design plan. The organic phase was preliminarily saturated with water to minimize changes in phase volume during extraction. 10 ml of the separately prepared aque-

Table 3.2.: Exemplary segment of the orthogonal design plan for experiments 47-56 with factor settings.

.	.	.	.	.	.	.	.	.
.	.	.	.	.	.	.	.	.
47	+	+	⊖	-	+	+	⊖	⊖
48	-	+	-	-	⊕	+	⊖	+
49	+	-	-	+	⊖	-	+	-
50	-	-	-	+	⊕	-	⊖	+
51	-	+	+	-	⊕	-	⊖	-
52	-	+	-	-	+	-	+	⊖
53	+	+	⊖	+	-	-	⊖	⊖
54	-	+	+	-	⊖	+	+	+
55	-	-	+	+	+	+	-	⊖
56	+	+	+	-	⊕	-	-	⊖
.	.	.	.	.	.	.	.	.
.	.	.	.	.	.	.	.	.

ous and organic phases were filled into PTFE tubes, sealed, and thoroughly mixed by shaking at 350 rpm in an HLC Thermomixer MHR 23 thermoshaker for 4 hours at the selected temperature. The samples were then centrifuged for 15 minutes at 2250 rpm to separate the phases. Next, the aqueous phase was extracted, and samples were drawn for concentration measurement by HPLC, and the density and pH were measured. Density was measured in a DAS 48 analyzer from Anton Paar KG and for pH measurement, a pH 1100L pH analyzer from VWR was used. After the removal of the aqueous phase, the solvent phase was extracted twice again by adding sodium hydroxide solution 10 mL 5 M. For both back extractions, 10 ml of 5 molar sodium hydroxide solution is added to the organic phase and the sample is shaken for two and twelve hours at 350 rpm in the thermoshaker. Phase separation and sample analysis were performed with the same procedure as extraction experiments. With the measured concentration and phase volumes, the

overall mass balance was calculated.

$$m_0 = m_{aq} + m_{BE} \tag{3.5}$$

$$m_{BE} = m_{BE,1} + m_{BE,2} \tag{3.6}$$

$$m_{err} = \frac{|m_0 - m_{BE} - m_{aq}|}{m_0} \tag{3.7}$$

The second back extraction step was considered the control to check whether all succinic acid was completely recovered from the solvent phase.

Analytical methods: The succinic acid concentration was determined by an Agilent 1100 series HPLC (Ratingen, Germany), equipped with an Organic Acid resin column (250 x 8 mm, CS Chromatography, Langerwehe, Germany). The succinic acid signal was recorded with a refractive index detector(RID) G1362A. 10 mM sulfuric acid solution 10 mM was used as eluent at 0.5 ml min^{-1} flow rate and a column temperature of 60 °C. All concentrations were determined in grams per liter of solution. The concentration of succinic acid in the aqueous phase was determined by HPLC Agilent 1100. Each HPLC sample was analyzed twice.

5 Statistical data evaluation

The data recorded for extraction yield and selectivity are given in table C.1. It was first evaluated by an analysis of variance (ANOVA) to identify factors with a statistically significant effect on the succinic acid extraction yield and on the selectivity toward anion co-extraction. Following the identification of factors with statistically significant effects, a multilinear regression is used to quantify the relevance of each factor in the results. The basis of the statistical analysis is the null hypothesis that says that the investigated factor has no effect on the results. If the null hypothesis is true, a deviation from the factor level would not cause any change in the results [104]. However, if a deviation in the results is

observed, the F-value and p-value determined by the ANOVA give the significance level of the observed effect. The principle is illustrated in fig. 3.3 An effect is considered statistically significant when the p-value

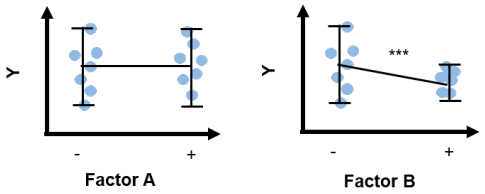

Figure 3.3.: Factor A does not have an effect on Y as results are evenly distributed independently of the factor level. For factor B a statistically significant trend is observed between the levels.

is < 0.05 [126]. With a p-value < 0.05 the probability of falsely verifying an effect while there is in fact none is below five percent. The codes for the significance level of an effect is given in table 3.3.

Table 3.3.: Significance codes

***	$0 < p \leq 0.001$
**	$0.001 < p \leq 0.01$
*	$0.01 < p \leq 0.05$
’	$0.05 < p \leq 0.1$
ns	$0.05 < p \leq 1$

3.2. Results and discussion

The experiments are evaluated with regard to the yield and selectivity of succinic acid extraction. The objective of ANOVA is to identify factors that show a statistically significant effect on the results. Identifying the factors with the largest impact on the results is beneficial in directing the focus of future studies on extraction behavior to the important factors. The maximum yields measured in the experiments are shown in fig. 3.4.

The highest yield of 76 % was observed for experiment no. 3 with THA and MIBK as solvents. The highest yield recorded for the commonly used TOA in the 1-octanol extraction system was 63 %. It should be noted that at the lower pH level, which was selected at 3, a major fraction but not all succinic acid was available for extraction. The higher pH probably explains the lower extraction yield compared to values in the range of 78 %-95 % which are reported in the literature [44].

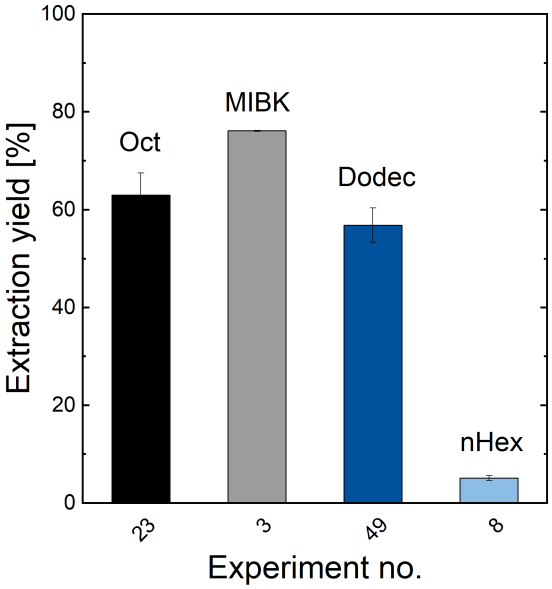

Figure 3.4.: Maximum yields observed in the DoE experiments

3.2.1. Main effects on yield

A statistically significant effect was observed on the yield of succinic acid extraction for pH, anion type, and extractant and diluent type (fig. 3.5).

On the other hand, no statistically significant effect was observed for the concentration of amine in the organic phase, the concentration of succinic acid in the aqueous phase, the concentration of ions in the aqueous phase, and the temperature (fig. 3.6). The orthogonal design plan also enables the investigation of effects within a group of one-factor factors, for example, the different types of anion present or the kind of extractant used.

Strong significance was found for the effect of the aqueous pH. This is in line with the known extraction mechanism for succinic acid extraction [134, 65, 108]. Only protonated succinic acid or hydrogen succinate with a proton is available for extraction; therefore, at pH 5 only a small fraction of the succinic acid can bind to the extractant. The significance level determined for the pH effect is the highest of all factors. This highlights the extraordinary importance of closely monitoring pH during the extraction of succinic acid. The results demonstrate that at an unfavorable pH, the extraction is easily limited by the equilibrium of succinic acid.

The limitation of the equilibrium of the aqueous pH cannot be overcome by the variation of other factors. The choice of the extractant has a significant effect on extractants with a steric hindrance like TEHA [65]. The difference between TOA and THA is small and not significant. Comparison of the results for extractant and diluent reveals a trend that more polar extractants or diluents tend to foster higher extraction yield. This trend was also reported before and is attributed to the ability of the diluent to stabilize the extractant-acid complex [62, 44]. The reduced yield observed with dodecanol is likely due to the formation of a third phase that occurs in the experiments. Active diluents with long alkyl chains and alkane extractants such as n-hexane show a poor solubility for the acid amine complex and tend to form a third phase [44, 57, 53]. Furthermore, the solubility of water in the organic phase is considered relevant as it also stabilizes the complex [135]. For both amine and extractant, the known effects were correctly identified by the screening method.

Interestingly, the type of anion has a significant effect on the extrac-

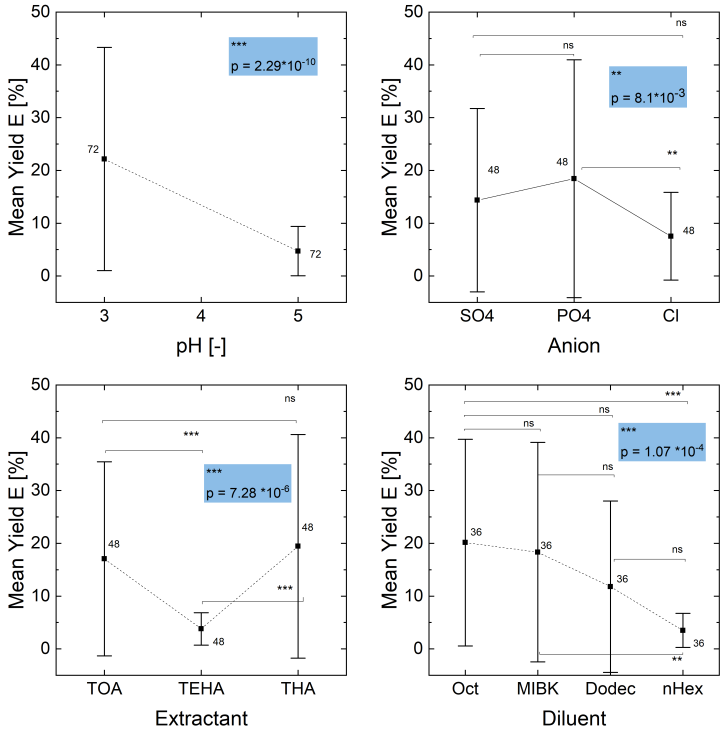

Figure 3.5.: pH (a), anion (b), extractant (c), and diluent (d) show a significant effect on the extraction yield.

tion yield as well. While there is no difference between sulfate and phosphate, chloride ions have a significant negative effect on the extraction yield. The negative impact of chloride ions was also reported by Kurzrock et al [44]. It may be attributed to the different charge densities and ion sizes. Sulfate is present mainly as bivalent SO_4^{2-} at the investigated pH and phosphate, although present in its monovalent $H_2PO_4^-$ form, is a larger ion compared to chloride. Consequently, the small chlo-

ride ion may bind more easily to a protonated amine and form stable ion-amine complexes. Therefore, the number of chloride ions in the aqueous phase should be limited if reactive extraction is employed to recover succinic acid from aqueous solutions. This leads to two conclusions: First, the use of hydrochloric acid for acidification before extraction should be avoided if amine-based extractants are to be used. Second, the use of chlorine-based nutrient salts during succinic acid fermentation should be minimized or preferably completely avoided. Phosphate- or sulfate-based nitrogen sources appear to be the better choice in this case. Especially when reactive extraction is intended for *in-situ* product removal during the fermentation [57, 132, 136].

The extractant concentration and the initial concentration of succinic acid do not reveal a significant effect on the yield fig. 3.6. This confirms that the experiments were conducted below the capacity limit, just as intended. Exceeding the stochiometric ratio of 1:1 succinic acid per amine causes the formation of acid-base complexes of higher order, like 2:1 [64].

Surprisingly, the total concentration of ions only has a small effect on the yield at the level of 0.5 M. By increasing the ion concentration to 1 M the yield increases simultaneously. This effect is likely caused by salting-out phenomena at high ion concentrations. The characteristics of the salting-out effect could also explain the smaller effect of sulfate and phosphate ions on extraction yield, as they exhibit a stronger salting-out behavior compared to chloride ions [137]. However, the presence of anions always reduced the maximum extraction yield fig. 3.7.

In contrast to previous studies, no significant effect of temperature is observed [100]. According to other reports[125, 112], we conclude that the effect of temperature is negligible for the extraction of succinic acid by tertiary amines. The results of Sprakel et al [138]. confirm the limited effect of temperature on the extraction equilibrium, as poor performance was found for temperature-swing extraction processes.

The identification of factors with insignificant effects and the differentiation from factors with significant effects allows one to focus on the important parameters that actually have an impact on the results in

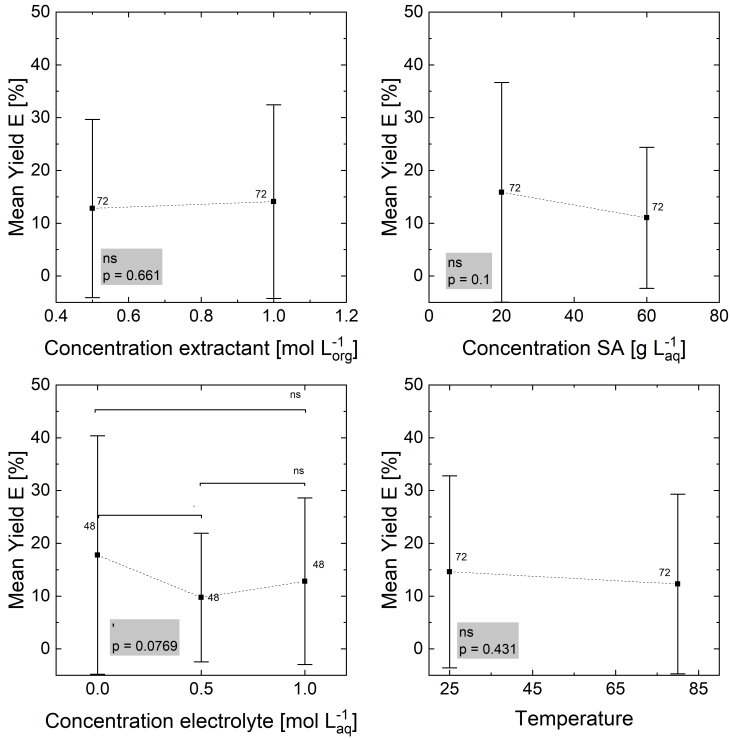

Figure 3.6.: Concentration of extractant (a), succinic acid (b), electrolyte (c), and temperature (d) have no significant effects on SA extraction yield. Siginificance code for p = 0 '***' 0.001 '**' 0.01 '*' 0.05 '.' 0.1 ' ' 1

future studies. As long as overload conditions are avoided, the results of extraction experiments are unlikely to be affected by the concentration of amines in the organic or succinic acids in the aqueous phase. The low significance of the effect of electrolyte concentrations can be partially explained by salting-out phenomena.

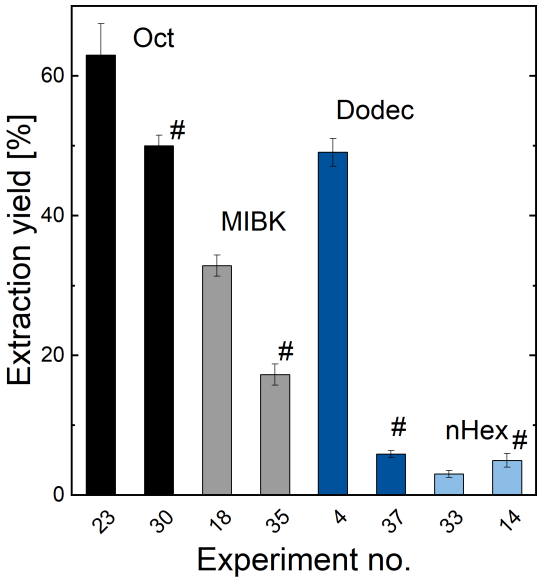

Figure 3.7.: The presence of anions reduces the achievable extraction yield for all active diluents. # denotes experiments with similar settings as the reference but with additional anions.

3.2.2. Main effects on selectivity

Maximizing extraction yield is an obvious objective when designing reactive extraction systems. But considering the latter application a selective separation is mostly always desired, too. Especially when the intended application is for product recovery in the field of biotechnological downstream processing. Although the coextraction of anions with a carboxylic acid is a known phenomenon, knowledge about the underlying factors that actually influence the selectivity is limited. Identification of these factors enables the targeted optimization of reactive extraction. Therefore, the results from extraction experiments containing 0.5 M or

1 M electrolytes were analyzed for selectivity as well. ANOVA revealed that the extractant, the diluent, the concentration of amines in the organic phase, the temperature, and the type of anion present in the aqueous phase do not show a statistically significant effect on the selectivity of succinic acid extraction fig. 3.8. There is a minor indication that selectivity might improve with MIBK compared to n-hexane, but significance is at the upper limit of becoming insignificant fig. 3.8 (c). However, since the highest yield for succinic acid extraction was obtained with MIBK, it could be a possible alternative to the commonly used TOA in the 1-octanol extraction system. Interestingly, the type of anion does not show any significance for the selectivity, as expected from the results for the yield fig. 3.5. This can be caused by the lower number of data points available for the evaluation of the selectivity. The design plan also considers experiments with no electrolyte concentration, which cannot be evaluated for selectivity. In contrast to the 144 data points from 72 factorial combinations available for the evaluation of the yield, only 94 data points are available for the evaluation of the selectivity. This may not provide a sufficient data set to differentiate the effect of the ions species on the selectivity. Comparing only results from extraction experiments with elevated ionic strength against each other has the drawback that only extraction experiments with already compromised extraction performance are considered. This can further mask the anion-specific effect. The striking finding for selectivity is that both the extractant and the diluent do not show a significant effect fig. 3.8 (a) and (b). As a consequence, the feasible improvement of the extraction selectivity by extractant and solvent optimization is likely limited by the number of mong extractants of similar chemical nature. In this study, only tertiary amines were considered to keep the extraction mechanism comparable. It should be taken into account that this finding cannot be generalized to extractions that differ in their extraction chemistry. For example, phosphine-based extractants such as trioctylphosphine oxide reportedly showed a much different extraction behavior and are a promising class of extractants for recovering carboxylic acid from solutions containing large amounts of inorganic anions [122, **?**].

For three of the investigated factors, a significant effect is identified on the selectivity of extraction. The highest level of significance was found for the concentration of succinic acid fig. 3.9 (c), followed by the ion concentration fig. 3.9 (b), and the pH fig. 3.9 (a). The effect of the pH appears consistent with the findings for the yield, as at lower pH a larger fraction of the succinic acid is available for extraction.

The significant effects identified for both the electrolyte concentration and the succinic acid concentration give an indication of where optimization efforts focused on selectivity should start. The high significance of the effect caused by pH and concentration also requires a careful determination of these measures when conducting extraction experiments. Any inaccuracy in the experimental execution or measurement of these parameters will likely cause erroneous results.

The differentiation between factors with and without a statistically significant effect allows us to focus on important factors for future optimization efforts. Factors that show only insignificant effects are unlikely to provide a major potential for the improvement of yield or selectivity. However, a statistically significant effect does not require that the factor have practical relevance.

3.2.3. Identification of main impact factors

An indicator of practical relevance is the t-value obtained from a multilinear regression. The t-value can be interpreted as a polynomial coefficient for each factor. A high t-value causes a high sensitivity of the result toward changes in the factor level. As a consequence, high t values indicate high practical relevance of the respective factor. The identification of factors with statistically significant effects followed by ranking the factors considered by their t value identifies the main factors that actually have a significant impact on the results.

The absolute t-values obtained from the regression are presented in fig. 3.10. It is obvious that factors with highly significant effects are prone to have a relevant impact on the results, as well. However, a significant effect does not require a relevant impact and *vie versa*. This

is the case for the electrolyte concentration with regard to yield and the extractant with regard to selectivity. In order to draw solid conclusions, both statistical measures should be taken into account.

With regard to the yield fig. 3.10 (a) an outstanding relevance of the aqueous pH is confirmed [64, 111]. Next, the type of diluent and extractant shows a relevant impact and a significant effect. This means that, in order to good extraction yields, controlling the aqueous pH is a mandatory task, and selecting the right extractant and diluent can improve the overall extraction performance. The presence of electrolytes has a minor, but non-negligible, impact. As indicated by the low significance, no practical relevance of the temperature was found. The practical consequence thereof is that precise control and measurements of the aqueous pH are crucial in order to get meaningful and reliable results in succinic acid extraction experiments. However, controlling the temperature is not as critical, and due to the low significance and relevance of its effect may allow extrapolation of the results determined at one temperature to other temperatures within the tested temperature range. As a consequence, the much stronger dependence of the extraction yield on the pH value of the aqueous phase compared to the temperature suggests that the stripping of succinic acid from the extractant by pH-swing is expected to work much better than stripping by temperature swing. A study by Sprakel et al. confirms that solvent regeneration by temperature swing alone was insufficient and the addition of an anti-solvent was required to achieve satisfactory removal of succinic acid from the extractant [138].

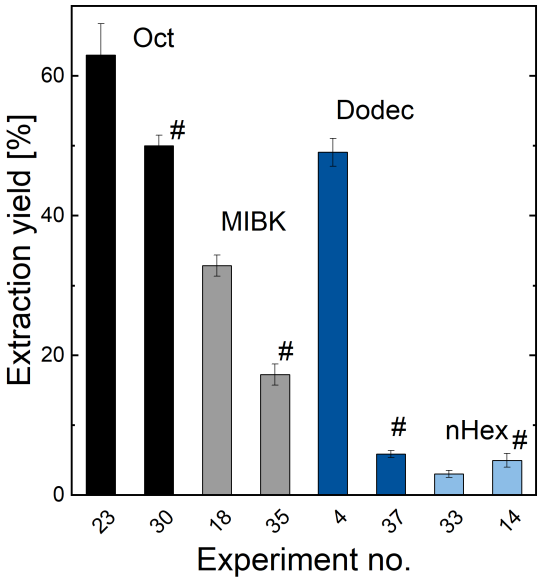

Figure 3.10.: Ranking of the factors according to the absolute t-values for yield (a) and selectivity (b).

Although the selection of extractant and diluent provides an optimization parameter with feasible potential for improvements in the extraction yield, the viable improvements on the selectivity appear limited. Extraction selectivity is mainly affected by the concentration of succinic acid and the electrolyte in the aqueous phase.

The high significance and relevance of the concentration and the ratio of succinic acid and electrolyte concentration is an indication that the co-extraction of inorganic anions also follows a mass-action relationship. In addition to the commonly used mass action relationship eq. (2.25) used to describe carboxylic acid extraction with tertiary amines[111, 64] the competing mass-action relationship for mineral acid extraction must

be taken into account.

Eyal and Canari suggested that mineral acid extraction by amine-based extractants is caused by proton transfer to the amine:

$$\mathrm{TAM} + \mathrm{H^+} \overset{\mathrm{pK}_n}{\rightleftharpoons} \mathrm{H{-}TAM^+}, \tag{3.8}$$

followed by an ionic complexation of the mineral acid anion:[65]

$$\mathrm{H{-}TAM^+} + \mathrm{A^-} \overset{\mathrm{K_{A^-,Ex}}}{\rightleftharpoons} [\mathrm{H{-}TAM^+{-}A^-}] \tag{3.9}$$

Thereof, the mass-action relationship for anion extraction by ion-pair formation with the protonated fraction of the amine

$$\mathrm{K_{A^-,Ex}} = \frac{[\mathrm{H{-}TAM^+{-}A^-}]}{\mathrm{H{-}TAM^+} \cdot \mathrm{A^-}}, \tag{3.10}$$

follows. The protonation of the amine is pH dependent and amine protonation eq. (3.8) also follows a dissociation equilibrium

$$\mathrm{K}_n = \frac{\mathrm{H{-}TAM^+}}{\mathrm{TAM} \cdot \mathrm{H^+}}. \tag{3.11}$$

The fraction of protonated amine β is calculated as

$$\beta = \frac{\mathrm{H{-}TAM^+}}{\mathrm{TAM_{tot}}} \tag{3.12}$$

$$= \frac{\mathrm{H{-}TAM^+}}{\mathrm{H{-}TAM^+} + \mathrm{TAM}}, \tag{3.13}$$

$$\tag{3.14}$$

which results with eq. (3.11) in

$$\beta = \frac{\mathrm{K}_n \cdot \mathrm{H^+}}{\mathrm{K}_n \cdot \mathrm{H^+} + 1}. \tag{3.15}$$

Inserting eq. (3.13) into eq. (3.10) yields the mass-action relationship

for anion extraction with regard to anion concentration, pH, and total amine concentration.

$$K_{A^-,Ex} = \frac{[H{-}TAM^+ {-}A^-]}{\beta \cdot TAM_{tot} \cdot A^-} \tag{3.16}$$

The proposed mass-action relationship can explain the trend observed in the experiments but is based on an idealized model of the extraction equilibrium. Especially the assumption of 1:1 stochiometry between amine and succinic acid only holds for conditions where the total succinic acid to amine ratio is below that value and no overloading of the amine occurs. At a higher acid-to-amine ratio, the stoichiometry of the carboxylic acid-amine interaction becomes more complex as the formation of 1:2 and 2:1 complexes can occur [111]. But especially with active diluents, the 1:1 complex is the most prominent and thus the most relevant one [64]. A rigorous quantitative description of the extraction equilibrium requires more detailed considerations of the exact stoichiometry, but the simplified model can already be used to derive some practical recommendations. The identified mass-action relationship has three consequences for the application of reactive extraction for the separation of succinic acid from ion-containing aqueous solutions. First, anion extraction requires prior protonation of the amine. As protonation of the amine depends on the amine basicity and the aqueous pH it is expected that the co-extraction of inorganic anions is more severe at a low aqueous pH. For this reason, the often found recommendation that reactive extraction requires acidification of the aqueous solution to low pH[113, 139] should state more precisely that reactive extraction requires the pH of the aqueous phase to be as low as possible in order to have as much protonated succinic acid as possible, while the pH of the aqueous phase must also be as high as possible to avoid protonation of the extractant. Both limits would frame a pH window where efficient operation of the reactive extraction of succinic acid is possible. Second, high concentrations of inorganic anions should be avoided in the feed of the extraction step, as they would inevitably compromise the feasible ex-

traction performance. Therefore, it is recommended to avoid the direct addition of inorganic acids for acidification prior to reactive extraction and preferentially uses ion exchange processes[108] or electrochemical methods[42, 140] to adjust the pH of the aqueous phase. Third, the selection of the diluent enables adjustment of the protonation propensity of the extractant. Active diluents such as 1-octanol or 1-decanol promote proton transfer to the amine [134]. Although this feature yields good performance in artificial systems[44, 141, 142] the application of reactive extraction to real fermentation broth requires diluents that are less prone to promote proton transfer.

3.3. Conclusion

The presented DoE method enabled rational screening and identification of main factors with a relevant impact on the yield and selectivity of a reactive extraction that features tertiary amines for the separation of succinic acid from aqueous solutions in the presence of inorganic anions. Aqueous pH was identified as the most significant and relevant factor for the extraction yield. The factor ranking obtained from the screening experiments revealed that a limitation caused by the aqueous pH cannot be compensated by other factors. For this reason, careful control and determination of the aqueous pH become crucial aspects when conducting reactive extraction experiments. Minor errors in aqueous pH will probably outweigh the effect caused by other factors. Likewise, the process performance of a reactive extraction used to recover succinic acid will be readily compromised by improper control of the aqueous pH value. Beyond that, the strong impact of pH indicates that pH-swing methods are well suited for stripping succinic acid from the extractant to regenerate the solvent.

The notable sensitivity of the selectivity toward concentration levels is interpreted as the result of a mass-action relationship describing the co-extraction of anions by tertiary amines at low aqueous pH. An implication of the derived mass-action relationship is that efficient reactive

extraction of succinic acid is expected within a pH range framed by the succinic acid dissociation equilibrium and the protonation of the extractant. In accordance with previous studies, chloride ions were found to have the most negative impact on extraction yield. Furthermore, a high concentration of any anion had a negative impact on the extraction yield. For this reason, anion-free methods are required for the acidification of pH-neutral fermentation broth prior to reactive extraction.

Electrochemical pH-swing processes are potential solutions for that purpose. The electrochemical pH-shift induced by water electrolysis enables acidification without adding more anions to the system. For that reason, electrochemical pH control is regarded as a promising tool for enabling efficient reactive extraction processes for succinic acid separation. The next chapter demonstrates the proof-of-concept for the electrochemical pH-swing extraction of succinic acid.

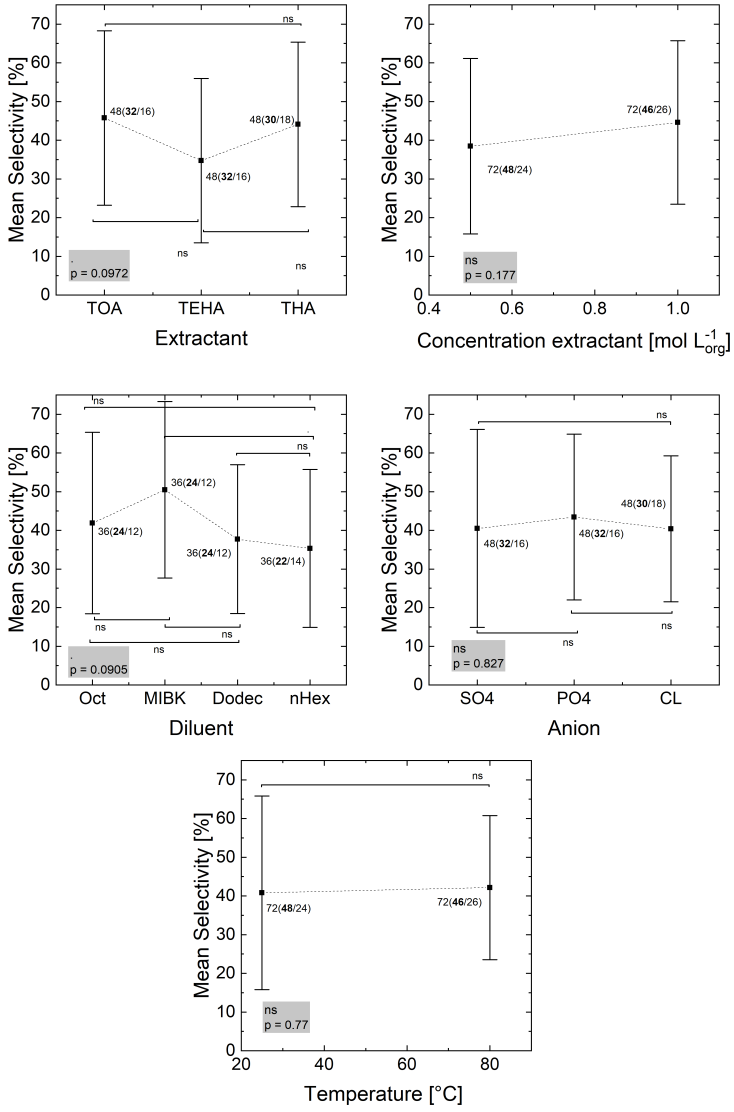

Figure 3.8.: Choice of extractant (a), extractant concentration (b), diluent (c), anion species (d), and temperature do not show a significant effect on extraction selectivity

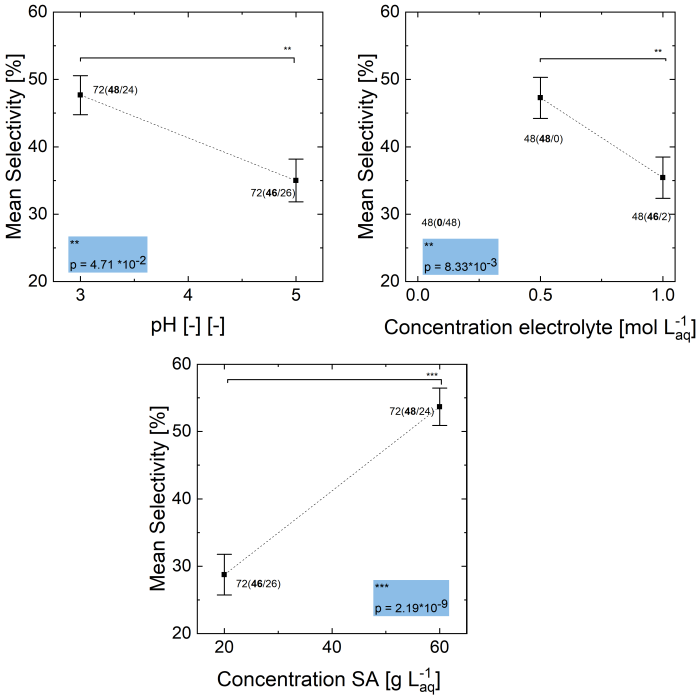

Figure 3.9.: pH (a), the concentration of the electrolyte (b), and the concentration of succinic acid (c) show a significant effect on extraction selectivity

4. Electrochemical pH-swing separation of succinic acid

[‡] Chapter 3 highlighted the importance of the aqueous pH value for the reactive extraction of succinic acid. The experimental results showed that in order to obtain high extraction yields acidification without the addition of further anions is required. In this chapter, the concept of electrochemical pH-swing separation is developed and demonstrated as a proof-of-concept experimentally with the example of succinic acid.

The newly developed separation process enables the recovery of crystalline succinic acid from diluted aqueous solutions while overcoming the need for acid and base addition so far required for controlling the pH and thus eliminating the issue of equimolar production of salt waste with the processed succinic acid [19, 63]. The electrochemically operated pH-shift is coupled with separation steps and thus produces the required acid and base by integrated water electrolysis. Thereby the suggested process allows the operation of the fermentation at optimal pH for maximal space-time yield. In the long-term perspective, electrochemical unit operations provide a way to utilize electricity for the purification of carboxylic acids.

4.1. Motivation

As discussed in section 2.3, maintaining thermodynamically favorable conditions for product export is crucial for maintaining a well-performing succinic acid fermentation. However, the excessive use of

[‡]Parts of this chapter have been published in Gausmann et al. "Recovery of succinic acid by integrated multi-phase electrochemical pH-shift extraction and crystallization" (2020), Separation and Purification Technology

base and acid in the downstream processing of succinic acid compromises the competitiveness of the bio-based production route [143]. The reactive extraction of succinic acid is considered a favorable separation method but also requires acidification before the extraction step if the fermentation is operated at near neutral pH [54, 61].

Bio-electrochemistry can overcome these difficulties by merging traditional fermentation with electrochemical methods [144]. Promising studies were conducted for the electrolytic extraction of fatty acids whereby the pH of the fermentation was controlled without additional base [38]. Also electrolytic extraction of short-chain carboxylic acids with subsequent esterification showed the potential to obtain bio-based fine chemicals by bio-electrochemical methods [37]. Direct electro-membrane extraction was also demonstrated for succinic acid production with promising results, yet process performance was limited by membrane-fouling [40].

In the following, an electrochemically driven pH-shift separation technique for the recovery of crystalline succinic acid from initially pH-neutral aqueous solution by a sequence of electrochemically operated extraction, back-extraction, and crystallization steps is presented. The separation process is founded on three main functionalities, spatially separated generation of pH gradient by water electrolysis and ion exchange fig. 4.9(a) [45], reactive extraction / back-extraction fig. 4.9(b), and fig. 4.9(c) pH-dependent solubility of succinic acid species and thereby pH-shift crystallization [21].

In order to close the electric circuit, ion transport between the anode and cathode chamber must be possible. In the most frequently employed setup, the ions transferred are either OH^- in alkaline electrolysis or H^+ in acidic proton exchange electrolysis [45]. In contrast, when the electric circuit is closed by the transport of ions like $K^+, Na^+, {SO_4}^{2-}, {PO_4}^{3-}, Cl^-$, the formed H^+ and OH^- ions remain in the respective compartment and thus alter the pH value of the solution near the electrode. The production of chlorine and sodium hydroxide solution from sodium chloride via chlorine-alkali electrolysis is a well-known example of a process featuring this principle [145].

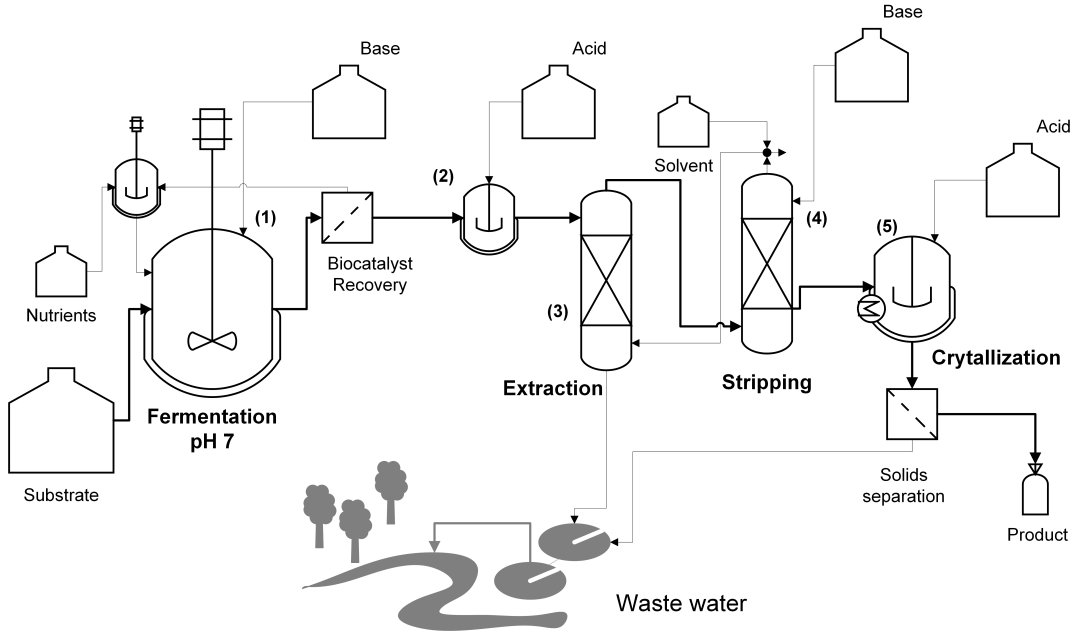

Figure 4.1.: Simplified flow-sheet of a pH-swing reactive extraction process for succinic acid separation. (1) Fermentation at neutral pH, (2) acidification of fermentation broth to low pH < pK_{a1}, (3) reactive extraction, (4) stripping (back-extraction) of succinic acid from the solvent by alkaline pH-shift and (5) acidification and cooling crystallization.

The electrochemical pH-swing extraction utilizes the H^+ and OH^- to trigger the reversible binding of the succinic acid with the tertiary amine as presented in fig. 2.7 and fig. 2.6. The efficiency of the electrochemically triggered pH-swing separation of succinic acid is defined as the molar ratio of separated succinic acid Δn_c and the number of ions (H^+ / OH^-) produced in the electrolysis as calculated with faraday's law eq. (2.12).

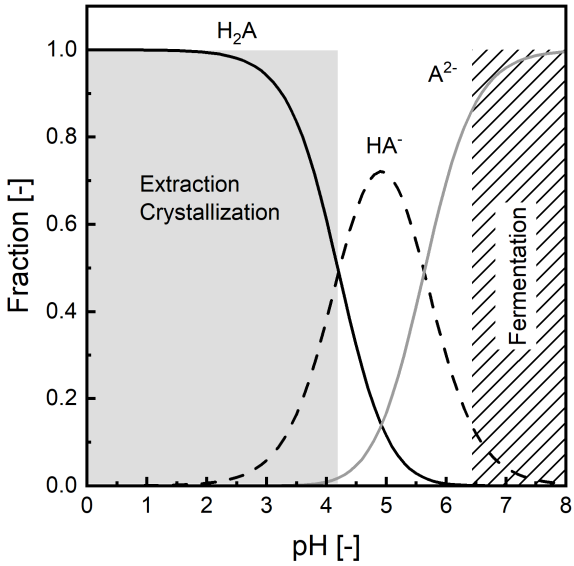

Figure 4.2.: Region of operational pH values for succinic acid fermentation and separation

H^+ and OH^- produced in the electrolytic half-cell reaction act on the aqueous pH equilibrium and shift the dissociation state of the succinic acid fig. 4.2. This enables the conversion of succinic acid from the succinate form present at neutral pH to the protonated

succinic acid form which is then available for extraction [54, 118]. In addition, the protonated form of succinic acid has a lower solubility than the ionic species, which enables electrochemically induced crystallization of the acid [21, 146]. The principles of pH-swing reactive extraction and back-extraction are described in detail in section 2.4.

4.2. Materials and Methods

In order to provide an experimental proof of principle, extraction, back-extraction and crystallization of succinic acid were investigated separately based on artificial aqueous solution.

4.2.1. Chemicals & Materials

Succinic acid (99 %) and tri-n-octylamine (TOA) (95 %) were supplied by ThermoFisher, Kandel, Germany. Sodium hydroxide (NaOH, 97 %) and di-sodiumsuccinate (for synthesis) were provided by MERCK, Darmstadt, Germany. Sodium sulfate (Na2SO4, 99 %) was obtained from Sigma Aldrich, Darmstadt, Germany. An EA-PS8360-10T power source from Elektro-Automatik GmbH & Co. KG, Viersen, Germany was used for electrolysis. In reactive extraction experiments anode and cathode chamber were separated by a porous glass membrane obtained from Robu Glasfilter, Hattert, Germany, measuring 25mm in diameter and 3mm in thickness with porosity grade 4 (10-16 µm). In order to prevent anion migration in back-extraction and crystallization, a cation exchange membrane Fumapem 14100 provided by Fumatec, Bietigheim-Bissingen, Germany was used as separator for the electrolysis chambers in these experiments. Platinum coated titanium anodes and ruthenium mixed metal oxide coated titanium anodes were provided by MAGNETO special Anodes B.V., Schiedam, Netherlands. Stripes of nickel sheet with 99 % metal purity were used as cathodes. The active side of all electrodes measured 25 x 40 mm. Nickel electrodes were selected because of their recent successful employment for electrochemical

production of carboxylic acids [69]. Ruthenium oxide and platinum are known highly active catalysts for the OER, whereas ruthenium oxide exhibits high catalytic activity and platinum is considered to be more stable catalyst compared to ruthenium oxide [147]. Because TOA is able to extract ruthenium from acidic aqueous solutions[148] Platinum was selected for extraction and back-extraction experiments and the application of ruthenium oxide electrodes was limited to crystallization.

4.2.2. Analytical Procedure

Samples were drawn from the aqueous phases of the anode and the cathode chamber, filtered by a syringe filter with pore size of 20 µm supplied by Macherey Nagel, Düren, Germany. Concentrations of succinic acid were determined by Agilent 1100 series HPLC, equipped with an organic acid resin column (250 mm × 8 mm, LC-OrganicAcid-CS-E, CS Chromatography) operated at 40 °C. A diode-array detector (DAD) G1315A was used to record the succinic acid signal at 210 nm wavelength. 2.5 mM aqueous sulphuric acid at a flow rate of 0.7 mL min^{-1} was used as eluent and sample injection volume of 5 µL was selected. pH was measured with a VWR pHenomenal pH1100L pH-meter. Error bars in the figures indicate analytical accuracy. Crystal size distributions were measured with the Camsizer X2 by Retsch technology using the free fall method. Pictures of crystal morphology were taken with an OLYMPUS DP25 microscope.

4.2.3. Experimental Procedure

Extraction: Electrochemically induced extraction was conducted in batch-mode electrolysis. The initial experiment (exp. 1) was repeated with similar settings in exp. 2. In both experiments, electrolysis was run for 6h under amperostatic conditions. A nickel cathode (-) was paired with a platinized titanium anode (+), both having an active electrode surface of approximately 10 cm^2. The anode and cathode chambers were separated by a porous glass membrane. An aqueous

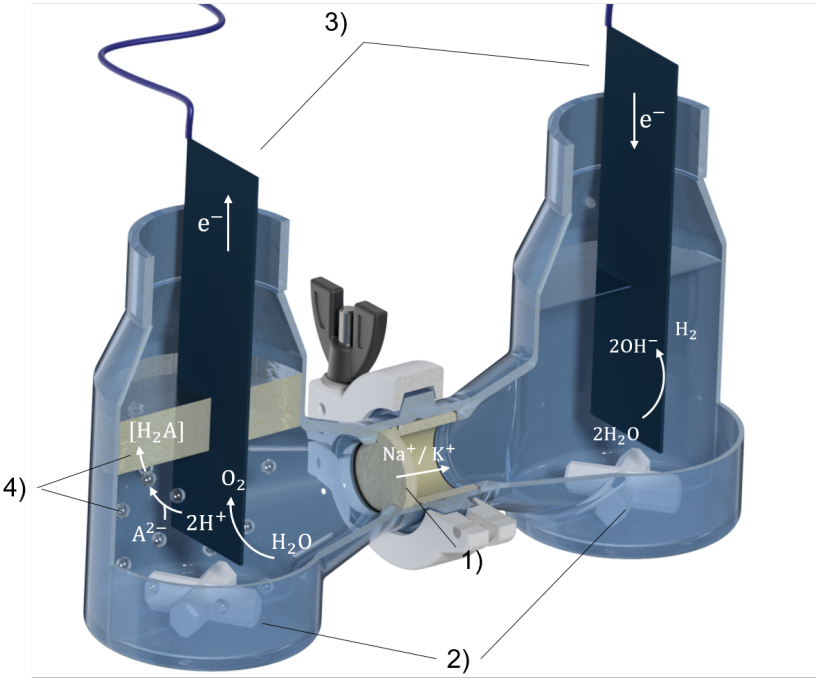

Figure 4.3.: Experimental two electrode setup used for the pH-swing separation experiments comprised by H-cell type glasses connected *via* an ion conducting separator (1). (2) magnetic stirring bars, (3) electrodes and (4) dispersed extractant.

solution containing approximately $47\,\mathrm{gL^{-1}}$ of succinic acid and 0.4 M Na_2SO_4 as background electrolyte was prepared. The initial pH was adjusted to pH 7(1) by the addition of sodium hydroxide. 115 mL of this solution were filled into the anode chamber and 155 mL to the cathode chamber. 40 mL of an organic solvent containing 50 w/w% of 1-Octanol and 50 w/w% TOA were added as extractant to the anode chamber. Prior to the electrochemically induced extraction, phases were equilibrated by rigorous stirring for 30 min. The temperature was held at 25 °C by a water bath. Electrochemically induced extraction

was carried out under amperostatic operation at a current of 0.3 A and thorough stirring throughout the 6 h experiment. Every hour pH was measured and a sample was drawn from each chamber and analyzed by HPLC. Subsequent to electrolysis, succinic acid was back extracted from the organic phase by the addition of 3.7 g solid sodium hydroxide. After back-extraction, concentration in the aqueous phase was determined by HPLC in order to close the mass balance and quantify any loss of succinic acid.

Back-Extraction: Electrochemically induced back-extraction was demonstrated in exp. 3 and repeated with similar settings in exp. 4. For back-extraction, a ruthenium oxide anode was paired with a nickel cathode, while back-extraction was conducted in the cathode chamber. Both chambers were separated by a cation exchange membrane, which was exchanged after each run. Again, an aqueous solution initially containing approximately $50\,\mathrm{g L^{-1}}$ succinic acid and 0.4 M Na_2SO_4 as background electrolyte was prepared as catholyte. 115 mL of this aqueous electrolyte and 40 mL organic solvent containing 50 w/w% of 1-Octanol and 50 w/w% of TOA. Both phases were thoroughly stirred at 25 °C overnight to establish extraction equilibrium. Afterward, the mixture was filled into the cathode chamber, and 155 mL aqueous electrolyte containing 0.4 M Na_2SO_4 was filled into the anode chamber. The same operating temperature, electrical current load, and sampling procedure, as stated for extraction experiments, were used. Wetting of the nickel cathode by the organic solvent was prevented by stirring thoroughly.

Crystallization: Electrochemical pH-shift crystallization experiments (exp. 5 and exp. 6) were conducted using a ruthenium-coated titanium anode paired with a nickel cathode. The anode and cathode chambers were separated by a cation exchange membrane. The cathode chamber was filled with 0.5 M of Na_2SO_4 as background electrolyte. The anolyte additionally contained $125\,\mathrm{g L^{-1}}$ succinic acid and pH was adjusted by sodium hydroxide addition to an initial value of 4.15. Both

cells were tempered to 20 °C and stirred by magnetic stirring bars. Electrolysis was run under amperostatic conditions at 0.5 A for the duration of the experiment. Every thirty minutes a sample was taken from each chamber. The pH was measured at the beginning and at the end of the experiments. The course of the pH was calculated assuming the H^+ production correlates linearly with the applied current. After terminating the electrochemically induced crystallization, the white crystalline product was filtered by a paper filter with retention size 8-12 µm, dried and the crystal size distribution was determined by the Camsizer X2. Crystal purity was determined by dissolving defined amounts of dried crystals in bi-distilled water and comparing the concentration determined by HPLC with the initially weighed portion.

Simultaneous Crystallization and Back-Extraction: Exp. 7 and 8 demonstrate the coupling of back-extraction and simultaneous crystallization. The anolyte was prepared by adding di-sodiumsuccinate and succinic acid at a molar ratio of 2:1 to a 0.4 M Na_2SO_4 electrolyte, which yielded a succinic acid solution with an initial pH of 4.11 and a total succinate concentration of approximately 120 gL^{-1}. In order to demonstrate that an increase of concentration can be achieved by electrochemical back-extraction, an organic solvent loaded with succinic acid was prepared by equilibrating an aqueous solution containing 0.4 M Na_2SO_4 and 50 gL^{-1} succinic acid overnight. For back-extraction, a new aqueous catholyte was prepared from Na_2SO_4 (0.4 M) and succinic acid as well as di-sodiumsuccinate at a molar ratio of 1:1 yielding a solution with approximately 50 gL^{-1} total succinic acid at pH 4.54. 20 mL of the loaded solvent were added to 96 mL of this freshly prepared aqueous catholyte and electrolysis was started. During the experiment, both cells were tempered to 20 °C and stirred by magnetic stirring bars. The current was kept constant at 0.3 A for the duration of the experiment. Every hour a sample was taken from each chamber and the pH was measured. The obtained crystals were filtered, dried, and purity was assessed as stated before.

4.3. Results and Discussion

4.3.1. Extraction

Figure 4.4 shows the concentration of succinic acid and the pH value in the aqueous phase over the electrical charge introduced to the system in two experimental runs. With increasing electrical charge, the initial loading of $47\,gL^{-1}$ succinic acid in the anode chamber decreases linearly to $33\,gL^{-1}$. This decrease is due to the advancing extraction of succinic acid into the organic phase. The extraction rate is independent of the initial succinic acid concentration and initial pH. Besides, it correlates well to the linear turnover of protons produced by electrolysis, which can be calculated from Faraday's law eq. (2.12). The Faraday efficiency for both runs varied between 31-36 % under the assumption that two protons were needed for succinic acid protonation (z=2). The succinic acid concentration in the cathode chamber slightly decreased, likely caused by the migration of ionic succinate species to the anode chamber. Extraction of succinic acid started at bulk pH above the pK_{a1} of succinic acid.

Current literature states that extraction of succinic acid was only observed for initial pH below the pK_{a1} [113, 149, 22]. Figure 4.4 depicts that electrochemically induced extraction starts instantaneously after applying an electrical current. Thus, acidification of the bulk phase to pH below pK_{a1} is not required for extraction. Here, two explanations seem plausible: First, extraction is initiated by local pH gradients around the anode that cause sufficient protonation and enable subsequent extraction. Second, by continuously providing protons and shifting the acid-base equilibrium, a fraction of succinic acid is always present in its protonated form and thus available for extraction. Independent of the exact mechanism causing extraction in pH ranges previously not reported we want to highlight the fact that electrochemically induced extraction started at neutral pH. As no prior acidification was necessary, this approach would enable the direct separation of

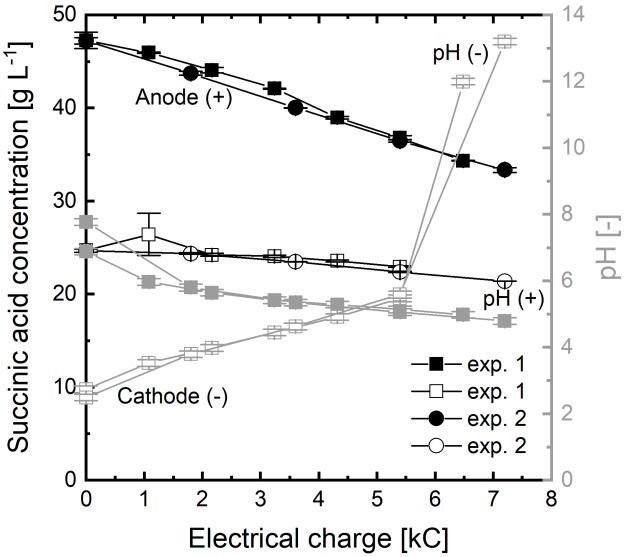

Figure 4.4.: Extraction of succinic acid and course of anolyte pH over electrical charge in exp. 1 (■, □) and exp. 2 (●, ○) for anode (+) and cathode (-) chamber. Error bars indicate analytical accuracy. Lines are only visual help.

succinic acid from a pH-neutral aqueous solution like fermentation broth. Subsequent to the electrochemical extraction, the organic phase was back-extracted, and succinic acid concentration was measured to close the mass balance. Mass balance error was determined at −3 % in exp. 1 and −4.9 % in exp. 2. The missing succinic acid is likely caused by handling issues with the viscous organic phase. The absence of any additional peaks in the HPLC data fig. E.1 and fig. E.2 suggests that no significant electrochemical decomposition of succinic acid occurred [140].

4.3.2. Back-extraction

Figure 4.5 shows a linear increase in succinic acid concentration in the cathode chamber during back-extraction, while pH remains between 5 and 6. From initially 23-25 gL^{-1} after equilibration, the succinic acid concentration increases to 37.29 gL^{-1}in exp. 4 and 34.23 gL^{-1}in exp. 3. Again, the linear trend of concentration change suggests that back-extraction is driven by the OH^--ions produced by water electrolysis. Assuming that a double negative charge of (z = 2) is required for splitting the succinic acid-TOA complex, the Faraday efficiency of electrochemically driven back-extraction is calculated to be 22.2 % in exp. 3 and 23.6 % in exp. 4. The assumption that two electrons are required per mole of succinic acid for back-extraction is supported when taking into account the acid species present at the respective pH. At a pH above 5 the fraction of SA_2^- increases. Therefore, succinic acid back-extracted from TOA must be stripped of its two protons.

For extraction and back-extraction the observed change in concentration can be well explained by the number of protons respectively hydroxide ions produced by water electrolysis during the experiment. Because immediate extraction was observed at pH values compatible conditions found in succinic acid fermentation[22, 48] applicability of this concept for *in situ* separation of succinic acid from fermentation broth should be investigated. Also by overcoming the need of adjusting bulk pH prior to extraction, the consumption of inorganic acid and thereby salt formation during the recovery of succinic acid could be reduced significantly [22].

4.3.3. Crystallization

The final objective in the downstream process is to recover succinic acid in a solid crystalline state[150, 119], which can be achieved by electrochemically induced crystallization [146]. Figure 4.6 displays the course of succinic acid concentration during electrochemically induced crystal-

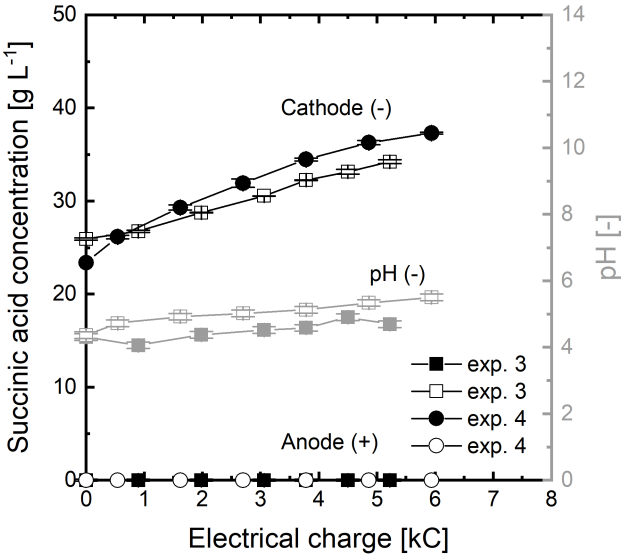

Figure 4.5.: Back extraction of succinic acid from loaded TOA and course of catholyte pH over electrical charge supplied during electrolysis in exp. 3 (■, □) and exp. 4 (●, ○). Lines are only visual help.

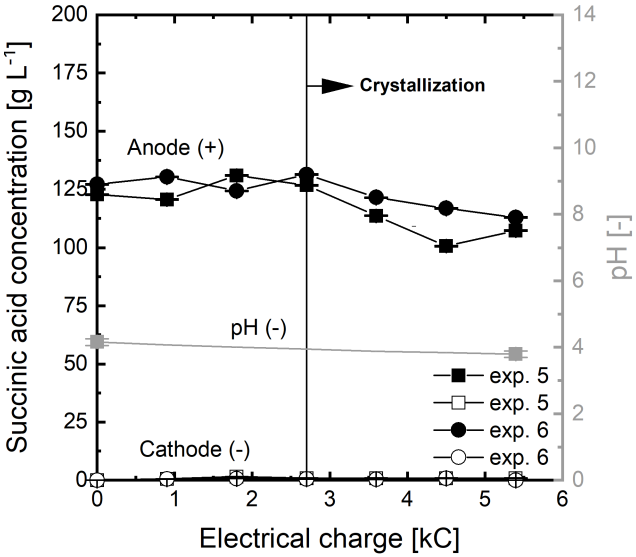

Figure 4.6.: Succinic acid concentration in the anode and cathode chamber in exp. 5 and exp. 6. Initial and end pH were measured. Lines are only visual help.

lization in the anode chamber for exp. 5 and exp. 6 over the electrical charge. Starting at an initial pH of 4.15 the pH in the anode chamber decreases during both experiments, while initially, the concentration remains constant. After a charge transfer of about 3 kC, the concentration of succinic acid in solution decreases due to nucleation and growth of succinic acid crystals. It was optically observed that nucleation occurs at the electrode surface and in the direct surrounding of the anode. This supports the assumption that crystallization is induced by protons produced from water electrolysis. The highest proton concentration, thus the lowest pH is obtained directly at the anode surface. Therefore, the anode surface is also the area of the highest supersaturation. By decreas-

ing the pH, the fraction of protonated succinic increases, and eventually saturation of dissolved succinic acid is reached. As protonated succinic acid has a lower solubility in water compared to the ionic species, local supersaturation can be created by electrolysis. This local supersaturation induces nucleation and subsequently crystal growth. At a high pH gradient between the vicinity of the anode and the bulk solution, all nuclei formed at the anode dissolve as soon they are transported to the bulk phase. After a charge turnover of 3 kC the nuclei appear to be stable in the bulk phase. Thus, small crystals that nucleated near the anode grow in the bulk phase resulting in the decrease of succinic acid concentration. Exp. 5 and 6 yielded each about two grams of solid crystals with an average purity of 94.3 % with a median of about X_{50}=468 µm. In the final purity assessment, no traces of other components besides succinic acid were found. The remaining fraction was likely water or traces of the background electrolyte that could not be quantified in the analytical method. The Faraday efficiency was calculated to 26.2 % and 32.3 % for exp. 5 and 6 respectively. However, it should be noted that efficiency would increase when the feed solution is closer to saturation. In this case, the produced protons would directly induce supersaturation. fig. 4.7 shows the crystal size distribution of commercial succinic acid and the crystals obtained in exp. 5.

Even under not optimized conditions, the electrochemical pH-shift crystallization process yielded a crystal size distribution with its maximum at 248 µm, which is comparable to the maximum of the commercial product at 200 µm. However, about 25 % of the produced crystals agglomerate to a size larger than 1500 µm. It was observed, that most of these agglomerates grew directly on the anode. Although large particles ease solid-liquid separation, narrow size distribution is generally more desired with regard to product quality. Therefore, measures like periodic mechanical scratching, ultrasonic cleaning, polarity reversal, seeding or current pulsation in order to reduce agglomerate formation are suggested to avoid the formation of large agglomerates [151, **?**]. Additionally, the influence of gas bubble-induced nucleation should be investigated. Microscopic images fig. 4.8 reveal that despite the agglomerate

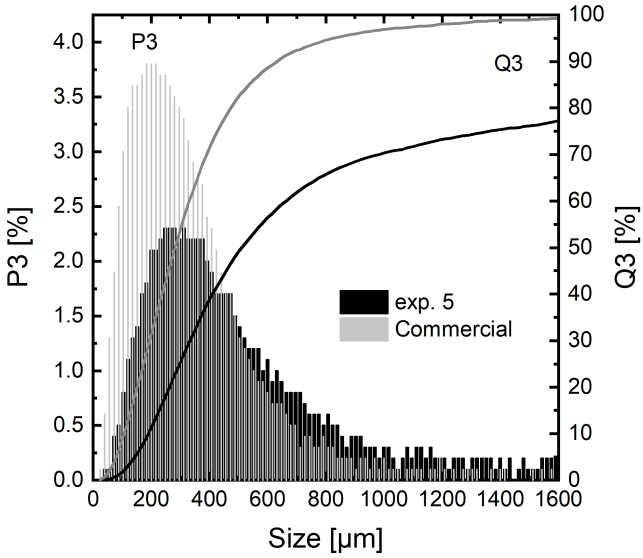

Figure 4.7.: Crystal size distribution of the commercial product (grey) and crystals obtained by electrochemical crystallization in exp. 5 (black). $50\,\%$ of crystals are <$500\,\mu m$, while $25\,\%$ form agglomerates >$1500\,\mu m$ the later fraction corresponds to the fraction of crystals which grow at the anode.

formation, single crystals from electrochemical pH-shift crystallization exhibit a similar size and shape as the commercial product. With the

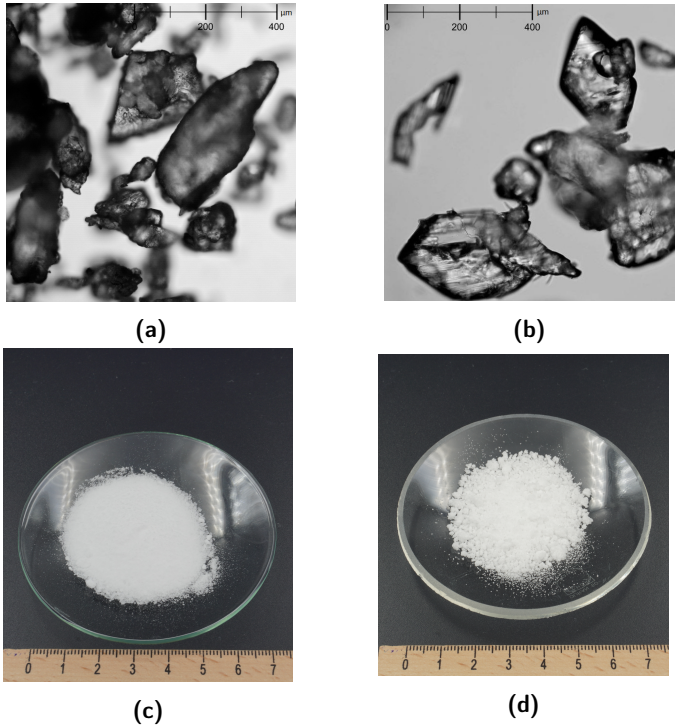

Figure 4.8.: Commercial succinic acid 99 % purity (left a),c)) from ThermoFisher and crystals obtained from electrochemical pH-shift crystallization (right b), d)) with the purity of 94.3 % based on HPLC analysis.

electrochemical separation, oxygen and hydrogen are produced from water electrolysis as "side products of separation". Oxygen can be supplied to aerobic fermentation and the hydrogen can be utilized for further processing steps [152]. Based on the presented electrochemical separation steps, an overall process for the recovery of succinic acid from aqueous fermentation broth is suggested fig. 4.9 [153]. Fermentation of succinic acid runs at neutral pH [16]. Thus, pH of the produced broth is above

pK_{a1} and pK_{a2}. The clarified broth is fed to the first anode chamber, where water electrolysis decreases the pH and thereby increases the fraction of protonated succinic acid. Then, succinic acid is extracted from the acidified broth into the organic phase. Following phase separation, the remaining broth is passed to the cathode chamber which is coupled to the previously mentioned anode chamber. Here, the OH^- ions from water electrolysis raise the pH and the stream can be recycled towards the fermenter also providing a base for pH control. This enables pH-shift extraction without detrimental salt production by acid and base addition. The loaded organic phase from reactive extraction is pumped into another cathode chamber, where the acid is back-extracted by OH^--ions from water electrolysis. By adjusting the phase ratio the concentration in the aqueous phase can be increased to enable crystallization. After phase separation, the unloaded organic phase is recycled into the reactive extraction step. The concentrated aqueous succinic acid solution obtained after back-extraction is passed to an anode chamber where crystallization is induced by the H^+-ions, eventually yielding solid succinic acid. Since the aqueous phase is recycled, a constant concentration of salt is maintained in the process. By pairing the electrode reactions in the presented way, each electrode reaction is utilized for separation.

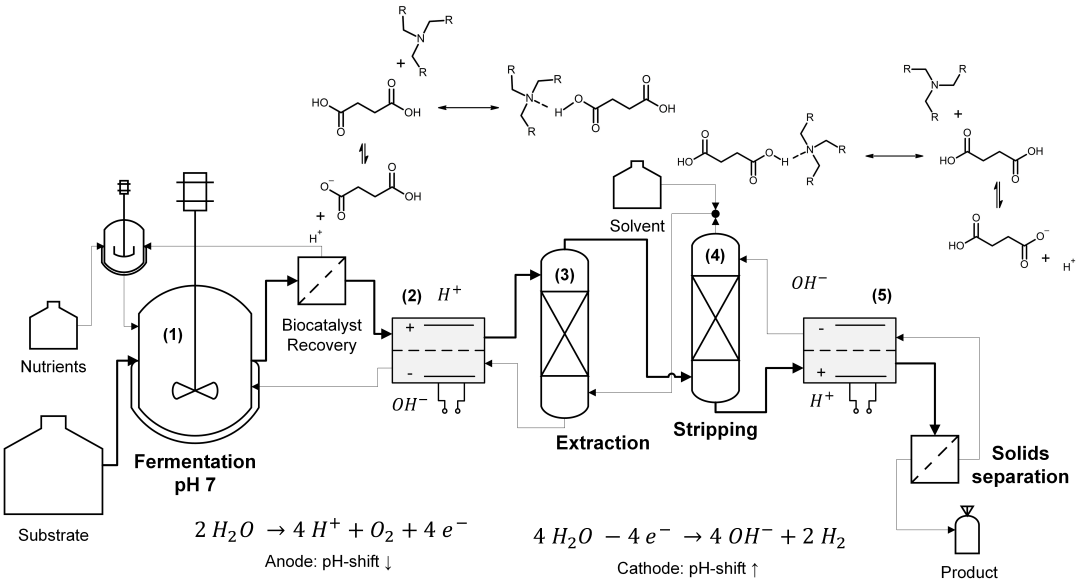

Figure 4.9.: Simplified flow-sheet of the electrochemical pH-swing reactive extraction process for succinic acid separation. (1) Fermentation at neutral pH maintained by alkaline solution provided by the pH-shift electrolysis (2) acidification of fermentation broth by the anodic water splitting reaction (3) reactive extraction of succinic acid, (4) alkaline back-extraction of succinic acid coupled with electrochemical crystallization (5).

The pairing of anodic crystallization and cathodic back-extraction was demonstrated in exp. 7 and 8 fig. 4.10. Again, the pH in the anode chamber decreases while the cathodic pH increases. Concentrations follow the same trend as in the separately conducted experiments. The crystallization runs coupled to back-extraction yielded 4.85 g and 5.57 g succinic acid crystals with a purity of 97 % and 99 %, respectively. It should be noted that the initial pH in these experiments was selected near the pK_{a1} of succinic acid. Thus, most of the protons produced by water electrolysis were efficiently utilized in pH-shift crystallization.

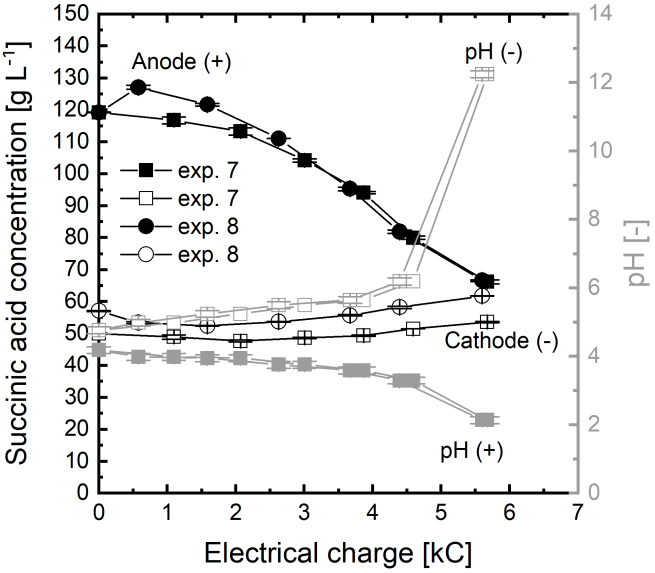

Figure 4.10.: Succinic acid concentration and pH during electrochemically coupled back-extraction at the cathode (-) and crystallization at the anode (+) in exp. 7 and 8. Lines are only visual help.

4.4. Conclusion

This chapter presented the experimental proof-of-concept for succinic acid downstream processing by electrochemical pH-swing separation. It was demonstrated that succinic acid could be extracted, back-extracted, and crystallized solely by means of an electrochemical pH-swing. The extraction was observed in a pH range compatible with conditions of known fermentation processes, while no pH adjustment by inorganic acid was necessary. Thereby, the co-production of salt waste was avoided during the recovery of the succinic acid. As electrochemically induced extraction runs at pH compatible with fermentation, this approach should be tested for continuous *in-situ* product removal.

Although this work shows the principle feasibility, future work must address the geometric design of devices for electrochemically induced separation steps to reduce the ohmic resistance to improve energy efficiency and align the electrochemical generation of protons with the throughput of the succinic acid, to achieve high Faraday efficiencies. Besides, the concept must be tested with real fermentation broth in order to evaluate the impact of co-products from fermentation on the separation performance and identify potential side reactions in long-term operation. However, the results already demonstrate that with non-optimized settings the recovery of succinic acid crystals with a purity >94 % from electrolyte-containing mother liquor is possible.

The technical realization of electrochemical pH-swing separation processes requires engineering tools to design and evaluate the unit operations with regard to the overall process. A relevant design question is, whether the direct integration of the electrochemical pH-swing with the reactive extraction step is mandatory. The proof-of-concept experiments showed that the advantage of short mass transfer distances comes at the expense of membrane degradation by the organic solvent. Beyond that, the electrolysis was identified as the rate-limiting step in the integrated setup. Next, a modeling approach is developed to facilitate the transfer from batch operation in an H-cell to continuous flow-cell operation.

5. Modelling of pH-swing electrolysis and reactive extraction kinetics

5.1. Motivation

The transfer from proof-of-principle experiments to technically applicable solutions requires a detailed understanding of the underlying physicochemical mechanisms. In the previous chapter, batch experiments were used to demonstrate the principle viability of electrochemical pH-swing extraction.

In this chapter, a 1D-dynamic model for the electrochemical pH-swing extraction of succinic acid is developed to provide an *in-silico* tool for model-based process analysis. The objectives of the 1D model are to:

- Enable model-based identification of rate-limiting steps and desirable operational conditions,
- Resolve potential sources of inefficiencies in terms of electricity usage,
- And facilitate design decisions for the transfer from batch experiments to continuously operable flow cells.

Key performance indicators for electricity usage in electrochemical processes are the Faraday efficiency η_F

$$\eta_F = \frac{\dot{n}_{H^+}}{\dot{n}_{e^-}} \tag{5.1}$$

and the specific energy consumption w:

$$w = \frac{U_{Cell} \cdot z \cdot F}{M} \cdot \frac{1}{3600} \qquad [\mathrm{kWh/kg}] \tag{5.2}$$

calculated from the cell voltage U [V], number of electrons z [−], Faraday's constant F [$\mathrm{C\,mol^{-1}}$] and the molar mass M [$\mathrm{g\,mol^{-1}}$]. The Faraday efficiency denotes the number of protons produced from the transferred electric charge and is affected by the selectivity of the electrode reaction. It is an indicator of the selectivity of the electrode reaction and can be regarded as the "electric current efficiency" [45, 154]. The specific energy consumption is directly related to the cell voltage U_{Cell}. A cell voltage above the reversible cell potential U_{rev} is an indication of irreversible losses in the electrochemical system. The specific energy consumption can be regarded as a measure of "voltage efficiency".

Two different layouts are considered. The integrated approach fig. 5.1a and the sequential layout fig. 5.1b. In the integrated layout, the organic phase flows with the electrolyte through the electrolysis cell. Thus protons, respectively hydroxide ions produced in the electrolysis can immediately act on the extraction equilibrium. Accordingly, a high utilization rate of the electrochemically produced protons, respectively hydroxide ions is expected.

However, the contact of organic solvent with the ion exchange membrane was observed to accelerate the membrane degradation which eventually may compromise the advantage of direct proton utilization. A central question to be answered in this chapter is: *Has the integrated approach operational benefits in terms of electricity usage, which outweigh the observed membrane degradation?*

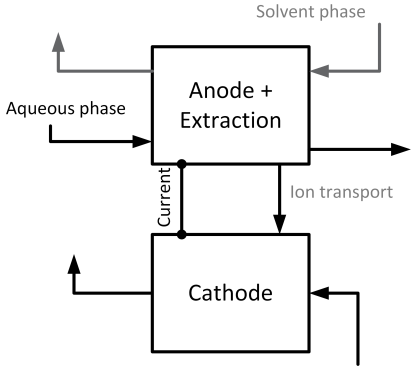

(a) Integrated design of pH-swing electrolysis and reactive extraction. The extractant is in direct contact with the electrolyte inside the electrolysis.

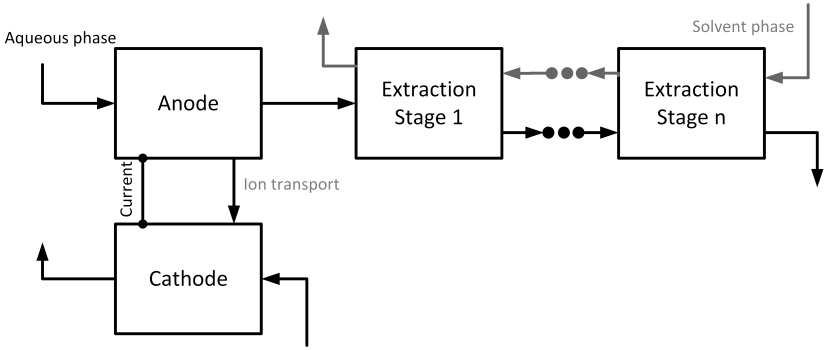

(b) Sequential design of pH-swing electrolysis and reactive extraction. pH-Swing electrolysis and reactive extraction are conducted in separate process steps.

Figure 5.1.: Conceptual designs for electrochemical pH-swing reactive extraction processes: (a) integrated, (b) sequential layout.

5.2. Modeling approach and model structure

The 1D model for electrochemical pH swing electrolysis and extraction is constituted by a set of differential and algebraic equations forming a differential algebraic system (DAE). This system was implemented as level-2 Sfunctions in a MATLAB (R2019b) Simulink simulation environ-

ment and solved with the *ode*15*s* solver.

The following simplifying assumptions were made:

- Constant thermodynamic properties and standard conditions (25 °C, 1 bar)
- Ideal solution chemistry
- Negligible cross-solubility between the aqueous and organic phase
- Stages are ideally mixed
- Change of volumetric flow rates are negligible

The general model structure is illustrated in fig. 5.2. The electrolysis cell is composed of two modeling domains. One is representing the anode, the other is representing the cathode compartment.

The state vector $\mathbf{x}^T$ denotes the states of the concentration in the aqueous phase and $\mathbf{y}^T$ lists the concentrations of the solvent phase.

$$\mathbf{x}^T = \left[\mathrm{H^+}, \mathrm{OH^-}, \mathrm{Na^+}, \mathrm{H_2Suc}, \mathrm{HSuc^-}, \mathrm{Suc^{2-}}, \mathrm{H_2SO_4}, \mathrm{HSO_4^-}, \mathrm{SO_4^{2-}}\right] \tag{5.3}$$

$$\mathbf{y}^T = \left[\mathrm{TOA}, \mathrm{H_2Suc_{sol}}, \mathrm{HSO_{4,sol}}, \mathrm{TOAH^+}\right] \tag{5.4}$$

In an aqueous solution containing up to $1\,\mathrm{mol\,L^{-1}}$ carboxylic acid change in concentration of the water content due to electrolysis is below 5 %. For that reason, constant volumetric flow rates are assumed:

$$\dot{S} = \dot{K} \tag{5.5}$$

$$\dot{F} = \dot{R} \tag{5.6}$$

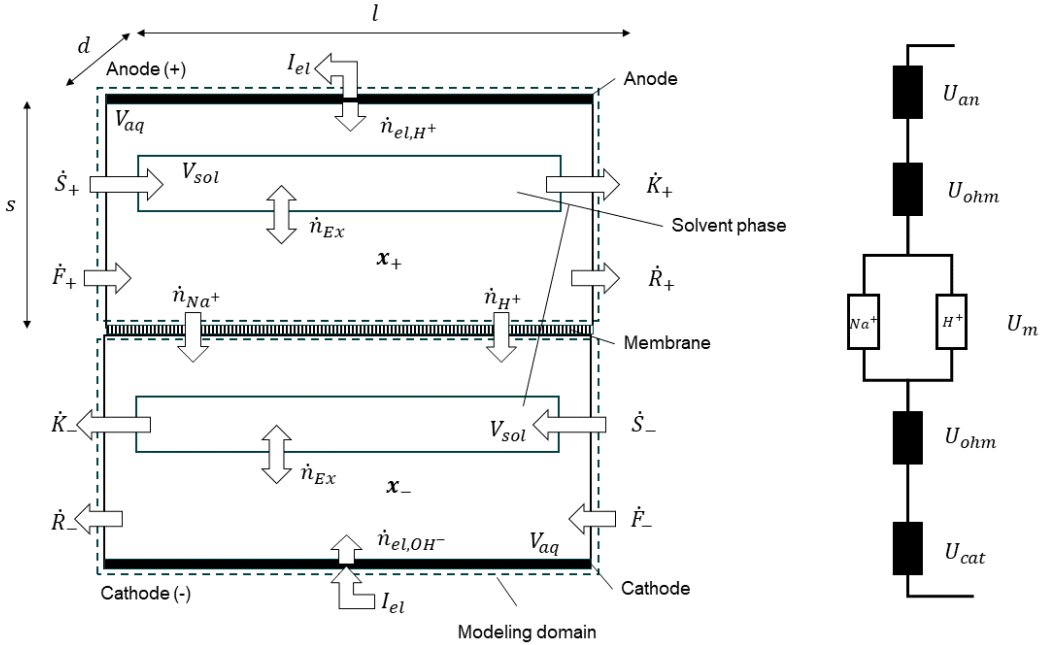

Figure 5.2.: General modeling domain of Sfunction blocks for the electrochemical pH-shift electrolysis and extraction model. The anode and cathode are modeled in separate domains connected by the electric current and an exchange term for the transferred electric charge.

5.2.1. Submodel: pH Equilibrium

The pH equilibrium of aqueous solutions is constituted by the dissociation of the weak acids present. In simple cases with few acid species, the dissociation state of each acid can be calculated from the mass-action law of the acid dissociation reaction section 2.1. For multi-species equilibrium systems solving the algebraic set of equations becomes more complex as each species adds another mathematically correct solution to the solution space that does not necessarily reflect a physically meaningful solution. Kip et al. [155, 156, 157] suggested a numerical method to solve complex pH equilibrium calculations.

A model applying a modified version of this approach was developed and published in [158]. The published model revealed the close interconnection of the pH equilibrium and the extraction equilibrium and suggested that the rate-limiting step of the electrochemical pH-swing extraction is the electrolysis kinetic. However, the algebraic model is limited in its ability to account for complex aqueous pH equilibria, constituted by more than one acid. The limitation comes from the algebraic approach used in the calculation of the weak acid equilibrium in the aqueous phase. In this approach, each acid-base equilibrium is transformed into a polynomial the set of all polynomials is then solved numerically for the proton concentration that fulfills all equilibrium conditions [159, 160]. In multi-equilibria systems, this approach is sensitive to numerical errors and was found to be often unreliable. Especially due to the fact that there can be more than one solution for the given sets of polynomials [161].

To overcome the limitations of the algebraic approach for pH and dissociation state calculations a dynamic approach, or rate-based model, was suggested by Glaser et al.[161]. The dissociation reactions of the weak acids are evolved into a set of ordinary differential equations (ODEs). The dissociation reactions of water and the dissociation reactions for each acid are included.

$$\frac{d[H^+]}{dt} = k_{w,f} - k_{w,b}[H^+][OH^-] + k_{i,f}[HA] - k_{i,b}[H^+][A^-] \tag{5.7}$$

$$\frac{d[OH^-]}{dt} = k_{w,f} - k_{w,b}[H^+][OH^-] \tag{5.8}$$

$$\frac{d[HA]}{dt} = -k_{i,f}[HA] + k_{i,b}[H^+][A^-] \tag{5.9}$$

$$\frac{d[A^-]}{dt} = +k_{i,f}[HA] - k_{i,b}[H^+][A^-] \tag{5.10}$$

The forward and backward reaction rates $k_{i,f}$ and $k_{i,b}$ are related by the equilibrium constant

$$K_{a,i} = \frac{k_{i,f}}{k_{i,b}} \tag{5.11}$$

In a steady state, the solution of the ODEs is equivalent to the equilibrium concentration. Advantageously, the ODEs can be easily extended to incorporate other reaction or mass transfer rates in the model. But in order to yield physically meaningful results, the reaction rates of the dissociation reactions must be known or selected in a way that the dissociation can be considered independent from other kinetic effects. Since the dissociation reactions are known to be fast, but the true reaction rate is not always known, Glaser et al. suggest selecting a value of 10^2 for $k_{i,f}$ [161].

5.2.2. Submodel: Electrolysis

The electrolysis is modeled with an amperostatic approach [162]. In comparison with the potentiostatic approach where a constant potential is set and the migration of ions is calculated with the Nernst-Planck equation [163, 9], the amperostatic approach sets the electric current,

and the cell potential is calculated based on the current state of the electrolysis cell. As illustrated in fig. 5.2 the cell voltage is constituted by the difference of the reversible cell potential U_{rev} the activation potential U_{act} and the potential to overcome ohmic losses in the electrolyte U_{ohm}. In non-ideally mixed systems concentration polarization can add additional potential losses U_{conc} which are negligible for ideally mixed conditions.

$$U_{Cell} = U_{rev} + U_{act} + U_{ohm} + U_{conc} \tag{5.12}$$

The reversible cell potential difference is calculated from the electrode potential $E_{0,i}$ obtained by the Nernst equation 2.10.

$$U_{rev} = E_{0,an} - E_{0,cat} \tag{5.13}$$

At standard conditions the Nernst equation for the water splitting reaction simplifies and the electrode potential can directly be calculated with the pH.

$$E_{0,an} = 1.229 - 0.059pH \tag{5.14}$$

and

$$E_{0,cat} = -0.059pH \tag{5.15}$$

The activation potential considers losses at the electrode-electrolyte interface accounting for the "activation" of the charge transfer from the electrode to the reactive species and calculated with the Butler-Volmer equation [9, 164, 162].

$$i = i_a + i_c = i_0 \left[exp\left(\frac{\alpha z F}{RT} U_{act} \right) - exp\left(-\frac{(1-\alpha)\, zF}{RT} U_{act} \right) \right] \tag{5.16}$$

In case $|U_{act}| >> \frac{RT}{zF}$, the counter-reaction becomes negligible [9] and eq. (5.16) reduces to:

$$U_{act} = \frac{RT}{\alpha_{an/cat} zF} arsinh\left(\frac{i}{2i_0} \right) \tag{5.17}$$

with i_0 being the exchange current density and $\alpha_{an/cat}$ the charge transfer coefficient of the anodic or cathodic electrode reaction. The parameters for platinum electrodes are listed in table table 5.1.

Table 5.1.: Charge transfer coefficients and exchange current densities for platinum electrodes [9]

Reaction	**Electrode**	$\alpha[-]$	i_0 [A cm^{-1}]
O_2/H^+	Anode	0.25	10^{-6}
H_2/OH^-	Cathode	0.5	10^{-3}

The potential loss due to the ohmic resistance of the cell can be calculated from the cell geometry, the conductivity of the electrolyte solution and the applied current.

$$U_{ohm} = RI = \frac{s}{A\kappa} \cdot I \tag{5.18}$$

The electrolyte conductivity is related to the concentration c_i and the ion mobility u_i of the charged species present in the electrolyte [165].

$$\kappa = F^2 \sum_{i=1}^{n} z_i^2 u_i c_i \tag{5.19}$$

The single ion mobility is related to the equivalent ion conductivity by the Nernst-Einstein relation eq. (5.20).

$$u_i = \frac{\lambda_i}{z_i F^2} = \frac{D_i}{RT} \tag{5.20}$$

Inserting eq. (5.20) into eq. (5.19) yields an expression for the electrolyte conductivity based on the ion concentration and the ion specific conductivity [166].

$$\kappa = \sum_{i=1}^{n} z_i \lambda_i c_i \tag{5.21}$$

The specific ion conductivities used in this model are given in table F.1 in the appendix. eq. (5.21) is based on the assumption of infinite di-

lution. The total electric current corresponds to the molar flow rate of protons produced at the anode, which can be calculated by faraday's law eq. (2.12)

$$\dot{n}_{CB,Total} = \dot{n}_{Elek,H^+} \tag{5.22}$$

The electric current in the electrolyte is distributed among the available ionic species, namely protons and sodium ions.

$$\dot{n}_{H^+} = \frac{\kappa_{H^+}}{\kappa_{H^+} + \kappa_{Na^+}} \dot{n}_{CB,Total} \tag{5.23}$$

$$\dot{n}_{CB,Na^+} = \frac{\kappa_{Na^+}}{\kappa_{CB,H^+} + \kappa_{Na^+}} \dot{n}_{CB,Total} \tag{5.24}$$

5.2.3. Submodel: pH-Swing reactive extraction

The kinetics of the reactive extraction are modeled with a simplified film theory [167]. It is assumed that the apparent concentration in the boundary layer of the organic phase $[\overline{X}]_{bl,sol}$ equals the equilibrium concentration of the aqueous succinic acid species with the organic phase $[\overline{X}]^*$.

$$[\overline{X}]_{bl,sol} = [\overline{X}]^* \tag{5.25}$$

For the succinic acid complex with TOA this expression becomes:

$$[\overline{H_2SA \cdot TOA}]_{bl,sol} = [\overline{H_2SA \cdot TOA}]^*_{bulk,sol} \tag{5.26}$$

$$\dot{n}_{Ex,H_2SA} = A_{Ex} \cdot k_{Ex,SA} \cdot ([\overline{H_2SA \cdot TOA}]_{bl,sol} - [\overline{H_2SA \cdot TOA}]_{bulk,sol}) \tag{5.27}$$

This assumption implies that the diffusion of the complex in the organic phase is the rate-limiting step. It should be noted that the complex formation can also be the rate-limiting step [10]. A clear identification of the rate-limiting step is so far not possible and for this reason a diffusion-limited process is assumed in the following. The apparent concentration in the boundary layer is calculated by a mass-action relationship between the free TOA concentration in the organic phase and the concentration

of protonated succinic acid in the aqueous phase.

$$[\overline{TOA \cdot H_2SA}]_{bl,sol} = K_{ex} \cdot [\overline{TOA_{free}}] \cdot [H_2SA] \tag{5.28}$$

With the data from table G.1 the mass transfer coefficient of the succinic acid complex with TOA in the organic phase can be estimated.

$$\begin{aligned} k_{Complex/1-octanol} &= k_{Iodine/kerosene} \frac{D_{Complex/1-octanol}^{2/3} \gamma_{1-octanol}^{-1/6}}{D_{Iodine/kerosene}^{2/3} \gamma_{kerosene}^{-1/6}} \\ &= 4.738 \cdot 10^{-6} \ \frac{m}{s} \end{aligned} \tag{5.29}$$

The equilibrium constant of the mass-action relationship K_{ex} can be calculated from correlations [111, 64] or fitted to experimental data.

5.2.4. Modeling domain: Anode

The dynamic pH-shift model of the anode chamber (AC) is constituted by the differential equations of the dissociation reactions, which are listed in the following. The electrolytic current is introduced as a molar flux of proton in the proton balance ($\dot{\mathbf{n}}_{\mathbf{Elek},\mathbf{H^+}}$).

Proton balance:

$$\begin{aligned}\frac{d[H^+]}{dt} &= k_{w,f} - k_{w,b}[H^+][OH^-] \\ &+k_{31,f}[H_2Suc] - k_{31,b}[H^+][HSuc^-]+ \\ &k_{32,f}[HSuc^-] - k_{32,b}[H^+][Suc^{2-}] \\ &+k_{61,f}[H_2SO_4] - k_{61,b}[H^+][HSO_4^-]+ \\ &k_{62,f}[HSO_4^-] - k_{62,b}[H^+][SO_4^{2-}] \\ &+\frac{1}{V_{AC}}\dot{\mathbf{n}}_{\mathbf{Elek},\mathbf{H^+}} - \frac{1}{V_{AC}}\dot{n}_{CB,H^+}+ \\ &\frac{\dot{M}}{V_{AC}}[H^+]_M - \frac{\dot{S}}{V_{AC}}[H^+]\end{aligned} \tag{5.30}$$

Hydroxide ion balance:

$$\frac{d[OH^-]}{dt} = k_{w,f} - k_{w,b}[H^+][OH^-] + \frac{\dot{M}}{V_{AC}}[OH^-]_M - \frac{\dot{S}}{V_{AC}}[OH^-] \tag{5.31}$$

Sodium ion balance:

$$\frac{d[Na^+]}{dt} = -\frac{1}{V_{AC}}\dot{n}_{CB,Na^+} + \frac{\dot{M}}{V_{AC}}[Na^+]_M - \frac{\dot{S}}{V_{AC}}[Na^+] \tag{5.32}$$

Dissociation reactions of succinic acid:

$$\begin{aligned}\frac{d[H_2Suc]}{dt} &= -k_{31,f}[H_2Suc] + k_{31,b}[H^+][HSuc^-]+ \\ &\frac{\dot{M}}{V_{AC}}[H_2Suc]_M - \frac{\dot{S}}{V_{AC}}[H_2Suc]\end{aligned} \tag{5.33}$$

$$\begin{aligned}\frac{d[HSuc^-]}{dt} &= k_{31,f}[H_2Suc] - k_{31,b}[H^+][HSuc^-]- \\ &k_{32,f}[HSuc^-] + k_{32,b}[H^+][Suc^{2-}] \\ &+\frac{\dot{M}}{V_{AC}}[HSuc^-]_M - \frac{\dot{S}}{V_{AC}}[HSuc^-]\end{aligned} \tag{5.34}$$

$$\frac{d[Suc^{2-}]}{dt} = k_{32,f}[HSuc^{-}] - k_{32,b}[H^{+}][Suc^{2-}] + \frac{\dot{M}}{V_{AC}}[Suc^{2-}]_{M} - \frac{\dot{S}}{V_{AC}}[Suc^{2-}] \tag{5.35}$$

Dissociation reactions of the sulfate background electrolyte:

$$\frac{d[H_2SO_4]}{dt} = -k_{61,f}[H_2SO_4] + k_{61,b}[H^{+}][HSO_4^{-}] + \frac{\dot{M}}{V_{AC}}[H_2SO_4]_{M} - \frac{\dot{S}}{V_{AC}}[H_2SO_4] \tag{5.36}$$

$$\frac{d[HSO_4^{-}]}{dt} = k_{61,f}[H_2SO_4] - k_{61,b}[H^{+}][HSO_4^{-}] - k_{62,f}[HSO_4^{-}] + k_{62,b}[H^{+}][SO_4^{2-}] + \frac{\dot{M}}{V_{AC}}[HSO_4^{-}]_{M} - \frac{\dot{S}}{V_{AC}}[HSO_4^{-}] \tag{5.37}$$

$$\frac{d[SO_4^{2-}]}{dt} = k_{62,f}[HSO_4^{-}] - k_{62,b}[H^{+}][SO_4^{2-}] + \frac{\dot{M}}{V_{AC}}[SO_4^{2-}]_{M} - \frac{\dot{S}}{V_{AC}}[SO_4^{2-}] \tag{5.38}$$

5.2.5. Modeling domain: Cathode

The dynamic pH-shift model of the cathode chamber (CC) developed analogously to the anode chamber. Here, the electrolytic current is introduced as a molar flux of in the hydroxide ion balance ($\dot{\mathbf{n}}_{\mathbf{Elek},\mathbf{H^{+}}}$).

Proton balance:

$$\begin{aligned}\frac{d[H^+]}{dt} &= k_{w,f} - k_{w,b}[H^+][OH^-] \\ &+k_{31,f}[H_2Suc] - k_{31,b}[H^+][HSuc^-]+ \\ &k_{32,f}[HSuc^-] - k_{32,b}[H^+][Suc^{2-}] \\ &+k_{61,f}[H_2SO_4] - k_{61,b}[H^+][HSO_4^-]+ \\ &k_{62,f}[HSO_4^-] - k_{62,b}[H^+][SO_4^{2-} \\ &+\frac{1}{V_{CC}}\dot{n}_{CB,H^+} + \frac{\dot{M}}{V_{CC}}[H^+]_M - \frac{\dot{S}}{V_{CC}}[H^+]\end{aligned} \tag{5.39}$$

Hydroxide ion balance:

$$\begin{aligned}\frac{d[OH^-]}{dt} &= k_{w,f} - k_{w,b}[H^+][OH^-]+ \\ \frac{1}{V_{CC}}\dot{\mathbf{n}}_{\mathbf{Elek},\mathbf{OH^-}} &+ \frac{\dot{M}}{V_{CC}}[OH^-]_M - \frac{\dot{S}}{V_{CC}}[OH^-]\end{aligned} \tag{5.40}$$

Sodium ion balance:

$$\frac{d[Na^+]}{dt} = \frac{1}{V_{CC}}\dot{n}_{CB,Na^+} + \frac{\dot{M}}{V_{CC}}[Na^+]_M - \frac{\dot{S}}{V_{CC}}[Na^+] \tag{5.41}$$

Dissociation reactions of succinic acid:

$$\begin{aligned}\frac{d[H_2Suc]}{dt} &= -k_{31,f}[H_2Suc] + k_{31,b}[H^+][HSuc^-]+ \\ &\frac{\dot{M}}{V_{CC}}[H_2Suc]_M - \frac{\dot{S}}{V_{CC}}[H_2Suc]\end{aligned} \tag{5.42}$$

$$\begin{aligned}\frac{d[HSuc^-]}{dt} &= k_{31,f}[H_2Suc] - k_{31,b}[H^+][HSuc^-]- \\ &k_{32,f}[HSuc^-] + k_{32,b}[H^+][Suc^{2-}] \\ &+\frac{\dot{M}}{V_{CC}}[HSuc^-]_M - \frac{\dot{S}}{V_{CC}}[HSuc^-]\end{aligned} \tag{5.43}$$

$$\frac{d[Suc^{2-}]}{dt} = k_{32,f}[HSuc^{-}] - k_{32,b}[H^{+}][Suc^{2-}] + \frac{\dot{M}}{V_{CC}}[Suc^{2-}]_M - \frac{\dot{S}}{V_{CC}}[Suc^{2-}] \tag{5.44}$$

Dissociation reactions of the sulfate background electrolyte:

$$\frac{d[H_2SO_4]}{dt} = -k_{61,f}[H_2SO_4] + k_{61,b}[H^{+}][HSO_4^{-}] + \frac{\dot{M}}{V_{CC}}[H_2SO_4]_M - \frac{\dot{S}}{V_{CC}}[H_2SO_4] \tag{5.45}$$

$$\frac{d[HSO_4^{-}]}{dt} = k_{61,f}[H_2SO_4] - k_{61,b}[H^{+}][HSO_4^{-}] - k_{62,f}[HSO_4^{-}] + k_{62,b}[H^{+}][SO_4^{2-}] + \frac{\dot{M}}{V_{CC}}[HSO_4^{-}]_M - \frac{\dot{S}}{V_{CC}}[HSO_4^{-}] \tag{5.46}$$

$$\frac{d[SO_4^{2-}]}{dt} = k_{62,f}[HSO_4^{-}] - k_{62,b}[H^{+}][SO_4^{2-}] + \frac{\dot{M}}{V_{CC}}[SO_4^{2-}]_M - \frac{\dot{S}}{V_{CC}}[SO_4^{2-}] \tag{5.47}$$

5.2.6. Modeling domain: pH-dependent reactive extraction

The pH-dependent reactive extraction is modeled by combining the aqueous pH equilibrium model with the constituting equations of the organic phase. In the following the constituting equations of the sequential model fig. 5.1b are presented. The mathematical formulation of the integrated approach fig. 5.1a is derived by integrating the extraction terms into the anode chamber model.

Proton balance:

$$\begin{aligned}\frac{d[H^+]}{dt} &= k_{w,f} - k_{w,b}[H^+][OH^-] \\ &+k_{31,f}[H_2Suc] - k_{31,b}[H^+][HSuc^-]+ \\ &k_{32,f}[HSuc^-] - k_{32,b}[H^+][Suc^{2-}] \\ &+k_{61,f}[H_2SO_4] - k_{61,b}[H^+][HSO_4^-]+ \\ &k_{62,f}[HSO_4^-] - k_{62,b}[H^+][SO_4^{2-} \\ &+\frac{\dot{S}}{V_{aq}}[H^+]_S - \frac{\dot{R}}{V_{aq}}[H^+]\end{aligned} \tag{5.48}$$

Hydroxide ion balance:

$$\frac{d[OH^-]}{dt} = k_{w,f} - k_{w,b}[H^+][OH^-] + \frac{\dot{S}}{V_{aq}}[OH^-]_S - \frac{\dot{R}}{V_{aq}}[OH^-] \tag{5.49}$$

Sodium ion balance:

$$\frac{d[Na^+]}{dt} = \frac{\dot{S}}{V_{aq}}[Na^+]_S - \frac{\dot{R}}{V_{aq}}[Na^+] \tag{5.50}$$

Extraction and dissociation reaction of succinic acid:

$$\begin{aligned}\frac{d[H_2Suc]}{dt} &= -k_{31,f}[H_2Suc] + k_{31,b}[H^+][HSuc^-] - \frac{1}{V_{aq}}\dot{\mathbf{n}}_{\mathbf{Ex},\mathbf{H_2Suc}} \\ &+\frac{\dot{S}}{V_{aq}}[H_2Suc]_S - \frac{\dot{R}}{V_{aq}}[H_2Suc]\end{aligned} \tag{5.51}$$

$$\begin{aligned}\frac{d[HSuc^-]}{dt} &= k_{31,f}[H_2Suc] - k_{31,b}[H^+][HSuc^-]- \\ &k_{32,f}[HSuc^-] + k_{32,b}[H^+][Suc^{2-}] \\ &+\frac{\dot{S}}{V_{aq}}[HSuc^-]_S - \frac{\dot{R}}{V_{aq}}[HSuc^-]\end{aligned} \tag{5.52}$$

$$\frac{d[Suc^{2-}]}{dt} = k_{32,f}[HSuc^{-}] - k_{32,b}[H^{+}][Suc^{2-}] + \frac{\dot{R}}{V_{aq}}[Suc^{2-}]_S - \frac{\dot{R}}{V_{aq}}[Suc^{2-}] \tag{5.53}$$

Dissociation reaction of the sulfate background electrolyte:

$$\frac{d[H_2SO_4]}{dt} = -k_{61,f}[H_2SO_4] + k_{61,b}[H^{+}][HSO_4^{-}] + \frac{\dot{S}}{V_{aq}}[H_2SO_4]_S - \frac{\dot{R}}{V_{aq}}[H_2SO_4] \tag{5.54}$$

$$\frac{d[HSO_4^{-}]}{dt} = k_{61,f}[H_2SO_4] - k_{61,b}[H^{+}][HSO_4^{-}] - k_{62,f}[HSO_4^{-}] + k_{62,b}[H^{+}][SO_4^{2-}] + \frac{\dot{S}}{V_{aq}}[HSO_4^{-}]_S - \frac{\dot{R}}{V_{aq}}[HSO_4^{-}] \tag{5.55}$$

$$\frac{d[SO_4^{2-}]}{dt} = k_{62,f}[HSO_4^{-}] - k_{62,b}[H^{+}][SO_4^{2-}] + \frac{\dot{S}}{V_{aq}}[SO_4^{2-}]_S - \frac{\dot{R}}{V_{aq}}[SO_4^{2-}] \tag{5.56}$$

Organic phase:

$$\frac{d[TOA]}{dt} = -\frac{1}{V_{sol}}\dot{\mathbf{n}}_{\mathbf{Ex,H_2Suc}} + \frac{\dot{L}}{V_{sol}}[TOA]_L - \frac{\dot{K}}{V_{sol}}[TOA] \tag{5.57}$$

$$\frac{d[H_2Suc_{sol}]}{dt} = \frac{1}{V_{sol}}\dot{\mathbf{n}}_{\mathbf{Ex,H_2Suc}} + \frac{\dot{L}}{V_{sol}}[H_2Suc_{sol}]_L - \frac{\dot{K}}{V_{sol}}[H_2Suc_{sol}] \tag{5.58}$$

5.3. Sensitivity of dynamic pH-equilibrium calculations

The implementation of the dynamic modeling approach presented in section 5.2 enables the handling of complex dissociation equilibria. It

overcomes the limitation of the algebraic approach [155, 156, 159, 160], whose applicability is limited to conditions where only succinic acid species dominate the aqueous dissociation equilibrium [158]. The dissociation reactions are generally considered to be fast reactions [168, 169]. Since the forward dissociation reaction rate is not known, an arbitrary but high enough value must be chosen in order to yield valid results [170]. Dissociation reactions are proton transfer reactions with a half-life of less than a millisecond which makes them fast compared to electrolysis or extraction kinetics [171, 10]. Consequently, the dynamic of the dissociation reactions does not interfere with the kinetic effects of the extraction or electrolysis when the aqueous dissociation equilibrium is reached within a few milliseconds. This is validated by a step-wise examination of the sensitivity imposed by different forward dissociation rates.

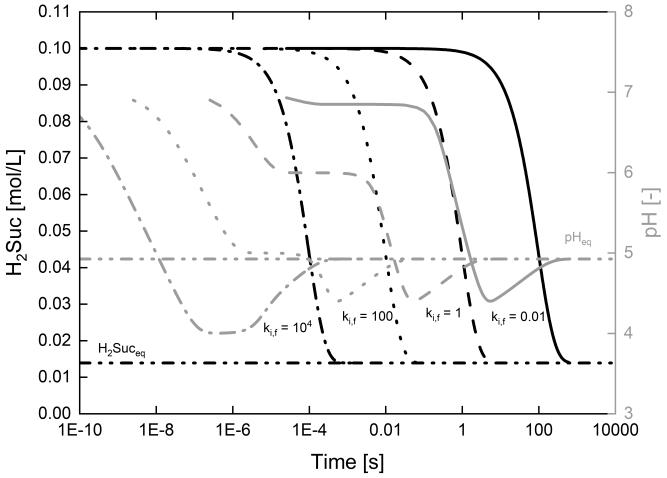

Figure 5.3.: Progression of the dissociation reaction towards equilibrium conditions with varying forward dissociation rates $k_{i,f}$ starting at non-equilibrium conditions: $H_2Suc_0 = 0.1\,\mathrm{mol\,L^{-1}}$, $NaOH_0 = 0.1\,\mathrm{mol\,L^{-1}}$, $H^+ = 1 \times 10^{-7}\,\mathrm{mol\,L^{-1}}$ and $OH^- = 1 \times 10^{-7}\,\mathrm{mol\,L^{-1}}$

Figure 5.3 presents the progression of the dissociation reactions start-

ing from non-equilibrium conditions. At dissociation rates larger than $1\,s^{-1}$ it takes seconds for the reaction to attain equilibrium. With dissociation rates of $100\,s^{-1}$ or below the dissociation equilibrium is reached within milliseconds as expected. Therefore, a forward dissociation rate of at least $100\,s^{-1}$ should be selected to yield reasonable results. This is in line with the recommendation by Glaser and Zars [161, 170].

Dissociation reactions are fast compared to extractive mass transport or electrolysis kinetics. Table 5.2 shows an exemplary comparison of rate constants for operational conditions typically encountered in reactive extraction or electrolysis. While the difference between the dissociation equilibrium and the reactive extraction as the second fastest reaction is about seven orders of magnitude the expected difference between the reactive extraction and electrolysis kinetic is still about three orders of magnitude. Consequently, the electrolysis kinetic is expected to be the rate-limiting step in an electrochemically driven pH-swing reactive extraction.

Table 5.2.: Comparison of rate constants for dissociation, extraction and electrolysis

Reaction	**Rate constant**	**Reference**
Dissociation acetic acid	$2.9 \times 10^{5}\,s^{-1}$	[168]
Reactive extraction succinic acid	$5.69 \times 10^{-2}\,s^{-1}$	*
Electrolysis	$9.85 \times 10^{-5}\,mol\,s^{-1}$	**

*Comparable rate constant calculated from $\frac{A_{Ex}}{V_{sol}} k_{Ex} = \frac{6 k_{Ex}}{d_{32}}$ assuming a mass transfer constant of $4.74 \times 10^{-6}\,m\,s^{-1}$[10] and a sauter mean diameter of d_{32} =0.5 mm.
**Calculated from faraday's law with 10 A.

An analysis of all kinetic effects lumped together is difficult to evaluate due to the intrinsically dynamic nature of the electrolysis reaction. While dissociation and extraction reactions progress toward equilibrium, this is not the case for electrolysis. Therefore, the interaction between the aqueous pH equilibrium and the reactive extraction equilibrium with regard to the forward dissociation constant is analyzed first.

fig. 5.4 denotes the difference in the equilibrium conditions attained with varying forward dissociation constants. If $k_{i,f} = 0.01\,\mathrm{s}^{-1}$ is selected, the simulation yields obviously unrealistic results as an intermediate pH above 12 would occur due to the H^+ deficiency caused by the removal of protonated succinic acid. At $k_{i,f} = 1\,\mathrm{s}^{-1}$ the dissociation attains its equilibrium together with the reactive extraction, which implies that both reactions might interfere with each other. With values of $100\,\mathrm{s}^{-1}$ or higher the dissociation equilibrium is attained before the extractive mass transport begins. Since pH-shift electrolysis is an intrinsically dy-

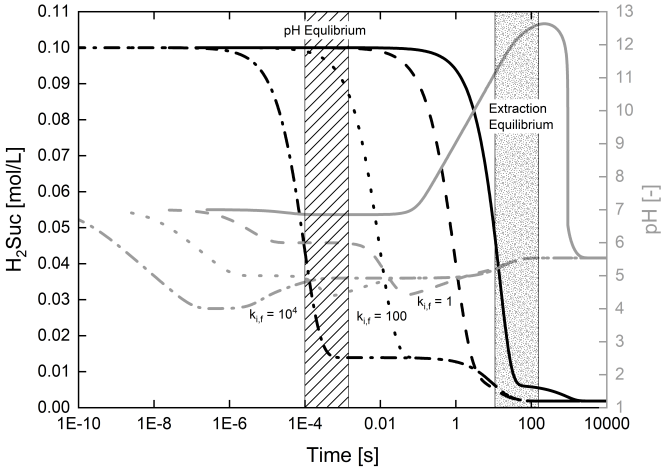

Figure 5.4.: Progression of the dissociation reaction and extraction towards equilibrium conditions with varying forward dissociation rates $k_{i,f}$. At $k_{i,f} \geq 100$ the pH equilibrium is reached more than three orders of magnitude faster than the extraction equilibrium.

namic process without a defined equilibrium condition, the sensitivity of the results is analyzed by simulating an electrolysis pulse fig. 5.5. Initially 2000 s were simulated to ensure the pulse is applied at equilibrium conditions. Then a 10 s pulse of 100 A is applied. The remaining deflection from equilibrium ΔpH and the deviation in the final protonated succinic acid concentration indicate whether the kinetic limitation

imposed by the dissociation reaction causes a deviation of the final results. Figure 5.5a shows an obvious deviation for the lowest kinetic constant. Again, for any rate above $100\,s^{-1}$ only small deviations are observed. This is confirmed by a log-log representation of the residual difference between the endpoint of the electrolysis pulse compared to the corresponding equilibrium concentration which is obtained when the electrolysis is stopped. The residual deviation is found to be below 1×10^{-3} for a dissociation constant above $100\,s^{-1}$. As a consequence, the deflection of the aqueous dissociation equilibrium is readily compensated and no artificial kinetic limitations are expected with a $k_{i,f} \geq 100\,s^{-1}$. The selected pulse conditions match the current upper limit for the current density feasible with commercially available electrolysis equipment [172, 66].

The selected kinetic values should therefore enable the correct modeling of the pH-shift during the electrolysis. The presented model thus enables the simulation of different operational conditions to identify suitable operating points. It also provides insights into inefficiencies occurring during operation. These insights are not accessible experimentally.

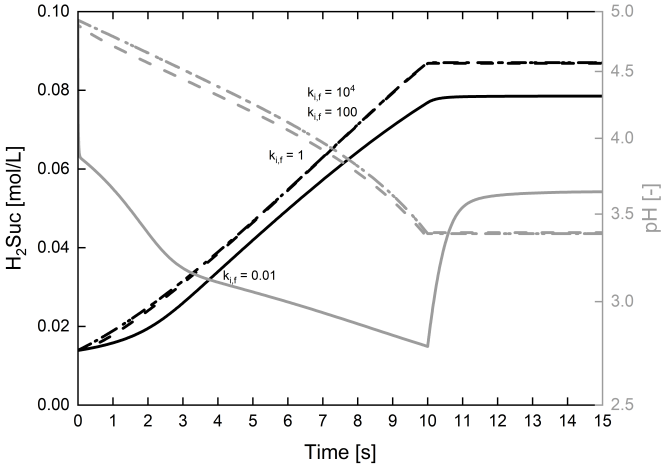

(a) Species distribution during electrolysis pulse for $10\,\mathrm{s}$. Beforehand $2000\,\mathrm{s}$ were simulated to ensure the electrolysis to start from equilibrium.

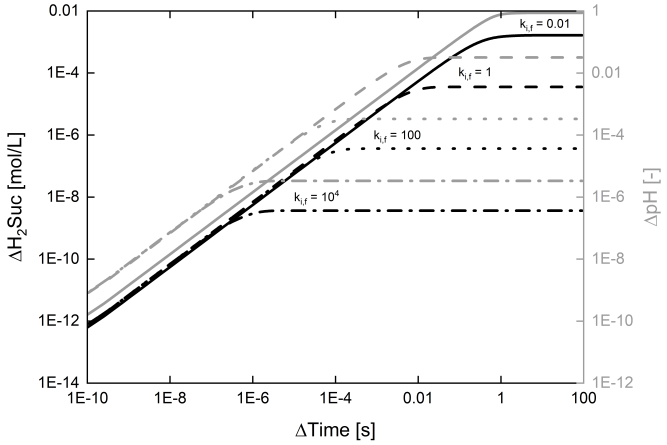

(b) log-log representation of the remaining deviation after the electrolysis pulse. pH refers to the endpoint of the $10\,\mathrm{s}$ pulse.

Figure 5.5.: Sensitivity of different forward dissociation rates $k_{i,f}$ on the final equilibrium pH (a) and the deflection from equilibrium during electrolysis (b) after the application of a $10\,\mathrm{s}$ pH-shift electrolysis pulse of $10\,000\,\mathrm{A\,m^{-2}}$.

5.4. Model extension for selectivity

The statistical analysis presented in chapter 3 revealed a significant effect of the electrolyte concentration on the extraction yield. Although the effect was found to be most prevalent for Cl^- the negative impact of high anion concentrations was reported for other ions as well [55, 102, 54]. In this thesis, sodium sulfate is used as a model component to represent the ionic load typically found in fermentation broths appendix F.0.1.

Although the extraction of inorganic anions from acidic solutions with TOA is known [173] the exact mechanism is not completely understood, yet. In principle, two binding mechanisms are plausible as presented in fig. 5.6.

Both mechanisms would be in line with the observed trend, that acidic conditions are required for the sulfate extraction to start. As the ionic complexation is known from metal extraction applications the mechanism suggested by [55] is selected for modeling the sulfate extraction in this work. First, the equilibrium conditions for the protonation of the amine and the extraction of sulfate species with protonated forms of the amine are added.

$$[\overline{TOAH^+}]_{bl,sol} = K_n \cdot [\overline{TOA_{free}}] \cdot [H^+] \tag{5.59}$$

$$[\overline{TOAH^+ \cdot SO_4^{2-}}]_{bl,sol} = K_{salt} \cdot [\overline{TOAH^+}] \cdot [SO_4^{2-}] \tag{5.60}$$

In addition to the molar extraction flow rate of succinic acid, the extraction rate for sulfate extraction,

$$\dot{n}_{Ex,SO_4^{2-}} = A_{Ex} \cdot k_{Ex,SO4} \cdot ([\overline{TOAH^+ \cdot SO_4^{2-}}]_{bl,sol} - [\overline{TOAH^+ \cdot SO_4^{2-}}]_{bulk,sol}) \tag{5.61}$$

and the protonation of the amine is added to the set of constitutive equations.

$$\dot{n}_{Ex,H^+} = A_{Ex} \cdot k_{Ex,TOA-H} \cdot ([\overline{TOAH^+}]_{bl,sol} - [\overline{TOAH^+}]_{bulk,sol}) \tag{5.62}$$

With this modification, the amount of free amine becomes the basis for

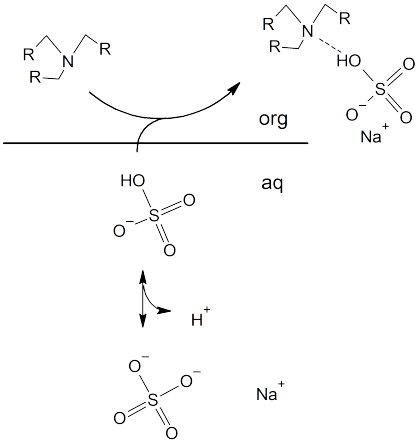

(a) Extraction of hydrogen sulfate by proton transfer complexation as proposed by [102]

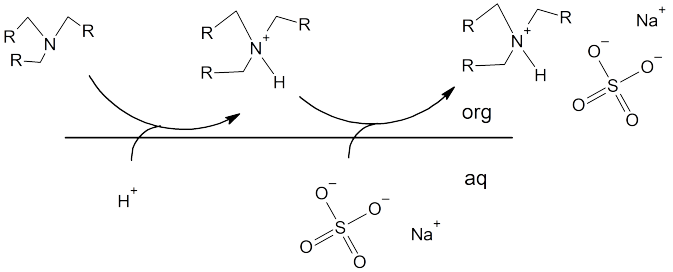

(b) Extraction of sulfate by ionic complexation as proposed by [55]

Figure 5.6.: Possible extraction mechanisms for the extraction of sulfate species with TOA.

the calculation of the kinetic driving force. It is obtained from the mass balance for all TOA species according to:

$$[\overline{TOA_{Total}}] = [\overline{TOA_{free}}]+[\overline{TOA \cdot H_2SA}]+[\overline{TOAH^+ \cdot SO_4^{2-}}]+[\overline{TOAH^+}] \tag{5.63}$$

$$[\overline{TOA_{free}}] = \frac{[\overline{TOA_{Total}}]}{1 + K_{ex} \cdot [H_2SA] + K_n \cdot [H^+](K_{salt} \cdot [SO_4^{2-}] + 1)} \tag{5.64}$$

The differential mass balance equations for each species are adjusted accordingly.

$$\begin{aligned}\frac{d[H_2SO_4]}{dt} = &-k_{61,f}[H_2SO_4] + k_{61,b}[H^+][HSO_4^-] + \\ &\frac{\dot{S}}{V_{col,aq}}[H_2SO_4]_S - \frac{\dot{R}}{V_{col,aq}}[H_2SO_4]\end{aligned} \tag{5.65}$$

$$\begin{aligned}\frac{d[HSO_4^-]}{dt} = &\, k_{61,f}[H_2SO_4] - k_{61,b}[H^+][HSO_4^-] - \\ &k_{62,f}[HSO_4^-] + k_{62,b}[H^+][SO_4^{2-}] \\ &+ \frac{\dot{S}}{V_{col,aq}}[HSO_4^-]_S - \frac{\dot{R}}{V_{col,aq}}[HSO_4^-]\end{aligned} \tag{5.66}$$

$$\begin{aligned}\frac{d[SO_4^{2-}]}{dt} = &\, k_{62,f}[HSO_4^-] - k_{62,b}[H^+][SO_4^{2-}] - \frac{1}{V_{aq}}\dot{n}_{Ex,SO_4^{2-}} \\ &+ \frac{\dot{S}}{V_{col,aq}}[SO_4^{2-}]_S - \frac{\dot{R}}{V_{col,aq}}[SO_4^{2-}]\end{aligned} \tag{5.67}$$

Organic phase with TOA protonation and sulfate extraction:

$$\frac{d[TOA]}{dt} = -\frac{1}{V_{sol}}\dot{n}_{Ex,H_2Suc} - \frac{1}{V_{sol}}\dot{n}_{Ex,H^+} + \frac{\dot{L}}{V_{sol}}[TOA]_L - \frac{\dot{K}}{V_{sol}}[TOA] \tag{5.68}$$

$$\frac{d[TOAH^+]}{dt} = \frac{1}{V_{sol}}\dot{n}_{Ex,H^+} + \frac{\dot{L}}{V_{sol}}[TOAH^+]_L - \frac{\dot{K}}{V_{sol}}[TOAH^+] \tag{5.69}$$

$$\frac{d[SO_4^{2-}]_{sol}}{dt} = \frac{1}{V_{sol}}\dot{n}_{Ex,SO_4^{2-}} + \frac{\dot{L}}{V_{sol}}[SO_4^{2-}]_L - \frac{\dot{K}}{V_{sol}}[SO_4^{2-}] \tag{5.70}$$

The extended set of equations now enables accounting for the competitive protonation of the amine and the co-extraction of sulfate species, once acidic pH values of the aqueous phase cause the protonation of the amine. The phase interface area is the last variable to be determined in order to calculate the molar flow rates. It is calculated from the volume

of the organic phase V and the Sauter mean diameter d_{32}. The extraction mechanism for sulfate implemented in the model assumes that overall hydrogen sulfate is extracted. In order to maintain a neutral charge balance of the organic phase the co-extraction of cations is inevitable. This implication should be validated in future experiments.

$$A_{Ex} = \frac{6V_{sol}}{d_{32}} \tag{5.71}$$

5.5. Experimental methods for model validation

In this section, the previously presented model for the pH-shift electrolysis and the reactive extraction of succinic acid under consideration of the weak acid equilibria of succinic and sulfuric acid is validated by comparison to experimental data. First of all, the pH-dependent extraction equilibrium of TOA and succinic acid is measured by titration and simulated cross-flow experiments.

5.5.1. pH dependent extraction equilibrium

As highlighted in chapter 3 the liquid-liquid extraction equilibrium of succinic acid is highly pH dependent. The pH reversible complexation is an elemental aspect of the successful implementation of electrochemically driven pH-swing extraction processes. A dispersion titration method was developed to study the extraction equilibrium in the pH range of interest.

Titration Extraction

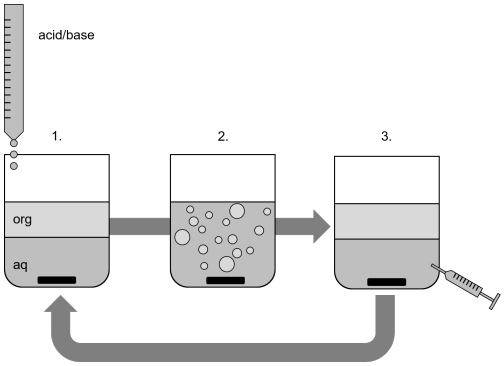

Figure 5.7.: Experimental procedure for dispersion titration.

The dispersion titration enables the recording of the LLE for the reactive extraction of succinic acid over a wide pH range in one experimental run. This is especially useful if dissociating background electrolytes are present. A schematic illustration of the experimental procedure is shown in fig. 5.7. An aqueous solution containing $35\,\mathrm{g\,L^{-1}}$ succinic acid and $0.5\,\mathrm{M}$ Na_2SO_4 was prepared. For the extraction experiments NaOH was added in an equimolar amount to the succinic acid to the solution. $60\,\mathrm{mL}$ of this solution was filled in a beaker and the extractant was added. The extractant was constituted by TOA and diluent (eg. 1-octanol) at a mass ratio of 1:1. The amount of the extractant was selected such that a molar surplus of TOA compared to succinic acid was maintained in order to avoid loading limited conditions in the extraction. The titration was conducted using $2\,\mathrm{M}$ sulfuric acid supplemented with $35\,\mathrm{g\,L^{-1}}$ of succinic acid for the extraction and $3\,\mathrm{M}$ sodium hydroxide supplemented with $35\,\mathrm{g\,L^{-1}}$ for the back-extraction. The supplementation of succinic acid to the acid and base used for the titration prevents the dilution of the aqueous phase over the course of the experiment. The samples drawn from the aqueous phase were used to calculate the extracted amount of succinic acid from the overall mass balance. In the extraction experi-

Table 5.3.: Experiment parameters LLE-experiments

	Extraction		Back-Extraction	
Set-No.	**initial pH**	n_{TOA}:n_{H2Suc}	**initial pH**	n_{TOA}:n_{H2Suc}
1	12	1.6	2.6	1.6
2	12	1.2	2.6	1.2

ments, the titration was stopped at a pH of approximately 3. After the last sample was drawn in the titration, a back-extraction was performed by adding sufficient sodium hydroxide to shift the pH to above 12. This enabled us to confirm the data calculated from the mass balance after each titration step by checking the overall mass balance. All experiments were carried out at an ambient temperature of 25 °C ± 2. Two sets of LLE measurements were conducted (table 5.3) and each set was repeated in a duplicate in order to minimize experimental error. Each sample was measured twice in the HPLC by the method described in table G.4.

Cross-flow extraction

Five-stage cross-flow extraction experiments were used to determine the maximally feasible recovery of succinic acid in a multi-stage extraction. In each stage, the aqueous phase from the previous stage is mixed with fresh solvent. This enables tracking the pH-shift during each stage of extraction fig. 5.8

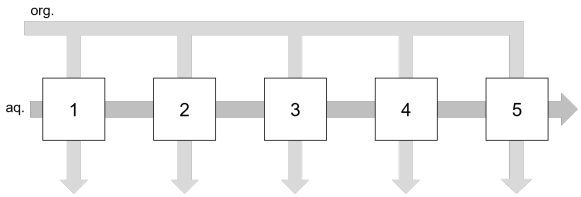

Figure 5.8.: Cross flow extraction scheme. In each stage, the aqueous phase (dark grey) is mixed with a fresh solvent (light grey) and brought into equilibrium by thorough mixing followed by phase separation.

Table 5.4.: Characteristic parameters for cross-flow-extraction experiments

Exp.-No.	**initial pH**	$n_{H_2SA} : n_{Na_2SA}$	$Na_2SO_4 mol\,L^{-1}$
CFE-06	2.6	100:0	0.5
CFE-03	4.6	50:50	0.5
CFE-04	7.7	0:100	0.5
CFE-07	2.6	100:0	0
CFE-08	4.6	50:50	0
CFE-05	7.7	0:100	0

The same succinic acid concentration $35\,g\,L^{-1}$ as used in the titration experiments was applied. Three different initial pH values were set by adjusting the ratio between succinic acid and sodium succinate. In order to test the effect of background electrolyte each pH set was recorded with 0.5 M and without 0 M Na_2SO_4 as stated in table 5.4. 70 g of aqueous succinic acid solution were mixed with 26 g solvent (TOA and 1-octanol 1:1) in a 100 mL glass separating funnel for 30 min and afterwards separated by sedimentation. Samples were drawn from the aqueous phase and pH and temperature were recorded. The aqueous phase was then used for the next stage of the cross-flow extraction. Using this setting, a molar surplus of at least 1.6 TOA over succinic acid was maintained in all stages. The organic phase from each stage was collected for a final back-extraction by 70 g of 3 M NaOH to check the mass balance of the

extraction. The values are reported as average from duplicates.

Results of titration experiments

The titration experiments revealed details of the pH dependency of the liquid-liquid extraction equilibrium as displayed in fig. 5.9. At neutral pH, no succinic acid is extracted into the organic phase. Once the pH is lowered, the extraction begins at pH values below 6. The extraction yield reaches a maximum at around pH 4.4 and decreases again in the acidic region. While the extraction shows a strong dependence on the aqueous pH, no significant difference is observed for different molar ratios between succinic acid and TOA fig. 5.9. The calculated yield of 42 %-52 % is in line with the values reported by Kurzrock et al. [44] for electrolyte-containing solutions.

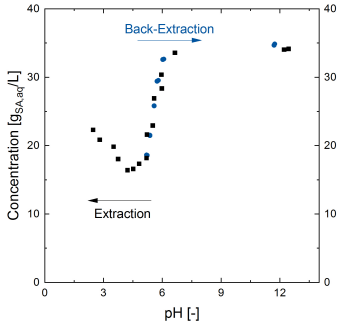

(a) Concentration in the aqueous phase

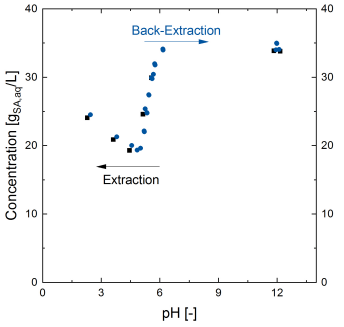

(b) Concentration in the aqueous phase

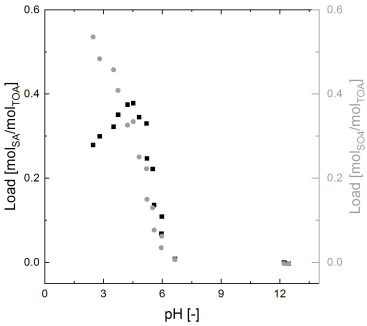

(c) Loading of the solvent

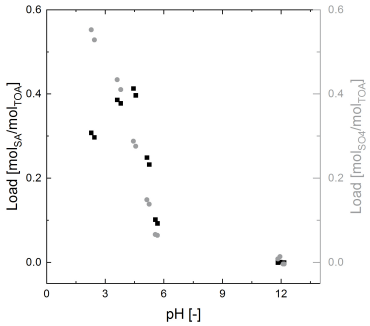

(d) Loading of the solvent

Figure 5.9.: The pH-dependent LLE is independent of the molar surplus of TOA. 1.2:1 (a,c) and 1.6:1 (b,d).

While the extraction of succinic acid is reversed at low pH values, the extraction of sulfate species continues. This is strong evidence that the sulfate species is preferred at low pH over the extraction of succinic acid. Consequently lowering the pH will not always yield more succinic acid extraction but increase the unwanted extraction of sulfate. The findings are in line with the mass-action law proposed in chapter 3. The displace-

ment of succinic acid from the organic phase at low pH is the result of two mechanisms acting against the desired succinic acid concentration. At low pH values, more TOA molecules become protonated, while succinic acid is practically completely protonated at pH values below 3. As a result, the protonated form of TOA and the protonated form of succinic acid cannot form the hydrogen-bond-based complexes necessary for the extraction. However, the protonated form of the TOA can form ionic complexes with anionic species e.g. sulfate. The results demonstrate that in order to achieve efficient utilization of protons in reactive extraction, the operational pH must be carefully controlled. It is likely that the best performance can be achieved within a certain pH range between 4 and 6 instead of the commonly propagated acidic regions [23]. The recorded data for the liquid-liquid equilibrium is used to obtain the equilibrium constant for TOA protonation K_n, and the equilibrium constants for succinic acid K_{Ex} and sulfate extraction $K_{\mathrm{SO}_{42}^{-}}$. Figure 5.10 shows the fitting results obtained for the equilibrium constants and the degree of protonation for succinic acid and TOA calculated from the equilibrium constants.

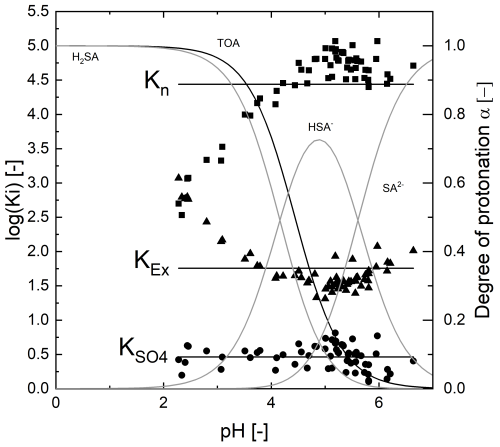

Figure 5.10.: Data points from titration experiments fig. 5.9 used to fit Kn, K_{Ex} and $K_{SO_4^{2-}}$.

Below an aqueous pH of 4 a deviation of K_{Ex} and K_n from the fitted value is observed. This deviation begins with the depletion of succinate ions. It could be caused by the interaction of protonated TOA and hydrogen succinate, which are simultaneously present between pH 4 and pH 6. The ionic complexation of hydrogen succinate by protonated TOA would be indistinguishable from the hydrogen-bond-based complexation of fully protonated succinic acid with TOA. An operation at acidic pH values is outside the focus of this work and most likely not desirable. For this reason, the obtained values are considered to be accurate within the targeted operational conditions. Nonetheless, resolving the underlying mechanisms that cause the deviation of the equilibrium constants at low values of the aqueous phase could be the objective of future fundamentals-oriented studies.

The obtained equilibrium constants were used to parameterize the competing sulfate extraction in the implemented model. This enables the model-based analysis of operational conditions for the reactive extraction of succinic acid with a competing extraction of sulfate species.

5.5.2. pH-shift Electrolysis

In order to assess the validity of the derived model pH-shift electrolysis experiments were executed and the results were compared with the results from the model. A 100 cm electrolysis cell with an electrolyte gap of 14 mm was operated in galvanostatic mode with 15 A. A more detailed description of the cell and the experimental setup is given in the application note chapter 8. The aqueous feed solution contained the equivalent of $35\,\mathrm{g\,L^{-1}}$ succinic acid adjusted to neutral pH with sodium as the cation. The required residence time to obtain complete protonation was calculated with faraday's law. From this set-point, the residence time was varied by $\pm 50\,\%$. In addition, an increased background electrolyte concentration of $0.5\,\mathrm{M}$ Na_2SO_4 was tested at the initial residence time.

5.6. Model validation with experimental results

5.6.1. pH-shift Extraction

The results from the cross-flow extraction experiments were compared with the results predicted by modeling the same conditions. Figure 5.11 presents the course of the succinic acid concentration and pH at the equilibrium of each stage. With the extraction of succinic acid, the pH of the aqueous phase raises. The modeling results for sulfate concentration and pH are well in line with the experimental data. The prevention of succinic acid extraction at elevated pH is well represented by the model. At lower pH values the succinic acid extraction is overestimated in cases where sulfate is present and underestimated for electrolyte-free conditions. This is likely caused by the deviation of the extraction constant from its original value, which causes a larger error at low pH conditions. However, these conditions would be below the desired operational pH for the succinic acid extraction which is 4.5. The model is therefore regarded to be sufficiently accurate in the operational region of interest.

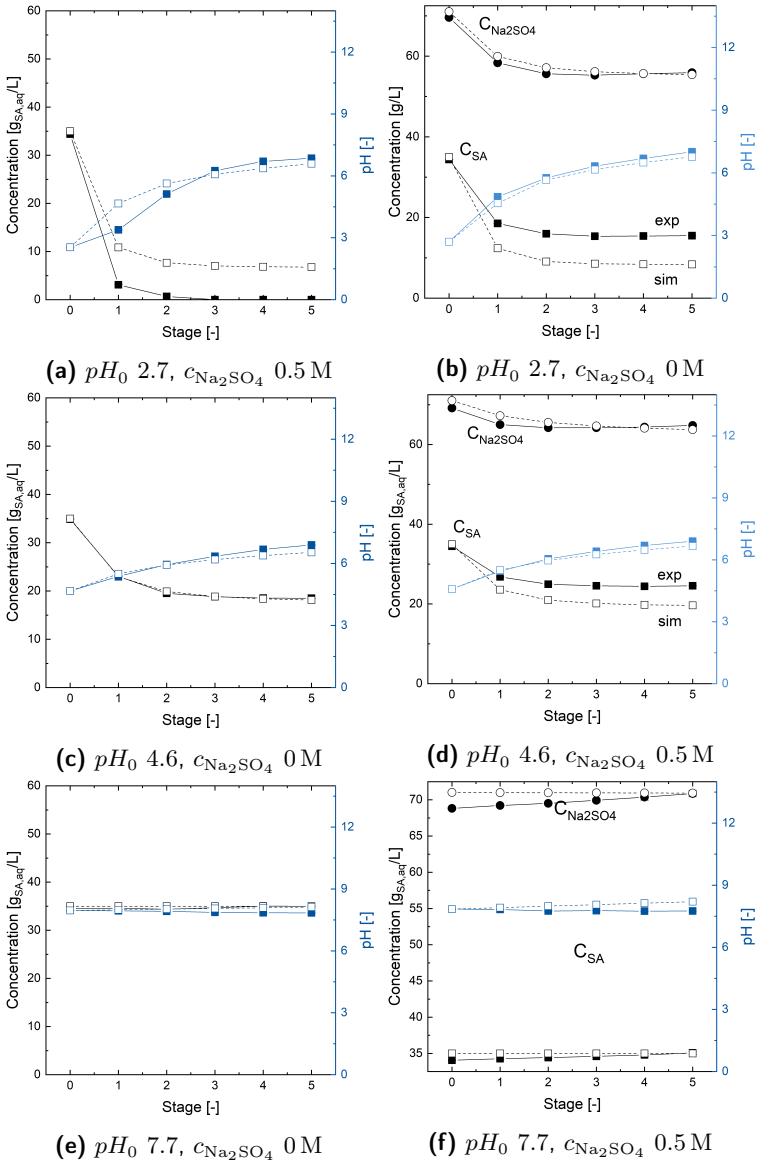

(a) pH_0 2.7, $c_{Na_2SO_4}$ 0.5 M **(b)** pH_0 2.7, $c_{Na_2SO_4}$ 0 M

(c) pH_0 4.6, $c_{Na_2SO_4}$ 0 M **(d)** pH_0 4.6, $c_{Na_2SO_4}$ 0.5 M

(e) pH_0 7.7, $c_{Na_2SO_4}$ 0 M **(f)** pH_0 7.7, $c_{Na_2SO_4}$ 0.5 M

Figure 5.11.: Concentration of succinic acid during cross-flow extraction without (a,c,e) and with(b,d,f) background electrolyte. Dashed lines show modeling results.

5.6.2. pH-shift Electrolysis

In fig. 5.12 the course of the pH in the electrolysis experiments is compared with the modeling results. The comparison was made without further tuning of the model parameters. After the run-in time, the pH of the anolyte calculated by the model is well in line with the experimental data. The pH of the catholyte is systematically overestimated by the model. The negligence of the water migration with the sodium ions may be a reason for this mismatch. For the over-protonation case, no simulation data is available as the simulation failed to converge with these settings.

Besides the pH, the calculated and measured degree of protonation as well as the cell voltage were compared. Figure 5.13 displays the results. The results calculated for the cell voltage at the reference set-point are close to the experimentally observed value. In the case of under-protonation and increased electrolyte concentration, the cell voltage is underestimated. The over-protonation did not achieve a stable operation as visible by the sharp increase of the cell voltage at 30 min run time. The maximal deviation observed in the calculated cell voltage was 29 % in the under-protonation case. For the reference set-point, the deviation in the cell voltage was around 4 % which is remarkably low taking into account that non-idealities were neglected in the model. It is therefore concluded that the derived model yields valid results at the technically desired operating point. The quantitative accuracy outside this region may be lower.

5.7. Model-based identification of inefficiencies

The validated model is used to analyze the sensitivity of operational parameters on the separation efficiency and the specific energy consumption. This enables the identification of desired operational conditions and potential sources of inefficiencies. The best performance is

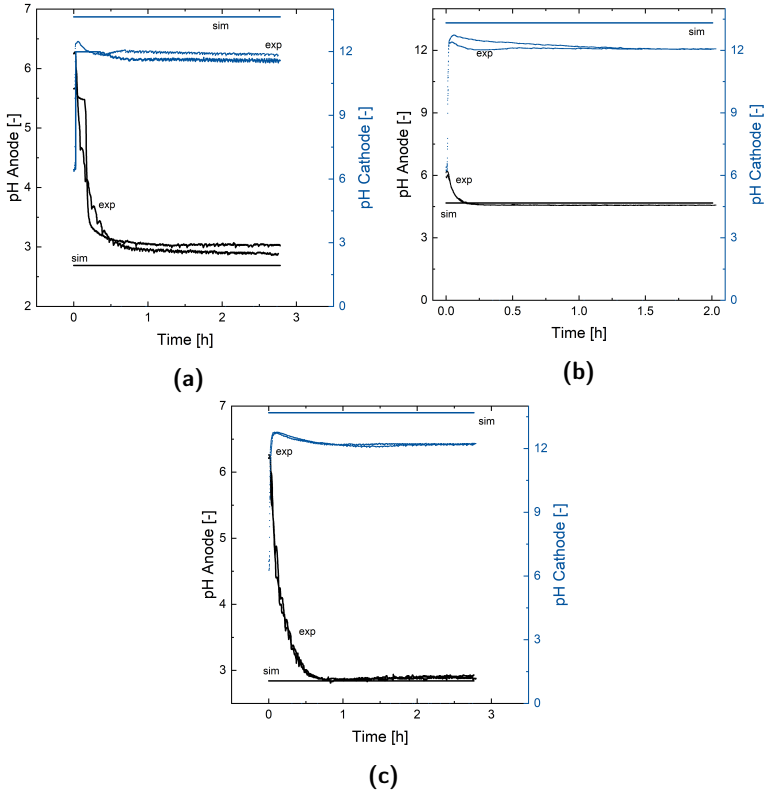

Figure 5.12.: Comparison of modeling results for the pH at the anode (black) and cathode (blue). Horizontal lines indicate the resulting pH value calculated by the model. (a) Reference setpoint, (b) under-protonation, (c) increased background electrolyte of $0.5\,\mathrm{M}$.

expected when all protons produced in the electrolysis yield completely protonated succinic acid which is also extracted in most parts. Any loss of protons or incomplete protonation would reduce the efficiency eventually. This idea leads to the concept of proton flux unity which is illustrated in fig. 5.14. The molar flux of succinic acid in the feed stream (dashed arrows) requires a certain flux of protons to become completely

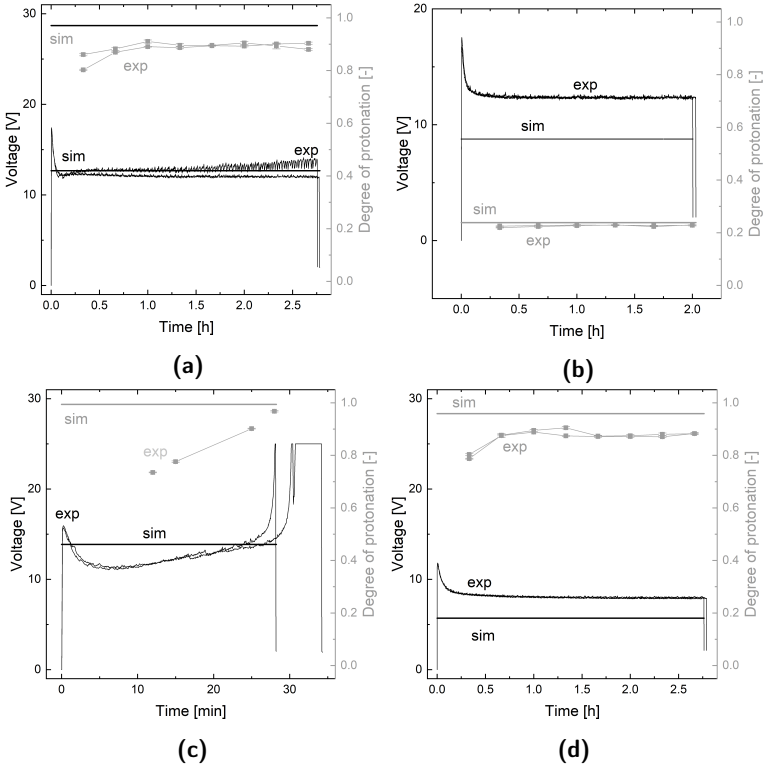

Figure 5.13.: Comparison of modeling results for the cell voltage and degree of protonation with experimental values. (a) Reference setpoint, (b) under-protonation, (c) over-protonation, (d) increased background electrolyte of 0.5 M.

protonated ($\alpha = 1$). The formulation in terms of flux $\mathrm{mol\,m^{-2}\,s^{-1}}$ instead of flow $\mathrm{mol\,s^{-1}}$ is preferred, since the kinetic properties of the electrolysis and extraction are largely determined by the active surface area. In addition, the electrode area and current density, which are important design measures for the electrolysis are thereby explicitly obtained.

Each proton produced by the electrolytic water splitting reaction

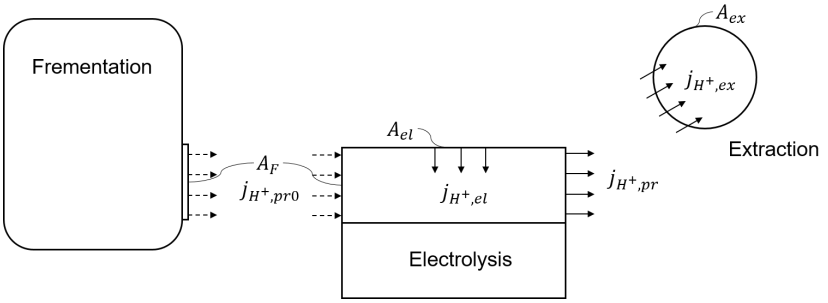

Figure 5.14.: Illustration of the proton flux model. Arrows indicate the flux of protons with succinic acid through the pH-shift electrolysis and reactive extraction. Dashed arrows indicate required protons to achieve complete protonation of the fermentation product.

should yield protonated succinic acid:

$$\dot{n}_{H^+,el} = \dot{n}_{H^+,pr} \tag{5.72}$$

which yields the following expression when reformulated in terms of molar flux:

$$\dot{n}_{H^+,el} = \frac{j\beta \cdot A_{el}}{zF} \tag{5.73}$$

$$\dot{n}_{H^+,pr} = \Delta\alpha c_0 \dot{V} \cdot 10^3 j_{H^+,pr} \tag{5.74}$$

$$= \Delta\alpha c_0 \frac{A_{el} h}{\tau} \cdot 10^3 j_{H^+,pr} \tag{5.75}$$

Thereof the first proton flux unity number Ju_I is formulated:

$$Ju_I = \frac{\tau_{el} j \beta}{\Delta \alpha c_0 h z F \cdot 10^3} \tag{5.76}$$

$$Ju_I = \begin{cases} > 1 : \text{Overprotonation} \\ = 1 : \text{Desired operational condition} \\ < 1 : \text{Insufficient protonation} \end{cases} \tag{5.77}$$

The proton flux unity number Ju_I can be regarded as the ratio of the proton flux from electrolysis and the convective flux of protons carried along the electrode with the succinic acid. Equation (5.76) indicates that the residence time of the electrolyte τ_{el} is a crucial operational parameter that must be controlled carefully, as concentration c_0, cell gap h and current density j are likely fixed by external boundary conditions. As a consequence, deviations from the optimal residence time are expected to lower the efficiency of the electrolytic pH-shift.

The optimal residence time τ_{el}^* for given operational conditions can be calculated with eq. (5.76). The dimensionless residence time θ is then calculated as follows:

$$\theta = \frac{\tau_{el}}{\tau_{el}^*} \tag{5.78}$$

The model-based approach now enables to study of the sensitivity of key performance indicators like the specific energy consumption, the electrochemical efficiency of protonation and extraction, and the cell voltage towards variations in the residence time. Figure 5.15 displays the results of this sensitivity study.

In general, an operation close to the $\theta = 1$ set-point is expected to yield the best results. The lowest specific energy consumption for protonation is found just below this set-point fig. 5.15 (a). At lower residence time the electrolytic pH-shift is insufficient to yield adequate protonation results. At higher residence times the specific energy demand increases

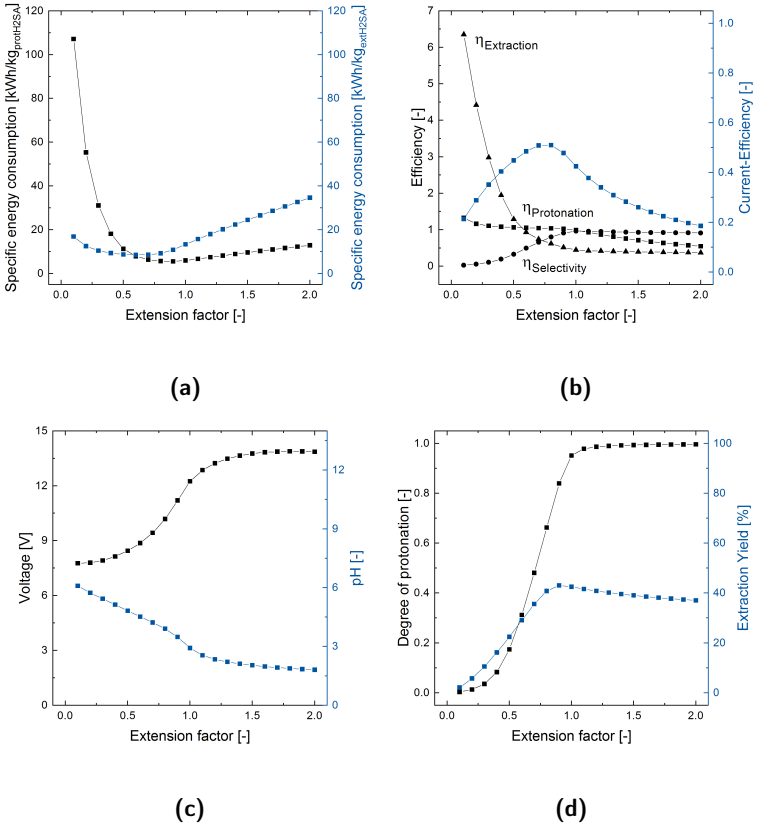

Figure 5.15.: Influence of a variation of the residence time from its optimal set-point.

again. This is mainly caused by the sharp increase of the cell voltage when approaching complete protonation fig. 5.15 (c).

The same trend is observed when analyzing the efficiencies of the electrochemical pH-shift extraction. The protonation efficiency η_{prot} indicates the fraction of the protons produced in the water electrolysis that causes a shift of the dissociation equilibrium of succinic or sulfuric acid.

$$\eta_{prot} = \frac{\dot{n}_{H^+ \rightarrow prot}}{\dot{n}_{e^-}} \tag{5.79}$$

Below the designated residence time, this number is close to 1 meaning that almost every proton produced in the electrolysis goes into the pH-shift. At higher residence times the succinic acid is completely protonated and additionally produced protons are lost by the effect known as "proton poisoning" [29]. When reaching the point of complete protonation, additionally produced protons accumulate in the anolyte. As the specific ionic conductivity correlates with the ion concentration, the fraction of the electric charge transported by proton conduction increases. Below an anodic pH of 3, the proton conductivity dominates over the conductivity contributed by the sodium ions. Operation in that region should be avoided in order to minimize the loss of protons.

Another potential source of proton losses are competing dissociation reactions. In this case, the sulfuric acid dissociation may compete with the succinic acid for protons at low pH values. Protons that are trapped by another dissociation reaction are not lost but lower the efficiency of the electrolytic pH-shift, since more protons are required to obtain complete protonation. This effect accounts for the protonation selectivity $\eta_{sel,SA}$. The protonation efficiency relates the fraction of protons that go into the desired protonation of the succinic acid with all protons that cause a shift of the aqueous dissociation equilibrium of any acid present in the anolyte.

$$\eta_{sel,SA} = \frac{\dot{n}_{H^+ \rightarrow \mathrm{H_2SA}}}{\dot{n}_{H^+ \rightarrow prot}} \tag{5.80}$$

Figure 5.15 (B) shows that the highest selectivity is achieved within the buffer range of succinic acid just before complete protonation is reached. At this point 96 % of the produced protons are utilized for the pH-shift. At higher residence times the protonation of sulfuric acid begins and reduces the selectivity. However, the loss of protons to the sulfuric acid protonation is not as dominant as the loss of proton conduction over the membrane. Nonetheless, the extraction yields $\eta_{ex,SA}$

gets compromised by the competitive extraction of sulfate fig. 5.15 (d).

$$\eta_{ex,SA} = \frac{\dot{n}_{\mathrm{SA},ex}}{\dot{n}_{\mathrm{SA},in}} \tag{5.81}$$

Although the competitive sulfate extraction is undesirable a small amount of background electrolyte like sulfuric acid with an active buffer range just below that of succinic acid has the potential to prevent the loss of proton to the electrolytic conduction.

In order to evaluate the best overall operating point the efficiencies and selectivities are multiplied and yield the overall current efficiency η

$$\eta = \eta_{prot} \cdot \eta_{sel,SA} \cdot \eta_{ex,SA} \tag{5.82}$$

A maximum in the current efficiency indicates the best molecular utilization of the electric current. In addition with the specific energy demand the best set-point for θ is found just below one.

The specific energy demand strongly depends on the cell voltage. A major contributor to the overall cell voltage is the loss caused by the ohmic resistance eq. (5.12). High ion concentrations increase the conductivity of the electrolyte and thereby reduce the ohmic losses. Despite the negative impact on the selectivity and the extraction yield increased electrolyte concentration thus may improve the specific energy consumption of the electrolytic pH-shift. Figure 5.16 presents the effect of increased electrolyte concentration.

The specific energy consumption is drastically lowered with the presence of background electrolyte fig. 5.16 (a). The most significant decrease is found for concentrations of 0.1 to 0.2 $\mathrm{mol\,L^{-1}}$. At higher concentrations, no further improvement is observed. The decrease of the specific energy consumption is associated with the expected decrease of the cell voltage fig. 5.16 (b).

As expected, the addition of background electrolyte prevents the loss of protons to the electrolytic ion transport which can be seen by the increase of the protonation efficiency with increasing background electrolyte concentration fig. 5.16 (b). However, the protonation selectivity

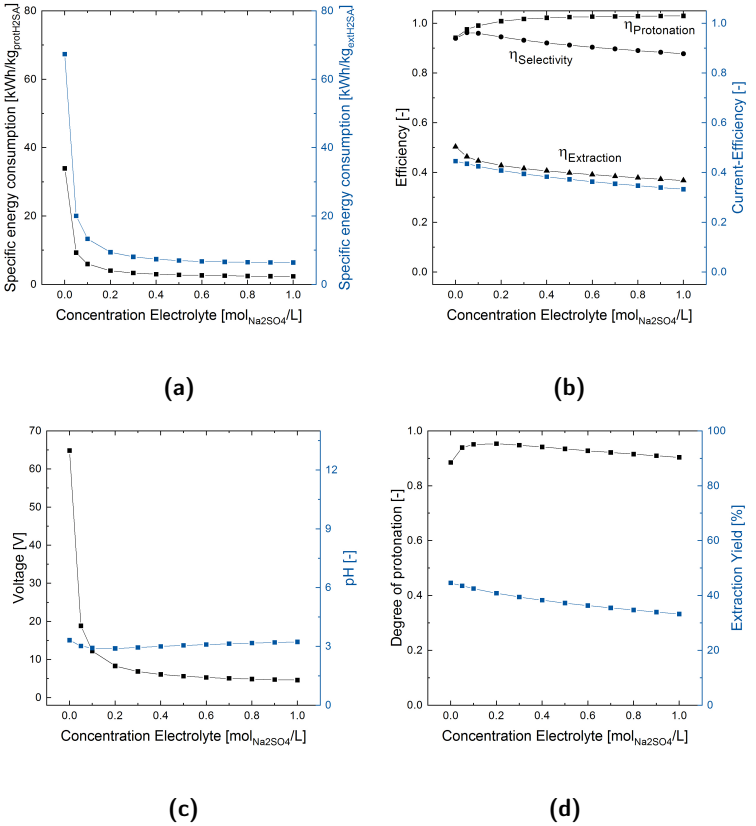

Figure 5.16.: Effect of the electrolyte concentration on the protonation and extraction performance for $\theta = 1$

is reduced with increasing electrolyte concentration. Beyond that, the extraction efficiency of succinic acid is reduced due to the competitive sulfate extraction. Because the extraction of sulfate also follows a mass action law, increasing sulfate concentration increases the competing sulfate extraction and thus shifts the competing extraction equilibrium towards an undesired direction.

5.8. Conclusion

In this chapter, a model-based approach for the pH-shift electrolysis and the pH-sensitive reactive extraction of succinic acid was presented. The model is based on a set of differential and algebraic equations describing the electrochemical properties, the dissociation reactions in the aqueous phase, and the reactive extraction equilibrium. The aqueous pH equilibrium is modeled by a dynamic approach which enables the straightforward implementation of additional weak acid species. In extension to a previous version, the important competitive extraction of sulfate species was parameterized and incorporated in the model and the updated model was compared to experimental data. The derived model was able to describe the pH-shift electrolysis and the pH-dependent extraction with satisfying accuracy in the region of interest. Deviations from the model predictions were observed at very acidic pH values. This is an indication that the extraction mechanism for the extraction of sulfate species deviates from the proposed mechanism at these conditions. A closer investigation of the competitive extraction behavior of sulfate species with TOA under these conditions would be beyond the scope of this thesis. But elucidating the extraction mechanism of sulfate species further may improve the understanding of the extraction mechanism of tertiary amines in the transition region where the complexation of a solute with the amine switches from a hydrogen bond-based mechanism to ionic complexation.

The derived model was used to identify inefficiencies that might increase the specific power consumption of the electrochemically driven pH-shift extraction. It was found that the best operational performance is achieved close to the point of complete protonation and that the residence time in the electrolysis cell must be well aligned with the electrochemical proton production in order to avoid the loss of proton to ion migration. A small concentration of background electrolyte was found to be beneficial as it reduces the cell voltage and thereby maintains a residual conductivity of the electrolyte when approaching complete protonation.

6. Model Aided Spatial Design and Identification of Limiting Conditions

The previous chapter highlighted the relevance of the operational conditions with regard to pH and background electrolyte concentration. However, the assumption of ideally mixing within the electrolysis cell likely holds only for laboratory- or small-scale electrolysis cells. Although gas formation promotes turbulence in the electrolyte gap and increases backmixing, the planar geometries of electrolysis cells make complete backmixing unlikely [174].

The objective of continuous pH-shift electrolysis is to obtain complete protonation at the outlet of the electrolysis cell. On the basis of the previous findings, it appears to be desirable if the point of complete protonation is reached only just before the end, to avoid the reduction of efficiency caused by overprotonation. On the contrary, turbulence promoters are often implemented in electrolysis cells to reduce mass transport limitations and improve the limiting current density [165].

In this chapter, the influence of the backmixing effect on the pH-shift electrolysis is analyzed by means of a numerical model with 1D spatial discretization in the flow direction. The degree of back-mixing is characterized by the dimensionless Bodenstein number, and both extremes of fluid flow patterns, the stirred tank and plug flow, are studied. The shape of spatial gradients in the pH and current distribution is evaluated with regard to potential inefficiencies such as proton crossover. The influence of cell length, electrolyte gap, and gas hold-up on the electrolysis performance is analyzed. A central design question that will be answered in this chapter is:

Which flow pattern is advantageous for ph-swing electrolysis: plug flow or high backmixing?

6.1. Flow Patterns in Reactor Modeling

The flow distribution in chemical reactors can be approximated with two limiting cases, the ideal plug flow reactor for operational conditions without backmixing and the stirred tank reactor for conditions with complete backmixing. [175] The flow pattern of real chemical reactors is often found to be a combination of both limiting cases. A characteristic measure is the residence time distribution $E(t)$. The residence-time distribution is obtained by measuring the time-dependent concentration of an inert tracer at the exit of the reactor.

$$E(t) = \frac{\dot{n}_{out}(t)}{n_{in,total}} = \frac{c_{out}(t)}{\int_0^\infty c_{out}(t)\ dt} \cong \frac{c_{out}(t)}{\sum_x c_{out,x} \cdot \Delta t_x} \tag{6.1}$$

The integral of the residence time distribution yields the cumulative residence time distribution $F(t)$, also referred to as the sum function of the residence time:

$$F(t) = \int_0^t E(t)\, dt \tag{6.2}$$

$$F(t) = \frac{n_{out}(t)}{n_{in,total}} = \frac{\int_0^t c_{out}(t)\ dt}{\int_0^\infty c_{out}(t)\ dt} \cong \frac{\sum_{x=0}^t c_{out,x} \cdot \Delta t_x}{\sum_x c_{out,x} \cdot \Delta t_x} \tag{6.3}$$

The residence time under ideal conditions is defined as $\tau = \frac{V}{\dot{V}}$. However, under non-ideal conditions the mean time of passage $\bar{t}$ is introduced to account for the effect of non-ideal flow distribution.

$$\bar{t} = \int_0^\infty t \cdot E(t)\ dt = \int_0^1 t \cdot F(t) = \frac{\int_0^\infty t \cdot c\ dt}{\int_0^\infty c\ dt} \cong \frac{\sum_x t_x \cdot c_x \cdot \Delta t_x}{\sum_x c_x \cdot \Delta t_x} \tag{6.4}$$

The spreading of the residence time distribution from a pulse experiment is characterized by the variance σ^2 of the concentration signal recorded

at the reactor exit.

$$\sigma^2 = \int_0^\infty (t - \bar{t})^2 \cdot E(t)\, dt = \frac{\int_0^\infty (t - \bar{t})^2 \cdot c\, dt}{\int_0^\infty c\, dt} \cong \frac{\sum_x (t_x - \bar{t})^2 \cdot c_x \cdot \Delta t_x}{\sum_x c_x \cdot \Delta t_x} \tag{6.5}$$

Transforming the variance calculated from the measured concentration data by division with the mean time of passage results in a normalized expression for the variance.

$$\sigma_\theta^2 = \sigma^2 / \bar{t}^2 \tag{6.6}$$

In principle there are two possible modeling approaches applicable for modeling deviations from ideal flow patterns in reactors: The axial dispersion model and the tank-in-series model. Both models allow for the consideration of non-ideal flow behavior, especially for back-mixing. The dispersion model superimposes an axial dispersion on the plug flow whose magnitude is characterized by the axial dispersion coefficient D_{ax}. When D_{ax} approaches infinity, the residence time distribution of the dispersion model approaches the residence time distribution of an ideally stirred tank reactor. This foundation makes the dispersion model well-suited to model flow conditions that are based on plug flow behavior. Such conditions are for example found for adsorption or chromatography processes where the dispersion model was very successfully applied [176].

The tank-in-series model, on the other hand, is composed of a cascade of equally sized stirred tanks. The degree of back-mixing is adjusted by the total number of tanks. Again, as the number of tanks approaches infinity, the resulting residence-time distribution becomes similar to the residence-time distribution of an ideal plug-flow reactor. Thus, both models are interchangeable to some extent. The dispersion model has the advantage that many flow correlations are directly applicable while the tanks-in-series model has the advantage that 2D or 3D compartment arrangements enable the modeling of spatially more complex flow patterns or the inclusion of recycle streams [175].

The relation between both models becomes apparent when taking into account that the Bodenstein number is often used to quantifiy the degree of back-mixing:

- No back-mixing, ideal plug flow: $Bo \rightarrow \infty$
- Completely mixed, ideal stirred tank reactor: $Bo \rightarrow 0$

Levenspiel and Smith derived a correlation between the Bodenstein number and the dimensionless variance [175].

$$\sigma_\theta^2 = \frac{2}{Bo} - \frac{2}{Bo^2} \cdot \left(1 - exp(-Bo)\right) \tag{6.7}$$

With the definition of the Bodenstein number:

$$Bo = \frac{u_{ax} \cdot L_{ax}}{D_{ax}} \tag{6.8}$$

where u_{ax} is the the fluid velocity in axial direction and L_{ax} is the axial tube length. Solving the correlation eq. (6.7) for Bo yields the equivalent value for D_{ax} for an experimentally determined or in this case simulated value of dimensionless variance.

The evolution of the gas is expected to impose a significant mixing on the electrolyte within the electrolysis cell [177] and accelerate the liquid phase due to the displacement of the volume. For that reason, the tank-in-series model is selected in this thesis. In addition to this, the tank-in-series model can be directly translatable to a finite-volume formulation of the mass transport within the electrolysis cell. Unlike the finite difference method and the finite element method, the finite volume method transforms partial differential equations of mass transport into discrete algebraic equations and formulates conservation laws over finite volumes [178]. The computational domain is discretized into finite control volumes, which means that each electrolysis chamber is divided into n_V control volumes fig. 6.1. The number of control volumes correlates

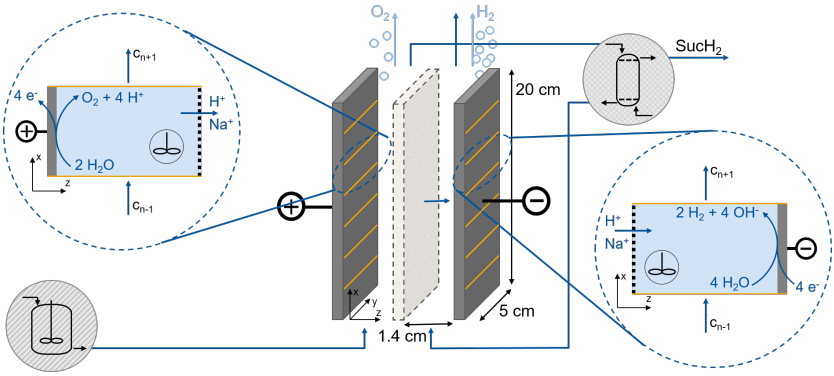

Figure 6.1.: Geometry and process interfaces of the modeled pH-shift electrolysis cell with indicated discretization in axial (x) direction.

with the degree of backmixing introduced; therefore, a sensitivity study must be performed to avoid a bias induced by the level of discretization.

6.2. Spatially Discretized Modeling of pH-Shift Electrolysis Cells

A finite volume method is used to solve the partial differential equations. The finite-volume method is based on conservation laws formulated for differential volumes, which transform the partial differential equation into discrete algebraic equations. The modeling domain is divided into equally sized, non-overlapping control volumes, as illustrated in fig. 6.2.

The peclet number Pe is an indicator of whether transport is dominated by convection or diffusion.

$$Pe = \frac{u \cdot \Delta x}{D} \tag{6.9}$$

If the Peclet number is lager than one, the transport is dominated by

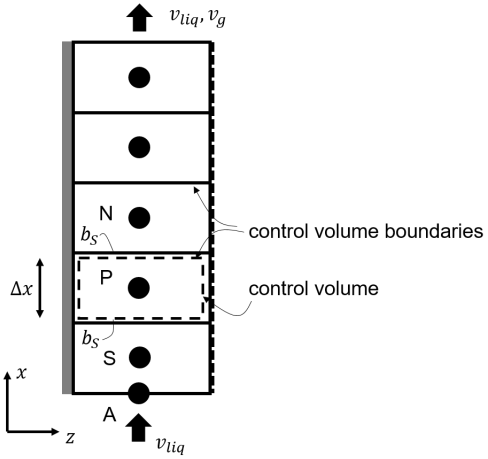

Figure 6.2.: Axial discretization into control volumes of a length Δx with a nodal grid point P and their neighboring control volumes S and N

convection. Taking into account the geometry of the cell, which is divided into up to 100 control volumes in axial direction, and considering the typical diffusivities for succinic acid and protons, a Peclet number greater than 100 is calculated. For this reason, diffusive fluxes are neglected in the following. The simplified electrolysis model is developed starting with a one-dimensional transport equation:

$$\frac{\partial(\rho\phi)}{\partial t} = -\frac{\partial}{\partial x}(\rho\phi u) + S_\phi \tag{6.10}$$

where ρ is the density that means molar mass per volume, $\rho\ \phi$ is the concentration with respect to molar mass, u is the velocity in the considered control volume.

The continuous equation is discretized by integration on a control volume (CV) which is then numerically approximated by ΔV.

$$\int_{CV} \frac{\partial(\rho\phi)}{\partial t}\ dV = -\int_{CV} \frac{\partial}{\partial x}(\rho\phi u)\ dV + \int_{CV} S_\phi\ dV \tag{6.11}$$

With the numerical approximation the respective terms are averaged over the control volume as indicated by the bars above the respective term.

$$\frac{\partial\overline{(\rho\phi)}}{\partial t}\,\Delta V = -\overline{\frac{\partial}{\partial x}(\rho\phi u)}\cdot A\cdot\Delta x + \bar{S}_\phi\,\Delta V \tag{6.12}$$

$$\frac{\partial\overline{(\rho\phi)_P}}{\partial t}\cdot V_P = (\rho\phi uA)_{b_S} - (\rho\phi uA)_{b_N} + \bar{S}_{\phi,P}\cdot V_P \tag{6.13}$$

The numerical approximation allocates the value of each cell to its center point. For this reason, the values at the interfaces, which define the entering (b_S) and leaving (b_N) convective flows, need to be approximated. In this work, the upwind scheme is used [179].

$$\frac{\partial\overline{(\rho\phi)_P}}{\partial t}\cdot V_P = (\rho uA)_{b_S}\phi_S - (\rho uA)_{b_N}\phi_P + \bar{S}_{\phi,P}\cdot V_P \tag{6.14}$$

Thereby the value at the boundaries is approximated by the center values of the neighbouring cells. Instead of the general transport property ϕ the molar concentration is of interest. Thus, the transport equation is formulated on a molar basis.

$$\frac{\partial\bar{c}_P}{\partial t}\cdot V_P = (uAc)_S - (uAc)_P + \bar{S}_{c,P}\cdot V_P \tag{6.15}$$

$$\frac{\partial\bar{n}_P}{\partial t} = \big(uAn/V\big)_S - \big(uAn/V\big)_P + \bar{S}_{n,P} \tag{6.16}$$

With the geometric relation between cell volume and interfacial area $V = A\cdot\Delta x$ the axial discretization is obtained.

$$\frac{\partial\bar{n}_P}{\partial t} = \frac{1}{\Delta x}\big(u_S\cdot n_S - u_P\cdot n_P\big) + \bar{S}_{n,P} \tag{6.17}$$

This results in the differential equation for the liquid phase:

$$\frac{\partial\bar{n}_P}{\partial t} = \frac{1}{\Delta x}\big(u_{l,S}\cdot n_{l,S} - u_{l,P}\cdot n_{l,P}\big) + \bar{S}_{n,P} \tag{6.18}$$

And the differential equation for the gas phase:

$$\frac{\partial \bar{n}_P}{\partial t} = \frac{1}{\Delta x}\left(u_{g,S} \cdot n_{g,S} - u_{g,P} \cdot n_{g,P}\right) + \bar{S}_{n,P} \tag{6.19}$$

Although the gas phase contains only one component, the liquid phase contains all of the constituents of pH equilibrium in the aqueous phase. In addition to the concentration, the change in the volume fraction of the gas- and liquid phases must be considered. The gas evolving from the electrolytic reaction displaces the liquid and thereby alters the velocity of the liquid phase.

Before the differential equation is solved, boundary conditions must be specified. Here, the following Dirichlet and Neumann conditions are set:
Dirichlet boundary conditions:

$$c_{\text{in,an}} = c_{\text{ferm}} \tag{6.20}$$

$$c_{\text{in,cat}} = c_{\text{out}*} \tag{6.21}$$

$$n_{\text{in,an,gas}} = 0 \tag{6.22}$$

$$n_{\text{in,cat,gas}} = 0 \tag{6.23}$$

As illustrated in fig. 6.1 the cathode feed concentration is assumed to have been depleted of succinic acid by reactive extraction. A reference case for fermentation with a succinic acid concentration of $0.66\,\text{mol}\,\text{L}^{-1}$ is taken as reported by Lee et al. [120]. Kurzrock et al. reported an extraction yield for succinic acid of 95 % [44, 139].

Neumann boundary conditions:

$$\frac{\partial c_{\mathrm{out,an}}}{\partial x} = 0 \quad \Rightarrow c_{\mathrm{n_V,an}} = c_{\mathrm{out,an}} \tag{6.24}$$

$$\frac{\partial c_{\mathrm{out,cat}}}{\partial x} = 0 \quad \Rightarrow c_{\mathrm{n_V,cat}} = c_{\mathrm{out,cat}} \tag{6.25}$$

$$\frac{\partial n_{\mathrm{out,an,gas}}}{\partial x} = 0 \quad \Rightarrow n_{\mathrm{n_V,an,gas}} = n_{\mathrm{out,an,gas}} \tag{6.26}$$

$$\frac{\partial n_{\mathrm{out,cat,gas}}}{\partial x} = 0 \quad \Rightarrow n_{\mathrm{n_V,cat,gas}} = n_{\mathrm{out,cat,gas}} \tag{6.27}$$

The dissociation equilibrium is calculated as presented in chapter 5. Because a multicomponent system is considered, the differential equation eq. (6.17) must be solved for each species individually. It is therefore transformed into vector notation.

$$\frac{\partial \bar{n}_{k,j}}{\partial t} = \frac{1}{\Delta x} \cdot \left(u_{j-1} \cdot n_{k,j-1} - u_j \cdot n_{k,j} \right) + \bar{S}_{k,j} \tag{6.28}$$

with $k = 1, ..., n_S$ indicating all species and $j = 1, .., n_V$ defining the control volumes.

$$\frac{\partial \bar{\boldsymbol{n}}_{\boldsymbol{k}}}{\partial \boldsymbol{t}} = \boldsymbol{A}_{\mathbf{conv}} \cdot \boldsymbol{n}_{\boldsymbol{k}} + \boldsymbol{b}_{\mathbf{conv}} + \bar{\boldsymbol{S}}_{\boldsymbol{k}} \tag{6.29}$$

with $\frac{\partial \bar{n}_{k,j}}{\partial t}$, $\boldsymbol{n_k}$, $\boldsymbol{b_{conv}}$, and $\bar{\boldsymbol{S}}_{\boldsymbol{k}}$ as vectors of the size $\mathbb{R}^{(n_V \times 1)}$ with each element accounting to a control volume and representing the component k. The matrix $\boldsymbol{A}_{\mathbf{conv}}$ has the size $\mathbb{R}^{(n_V \times n_V)}$ and defines the convection factors for each control volume. $\boldsymbol{b_{conv}}$ defines the concentration in the inlet flow. The gas evolution displaces the liquid in each control volume and reduces the free cross-sectional area for the liquid flow. Accordingly the velocity of the liquid phase changes with the gas hold-up.

The convection term in matrix form is for a component in the elec-

trolyte specified by:

$$\boldsymbol{A}_{\mathbf{conv}} \cdot \boldsymbol{c}_{\boldsymbol{k}} + \boldsymbol{b}_{\mathbf{conv}} = \tag{6.30}$$

$$= \frac{1}{\Delta x} \cdot \begin{pmatrix} -1 & 0 & 0 & \dots & 0 & 0 \\ 1 & -1 & 0 & \dots & 0 & 0 \\ 0 & 1 & -1 & \dots & 0 & 0 \\ 0 & 0 & 1 & \dots & 0 & 0 \\ \vdots & \vdots & \vdots & \ddots & \vdots & \vdots \\ 0 & 0 & 0 & \dots & 1 & -1 \end{pmatrix} \cdot \begin{pmatrix} u_1 \cdot n_{\mathrm{k},1} \\ u_2 \cdot n_{\mathrm{k},2} \\ u_3 \cdot n_{\mathrm{k},3} \\ \vdots \\ u_{n_V-1} \cdot n_{\mathrm{k},\mathrm{n_V}-1} \\ u_{n_V} \cdot n_{\mathrm{k},\mathrm{n_V}} \end{pmatrix} + V_{dot} \cdot \begin{pmatrix} c_{\mathrm{k,in}} \\ 0 \\ 0 \\ \vdots \\ 0 \\ 0 \end{pmatrix} \tag{6.31}$$

For the source and sink terms the vector notation follows accordingly:

$$\bar{\boldsymbol{S}}_{\boldsymbol{k}} = \begin{pmatrix} S_{\mathrm{k},1} \\ S_{\mathrm{k},2} \\ S_{\mathrm{k},3} \\ \vdots \\ S_{\mathrm{k},\mathrm{n_V}-2} \\ S_{\mathrm{k},\mathrm{n_V}-1} \end{pmatrix} \tag{6.32}$$

where each term is the sum of the changes induced by dissociation, electrolysis and ion migration over the membrane.

$$\bar{S}_{k,j} = \underbrace{\left(\frac{\partial c_{\mathrm{dissociation,k}}}{\partial t}\right)_j \cdot V_j}_{\text{dissociation}} + \underbrace{\left(\frac{\partial n_{\mathrm{electrolysis,k}}}{\partial t}\right)_j}_{\text{electrolysis } (H^+,\ OH^-,\ O_2 \text{ and } H_2)} - \underbrace{\left(\frac{\partial n_{\mathrm{membrane,total}}}{\partial t}\right)_j}_{\text{ion migration } (H^+ \text{ and } Na^+)} \tag{6.33}$$

Because a cation exchange membrane is considered, it is assumed that only H^+ and Na^+ ions migrate over the membrane. The migration of the membrane is calculated based on a charge balance approach as presented in chapter 5 and appendix F. The accumulation of gas in the control volumes creates a gas holdup in the electrolysis cell.

$$\epsilon_g = \frac{V_g}{V_g + V_l} = \frac{V_g}{V_{CV}} \tag{6.34}$$

The gas volume created by the electrolytic reaction is calculated with the ideal gas law:

$$V_g = \frac{n_g \cdot R \cdot T}{p_g} \tag{6.35}$$

For the gas velocity calculation a simplified swarm model is implemented. Regarding the average size of the gas bubbles formed during an electrolysis different values are found in the literature. Values ranging from 50 µm to 200 µm are reported [180, 181, 177, 182]. In the following a uniform bubble size of 200 µm is assumed. The stationary bubble velocity is calculated from the commonly known balance of the weight force F_G, buoyancy force F_B and resistance force F_R:

$$0 = -F_G + F_B - F_R \tag{6.36}$$

$$0 = -V_g \cdot g \cdot \rho_g + V_g \cdot g \cdot \rho_l - A_{ref} \cdot \zeta \cdot \frac{\rho_l \cdot u_g^2}{2} \tag{6.37}$$

$$0 = \frac{\pi}{6} \cdot d_g^3 \cdot g \cdot (\rho_l - \rho_g) - \frac{\pi}{8} \cdot d_g^2 \cdot \zeta \cdot \rho_l \cdot u_g^2 \tag{6.38}$$

$$u_{g,swarm} = \sqrt{\frac{4 \cdot d_g \cdot g \cdot (\rho_l - \rho_g)}{3 \cdot \rho_l \cdot \zeta_{swarm}}} \tag{6.39}$$

where $u_{g,swarm}$ is the velocity of the bubble, d_g the bubble diameter, g is the gravitational acceleration, ρ_g is the gaseous density of oxygen or hydrogen, respectively, ρ_l is the electrolyte density, which is approximated by the water density, and ζ is the drag coefficient.

The drag coefficient is calculated based on the Stokes' correlation. It should be noted that this may limit the accuracy of the hold-up model as the Reynold's number of a gas bubble in an electrolysis cell may be outside its validity range.

$$\zeta_{g,1} = \frac{24}{Re_g} \cdot \frac{\frac{2}{3} + \frac{\eta_g}{\eta_l}}{1 + \frac{\eta_g}{\eta_l}} \qquad \text{with} \quad \eta_g << \eta_l \quad \Rightarrow \quad \zeta_{g,1} = \frac{24}{Re_g} \cdot \frac{2}{3} = \frac{16}{Re_g} \tag{6.40}$$

Parisien et al. suggest a swarm correction for the drag coefficient,

which is applicable with gas hold-ups up to 66 %[183]:

$$\zeta_{g,swarm} = \zeta_{g,1} \cdot (1 - \epsilon_g) \cdot \left((1 - \epsilon_g)^{1.39} \cdot (1 + 2.55 \cdot \epsilon_g^3)\right)^{-2} \tag{6.41}$$

The bubble drag coefficient $\zeta_{g,swarm}$ is used to calculate the swarm velocity $u_{g,swarm}$ which is added to the velocity of the surrounding liquid u_l to yield the velocity of the gas phase u_g:

$$u_g = u_{g,swarm} + u_{l,0} \tag{6.42}$$

The velocity of the liquid is again calculated with the continuity law for incompressible fluids.

$$u_l = \frac{1}{A_l} \cdot \left(\dot{V}_{l,0} + \dot{V}_{\mathrm{g,acc}}\right) = \frac{1}{A_{CV} \cdot (1 - \epsilon_g)} \cdot \left(\dot{V}_{l,0} + \dot{V}_{\mathrm{g,acc}}\right) \tag{6.43}$$

$\dot{V}_{l,0}$ is the volumetric flow of the liquid. The accumulation of the gas phase $\dot{V}_{\mathrm{g,acc}}$, which displaces some of the liquid and thus changes the available cross-sectional area for liquid flow, is taken into account.

The implemented hold-up model is expected to have some limitations as experimental data for the bubble size distribution is rare and the assumption of uniform size distribution is unlikely to represent reality completely. Besides, the flow regime inside the cell is expected to be more complex and may cause effects that cannot be covered by a simplified 2D model. Those limitations must be taken into account in the quantitative interpretation of the modeling results.

6.3. Validation of Gas Hold-Up Model

The validity of the gas hold-up model implemented is verified by comparing with data from the literature [7, 184]. The results of the implemented hold-up model are in the same range compared to the hold-up data from literature fig. 6.4. Preliminary tests revealed a great sensitivity towards the assumed bubble size. In order to yield quantitatively accurate results this aspect should be given special attention. However,

a quantitatively accurate hold-up model is beyond the scope of this work and therefore the results are considered to have a satisfying accuracy for the desired investigations.

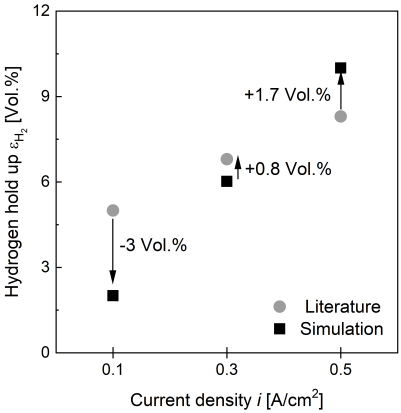

Figure 6.3.: Hydrogen hold up comparison with literature data from [7]; The respective absolute deviations are given in the diagram; Settings: i = 0.1 A/cm^2, 0.2 A/cm^2, 0.3 A/cm^2; L_{cell} = 30 cm; d_{gap} = 2 cm; B_{elec} = 1.5 cm; $\dot{V}$ = 1000 mL/min; τ_{id} = 0.09 min

6.4. Results and Discussion

The reference state of the simulation represents the electrolysis cell used in the experiments presented in chapter 5. The cell measures 20 cmx5 cm with an electrode distance of 28 mm. It was experimentally observed that the gas evolution caused a liquid displacement from the cell. Due to this liquid displacement a stable operation was limited to current densities of 0.15 A cm^{-1}. For all simulations a temperature of 25 °C and an atmospheric pressure of 1 bar is assumed.

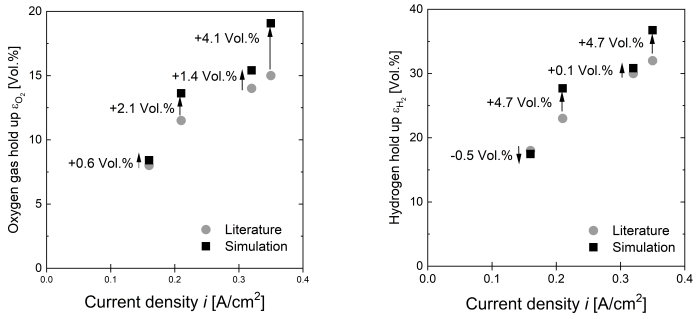

(a) Oxygen hold-up **(b)** Hydrogen hold-up

Figure 6.4.: Comparison of the implemented gas hold-up model with hold-up results from literature, Settings: $i = 0.16\,\mathrm{A/cm^2}$, $0.21\,\mathrm{A/cm^2}$, $0.32\,\mathrm{A/cm^2}$, $0.35\,\mathrm{A/cm^2}$; $L_{cell} = 60\,\mathrm{cm}$; $d_{gap} = 20\,\mathrm{cm}$; $B_{elec} = 1.3\,\mathrm{cm}$; $\dot{V} = 3360\,\mathrm{mL/min}$; $\tau_{id} = 0.46\,\mathrm{min}$

6.4.1. Fluid Flow Patterns: Stirred Tank vs. Plug-Flow

The axial discretization and the number of control volumes determine the Bo number and thereby the degree of axial back-mixing. Figure 6.5 displays the change of the Bo number with different numbers of control volumes. One control volume corresponds to operation under ideally mixed conditions, while 30 control volumes are considered to represent the plug flow. The effect of the back-mixing on the current distribution is shown in fig. 6.6. Under ideally mixed conditions the current distribution is uniform. With more distinct flow patterns a cell internal rearrangement of the current flow is observed in the model. The current density increases shortly after the inlet of the electrolysis cell and then decreases towards the exit.

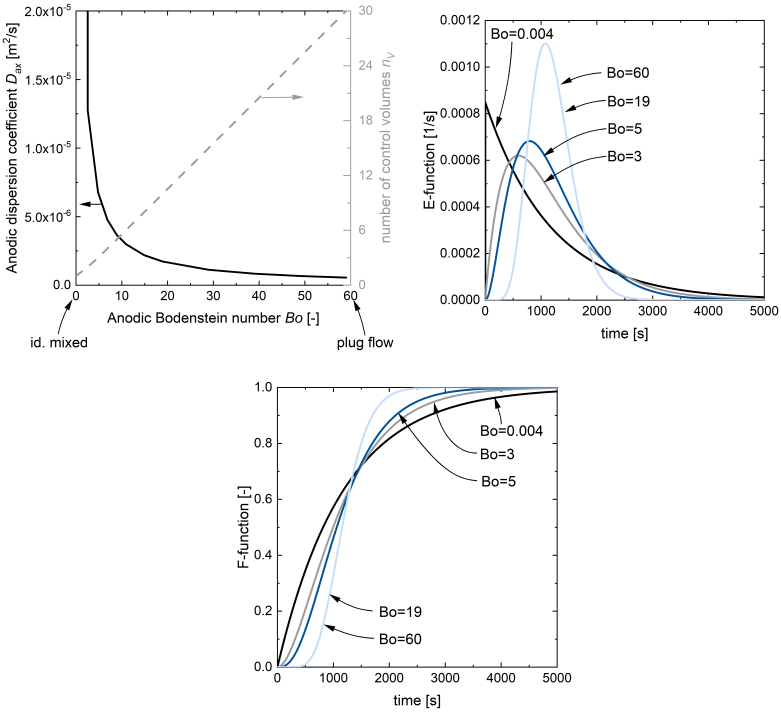

Figure 6.5.: Bodenstein number as a fuction of control volumes with resulting E-function and F-function. Settings: $i = 0.15\,\mathrm{A/cm^2}$; $L_{cell} = 20\,\mathrm{cm}$; $d_{gap} = 1.4\,\mathrm{cm}$; $B_{elec} = 5\,\mathrm{cm}$; $\dot{V} = 6.86\,\mathrm{mL/min}$; $\tau_{id} = 20.41\,\mathrm{min}$; $0.004 \leq Bo \leq 60$

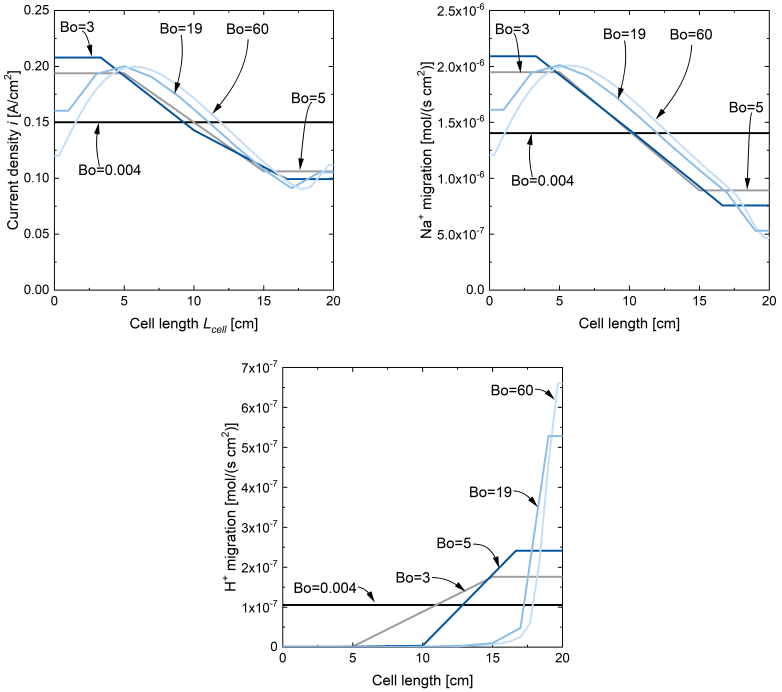

Figure 6.6.: Current density, and ion migration distribution along the cell. Settings: $i = 0.15\,\mathrm{A/cm^2}$; $L_{cell} = 20\,\mathrm{cm}$; $d_{gap} = 1.4\,\mathrm{cm}$; $B_{elec} = 5\,\mathrm{cm}$; $\dot{V} = 6.86\,\mathrm{mL/min}$; $\tau_{id} = 20.41\,\mathrm{min}$; $0.004 \leq Bo \leq 60$

A detailed look at the ion migration reveals a similar pattern for the charge transfer of Na^+ ions within the cell. The minimum of the current density is found just before the end of the module. With that, an increase of the current density right after is observed, which can be attributed to H^+ migration. The H^+ migration starts immediately when the total protonation of the succinic acid is reached. Since protons migrating over the membrane are lost, this is identified as the origin of the so-called "proton poisoning" of electrodialysis membranes [29]. In that case, the conductivity of the protons is high compared to other ions and major fractions of the electric charge are being carried by them instead of the desired Na^+ ions. This significantly reduces the pH-shift efficiency and should be avoided during operation.

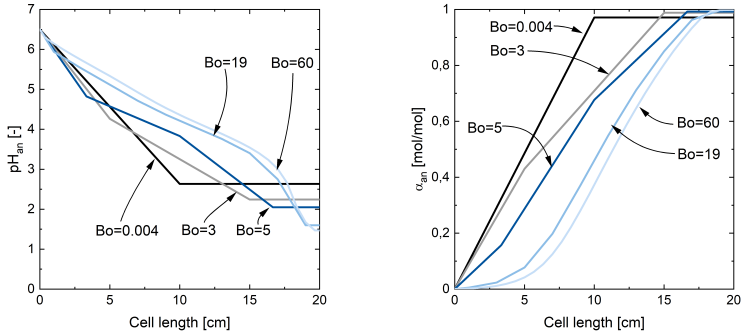

Figure 6.7.: Anodic pH and protonation degree over the cell length for varying Bodenstein numbers; Settings: $i = 0.15\,\mathrm{A/cm^2}$; $L_{cell} = 20\,\mathrm{cm}$; $d_{gap} = 1.4\,\mathrm{cm}$; $B_{elec} = 5\,\mathrm{cm}$; $\dot{V} = 6.86\,\mathrm{mL/min}$; $\tau_{id} = 20.41\,\mathrm{min}$; $0.004 \leq Bo \leq 60$

Figure 6.7 shows that with stronger backmixing the point of complete protonation is reached earlier but at the expense of a greater flow of current through regions of less desirable conductivity. In a flow regime closer to plug-flow conditions, the point of complete protonation is reached at the end and most of the current can be transferred with good conductivity. In other words, the point of operation should prefer-

ably be reached directly at the end of the electrolysis cell and not earlier as that would cause subefficient electrical operation. For this reason, it does not appear desirable to increase the axial back-mixing extensively. Operation in a plug flow regime or stage-wise operation with a series of well-mixed electrolysis cells is expected to be more efficient based on the simulation data.

A similar trend is found for the gas hold-up fig. 6.8. With stronger backmixing, the average hold-up in the electrolysis cell increases. Gas hold-up blocks the free electrode area and increases the cell voltage, which is an undesirable effect.

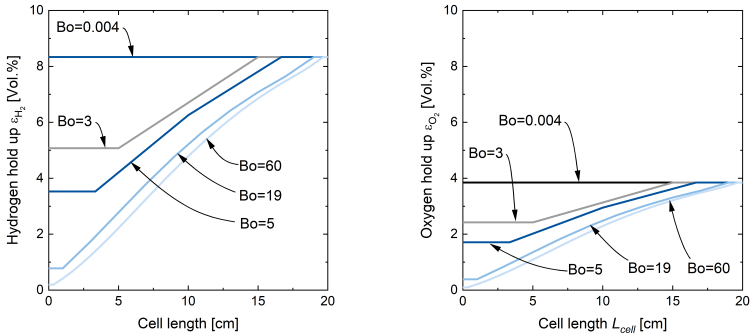

Figure 6.8.: Hydrogen and oxygen hold-up over the cell length. Settings: $i = 0.15\,\mathrm{A/cm^2}$; $L_{cell} = 20\,\mathrm{cm}$; $d_{gap} = 1.4\,\mathrm{cm}$; $B_{elec} = 5\,\mathrm{cm}$; $\dot{V} = 6.86\,\mathrm{mL/min}$; $\tau_{id} = 20.41\,\mathrm{min}$; $0.004 \leq Bo \leq 60$

6.4.2. Cell Length, Electrolyte Gap and Gas Hold-up

The obtained results suggest that a plug flow pattern is to be preferred. Next, the influence of the cell length, the electrolyte gap, and the resulting gas hold-up on the performance of the electrolysis cell follow. The influence of a cell is displayed in fig. 6.9. The residence time was adjusted accordingly to obtain a leveled basis for the comparison. It is noted that a short cell does not achieve complete protonation, whereas a long cell results in overprotonation.

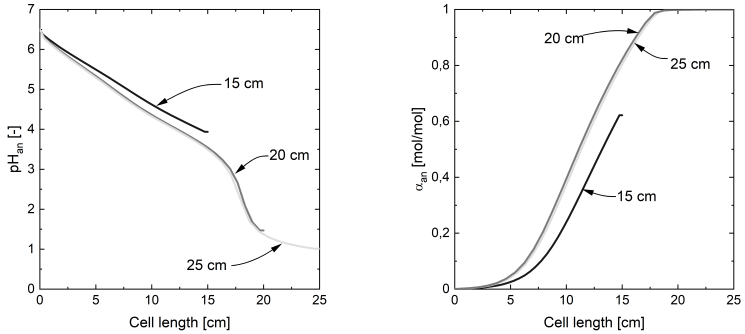

Figure 6.9.: Anodic pH and degree of succinic acid protonation over cell length. Settings: $i = 0.15\,\mathrm{A/cm^2}$; $L_{cell} = 15\,\mathrm{cm}$, $20\,\mathrm{cm}$, $25\,\mathrm{cm}$, $d_{gap} = 1.4\,\mathrm{cm}$; $B_{elec} = 5\,\mathrm{cm}$; $\dot{V} = 6.86\,\mathrm{mL/min}$; $\tau_{id} = 15.31\,\mathrm{min}$, $20.41\,\mathrm{min}$, $25.52\,\mathrm{min}$; $Bo = 60$

The issue with overprotonation becomes more visible in fig. 6.10. It displays how the distribution of current density over cell length evolves over time. Shortly after the ideal residence time is reached at approximately 1200 s, the migration of H^+ begins. As stated above, this causes a loss of electrochemically produced protons and reduces the protonation efficiency. The last aspect is the selection of a suitable electrolyte gap. From the electrical perspective, a gap as small as possible would be desirable as a small gap minimizes the ohmic losses and thus benefits the overall energy efficiency of the pH-shift electrolysis.

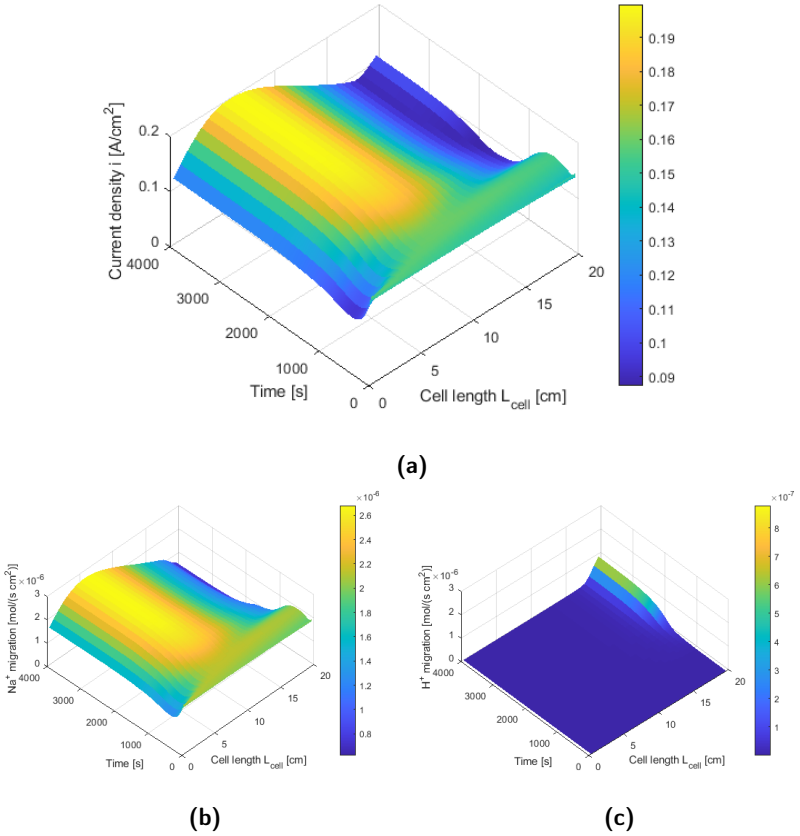

Figure 6.10.: Current distribution and ion migration over time and cell length. Settings: $i = 0.15\,\mathrm{A/cm^2}$; $L_{cell} = 20\,\mathrm{cm}$, $d_{gap} = 1.4\,\mathrm{cm}$; $B_{elec} = 5\,\mathrm{cm}$; $\dot{V} = 6.86\,\mathrm{mL/min}$; $\tau_{id} = 1224\,\mathrm{s}$; $Bo = 60$

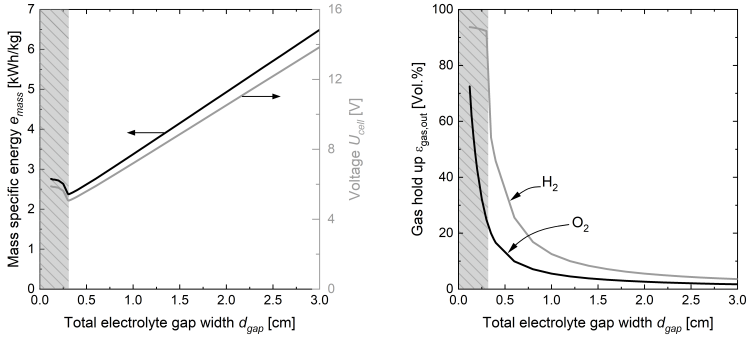

Figure 6.11.: Energy demand and gas hold-up as a function of electrolyte gap size. Settings: $i = 0.15\,\mathrm{A/cm^2}$; $L_{cell} = 20\,\mathrm{cm}$; $d_{gap} = 1.4\,\mathrm{cm}$; $B_{elec} = 5\,\mathrm{cm}$; $\dot{V} = 6.86\,\mathrm{mL/min}$; $\tau_{id} = 20.41\,\mathrm{min}$; $Bo = 60$

However, fig. 6.11 gives a slightly different picture. As expected, the cell voltage and the specific energy demand increase linearly with increasing gap sizes, which correlate with the increase in ohmic resistance. But below 3 mm the specific energy demand increases. This is caused by a steep increase in the gas hold-up when the gap between the ions is approaching small electrolyte gaps. In small gaps, the gas evolution from the electrode reaction seems to displace a significant fraction of the electrolyte. For that reason, the electrolyte gap should be selected small but sufficiently large to enable the removal of the evolving gases without blocking the electrolyte. An option to reduce the gas volume would be operation under pressure.

6.5. Conclusion

In this chapter a spatially structured simulation model was developed. The spatially structured model is based on the 0D-model presented in the previous chapter. A simplified model to calculate the gas hold-up in the electrolysis cell was implemented and compared with literature data. The results were found to have a satisfying accuracy for the de-

sired investigations. First, the influence of the flow pattern revealed that strong back mixing in the electrolysis cell is not desirable. With the progress of the pH-shift the electrolysis becomes more inefficient to operate. Once all available succinic acid is protonated, the surplus protons easily participate in charge transfer over the membrane and are lost. This phenomenon was reported in the literature and is correctly predicted by the developed model. It is therefore advisable to perform pH-shift electrolysis in the plug flow regime or in a series of at least 3-4 cells when strong backmixing cannot be prevented.

Second, correct alignment of residence time, current density and module lenght is important to obtain a good result for the protonation and avoid the proton migration. Lastly, the modeling results suggest that small electrolyte gaps are preferable to the extent that they still provide sufficient free cross sectional area for the exit of the gases evolving at the electrodes.

The gas liquid separation and gas withdrawal from the electrode compartment without the loss of liquid is a crucial aspect to ensure stable operation. With the implemented hold-up model a minimal reasonable gap size for the tested cell geometry of around 3 mm is identified. This value should be verified by more detailed experimental investigations or computational fluid simulation.

7. Application Note 1: Electrochemical pH-swing extraction of lactic acid with membranes

7.1. Motivation

[†] In this chapter the concept of electrochemical pH-swing electrolysis is applied to improve the recovery of lactic acid with membrane-supported extraction. Lactic acid is one of the most relevant carboxylic acids in the industry. An experimental setup is designed which integrates an electrolysis cell into a membrane extraction setup. The electrochemical pH-shift is used to adjust the pH of the feed to the membrane module. Its successful application for extraction and back-extraction is presented. On the basis of the dynamic models developed in the previous chapters, the influence of the pH on the membrane extraction performance is studied. An experimental analysis supported by a model confirms the extraordinary importance of the pH of the feed on the extraction performance of the membranes. The state-of-the-art design framework for the calculation of the required membrane area is extended and a new mathematical framework is developed to account for the extraction of

[†]This chapter is based on a collaboration between the University of Life Sciences FHNW, the University of Twente and the RWTH Aachen University. Parts of this chapter have been published as "Gausmann & Gössi et al. "Electrochemical membrane-assisted pH-swing extraction and backextraction" (2022), Separation and Purification Technology" Parts of this chapter are also used in the dissertation of Angelo Gössi, " Membrane-supported reactive extraction using membranes with enhanced stability".

dissociating solutes with membrane contactors.

7.2. Background of Lactic Acid Production

The demand for biobased chemicals has increased tremendously in the last few years [185], and a wide range of pharmaceuticals and chemicals is produced today by fermentation. Lactic acid is an emerging biobased chemical produced by fermentation at large scale. [186, 187]. Large fermentors are often required as the concentration of the main product in the fermentation broth is low (usually << 10 wt%) due to inhibition of the microorganism by the product and/or the substrate [188]. For pH control during fermentation to counteract acidification due to the produced acids, calcium hydroxide or calcium carbonate is typically used. When the fermentation process is finished, the microorganisms are removed by filtration. After that, sulfuric acid is added to release lactic acid from the lactate form. The free acid is further purified by evaporation and distillation. During this process, calcium sulfate (gypsum) is formed at a rate of about one ton per ton of lactic acid. At current levels of lactic acid, still practical uses are found, but especially when acid production is ramped, gypsum production will pose disposal and environmental problems [189, 190]. An alternative to the use of neutralizing agents is the in-situ separation of the produced acid during fermentation. However, selective removal of a highly hydrophilic carboxylic acid in the presence of numerous substrates and active microorganisms is challenging. The use of Ionic liquids (ILs) as solvents is promising due to their negligible vapor pressure, high thermal stability, and low chemical reactivity. Several published ILs have been shown to have high capacity and low toxicity toward microorganisms [191, 192, 193]. However, recent work on recovery from ILs showed that direct thermal recovery is not possible at low loadings, and an additional back-extraction is needed, followed by thermal decomposition of the formed complexes [194]. This is less suited for lactic acid, as it is prone to polymerization at elevated temperatures. Therefore, reactive extraction with ter-

tiary amines [195, 196, 197, 198, 127] still appears to be the solvent of choice. The reactive extraction of carboxylic acid has been subject to numerous studies [189, 64, 61]. Typically, a tertiary amine, such as tri-n-octylamine (TOA), is used as an extractant. However, the pH optima difference for fermentation and extraction poses a significant challenge. While a neutral pH value is required for fermentation, higher extraction yields are achieved at low pH since tertiary amines only extract unprotonated acids. Several publications report reduced extraction efficiency of tertiary amines at higher pH values[196, 197, 101, 199]. An option to improve the efficiency of tertiary amines at higher pH values is to add highly water-soluble salts[200]. However, this approach requires the addition of large amounts of salts and therefore cannot be used as an in-situ product removal technique. Thus, this process can only be used for fermentation processes with continuous neutralization or fermentations, which result in low concentrations of lactic acid. However, since carboxylic acids are promising platform chemicals used in large scale, in-situ extraction represents the key towards continuous fermentation and hence, a large scale production. Another approach to increase the extraction efficiency of tertiary amines is electrochemical pH-shift. Recently, separations have been shown in combination with electrochemical stimuli, such as electrodialysis or electro-deionization [140, 42, 146]. Furthermore, recent publications presented combinations of electrochemical separation technologies and biobased production [201]. For example, electrochemical extraction of carboxylic acid [140, 39] or capture of CO2 with amines [202].

The positive effect of the combination of electrochemical pH-shift and reactive extraction has already been demonstrated in a previous publication [140]. However, in-situ extraction of fermentation broths is challenging due to the formation of stable emulsions, limited phase ratios applicable, and solvent toxicity. A previous publication demonstrated the benefits of a membrane as an extraction interface with respect to these issues [195]. Herein, the concepts of electrochemical pH-swing and membrane assisted reactive extraction, respectively back-extraction are combinded to enable the recovery and up-concentration of lactic acid

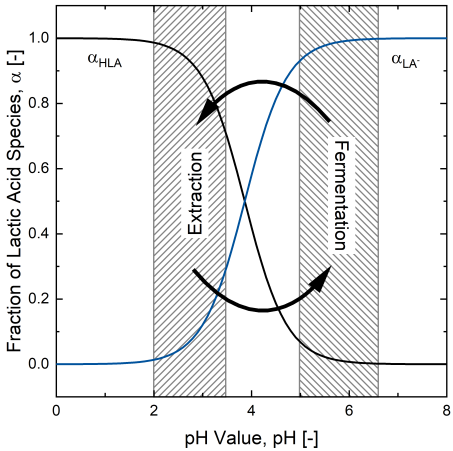

Figure 7.1.: Optimal ranges of the aqueous pH value for the fermentation and reactive extraction of lactic acid, the blue lines show the reversible pH changes introduced in the cathode/ anode chamber of the electrolysis for optimal fermentation, extraction, and back-extraction.

from aqueous solution at physiological pH values [203]. The relevance of the aqueous pH on the lactic acid extraction performance is investigated experimentally. Based on the experimental observations a mathematical model is derived, that takes the weak-acid equilibrium of lactic acid into account and enables design calculations to determine the membrane area required for the extraction at varying pH values in the feed which is an important aspect in the development of well performing in-situ separation technologies [204, **?**].

7.3. Materials and Methods

7.3.1. Chemicals

All chemicals used were purchased from Sigma Aldrich Switzerland. Tri-n-octylamine (TOA) 98%, sodium sulfate > 99%, mandelic acid (Standard for quantitative NMR, TraceCERT), 1-decanol > 99%, sodium hydroxide solution $1M$, sulphuric acid $1M$, deuterium oxide 99.9% The aqueous lactic acid solutions were prepared using 85 wt% FCC lactic acid.

7.3.2. Experimental setup

Figure 7.2 shows a schematic representation of the used electro-swing membrane extraction setup. It consists of two temperature-controlled 2 L tanks for the aqueous and organic phases. Two Ismatec Micropump gear pumps (Z 140, 5 - 60 L / h), were used to pump the phases through the electrochemical cell, the membrane module, and back into the container, which can be adjusted to 10-60 °C. Needle valves were used to adjust pressure. Coriolis flow meters were used to record the flows as well as the densities of both phases. All phase-contact parts made from PVDF, PTFE, glass, or stainless steel (1.4404). The electrolysis cathode consists of platinum and the anode of titanium coated with titanium coated with iridium mixed metal oxide, provided by Magneto special anodes B.V., Netherlands; the electrolysis membrane was a Fumasep FS-990-PK, Fumatech, Germany. A quasi-continuous operation was used to study the effect of pH on membrane extraction and potential improvements by applying the electrochemical pH-shift. Therefore, the lactic acid containing the aqueous phase was first pumped through the anode chamber, where the protons produced by the electrolysis acidify the solution before it enters the membrane contactor. The base produced with the electrochemical pH-shift was recovered in a second loop (Base loop).

For the back-extraction, the aqueous receiving phase was pumped through the cathode chamber of the electrolysis as depicted in fig. 7.8.

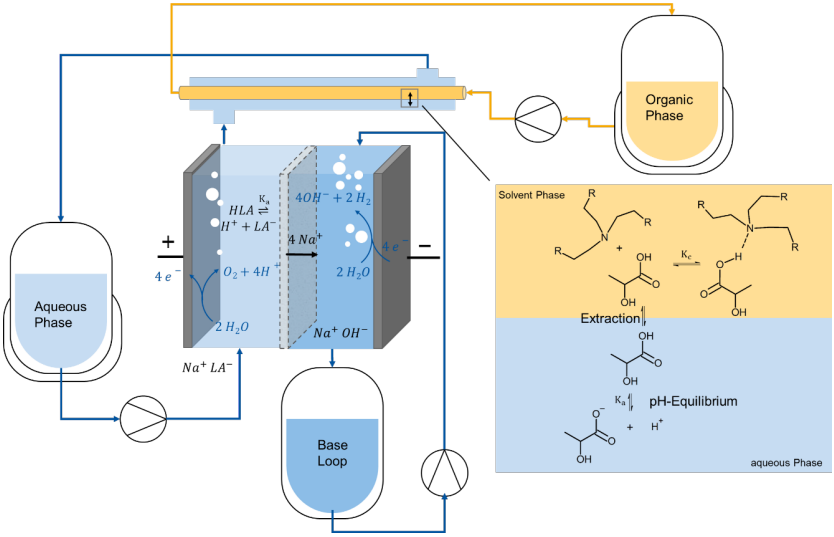

Figure 7.2.: Electro-swing MSE-Setup and extraction equilibrium system, HLA=protonated lactic acid, Kc=lactic acid-TOA complexation constant, Ka=lactic acid dissociation constant.

7.3.3. Experimental methods

If not stated differently, 20 wt% tri-n-octylamine (TOA) in 1-decanol was used as solvent for the experiments. Membrane supported extraction (MSE) experiments were started by pumping the aqueous phase with an overpressure of about 60 mbar to ambient pressure. Subsequently, the organic phase flow was started, keeping the pressure about 50 mbar lower than that of the aqueous phase. This avoids the introduction of the organic phase into the aqueous phase. The organic phase was pumped through the fibers and the aqueous phase through the membrane contactor shell side. The outer diameter of the fibers was used to calculate the contact area because the hydrophobic membranes are penetrated only by the organic phase. Table 1 shows the properties of the used PTFE fibers purchased from Memo3 GmbH, Switzerland.

Since only a small membrane module (0.059 m) was used, both

Table 7.1.: Used PTFE membrane. The tortuosity was determined using Field Emission Scanning Electron Microscopy (FESEM)

Material	Porosity [%]	d_p [µm]	d_i [mm]	D_a [mm]	Thickness [µm]
PTFE	54	0.47	2.97	3.49	260

the aqueous and organic phases were circulated until equilibrium was reached. If not stated otherwise, all experiments were carried out at room temperature and with 0.15 M Na_2SO_4 as the background electrolyte, to represent the ionic strength encountered in lactic acid fermentation.[30,31]

7.3.4. Analytical methods

All samples were analyzed by either High-Performance Liquid Chromatography (HPLC) or quantitative Nuclear Magnetic Resonance (NMR) measurements. Lactic acid concentrations in the preliminary equilibrium study (Figure A2) were measured by HPLC on an 1100 Series HPLC (Agilent Technologies) equipped with an Organic Acid Resin 250 X 8 mm Column (CS Chromatographie) and a refractive index (RI) detector (G1362A). As a mobile phase, 10 mmol H2SO4 at an isochratic flow rate of 1 mL/min was used. Quantitative 1H-NMR measurements were used to measure the carboxylic acid concentration in membrane extraction experiments. Measurements were performed at ambient temperature on a Bruker Avance III 400 NMR spectrometer (Bruker BioSpin AG) fitted with a 5 mm i.d. BBO prodigy probe and operating at 400.13 MHz. Maleic acid was used as an internal standard in D_2O.

7.4. Theory and Reactive Extraction Modeling

Small carboxylic acids are difficult to extract out of aqueous streams due to their hydrophilic nature. Thus, it is highly beneficial to apply a reactive extraction process instead of a conventional physical extraction. Tertiary amines such as tri-n-octylamine (TOA) are state-of-the-art for the reactive extraction of carboxylic acids out of aqueous streams, due to their high selectivity and capacity [196, 205, 23, 123]. Both are needed when working with fermentation broths since the carboxylic acid is highly diluted (<10 wt% in water) and the fermentation broths contain numerous compounds that preferentially are not co-extracted. The pH of the fermentation broth determines the concentration of protonated lactic acid and thus the extraction rate and efficiency. A mass transfer model was developed to describe the extraction rate and, hence, to predict the required membrane area for the desired production rates. A detailed description of the model and derivations can be found in the supplementary electronic information published with [8]. Figure 7.2 displays the reactive extraction mechanism assumed for lactic acid [206]. The overall mass transfer coefficient k_{ov} can be determined experimentally from:

$$\dot{n}_{ex} = \frac{dn}{dt} = k_{ov} A_o \left([HLA]_{aq} - \frac{[HLA \cdot TOA]_{org}}{K_c [TOA]_{org}} \right) \tag{7.1}$$

with Kc as the lactic acid-tri-n-octylamine complexation constant and k_{ov} as the overall mass transfer coefficient and HLAC as the lactic-acid-tri-n-octylamine complex. The bracket is the driving force described by the concentration difference between protonated acid in the aqueous phase $[HLA]_{aq}$ and the organic phase $[HLA]_{org}$. Ao stands for the membrane contact area. It is essential to mention that the membrane only serves as a solid extraction interface, meaning that the membrane does not influence the phase equilibrium in any way. The total mass transfer coefficient k_{ov} can be calculated as shown in the ESI of [8] or

can be fitted from mass transfer experiments [207]. The pH of the aqueous is calculated using the dynamic approach [208, 170], which includes solving the differential equations for the concentration of protons, sulfuric and lactic acid in the aqueous phase. The constituting equations of the kinetic model used in the calculation presented in Figure 7.3 are given in the ESI of (S8-S25) [8]. It should be noted that because of the low membrane area and high volumetric flow, the concentration difference between the membrane input and outlet was negligible. Although such settings are well suited to investigate the kinetics of the reactive extraction, a kinetically limited reactive extraction caused by insufficient contact area is not desirable for any process application. For this reason, the calculation of the required membrane area is an essential step in the designing of processes featuring membrane assisted in-situ extraction. The herein-derived model is based on the classic design approach for membrane-assisted extraction from [209]. For a detailed explanation of the derivation, the reader is referred to the original work and appendix G.2. In summary, mass balances for a differential volume of the membrane contactor and the overall module are formulated, approximated with a Taylor series expansion and rearranged to yield a differential expression for the membrane area concerning the desired change in lactic acid concentration:

$$\frac{dA_m}{d[HLA]} = -\frac{\frac{\dot{V}_{aq}}{k_{mem}}}{\left([HLA]K_c[TOA] + \frac{\dot{V}_{aq}}{\dot{V}_{org}}([HLA_{tot}]_\alpha - HLA_{tot}) - [HLA_{tot}]_\omega\right)} \tag{7.2}$$

This approach is analogous to the modeling of plug flow reactors (PFR). Integration of the right-hand side of eq. (7.2) for the respective concentration $[HLA_{tot}]_\alpha$ at the inlet and at the outlet $[HLA_{tot}]_\omega$, where $[HLA_{tot}]_\omega$ is the desired outlet concentration, yields the required membrane area for the extraction. In order to take into account that only the protonated lactic acid is extracted, the integration variable is altered from the concentration of protonated lactic HLA to the total

concentration of lactic acid HLA_{tot} by changing the integration variable:

$$\frac{dA_m}{d[HLA_{tot}]} = \frac{dA_m}{d[HLA]} \frac{d[HLA]}{d[HLA_{tot}]} \tag{7.3}$$

The derivation of the differentials resulting from this change of variables is presented in the appendix appendix G.2.

And further:

$$\frac{d[HLA]}{d[HLA_{tot}]} = \frac{[H^+]}{[H^+] + K_{LA}} + [HLA_{tot}] \frac{d[H^+]}{d[HLA_{tot}]} \frac{K_a}{([H^+]K_a)^2} \tag{7.4}$$

The term defined in Eeq. (7.4)is in essence the inverse of the aqueous phase enhancement factor as defined by Gössi et al. [207]. A derivation of the remaining differentials caused by the change in the integration variable is given in the appendix appendix G.2. The resulting set of differential expressions equations is solved numerically for the required membrane area using the MATLAB ode15s solver.

7.5. Results and Discussion

7.5.1. pH-dependent Extraction kinetic Modeling

The model described in ESI (S8-S25) of [8] was experimentally verified. For that, membrane assisted extractions were performed with a membrane contactor with 0.059 m and 1200 g of aqueous phase with 10g/L lactic acid and 500g of 20wt% TOA in 1-Decanol. A lactic acid concentration of 10g/L represents a realistic concentration during a continuous fermentation with in-situ removal. Both phases were continuously recirculated at 15 kg/h through the membrane until equilibrium was reached. Three experiments were performed at pH 4.5, 5 and 6. A mass transfer coefficient of 2·10-7 m/s working with the same membrane contactor and aqueous feed has been published before [207]. From the results in fig. 7.3, it can be concluded that at higher pH values, hardly any extraction is observed. While these results are entirely in line with what would

be expected based on literature, it proves that using tertiary amines to extract lactic acid from buffered solutions is highly inefficient [199, 210].

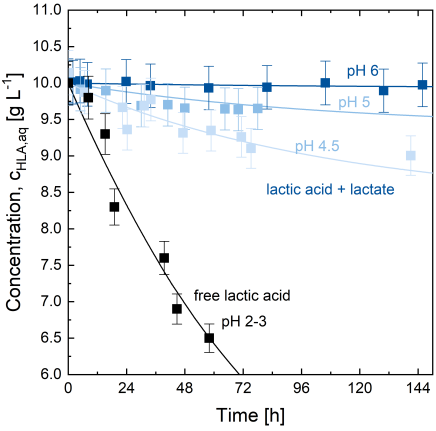

Figure 7.3.: Aqueous phase lactic acid concentration-in-time-profiles for extractions at initial pH values of pH 6, pH 5, pH 4.5.

Figure 7.3 shows the experimental and simulative results for various pH values, the initial lactic acid concentration was 10g/L, and the organic phase consisted of 20 wt% TOA in 1-decanol. The black line represents the predicted concentration profile using the model from [209] without any pH-dependency included. The blue lines show the predicted concentration profiles based on the model presented in this work, which can be regarded as a further development of the models from [140, 207]. The experimental and simulative results are in excellent agreement. It is evident that the aqueous pH has a striking effect on the kinetics of the membrane-assisted extraction. Therefore, it is crucial to consider its impact in the design process and maintain a suitable pH during the operation to ensure satisfying extraction rates. This can either be done by employing the electrochemical pH-shift prior to extraction or by developing acid tolerant strains of lactic acid producing microorganisms

[211, 212, 213].

7.5.2. Design of Membrane Contactor Area for Dissociating Solutes

The classical design equations which are used to calculate the membrane area required for the membrane supported extraction do not consider the pH effect imposed on the extraction by the weak-acid equilibrium [209]. Based on the modeling results, an extensioon of the design framework by Melin et al. is derived and a new mathematical model to calculate the membrane area required for ISPR at different feed conditions (concentration and pH) is developed. Figure 7.4 shows the required areas for a fictive fermenter of 10 L operated with a productivity of 2 g L-1 h-1, depending on the pH and lactic acid concentration. In the hatched area, the pH equilibrium prohibits the complete extraction and causes a steep exponential increase of the required membrane area, which makes the junction region sensitive towards numerical errors.

Two major influences can be identified in fig. 7.4: The reduced membrane area required at low acid concentrations and the strong influence of the pH value. The first influence can be explained by the higher amine-acid ratio at low concentrations, which is also reflected in the last term of Equation S13 in the ESI of [8]. The increasing enhancement factor outweighs the decreasing driving force at low concentrations and leads to higher mass transfer rates. This also demonstrates that the reactive extraction with tertiary amines is especially suitable for in-situ extractions, where lactic acid must be recovered from low concentrations [214, 215]. The second influence, the influence of the pH on the required membrane contact area, is apparent, demonstrating the immense improvement that could be reached when applying an electrochemical pH-shift or . The membrane area required for extraction rises exponentially when the aqueous pH approaches 4. Above this pH, the removal of protonated lactic acid causes an immediate increase of the aqueous pH, which triggers the dissociation of the remaining lactic acid and thereby makes it unavailable for extraction. A starting pH well be-

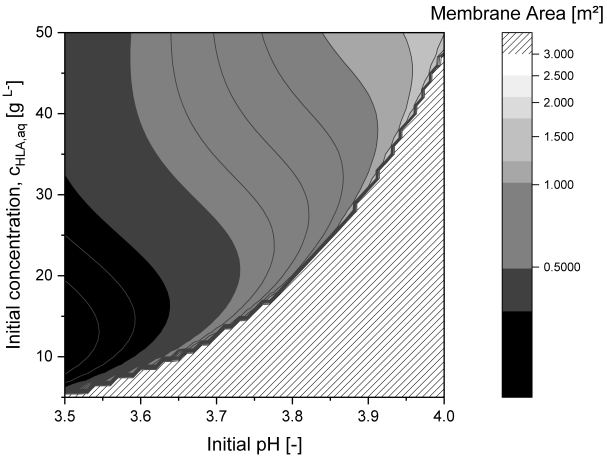

Figure 7.4.: Membrane area required for the extraction of lactic acid, dependent on pH and total lactic acid concentration.

low 4 is mandatory to achieve an efficient extraction. This requirement is not compatible with the thermodynamic limits imposed by microbial lactic acid production and product export from the cell in currently used microorganisms (Figure A3) [8]. As a consequence, there is a gap between the optimal operational conditions required for fermentation and extraction with regard to the pH value, which can be closed by electrochemical pH-shift. By doing so, the pH of the aqueous solution can be reduced prior to the membrane module and the extraction efficiency can be highly increased. Figure 5 shows the influence of an electrochemical pH-shift from pH 4.5 to pH 4. In both experiments, the initial lactic acid concentration was 10g/L, and the organic phase consisted of 20 wt% TOA in 1-decanol. The black symbols represent an experiment with an initial pH of 4 and without electrochemical pH-swing, the grey symbols an experiment in which the pH of the aqueous feed phase was reduced in the electrochemical cell prior to the membrane-assisted extraction to a pH 4.

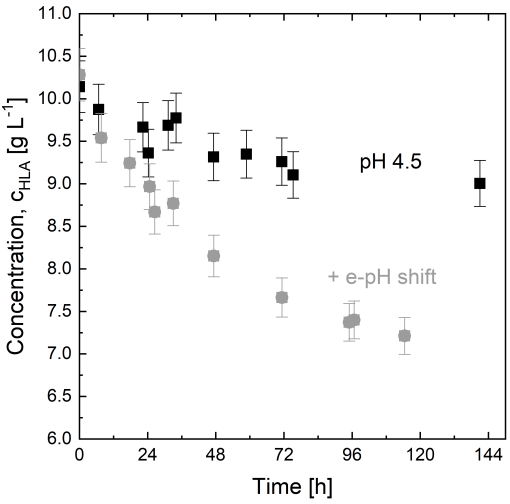

Figure 7.5.: Aqueous phase lactic acid concentration-in-time-profiles for the extraction with and without electrochemical pH-shift.

The improvement depicted in fig. 7.5 is apparent. However, the benefit can be even: The electrolysis allows a change of pH at a given lactic acid concentration and can therefore lead to strongly reduced membrane contactor sizes required. The electrochemical pH-shift improves the extraction rate at the expense of electric power consumption. The degree of the pH-shift depends on the amount of protons $\dot{n}_{H^+}$ produced in the electrolysis and is proportional to the electric current I according to Faraday's law. With t being the time, z the number of electrons transferred in the electrochemical reaction and F being the Faraday constant. As a consequence, a high degree of pH-shift requires a high input of electricity. This results in a trade-off between the power consumption required for the pH-shift and the membrane area required for extraction. Finding the sweet spot for the process operation thus requires an understanding of the relation between the membrane area required for

extraction and its dependence on the initial lactic acid concentration and the initial pH at the module entrance. For this purpose, the design method presented in appendix G.2 is used to calculate the required membrane area with regard to the initial condition at the module entrance.

Figure 7.5 implies that a lower pH value is always better for extraction. However, culture media typically contain various salts, like NaCl, Na_2SO_4, or K_2HPO_4. Their presence should initiate the salting-out of the produced acids and increase the distribution coefficient. Contrarily, studies showed that the presence of salts reduces the extraction efficiency of carboxylic acids [210, 216]. For example, sodium chloride results in the formation of hydrochloric acid, which then competes with lactic acid for extraction. This leads to a reduced extraction efficiency. Therefore, the number of undissociated acids in the fermentation broth should be kept at a minimum to reduce co-extraction. Further information about the co-extraction of salts can be found in fig. 7.6. As an alternative, the extractant Trioctylphosphine oxide (TOPO) showed only negligible co-extraction of sulphuric acid and thus might be a promising alternative to TOA [122].

Another opportunity to close the gap between the fermentation and extraction pH values is the development of more acid-resistant bacteria, which have been investigated lately [212]. These microorganisms allow a more efficient extraction process due to an increased driving force and reduced electrolysis's required power input. If low pH tolerant strains are available [197, 212], the direct extraction of lactic acid is viable without an electrochemical pH-shift prior to extraction. However, at low pH, the lactic acid production and export from the cell of the biocatalyst require additional metabolic energy for the active product export. This energy is inevitably gained at the expense of substrate yield, which causes a trade-off between ease of separation and substrate utilization efficiency [5]. Nevertheless, using an electrochemical pH-shift in the back-extraction process will still be highly beneficial. The following section describes this back-extraction approach in detail.

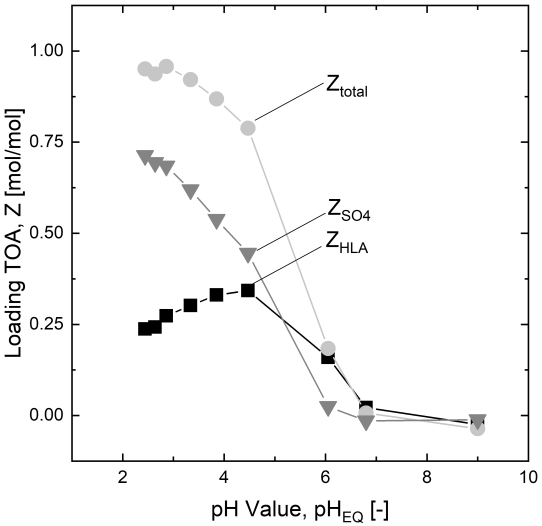

Figure 7.6.: Loading of tri-n-octylamine (TOA) with lactic acid and sulphuric acid depending on the pH. Lines are only visual help. Initial lactic acid concentration 0.5 mol/L. Initial sodium sulfate concentration 0.15 mol/L. Adjustment of pH using 2 M sulphuric acid. Experimental procedure stated in [8]

7.5.3. Electrochemical pH-swing back-extraction

A continuous process raises the need for a continuous solvent recycling process; thus, a back-extraction is needed. Different strategies have been reported for the back-extraction of carboxylic acids out of tertiary amines. In the case of volatile acids or solvents, the most straightforward option appears to be evaporation or distillation. A temperature- and solvent-swing process can be applied if neither the carboxylic acid or the solvent is volatile[61]. Since the complexes are stabilized by hydrogen bonds with the solvent n-decanol, adding a solvent that cannot donate or accept hydrogen bonds - like heptane - reduces the complex's stability [61, 55, 134]. Additionally, an increase in the organic phase temperature

reduces the complexation constant, increasing the recovery rate[55, 217]. However, the added heptane needs to be recycled after back-extraction by evaporation[195]. Instead, using an electrochemical pH-shift for the back-extraction enables effective solvent regeneration. Back-extraction with a receiving phase at alkaline pH conditions is known for its high efficiency[204]. In the herein presented setup, the alkaline conditions in the receiving phase are established by pumping the receiving phase through the cathode chamber of an electrolysis cell. Experiments with lactic-acid saturated 20 wt% TOA in 1-decanol (55 g/L lactic acid) and an aqueous receiving phase with 0.15 M Na2SO4 set to a pH of 12 led to extraction efficiencies of > 90%. fig. 7.7 shows the back-extraction process using an electrochemical pH-shift to increase the pH of the receiving aqueous phase to 12 before the actual back-extraction.

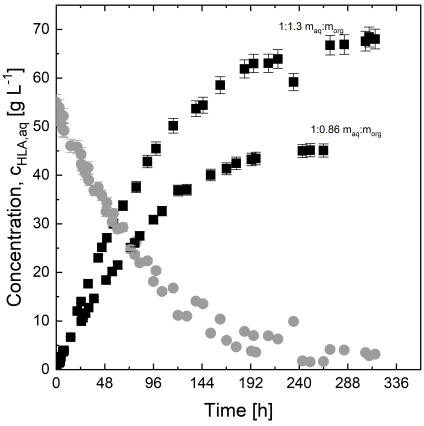

Figure 7.7.: Back-extraction with electrochemical pH-shift, with LA-saturated 20 wt% tri-n-octylamine in 1-decanol. Electrochemical pH-shift to pH 12 prior to back-extraction.

Compared to the temperature- and solvent-swing process, the mass transfer coefficient is reduced when applying an electrochemical pH-

shift: The mass transfer coefficient with temperature- and solvent-swing is 2.1*10-7 m/s (Solvent/Feed/Wash with a volumetric ratio of 1/1/3), and 1.4*10-7 m/s with the electrochemical pH-shift (Solvent/Feed with a 1/1 volumetric ratio). The reduced viscosity with heptane as antisolvent and working at increased temperature can explain the increased extraction rate. However, the extraction efficiency with pH-shift can be increased significantly, from 40% [195] to > 90%, depending on the chosen parameters. Thus, by applying an electrochemical pH-shift, a much higher concentration factor is achievable. Moreover, the subsequent distillation process for water removal requires less energy, and the whole process becomes more energy efficient. Additionally, evaporating three parts of antisolvent per part extractant phase after back-extraction is no longer necessary.

7.5.4. Outlook

Based on the results presented in this chapter it is proposed to combine membrane supported extraction and electrochemical pH-swing for lactic acid purification. Depending on the pH value of the fermentation a first electrochemical pH-swing could be used to adjust the pH value in the feed of the membrane supported extraction [8]. If the fermentation pH is sufficient for direct extraction, the process scheme presented in fig. 7.8 is suggested. The lactic acid is recovered by in-situ product removal by membrane supported extraction. In-situ extraction with membrane supported extraction have been previously reported by [195]. The loaded solvent is then regenerated with an alkaline solution produced in the electrochemical pH-swing electrolysis. Afterwards the lactate solution is fed to the anode chamber to produce the free lactic acid, which is then further purified by distillation and short-path evaporation.

Further investigation is required to clarify whether an initial pH-shift by electrolysis or a slightly acidic fermentation is the more economically way to enable the membrane supported extraction. Besides, the final purification may require additional ion removal steps to keep the concentration of divalent ions, which complicate the lactic acid distillation,

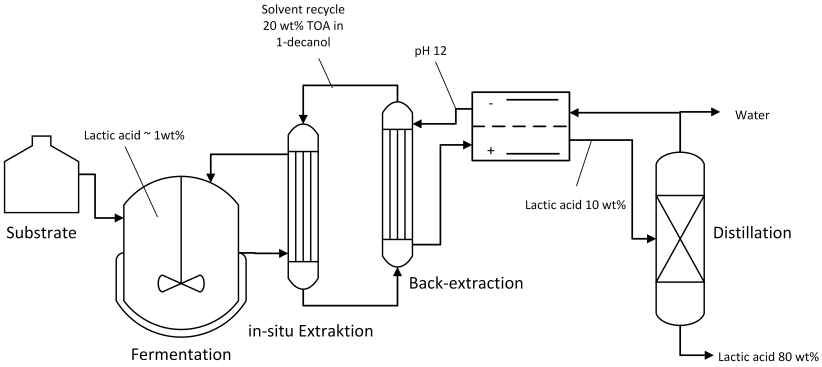

Figure 7.8.: Process scheme for the in-situ extraction and continous production of lactic acid. Additional ion removal steps may be required before the distillation to avoid oligomerization and racemization.

within tolerable limits. Overall such a process layout would overcome the costly initial recovery of lactic acid from very dilute aqueous solution.

7.6. Conclusion

The developed pH-dependent reactive extraction model enables the calculation of the necessary contact area for membrane-assisted extraction, an essential step in the design of extraction processes to separate lactic and other carboxylic with membrane contactors. Implementing a pH-shift electrolysis can overcome the pH gap between the optimal operating conditions of fermentation and extraction, reducing the required membrane. The significant reduction of the required area is advantageous since membrane contactors often represent substantial investment costs. The presented electrochemically driven back-extraction enables high concentration factors reducing the required energy input for thermal purification tremendously.

8. Application Note 2: pH-T-swing Separation of Itaconic Acid

8.1. Motivation

[‡] This chapter presents the development of an electrochemical pH-T-swing separation process, which is applied for the recovery of bio-based itaconic acid. In contrast to succinic acid, where low pH fermentation is limited by the energy balance of microbial metabolism, acid tolerant strains for itaconic acid production are feasible. This chapter demonstrates how sophisticated microbial engineering and electrified downstream processes enable itaconic acid production with a promising economic perspective.

8.2. Background of Itaconic Acid Production

Itaconic acid is considered a promising platform chemical due to its versatile molecular properties and potential applicability for biobased resins, polymers, and solvents [218, 219, 1, 212]. Despite these characteristics, the industrial applications of bio-based itaconic acid are relatively rare compared to, e.g. citric acid due to high production costs [220]. Aside the costs, a major drawback of the bio-based production route for itaconic acid is the production of waste salt due to the use of pH-adjusting agents in the fermentation and downstream processing [218, 20, 23, 24, 221]. Controlling the pH value is necessary for optimal

[‡]Parts of this chapter have been published in "Gausmann & Kocks et al. "Electrochemical pH-T-Swing Separation of Itaconic Acid" 2021, ACS Sustainable Chemistry & Engineering"

operating conditions during fermentation and recovery [222]. In order to render the bio-based production of itaconic acid ecologically and economically more attractive, minimizing the use of pH-adjusting agents, which is inevitably associated with waste salt production, as well as waste free solvent regeneration strategies are required [223, 224, 225].
A promising concept is the development of low pH value tolerant microorganism for itaconic acid production. The pH value is not controlled throughout the fermentation and drops due to the production of itaconic acid to acidic values. Heverkerl et al. produced itaconic acid in acidic fermentations of *Aspergillus terreus* because of the high possible titers [226]. However, the filamentous morphology of *A. terreus* causes challenges regarding reproducibility and handling during the fermentation process such as high viscosities and sufficient oxygen supply [227, 228, 229]. These drawbacks can be avoided in itaconic acid fermentation with the smut fungus *Ustilago maydis*, with its characteristic haploid single-cell morphology [227, 230]. However, *U. maydis* performs best at neutral pH values, which requires the use of additional pH-adjustment agents in up- and downstream processing [231, 232, 233]. At low pH values, losses in volumetric productivity and titer are reported for the fermentation of *U. maydis* [234]. Morphologically engineered strains of *Ustilago cynodontis* present a promising possibility to combine the advantages of *A. terreus* and *U. maydis*. Tehrani et al. achieved titers comparable to fermentations with *U. maydis* of up to $82.9\,\mathrm{g\,L^{-1}}$ of itaconic acid in a low pH value fermentation with *U. cynodontis* while maintaining yeast-like growth. However, itaconic acid production is significantly reduced at concentrations of itaconic acid above $50\,\mathrm{g\,L^{-1}}$ and completely inhibited at concentrations above $80\,\mathrm{g\,L^{-1}}$ making the process a potential application for *in situ* product removal [235, 236]. Synergies between low pH production and *in situ* product removal techniques such as increased productivity and space-time-yield were highlighted by several authors [63, 131, 237]. Furthermore, the fermentation process with low pH is beneficial for further downstream processing of itaconic acid, since a large fraction of itaconic acid is present in its protonated form after the fermentation. This enables direct extraction without further

pH-adjustment [63, 131, 237]. Nevertheless, the presented downstream processes still produced significant amounts of salt-rich waste streams due to pH-management during the purification. Electrochemical unit operations such as electrodialysis (ED) have the potential to reduce salt emissions and were successfully applied for carboxylic acid recovery from aqueous solution [26, 238, 239, 38, 240, 241]. Yet, bi-polar membranes often used in water-splitting ED, require careful pretreatment of the fermentation broth in order to avoid irreversible membrane fouling [42]. Furthermore, selective removal of the targeted carboxylic acid from complex fermentation broths is considered challenging [242]. Economic competitiveness of processes featuring electrodialysis for itaconic acid recovery were often found unfavorable if operated at low current density [219]. Herein, we demonstrate the production of itaconic acid from fermentation broth to the crystalline product by an electrochemical pH-T-swing process. By proper selection of the water splitting electrode material, product degradation at the electrodes can be avoided while the pH-shift induced by water electrolysis is used to trigger back-extraction and crystallization of itaconic acid. This enables the use of more robust ion exchange membranes or potentially membrane free processes [140, 146]. While the single processing steps presented in this work were conducted separately, the joint application of low pH value itaconic acid fermentation with *U. cynodontis* and electrified pH-T-swing downstream processing enables itaconic acid production with a significant reduction of pH-adjusting agents.

8.2.1. pH-shift Water Electrolysis

The cathodic hydrogen evolution reaction of water electrolysis is accompanied by the production of hydroxide ions (OH^-) while the anodic oxygen evolution reaction goes along with the formation of protons (H^+). In contrast to conventional proton exchange membrane electrolysis (PEM) or alkaline electrolysis, where H^+ ions respectively OH^- ions carry out the charge transfer, pH-shift water electrolysis features charge transfer by other ions such as Na^+, K^+ or ${SO_4}^{2-}$. By closing the electric circuit

of water electrolysis with ions other than H^+ ions or OH^- ions, both accumulate in the respective chamber and thus, water splitting can be used to adjust the pH value of the anolyte and catholyte either to acidic or to alkaline conditions, respectively. A well-known industrial application using this principle is the production of sodium hydroxide from sodium chloride via chlorine alkali electrolysis. The presented approach aims for the control of back-extraction and crystallization processes by altering the pH value as their driving force via water splitting. The amount of H^+ ions and OH^- ions produced at the respective electrode can be calculated by Faraday's law.

The efficiency of electrolysis is defined as the ratio of produced H^+ ions or OH^- ions to the electrons e^- introduced into the system and is mainly influenced by side reactions, which can be identified for example by cyclic voltammetric measurements with the specific electrodes. If no side reactions are detected, the efficiency of the electrolysis is close to one [243, 244].

$$\eta_{el} = \frac{n_{H^+,OH^-}}{n_{e^-}} \tag{8.1}$$

Both, OH^- ions and H^+ ions, alter the pH value and the dissociation of itaconic acid. The degree of dissociation defines the amount of acid present in its dissociated forms (HIA^-, IA^{2-}) or protonated form (H_2IA) fig. 8.1. The knowledge of the dissociation of itaconic acid is especially important since it defines efficiency and yield of extraction, back-extraction and crystallization. The extraction of itaconic acid from the aqueous phase via reactive extraction aims for the protonated species of itaconic acid. Reactive extractants such as Tri-n-octylamine (TOA) can form complexes with the H_2IA form of itaconic acid *via* hydrogen bonds and thereby extract the acid into the organic phase. Hence, for a removal of itaconic acid from the aqueous phase via reactive extraction the pH value should be low. A similar effect is observed for the crystallization of itaconic acid. The H_2IA has a lower solubility, which enables crystallization, compared to most of the itaconates present at higher pH values fig. 8.1. Therefore, crystallization of carboxylic acid

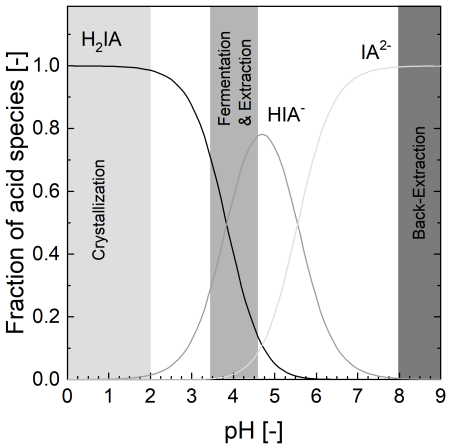

Figure 8.1.: Dissociation of itaconic acid calculated with the equilibrium constants $K_{a1,2}$ at room temperature $pKa1,2 = -log(K_{a1,2}) = 3.84$ and 5.55. The operating pH value ranges of the fermentation, extraction, back-extraction and crystallization is indicated by the respective areas.

is usually performed under acidic conditions at low temperatures [21]. The back-extraction is enabled by the opposing effect, and relies on a high pH value in the aqueous phase. Under these conditions the complex in the organic phase is broken and the dissociated itaconic acid (HIA^- or IA^{2-}) is transferred back into the water. For the electrochemically induced downstream the adjustment of the pH value is realized by the produced amount of H^+ ions and OH^- ions. Hence, the dissociation of the targeted itaconic acid is changed enabling either electrochemical induced back-extraction or crystallization. The pH-shift efficiency η_{pH} correlates the H^+ ions or OH^- ions which are used for the change in dissociation of itaconic acid $n_{H^+ \rightarrow IA}$ or $n_{OH^- \rightarrow IA}$ with the overall produced amount of protons (n_{H^+}) or hydroxide ions (n_{OH^-}) by water splitting

electrolysis at the respective electrode.

$$\eta_{\mathrm{pH,Anode}} = \frac{n_{H^+ \rightarrow IA}}{n_{H^+}} \quad \text{or} \quad \eta_{\mathrm{pH,Cathode}} = \frac{n_{OH^- \rightarrow IA}}{n_{OH^-}} \tag{8.2}$$

Furthermore, the efficiency of the crystallization can be defined as the ratio of solid product $n_{IA,(s)}$ to the amount of H^+ ions used to protonate the itaconic acid. This crystallization efficiency depends on the operating conditions such as initial pH value, concentration and solubility of itaconic acid.

$$\eta_{\mathrm{cry}} = \frac{n_{IA,(s)}}{n_{H^+ \rightarrow IA}} \tag{8.3}$$

Equations (8.1), (8.2) and (8.3) result in the overall efficiency η of the electrochemical crystallization process:

$$\eta = \eta_{\mathrm{el}} \cdot \eta_{\mathrm{pH,Anode}} \cdot \eta_{\mathrm{cry}} = \frac{n_{IA,(s)}}{n_{e^-}}. \tag{8.4}$$

8.2.2. Process

This work presents all necessary single steps towards a bio-based production process from the substrate glucose to the final product, crystalline itaconic acid. The envisioned concept for a combined process is displayed below fig. 8.2.

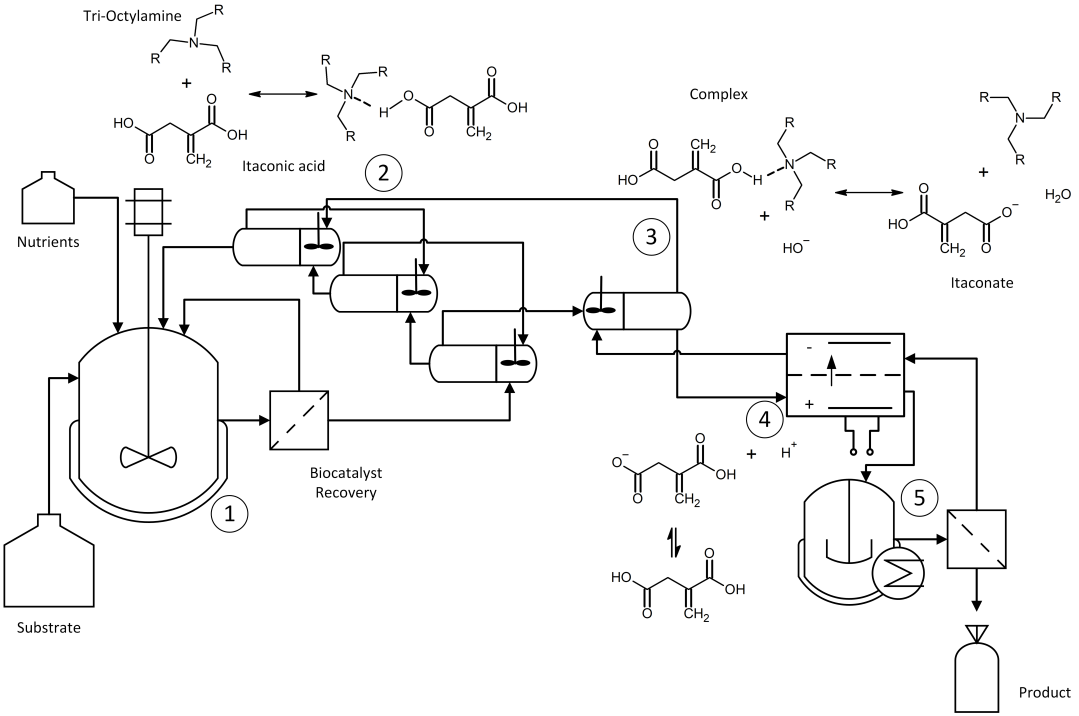

Figure 8.2.: Envisioned electrified downstream process concept for bio-based itaconic acid production: (1) fermentation at low pH values, (2) extraction of the protonated itaconic acid into the organic phase at low pH values, (3) back-exctraction of itaconic acid in the aqueous phase induced by an electrochemical pH-shift to high pH values, (4) electrochemical protonation of itaconic acid and (5) final cooling crystallization.

After the fermentation with *U. cynodontis*, the produced itaconic acid is extracted via reactive extraction from the acidic fermentation supernatant into the organic phase. TOA is a ternary amine, which shows good results as a bio-compatible reactant for itaconic acid due to its low solubility in the aqueous phase ($\log P_{ow} = 10.35$) [131]. Usually TOA is diluted in octanol or similar organic compounds to simplify processing and to avoid the formation of a third TOA-rich phase. The selective recovery of itaconic acid by reactive extraction has been shown successfully in literature [63, 237]. TOA builds a complex with the protonated itaconic acid and thereby itaconic acid is concentrated in the organic phase. The subsequent downstream processing was studied by Eggert et al., choosing a back-extraction with pH-control by sodium hydroxide (NaOH) followed by a final pH-shift crystallization by using hydrochloric acid (HCl) [63]. The process highlighted in this work uses a comparable approach by shifting the pH value for an alkaline back-extraction induced by electrical current followed by a crystallization at low pH values and temperature. In this case the organic solution is brought into contact with an alkaline aqueous phase coming from the cathode chamber of the electrolysis stack as displayed in figure fig. 8.2. Hence, the complex is split by the high pH values and the dissociated itaconic acid is released into the aqueous phase. By adjusting the phase ratio of organic and aqueous phase during back-extraction a concentration increase of itaconic acid in the aqueous phase can be reached. The elevated concentration enables product recovery by pH-shift crystallization. For that purpose, the aqueous solution is transferred into the anode chamber of the electrolysis stack to lower the pH value and protonate the itaconic acid, before entering the final cooling crystallization.

8.3. Experimental Procedure

8.3.1. Materials

Itaconic acid (99%) and Tri-n-octylamine (95%), Sodium hydroxide (99%) and sodium sulfate (99%), were purchased from VWR, Lan-

genfeld Germany. Potassium sulfate (99%), 1-Octanol (99%), sodium chloride (99%), iron(II) sulfate heptahydrate (99.5%), zinc sulfate heptahydrate (99.5%), manganese(II) chloride dihydrate (96%), copper sulfate pentahydrate (99%) and sodium molybdate dihydrate (99.5%) were obtained from Merck, Darmstadt Germany. Sulfuric acid (96%), ammonium chloride (99.7%), glucose (ACS), potassium dihydrogen phosphate (99%), magnesium sulfate heptahydrate (99%), cobalt chloride hexahydrate (99%), calcium chloride dihydrate (99%), boric acid (99.8%), potassium iodide (99%), potassium hydroxide (85%) and 2-(N-morpholino)ethanesulfonic acid (MES) monohydrate (99.5%) were purchased from Carl Roth, Karlsruhe Germany. EDTA (99%) was purchased from Thermo Scientific, Langerwehe Germany.

8.3.2. Fermentation

An acid tolerant strain of *Ustilago cynodontis* was used for itaconic acid fermentation. The fermentation was carried out as part of research collaboration by AVT.BioVT. For a detailed description of the fermentation conditions and the analytical procedures applied in the fermentation, the reader is referred to the published paper [245].

8.3.3. Extraction Equilibrium of Itaconic acid

The optimal pH value for extraction was determined by titration experiments. An aqueous solution containing $40\,\mathrm{g\,L^{-1}}$ itaconate with a near neutral pH value was prepared from itaconic acid and sodium hydroxide. A 50:50 w/w% mixture of TOA and 1-Octanol was used as extractant. 2 M solution of sulphuric acid containing $40\,\mathrm{g\,L^{-1}}$ itaconic acid was used for titration. The itaconic acid was added to the titration solution in order to eliminate the dilution effect of itaconic acid in the aqueous phase during titration and thus isolate the pH-dependent extraction effect. 37.5 mL extractant was added to 60 mL of aqueous solution establishing a molar excess ratio of 1.6 TOA to itaconic acid. Small volumes of the titration solution were added. Both phases were

well mixed for 30 min after each separation step and allowed to settle afterwards. When satisfying phase separation was reached, the pH value of the aqueous phase was recorded and a sample for HPLC analysis of itaconic acid concentration in the aqueous phase was drawn. The concentration of itaconic acid was determined by an Agilent (Ratingen, Germany) 1100 series HPLC, equipped with a LC-OrcanicAcid-CS-E resin (2500 x 8 mm, CS Cromatography, Langerwehe, Germany). The itaconic acid signal was recorded with a refractive index detector (RID) G1362A and 10mM of aqueous sulfuric acid solution was used as eluent, with a flow rate of $0.75\,\mathrm{mL\,min^{-1}}$ at a temperature of $40\,^{\circ}\mathrm{C}$. All concentrations were determined in gram IA per liter solution. From the itaconic acid concentration of the aqueous phase and the added titration solution, the loading of the extractant was calculated by mass balances. The maximal back-extraction yield was determined by a similar procedure, yet starting with loaded extractant. The loaded extractant was prepared by adding 13.6 mL extractant to 20 mL of an aqueous solution containing $40\,\mathrm{g\,L^{-1}}$ itaconic acid. The aqueous phase additionally contained 0.2 M Na_2SO_4 in order to account for the background electrolyte used in the electrochemical pH-swing. A 5 M NaOH solution containing additional $40\,\mathrm{g\,L^{-1}}$ itaconic acid and 0.2 M Na_2SO_4 was used for back-extraction titration. Again, the loading of the organic phase was calculated with the concentration data obtained after each titration step by mass balances. Both titration experiments were conducted in triplicates.

The maximal loading of the extractant and the maximal recovery of itaconic acid from fermentation broth was determined by conducting two five stage cross-current batch extractions. Maximal depletion was determined by adding 5.5 mL of fresh extractant to the same 25 mL fermentation broth in each stage. By this setting, the extraction capacity in each stage was limited, which yielded in more data points for the course of pH value during extraction. The samples were shaken at $700\,\mathrm{min^{-1}}$ for 30 min and separated by centrifugation at $2000\,\mathrm{min^{-1}}$ for 5 min afterwards. After phase separation the organic phase was withdrawn and fresh extractant was added for the next stage. The maximal

loading of the organic phase was determined in a similar way by adding 15 mL of fresh fermentation broth to the same 13.3 mL extractant. Thus, sufficient itaconic acid was supplied in each stage and extraction was only limited by the aqueous pH value. All cross-current extraction experiments were conducted in triplicates.

8.3.4. Solid Liquid Equilibrium of Itaconic acid

For a detailed description of the experimental procedure applied for solid liquid equilibrium determination, the reader is referred to the published paper [245].

8.3.5. pH-T-swing Separation

Cell free supernatant from the fermentation broth was used to prepare an itaconic acid loaded extractant. The extraction was carried out as a one-stage reactive extraction with a TOA-octanol (50:50 w/w%) at a phase ratio of 3:1 (aq:org) by mixing both phases for 12 h on a magnetic stirring plate followed by 4 h sedimentation and decantation. 600 mL of loaded extractant were prepared in each extraction. The loaded extractant was used for electrochemical pH-swing back-extraction with simultaneous acidification. The aqueous solution on the cathode side was pumped at a flow rate of $60\,\mathrm{mL\,min^{-1}}$ through the electrolysis module and the packed extraction column and contacted with the loaded extractant which circulated at a flow rate of $20\,\mathrm{mL\,min^{-1}}$. The anolyte was constituted by the solution harvested in the previous back-extraction run and also circulated at a flow rate of $60\,\mathrm{mL\,min^{-1}}$. Itaconic acid was eventually recovered from the acidulated anolyte by cooling crystallization. Since no back-extracted itaconic acid was available for the inital start-up run, an artificial itaconic acid anolyte was used for the experiment which produced the first itaconic acid enriched solution from back-extraction (data not shown).

For the purpose of establishing similar conditions in the back-extraction as expected with closed recycling streams for the mother

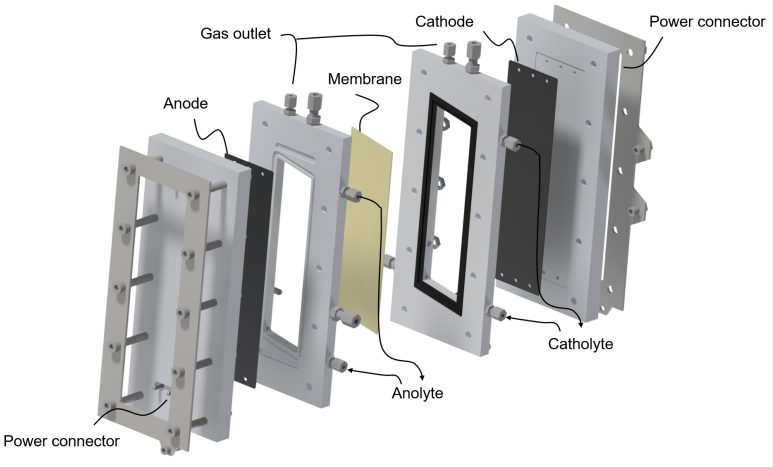

Figure 8.3.: Internal view of custom made $100\,\mathrm{cm}^2$ PTFE pH-shift electrolysis cell

liquor, a solution containing $80\,\mathrm{g\,L}^{-1}$ itaconic acid and 0.2 M Na_2SO_4 was used. Images of the electrolysis cell Figure 8.4 shows the experimental setup and fig. 8.3 a detailed view of the electrolysis cell for the pH-shift water electrolysis. The $100\,\mathrm{cm}^2$ custom made PTFE-electrolysis cell was equipped with a platinum coated titanium cathode and a ruthenium mixed metal oxide coated titanium anode supplied by Magneto special anodes, Schiedam Netherlands. The electrode chambers were separated by a fumasep F-10120-PK cation exchange membrane (Fumatech, Bietigheim-Bissingen Germany). An EA-PS9040-40T-640 power source from Elektro-Automatik, Viersen Germany, was used for power supply and continuous recording of voltage and current. The electrolysis was operated at a current density of $0.1\,\mathrm{Acm}^{-2}$. Temperature was controlled via the heat exchangers at 36 °C (±2 °C). Data for temperature, pH value, voltage and electrical current was recorded by a LABView control. The aqueous solution obtained from the back-extraction was used as the anolyte solution for the following experiment.

All cooling crystallization experiments were carried out using a one-

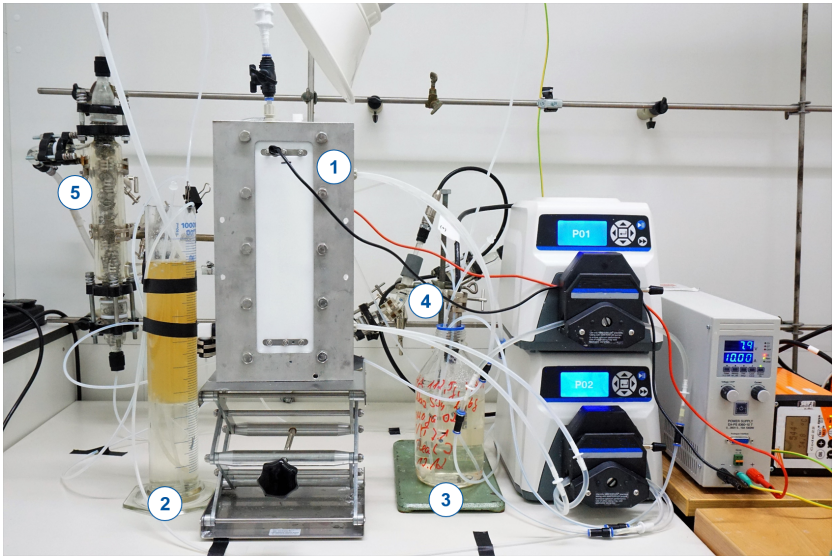

Figure 8.4.: Experimental setup: 1 $100\,\mathrm{cm}^2$ electrolysis cell, 2 Catholyte reservoir, 3 Anolyte reservoir, 4 pH sensor, 5 Catholyte heat exchanger and extraction column, Anolyte heat exchanger not visible

liter stirred double-jacketed glass crystallizer stirred at 200 rpm. Temperature was controlled via a Julabo Presto A40 thermostat with the thermal fluid Thermal HL 60 (Julabo). A PT100 temperature sensor was used to measure the temperature of the solution inside the crystallizer to regulate and record the temperature. The crystallizer was made air-tight to minimize eventual loss of solvent due to evaporation. The solution obtained from the electrolysis stack was filled into the crystallizer and held at 35 °C for 30 min, which is approximately the end temperature of the protonation. Then the solution was cooled with a rate of $0.3\,^{\circ}\mathrm{C}\,\mathrm{min}^{-1}$ to 20 °C and held for 10 min at 20 °C. The gained solids were separated from the mother solution via vacuum filtration through a paper filter (MN 640w Machery-Nagel). Subsequently, the crystals were dried and the crystal size distribution was measured with the Camsizer X2 by Retsch Technology (Haan, Germany) using the free

fall method. Pictures of crystal morphology were taken with a Table Top TM 3030Plus electron microscope by Hitachi . The purity of the crystals was measured by dissolving a specified concentration in water and then measured with the HPLC method mentioned in the extraction section.

8.4. Results and Discussion

8.4.1. Equilibrium data

Reactive extraction of itaconic acid is based on reversible formation of complexes between the acid and the reactive extractant soluble in the solvent. TOA reacts with the protonated itaconic acid by formation of hydrogen bond complexes [61]. The aqueous pH value is a critical process parameter, since only protonated itaconic acid is available for extraction. Results obtained from the titration experiment fig. 8.5 reveal the impact of the aqueous pH value on the extraction equilibrium. When the aqueous pH value is lowered by addition of sulphuirc acid, protonated itaconic acid becomes available for extraction eq. (8.5). The extractant reaches its peak loading at a pH value of approximately 4. Further acidification of the aqueous phase reduces the itaconic acid loading of the solvent due to undesired co-extraction of SO_4^{2-} anions eq. (8.6), which is a known issue in carboxylic acid extraction [44].

$$H_2IA + TOA \rightleftharpoons [TOA{-}H_2IA] \tag{8.5}$$

$$HSO_4^- + TOA{-}H^+ \rightleftharpoons [TOA{-}H^+HSO_4^-] \tag{8.6}$$

The pH value at which the maximum loading of the extractant was observed, suits the conditions maintained during fermentation. In order to assess the extraction performance, the recovery of the extraction and back-extraction step is defined as:

$$R = \frac{n_{IA,ex}}{n_{IA,0}}. \tag{8.7}$$

$n_{IA,ex}$ is the amount of extracted and back-extracted itaconic acid respectively and $n_{IA,0}$ the amount of itaconic acid initially present.

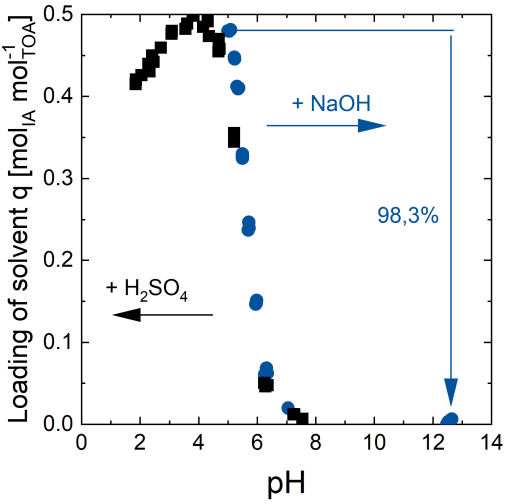

Figure 8.5.: pH-dependent extraction equilibrium of itaconic acid for extraction ■ and back-extraction ●. The maximum extraction was found near a pH value of 4.

The pH-dependent liquid-liquid equilibrium data fig. 8.5 was obtained from titration experiments. It indicates that almost complete back-extraction is achievable by a one step pH-shift to alkaline conditions. 98.3 % of the itaconic acid initially bound to the extractant were recovered when the pH value was elevated to pH = 12.5. The maximum recovery for extraction fig. 8.6 (A) and the maximal loading of the extractant fig. 8.6 (B) were determined by a five-stage cross-current batch extraction. The maximal average recovery for extraction was determined to 67.2 % for direct extraction of itaconic acid from the initially acidic fermentation broth. During extraction, the aqueous pH value increases due to the removal of protons from the aqueous phase with the

proceeding extraction of IA and eventually approaches neutral conditions fig. 8.6 (A). At the final pH value of 6.59, less than 0.1 % of the itaconic acid is present in its protonated form and thus the remaining itaconic acid becomes unavailable for extraction. The remaining fraction of itaconic acid corresponds to the 30.4 % of the total IA which were neutralized by the 3.8 L 3 M KOH added during fermentation. This has three implications: First, multi-stage reactive extraction can recover almost all itaconic acid that is available for extraction. Second, achieving a recovery of more than 98 % in a sequential process seems challenging as a pH value below 2 would be necessary with regard to itaconic acid equilibrium fig. 8.1. Third, co-extraction of inorganic anions will become a problem at such conditions. The maximal feasible loading of the extractant was determined at $0.88\,\mathrm{mol_{IA}mol_{TOA}^{-1}}$ for a multi-stage extraction from fermentation broth with a final pH value of approximately 4 fig. 8.6 which is close to the reported 1:1 complexes observed under ideal conditions [57]. Thus, the greatest potential is expected for process concepts running a fermentation at a pH value of 4 with *in situ* product removal by multi-stage extraction.

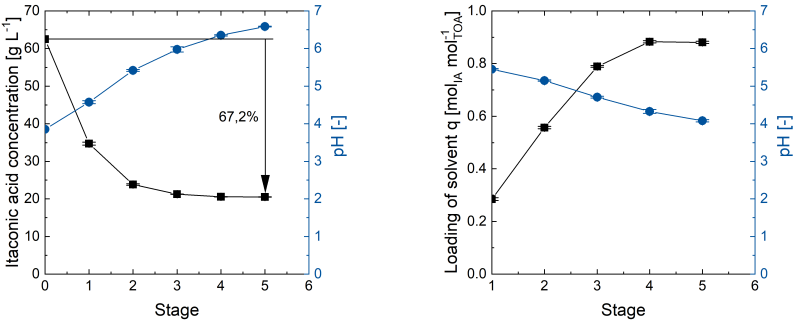

Figure 8.6.: Multi-stage "cross-current" batch extraction equilibrium of itaconic acid from fermentation broth. (A) Multi-stage extraction yield a maximal recovery of $67.2\,\%$ limited by the aqueous pH value. (B) A maximal loading of 0.88 $\mathrm{mol_{IA}mol_{TOA}^{-1}}$ is obtained from multi-stage extraction. Measured concentrations are displayed by ■ and pH values by ●, while the lines are visual help.

For the evaluation of crystallization processes the solid liquid equilibrium (SLE) is essential. It defines the solubility of itaconic acid at a given temperature, pH value and composition of solution. Hence, the yield of the crystallization process can be defined by:

$$\mathrm{Y} = \frac{\mathrm{n_{IA,(s)}}}{\mathrm{n_{IA,0} - n_{IA,SLE}}}. \tag{8.8}$$

Y is the yield, $\mathrm{n_{IA,(s)}}$ is the amount of produced solid itaconic acid, $\mathrm{n_{IA,0}}$ the initially dissolved amount of itaconic acid and $\mathrm{n_{IA,SLE}}$ the amount of itaconic acid dissolved due to the SLE. For a detailed explanation of the SLE the reader is referred to the paper [245].

8.4.2. Electrochemical pH-T-swing Separation

The low pH value of the fermentation broth enables direct extraction of itaconic acid. Solvent regeneration was realized by the cathodic reaction

of water electrolysis which supplied the OH^- ions to transfer the itaconic acid from the extractant to the aqueous phase. Simultaneously, the anodic reaction was used to convert the itaconate obtained during back-extraction, to itaconic acid which was isolated by a subsequent cooling crystallization. The courses of pH value and itaconic acid concentration in the aqueous phase are shown in fig. 8.8 (A) and (B). Cell voltage and power consumption during the pH-shift electrolysis are displayed in fig. 8.7.

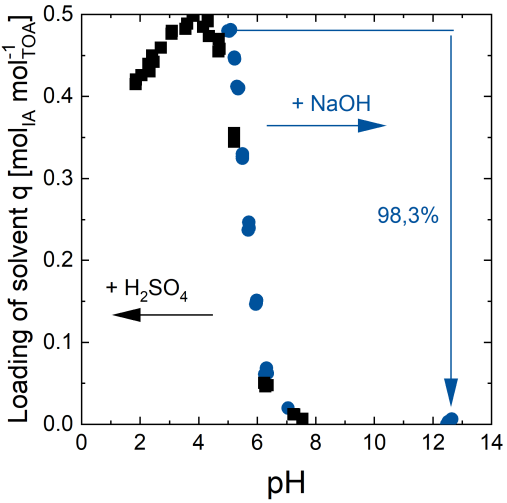

Figure 8.7.: Electrical power consumption, Cell voltage and total current during the pH-shift electrolysis.

The phase ratios of extractant and aqueous phase in the back-extraction were selected in such a way that an increase of itaconic acid concentration in the aqueous phase was obtained during back-extraction, overcoming the need for thermal energy for water evaporation prior to crystallization [219]. By conducting the back-extraction and protonation at elevated temperature, crystallization of itaconic acid in the electrol-

ysis module can be prevented. Both runs yielded comparable results for protonation, whereas the deviation observed for the course of the pH value is likely caused by the different initial pH values. The itaconic acid concentration in the aqueous phase of the cathode chamber decreases at the beginning of the experiment indicating that some itaconic acid from the aqueous phase is extracted due to the initially low pH value and high itaconic acid concentration in the cathode chamber. After passing a pH value of approximately 4 the concentration of the aqueous phases rises constantly and the itaconic acid is back-extracted into the aqueous phase. The produced OH^- ions cause the dissociation of itaconic acid and the complex formed in the organic phase breaks. The pH value rises from about 3 to a value of 6 showing the expected logarithmic course. The concentration of itaconic acid reaches a plateau of around $120\,g\,L^{-1}$. This demonstrates that electrochemical stripping is able to recover itaconic acid from the extractant and yield an aqueous solution with sufficiently high itaconic acid concentration to trigger crystallization after electrochemical acidification and cooling. During acidification conducted within the anode chamber fig. 8.8 (A), the concentration remains constant over the experiment until it reaches the SLE concentration at a pH value of approximately 4. The drop in the pH-curve after 4.5 h shows a sudden depletion of buffer capacity indicating complete protonation of itaconic acid. Shortly after, crystallization of itaconic acid in the samples drawn for HPLC analysis is observed. The samples were stored at a room temperature of 20 °C and filtered prior to analysis.

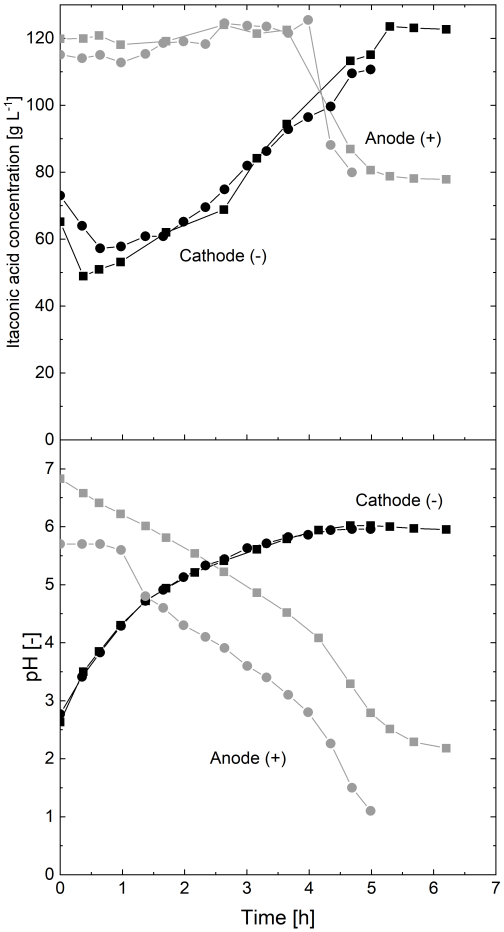

Figure 8.8.: Itaconic acid concentration (A) and pH value (B) in the aqueous phase of two experiments in anode (■ and ●) and cathode (■ and ●) chamber during pH-T-swing back-extraction with simultaneous protonation of itaconic acid. Crystallization of itaconic acid in the samples drawn after $4.5\,\mathrm{h}$ is observed. Symbols are measured pH values and concentrations and lines are visual help.

Inside the anode chamber no crystals were formed due to higher temperatures of around 35 °C. Once the itaconic acid on the anode side was protonated completely, no further back-extraction was observed. This is likely linked to a change of the main charge carrier once itaconic acid is protonated completely. The contribution of each ion species to the overall conductivity κ which is related to the ohmic resistance R by the geometric properties of the electrolyte $\frac{l}{A}$ is defined by [75].

$$R = \frac{l}{A \cdot \kappa}. \tag{8.9}$$

The conductivity is calculated from the charge number, the ion concentration in $\mathrm{mol/cm^{-3}}$, the concentration and the ion specific limiting conductivity λ_i by [246]

$$\kappa = \sum |z_i| c_i \lambda_i. \tag{8.10}$$

Under the assumption that only cations can participate in the charge transfer across the cation exchange membrane, H^+ ions and Na^+ ions are the major charge carrier during pH-swing electrolysis. Taking into account the initial and final concentration of H^+ ions and Na^+ ions in the anolyte into account, the ion specific contribution to the overall conductivity is calculated and displayed in table 8.1. Comparing the

Table 8.1.: Change in ionic conductivity [2]

	c_{init}	c_{end}	λ_0	κ_{init}	κ_{end}
H^+	10^{-7}	0.1	349.65	$3.50 \cdot 10^{-7}$	$1.75 \cdot 10^{-2}$
Na^+	1.8	0.4	50.08	$9.01 \cdot 10^{-2}$	$5.01 \cdot 10^{-4}$

conductivity in the beginning and in the end reveals that initial Na^+ ions associated conductivity is $2.85 \cdot 10^5$ times higher than the conductivity constituted by H^+ ions. Yet, in the end the proton associated conductivity increases and becomes two times higher than the conductivity provided by Na^+ ions. To conclude, as long as Na^+ ions are present on the anode chamber, they remain the major charge carrier. When the pH

value drops and Na^+ ions become depleted, protons start to participate in charge transfer, which inhibits further pH-shift on the cathode side because H^+ ions migrate to the cathode and neutralize the OH^- ions immediately. As a result, the pH-shift efficiency η_{pH} deceases due to the loss of H^+ ions and results in values of 63 % and 79 %. Another reason for the drop of the efficiency is that nearly all of the itaconic acid is already protonated so that the produced H^+ ions can no longer bind to itaconic acid molecules. Consequently, the electrochemical pH-shift should be stopped when pH values of around 2.5 are reached in order to achieve both, maximum efficiency and yield at the same time. The yield will not be improved if the pH value drops under 2.5, since the SLE is nearly constant.

The repeated execution leading to comparable results, demonstrates that the process layout presented in fig. 8.2 is feasible. Itaconic acid was subsequently recovered by cooling crystallization. Analysis of the crystal material revealed a purity of >99 % for the itaconic acid obtained in each run. The three selective processing steps, extraction, back-extraction and crystallization, allow the production of pure itaconic acid from fermentation broth. An image of the product of each process step and the crystalline product is given in fig. 8.9. The yield Y reaches values of 91.2 % and 90.9 %. The itaconic acid crystals exhibited the typical rhombic shape fig. 8.9.

Cooling crystallization has the advantage that no energy intensive water evaporation is required and particle size distribution as well as product purity can be further improved by optimized cooling profiles. Afterwards, the mother solution can be recycled to the cathode side and reloaded with itaconic acid in the back-extraction fig. 8.2.

From the mass of crystalline itaconic acid obtained after crystallization and the recorded power input the overall energy input was calculated to $10.9\,\mathrm{kWh\,kg_{IA,s}^{-1}}$. For energy calculations only the solid fraction of itaconic acid is considered. The overall efficiency in this case is determined to 25 % eq. (8.4). Taking into account the $80\,\mathrm{gL^{-1}}$ of protonated itaconic acid left in the mother liquor after cooling to 20 °C into account and considering that complete protonation was reached after

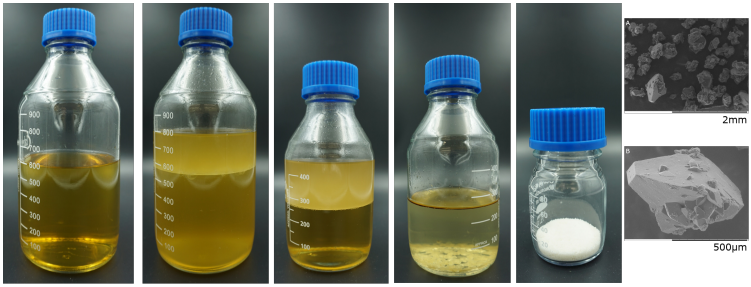

Figure 8.9.: Images of processing steps: 1) Filtrated fermentation broth 2) Extraction 3) pH-swing back-extraction 4) pH-T-swing crystallization 5) itaconic acid crystals after filtration and drying 6) the recovered crystals (A) and a close-up (B).

5.3 h, the protonation efficiency η_{pH} of itaconic acid was 96.2 %. Afterwards, the efficiency drops drastically due to the depletion of Na^+ and the corresponding loss of H^+ ions as discussed above. With regard to the overall process leaving behind protonated itaconic acid in the mother liquor inevitably lowers the overall efficiency for separation. As the protons will be lost once the mother liquor is returned to the cathode. This results in a trade-off between energy demand for cooling and protonation because at lower temperatures a larger fraction of the itaconic acid can be recovered in the cooling crystallization. With the power input of 80 W and the Na^+-ion transfer rate a minimal power consumption of 4.2 $\mathrm{kWh\,kg_{IA}^{-1}}$ protonated is determined for this electrolysis cell. When exploiting the full capacity of itaconic acid solubility at the pH value of 4 (300 $\mathrm{g\,L^{-1}}$) and conducting cooling crystallization at 5 °C a minimal power consumption of 4.8 $\mathrm{kWh\,kg_{IA,s}^{-1}}$ is expected. Considering the comparably wide electrolyte gap of 28 mm, recovery of crystalline itaconic acid with a high purity and a power consumption below 5 $\mathrm{kWh\,kg_{IA,s}^{-1}}$ seems feasible. It should be pointed out that comparable electrodialysis processes operate at lower current densities and the current densities achieved in this setup operate in the same magnitude

like recent bipolar membrane (BPM) processes [242]. Comparing the operational costs expected for electricity with the material costs for pH-adjustment by acid and base reveals the promising economic potential of the pH-T-swing process. H_2SO_4 and NaOH are considered the industrially established standard for pH-controlling agents. With the current costs for H_2SO_4 ($140\,\mathrm{EUR\,t^{-1}}$) and NaOH ($300\,\mathrm{EUR\,t^{-1}}$) this amounts to $29\,\mathrm{ct\,kg_{IA}^{-1}}$. Assuming an electricity price for industrial customers in Germany of $6\,\mathrm{ct\,kWh^{-1}}$, the electricity costs for itaconic acid recovery amount to $28.8\,\mathrm{ct\,kWh^{-1}}$ [247]. In sweet spots for renewable energy, electricity is available at prices below $2\,\mathrm{ct\,kWh^{-1}}$ [248], meaning electricity costs for itaconic acid recovery would be reduced to $9.6\,\mathrm{ct\,kWh^{-1}}$. This back of the envelope calculation and comparison of operational expenses demonstrates the economic potential if waste producing additives are replaced by electrochemically driven process steps operated with renewable electricity. However, in order to validate the cost advantage of electrochemical pH-swing separation processes the capital expenses for electrolyzers must be taken into account, too. This also requires detailed analysis and experimental data for the lifetime of key equipment such as electrodes and membranes used in pH-swing electrolysis. Beyond reduced additive costs, the utilization of renewable electricity can provide additional value if the process is operated with a suitable demand side management [249]. Especially creating value by harnessing times of abundant electricity supply from renewable sources or the ability to provide fractions of the nominal power consumption as primary control power for electricity grid stabilization can become a competitive advantage for companies looking for a sustainable future.

8.5. Conclusion

The joint application of low pH value itaconic acid fermentation followed by an electrochemically driven pH-T-swing separation process enabled the production of pure bio-based itaconic acid in crystalline form. An assessment of the electrochemical stability revealed no major

degradation of itaconic acid at water splitting catalysts. Thus, direct pH-shift water electrolysis can be used to drive pH-reversible reactive extraction and crystallization of itaconic acid [38, 241, 140, 146]. The $100\,cm^2$ laboratory pH-shift electrolysis cell already showed a performance comparable to other ED processes reported for di-carboxylic acid recovery [42].An assessment of the pH-dependent extraction behavior of itaconic acid showed the best extraction performance for an aqueous pH value of 4 and almost complete regeneration of the extractant by alkaline stripping. Investigations of multi-stage cross-current extraction demonstrated that a high loading of the extractant is feasible, if the aqueous pH value is maintained at its optimum. The extraction yield is limited by the fraction of itaconic acid available in its protonated form. The best performance is expected for a setup featuring low pH value fermentation, with pH-management by *in situ* removal of itaconic acid via multi-stage reactive extraction, followed by the presented electrochemical pH-T-swing process. Herein, the water electrolysis has to be adjusted precisely to operating conditions, as for example pH value and salt concentration, in order to minimize power losses. Furthermore, the measured pH-dependent SLEs of itaconic acid indicate that the final pH value for the electrochemically induced crystallization of itaconic acid should not be lower than 2.5, in order to achieve a high efficiency. To fully exploit the synergies of low pH value fermentation and pH-T-swing separation the implementation of a process setup with *in situ* product removal is the next step. To further validate the promising results, future investigations should address the long term stability of the ion exchange membranes if exposed to solvent traces and biogenic material and thoroughly analyse the overall processing costs in order to validate the economic potential. Nonetheless, it is expected that the herein presented findings for itaconic acid can be transferred to the recovery of other di-carboxylic acids such as adipic or succinic acid and foster the development of sustainable production routes for bio-based platform molecules.

9. Techno economic assessment of bio-SA downstream technologies

[‡] Finding economically viable ways to produce biobased chemicals is a major challenge in the transformation from fossil to renewable resources. The rally in crude oil prices in the 2000s started a first wave of research and development in industrial biotechnology that led to the concept of bio-based platform molecules[250, 251] accompanied by the identification, characterization and development of high performance microbial catalysts [252, 253, 254, 255].

Among the potential molecules, succinic acid was regarded a high profile candidate [256, 257, 258]. This led to commercial interest and the founding of several companies like BioAmber, Succinity (BASF/Corbion), Myriant and Reverdia (DSM/Roquette) who targeted the industrialization of the bio-based succinic acid (bio-SA) production [259]. The global market for succinic acid was estimated at 40.000 MT in 2010 and was expected to grow with a CAGR between 20 %-35 % from 2010 to 2020 [260]. This was partially driven by the expectation that the availability of natural gas supplied by the North American shale-gas boom would lead to a shift of the refining and steam-cracker capacity from naphtha toward natural gas as the main feedstock. The substitution of naphtha with natural gas reduces the amount of benzene, toluene, and xylene as well as butene produced by the steam cracking process, thus providing a potential niche for bio-based C4 platform chemicals like succinic acid. [261] In addition, development of new microbial strains capable of producing succinic acid at low pH was considered a break-

[‡]Parts of this chapter are intended for publication in Gausmann et al. "Techno economic assessment of downstream technologies for CO2-negative bio-succinic acid production" (2023), (Manuscript in preparation)

through that would increase the economic success of bio-SA [262]. Despite the promising perspective and the momentum that bio-SA technology has gained from market observers [263], commercial success has stalled and in recent years all companies that were pioneering the development have ended or refocused their business activities. In 2018 the last remaining player BioAmber declared bankruptcy [264] and liquidated the 141 mio USD investment in the Sarnia plant, which was originally designed to produce 30 kT/a succinic acid. In a recent case study, Li and Mupondwa analyzed the BioAmber bio-SA process and identified technological and economic obstacles that led to the demise of BioAmber's business. They concluded that higher than expected production costs combined with lagging demand from the market made the plant unable to operate at full capacity [265]. Additionally, a strong reliance on licensed technology from external partners and the lack of company owned process know-how and R&D experience limited the ability to solve the engineering challenges encountered during scale-up. A major cost driver were the purification costs which represented 40 % of the overall production costs, while above 80 % of the total utility consumption was attributed to downstream processing [265]. The economic fate of bio-SA is determined by three key aspects: 1. upstream performance (yield, titer, productivity), 2. low-cost secondary or tertiary feedstock (waste streams, non-food, lignocellulosic) and 3. Cost effective recovery and purification of the product [266]. With the development of high-performance microbial catalysts table 9.2 which reach titers up to 110 g/L and yields >1 g_P/g_S due to the fixation of CO_2 as a secondary carbon substrate [119, 267, 3], production is no longer the bottleneck of bio-SA production [268]. For this reason, cost-effective downstream processing is a key enabling technology for the commercial success of bio-SA [20]. This is underlined by the results from previous life cycle (LCA) and techno economic assessment (TEA) studies which revealed potential ecological advantages of bio-SA over petroleum-based succinic acid synthesised *via* maleic anhydride [15]. However, the ecological advantage and the feasibility of economic competitiveness are lost with inefficiencies in the downstream process. Although the uti-

lization of waste and residue streams provides a viable option to reduce raw material costs[269] the impact of the downstream process is reportedly dominant in overall process competitiveness [114]. The layout of the downstream process is largely dependent on the type and strain of the biocatalyst. While prokaryotic strains such as *Mannheimia succiniciproducens* or *Escherichia coli* grow at neutral pH conditions [252, 270], eukaryotic strains such as yeasts *Sacharomyces cerevisiae* and *Yarrowia lipolytica* [271, 272] tolerate more acidic conditions. In neutral-pH fermentation, bio-SA is produced in its succinate form and must be converted to free acid during recovery. This conversion requires an at least equimolar addition of base and acid [19]. Despite the high yield, productivity, and titer that have been reported for prokariotic succinic acid producerstable 9.2 the latest LCAs advocate low-pH fermentation as superior process technology due to ease of downstream processing [114, 265, 273, 268]. However, these processes apply aerobic cultivation conditions and the ease of downstream processing is earned at the expense of CO_2 emissions [49]. On the other hand, fixing prokaryotic strains require strategies for pH control that do not rely on the extensive utilization of acid and base [274, 3]. In this light, the recent emergence of electrochemical separation technologies could provide the separation technology needed [42, 43]. Reports of the electrochemical separation of bio-SA by electrodialysis (ED) date back more than 30 years [275, 19]. But their application was considered costly due to high electricity prices [114] and limitations of the achievable current density [276]. However, innovative processes such as direct electrochemical anion extraction or electrochemical pH swing reactive extraction concepts [37, 39, 40, 140, 277] not only mitigate acid and base usage but also enable continuous *in situ* product removal and thus extended batch or potentially continuous bio-SA fermentation processes with closed recycle loops for process water and pH control agents. A key element for the revival of electrochemical separation technologies is the drop in electricity production costs facilitated by the improvements of renewable energy sources [30]. However, to profit from the low generation costs, electrochemical separation processes must be able to cope with the in-

termittent supply of renewable energy sources such as wind and solar. The objective of this chapter is to analyze the technological limits and evaluate the economic performance and environmental footprint of different downstream technologies for the production of bioSA. Based on current scientific and patent literature, five downstream process alternatives that have not been covered by other TEA or LCA studies are identified. These process routes were modeled by flowsheet simulations in ASPEN, which yielded mass- and energy balance data and estimations for the equipment size. The simulation results are analyzed and discussed with regard to the thermodynamic limits of microbial succinic acid production and the measures required to adapt for the utilization of renewable electricity for the separation of bio-SA.

9.1. Biothermodynamic of succinic acid fermentation

The thermodynamic limits of microbial bio-SA production were derived in chapter 2. Bio-SA production is only viable below the limiting line for the respective export mechanism. Sustaining an extracellular pH value below tree requires additional ATP to drive product export by ABC or antiport combined with H^+ export by H+-ATPase, which maintains the homeostasis of inner cellular pH [47]. As a consequence, acidic fermentation has the drawback that a lower extracellular pH is sustained at the expense of increased energy demand for product export. Concentrations and pH values required for technical operations seem only feasible if additional metabolic energy is available, for example from aerobic respiration or side product formation. Furthermore, the back-diffusion of protonated succinic acid becomes more severe at low extracellular pH and high extracellular succinate concentrations [50, 51]. From these findings, it is concluded that the development of low-pH tolerant strains has the potential to reduce the separation effort but the metabolic energy gain imposes operational limits, which must be taken into account in order to not compromise the metabolic carbon yield.

9.2. Conceptual process design and evaluation of bio-SA recovery

A detailed LCA of the whole bio-SA process was covered including a comparison of different raw materials was covered in other studies[114, 278, 273] thus, this analysis focuses on evaluating the performance of different separation technologies for similar initial conditions. Figure 9.1 displays the methodological steps of the study presented in this chapter.

9.2.1. Goal & scope

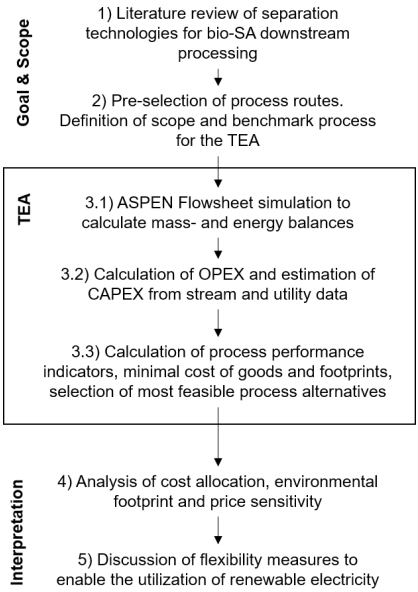

Figure 9.1.: Steps for the techno economic assessment

The challenge of succinic acid separation is the recovery of the product (300) fig. 9.2 after fermentation, which focuses primarily on the separation from water and the removal of the main organic impurities such

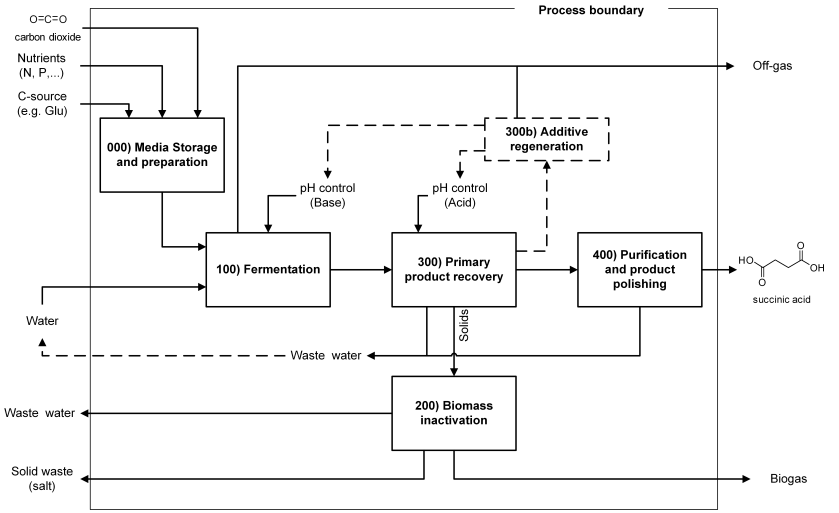

Figure 9.2.: Conceptual bio-SA process. Dashed lines indicate potential recycle streams enabled by additive regeneration or ISPR.

as biomass or substrate residues. Product recovery is accompanied by a biomass inactivation processing step (200) and followed by a product purification and polishing step (400) fig. 9.2 that yields pure bio-SA in crystalline form. López-Garzón and Straathof provide an extensive review of the state-of-the-art downstream processing technologies applicable to bio-SA processing [23].

Table 9.1.: Downstream processes for succinic acid recovery

Process	**Selected for TEA**	**Rationale**	**Acronym**
Calcium precipitation and resolution with sulphuric acid	yes	Considered as the benchmark process	1-Ca
Magnesium precipitation and thermal salt cracking	yes	New technology for the salt waste free recovery of carboxylic acids	2-MgCl
pH swing extraction	yes	Low-energy process suggested for the recovery and ISPR of carboxylic acids	3-Ex
Acidic fermentation	yes	Low pH fermentation with direct crystallization is considered the most promising option for bio-SA production	4-Ac
Electrochemical pH swing extraction	yes	Electrochemical pH swing overcomes the pH missmatch between up- and downstream thus enabling ISPR and salt waste free bio-SA recovery	5-eEx
Electrodialysis	no	Inferior performance due to high equipment costs and energy demand for water removal [114]	-
Ion exchange process	no	High additive demand for IEX regeneration leads to inferior process performance[114]	-
Direct electrochemical carboxylate extraction	no	Recently covered in another study[273]	-

Table 9.1 gives an overview over the most relevant recovery technologies applicable in the separation of succinic acid. The calcium precipitation process (1-Ca) is commonly applied for the recovery of (di-)carboxylic acids [19, 23]. The thermal salt cracking process (2-MgCl) is a proprietary technology of corbion, originally developed for the salt waste free recovery of lactic acid [279]. Eggert et al. proposed the pH swing extraction (3-Ex) for the recovery of itaconic acid, which is considered applicable to succinic acid due to its molecular similarity [63]. Low pH fermentation (4-Ac) is regarded as having the most promising perspective for the commercialization of bio-SA [114, 280, 265, 268, 273]. In this thesis, the concept of electrochemical pH swing extraction was developed, which enables the separation of succinic acid [140, 158] and other carboxylic acids with closed recycle loops for water and base and features electrochemical regeneration of acid and base [281, 8].

9.2.2. Microbial succinic acid production

The microbial succinic acid production is modeled by a lumped reaction that is calculated based on experimentally reported prokariotic fermentation values of Lee et al. and Becker et al [120, 282]. The elemental composition of the biomass is represented by an average formula:

$$\text{CDW:} \quad C_1H_{1.7}O_{0.387}N_{0.24}P_{0.02} \tag{9.1}$$

It represents the average composition of 1 gDW of cell mass determined experimentally and by metabolic flux analysis [252] and resembles the values used in recent LCA studies [114]. For eukariotic fermentation, Li et al. and Xiberras et al. are used [283, 284]. The fermentation is split in a seed train and the main fermentor. Practically, fermentation would be operated batch-wise with multiple reactors in parallel. The harvest tank after fermentation can store the volume of one fermentor, enabling the continuous operation of the subsequent downstream.

While the seed train is used to cultivate the biomass required to inoculate the main fermenter, succinic acid is solely produced in the main

fermenter according to the following equation:

$$1\,C_6H_{12}O_6 + 1.3\,CO_2 + 0.013\,(NH_4)_3PO_4 + 0.114\,NH_3 \tag{9.2}$$

$$\longrightarrow 1.53\,C_4H_6O + 0.24\,C_2H_4O_2 + 0.6339\,C_1H_{1.7}O_{0.387}N_{0.24}P_{0.02} \tag{9.3}$$

The formation of acetic acid is included in the reaction to account for the formation of potential by-products. By-products such as acetic, formic, lactic acid or ethanol are formed by prokariotic organisms under CO_2 limiting conditions [267]. Thus, acetic acid is often found in significant amounts and is chosen as the exemplary by-product [285, 282].

Table 9.2.: Summary of succinic acid producing strains

Strain	**Substrate**	**Titer** (g/L)	**STY** (g/L/h)	**Yield** (g_P/g_S)	**pH**	**Ref.**
A. succinogenes FZ53	Glu	105.8	1.36	0.82	6-7.2	[286]
M. succiniciproducens MBEL55E	Glu	10.5	1.75	0.95	6.5	[119]
M. succiniciproducens PALKG	Sucr	78.4	6.02	1.07	6.5	[120]
B. succiniciproducens	Glu	20	1.02	0.71	7*	[282]
B. succiniciproducens LU15224	Gly + Mal	69.8	2.91	1.11	6.5	[287]
B. succiniciproducens DD1	Sucr	71	0.78	0.86	6.5	[288]
E. coli AFP111	Glu	99.2	1.31	1.1	6.8-7	[289]
E. coli SD121	Glu	116.2	1.55	1.13	6.7	[270]
C. glutamicum BOL	Glu	133.8	2.53	1.09	6.9	[290]
C. glutamicum NC-3-1	Glu	113.0	2.35	0.94	7**	[291]
S. cerevisiae PMCFfg	Glu	13.0	0.11	0.13	4.0-4.5	[271]
S. cerevisiae CEN.PK113-1A	Gly	10.7	-	0.22	5.0	[284]
Y. lipolytica PGC202	Gly	110.7	0.8	0.53	3.6	[280]
Y.lipolytica PGC202	Glu	71.6	0.6	0.61	2.8	[283]

*Buffering with $MgCO_3$ reported

**Buffering with $NaHCO_3$ reported

Glucose (Glu), Sucrose (Sucr), Glycerol (Gly), Maltose (Mal)

9.2.3. Separation process description and simulation

Simplified flowsheets of the downstream processes investigated are shown in figs. 9.3 to 9.7. Pumps and heat exchangers are omitted for the sake of clarity, but are considered in the Aspen model. Physical property data was retrieved from the Aspen database. The electrolyte non-random-two-liquid Redlich-Kwong (ENRTL-RK) property method and the true component approach was used to calculate the electrolyte chemistry of weak acid and salt in water. Missing NRTL parameters were estimated using the UNIFAC method. Physical properties of the acid species were approximated with the parameters of the free acid form with manually modified molecular weight and charge.

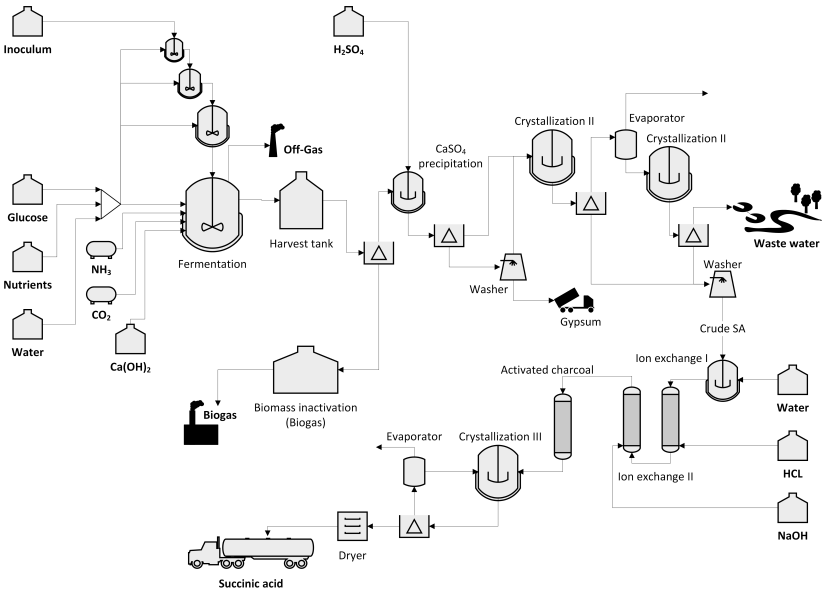

Figure 9.3.: Flowsheet for the bio-SA production process with calcium precipitation (1-Ca)

Calcium precipitation (1-Ca). The entire bio-SA process with all sections is shown exemplarily in fig. 9.3. The polishing section (400)

is not shown in the other process flowsheets, as its layout is not modified and is always considered equal. However, depending on the purity of the crude SA after recovery, the additive and energy consumption vary. Calcium precipitation purification is probably the most widely applied downstream method for carboxylic acid purification [19, 250]. It operates with anaerobic fermentation whose pH is maintained under neutral conditions by adding calcium oxide or calcium hydroxide. Due to its low solubility, calcium succinate precipitates in fermentation and is withdrawn as a suspension [23]. After biomass separation, succinic acid is recovered by adding concentrated sulfuric acid. This yields a concentrated solution of succinic acid and gypsum$CaSO_4$ in an equimolar ratio. The concentrated succinic acid is purified by a sequence of cooling and evaporation crystallization, which yields crude bio-SA crystals. The remaining ionic and organic impurities are then removed by a sequence of ion exchange and activated carbon adsorption.

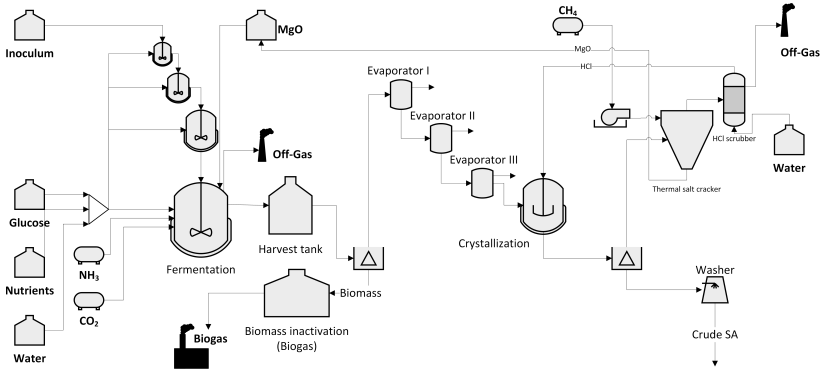

Figure 9.4.: Flowsheet for the bio-SA production process with thermal cracking of MgCl (2-MgCl)

Thermal cracking of MgCl (2-MgCl). Acid and base recycling technology by thermal cracking of MgCl fig. 9.4 was developed by Corbion for the salt waste free processing of lactic acid[213] but also tested for succinic acid purification [279]. The pH in fermentation is controlled

by MgO and $Mg(OH)_2$. This presents two advantages. First, the use of magnesium appears to promote fixation of CO_2 [292, 293]. Second, HCl and MgO can be regenerated from MgCl by thermal cracking. Compared to calcium salt, magnesium succinate has a high solubility of up to 500 g/L as reported in the patent [279]. The biomass-free fermentation broth is concentrated by multieffect evaporation up to the saturation concentration of magnesium succinate. pH shift and cooling crystallization are used to recover the crude succinic acid. The remaining mother liquor containing the $MgCl_2$ and residual succinic acid is fed into a hot gas flame for thermal cracking. At 350-450 °C magnesium chloride decomposes:

$$MgCl_2 + H_2O \longrightarrow MgO + 2\,HCl \tag{9.4}$$

The regenerated MgO is separated from the exhaust gas, washed with water, and returned to fermentation. HCl is recovered from the exhaust gas by scrubbing and returned to the fermentation.

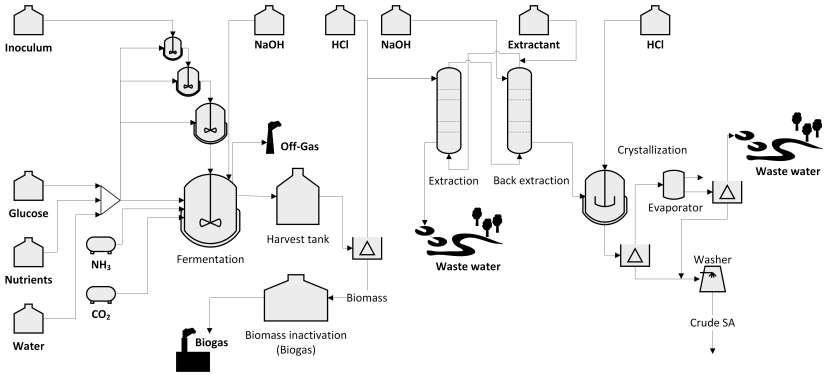

Figure 9.5.: Flowsheet for the bio-SA production process with pH swing extraction (3-Ex)

pH swing extraction (3-Ex). Reactive extraction fig. 9.5 is extensively studied for its application to the separation of carboxyclic acids [62, 100, 101, 103, 142, 63]. Reactive extraction has the advantage of

mild process conditions that do not require energy for evaporation [20]. In addition, the high recovery rates demonstrated for reactive extraction make the technology a viable option to prevent product losses and achieve high yields [294, 44, 139]. The extraction mechanism is based on reversible complexation of the protonated succinic acid with a tertiary amine [62, 134]. In this study tri-n-octylamine (TOA) mixed with n-decanol is used [295]. Sodium hydroxide is used to maintain a neutral pH in fermentation. Afterwards, the fermentation broth is clarified and acidified before extraction. A pH swing is used to recover succinic acid from the organic phase in a concentrated solution. The crude bio-SA is then recovered by cooling crystallization followed by a final evaporation step to avoid product losses with the salt-containing waste water.

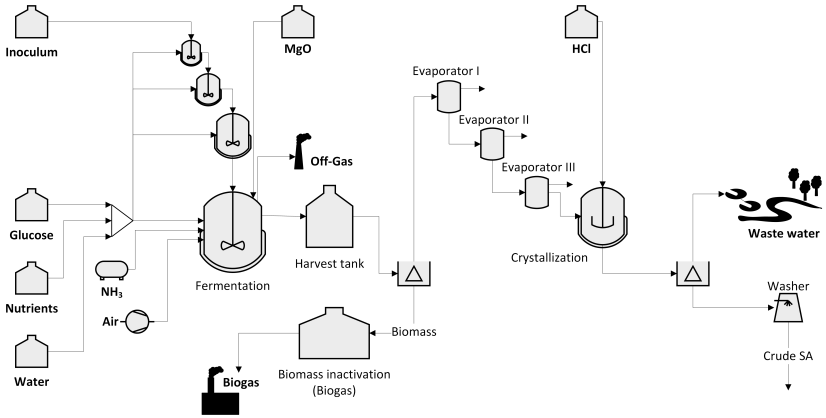

Figure 9.6.: Flowsheet for the bio-SA production process with low pH fermentation (4-Ac)

Low pH fermentation (4-Ac) fig. 9.6 The development of low pH tolerant strains significantly simplifies the downstream processing of bio-SA significantly [296, 283, 297, 284]. At pH 2.8 95 % succinic acid is present in the protonated form. The base consumption during the fermentation is accordingly reduced. This enables direct crystallization of the fermentation broth after water removal by multi-effect evaporation

[21]. Since small amounts of base are still necessary in the fermentation, the remaining succinate fraction is converted by the addition of hydrochloric acid. In contrast to the other processes, low-pH fermentation operates aerobically and requires the supply of additional oxygen.

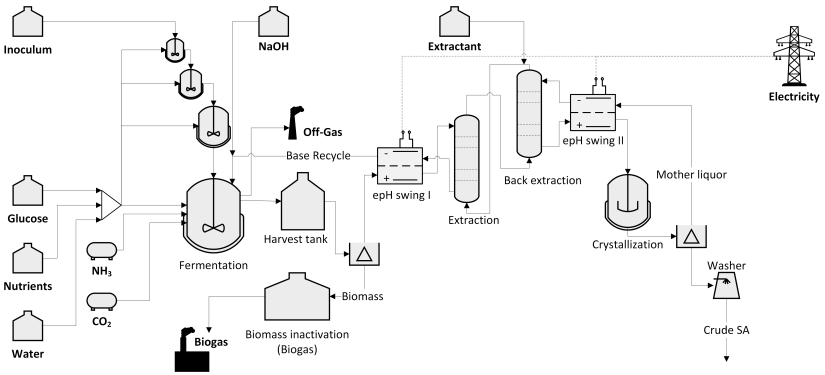

Figure 9.7.: Flowsheet for the bio-SA production process with electrochemical pH swing extraction (5-eEx)

Electrochemical pH swing extraction (5-eEx) The electrochemical pH swing extraction process uses protons and hydroxide ions generated by electrochemical water splitting to provide the acid and base that drive the pH swing extraction [140]. Its layout is comparable to fig. 9.5 but instead of discharge of waste water, the fermentation broth and the mother liquor are recycled within the process. This enables closed-loop operation and mitigation of most of the salt discharge from the process. To avoid the accumulation of trace components in recycling, purge rates on the order of 2 % are required. The clarified fermentation broth is fed to the anode side of a water electrolyzer where the protons produced at the anode pronate succinic acid. Meanwhile, the electric circuit of the pH swing electrolysis is closed by the cations from the base that was used to control the pH in fermentation, e.g. Na^+. This electrodialytic recovery of cations generates an alkaline solution on the cathode side which is returned to the fermenter for pH control. The succinic acid is recovered from the loaded solvent by a second pH swing. By adjusting

the phase ration in the back extraction, a concentrated succinate solution is obtained. This solution is then acidified at elevated temperature by a second pH swing electrolysis [281]- Finally, the crude bio-SA is obtained by cooling crystallization, and the mother liquor is recycled to the cathode side of the second pH swing electrolysis. Electrochemical separation technology also enables the use of renewable electricity for separation. To adapt the process to the intermittent supply from renewable sources, additional storage tanks are required for the fermentation broth and catch-up capacity reserves for the electrolysis cells. A scaling exponent of 0.8 is assumed for the additional tank capacity and that the investments costs per kW installed electrolysis capacity will reduce from $600\,\mathrm{EUR/kW_{in}}$ to $300\,\mathrm{EUR/kW_{in}}$ due to the ongoing development and industrialization of electrolyzer production [31].

9.2.4. Process footprint and economic assessment

Process performance & footprints The process footprint analysis covers scope 1 emissions for CO_2, production of solid waste and the consumption of fresh water. In addition, emissions from scope 2 CO_2 for utilities are considered.

$$E_{\mathrm{s}} = \frac{\dot{m}_s}{\dot{m}_{\mathrm{bio-SA}}} \tag{9.5}$$

A scope 3 analysis is outside the scope of this study, as it would mix results affected by downstream technology with results determined by the selection of raw materials, the location of the site and the actual structure of the plant supply chain. The downstream yield is calculated according to:

$$Y_{\mathrm{DSP}} = \frac{\dot{m}_{i,\mathrm{SA}}}{\dot{m}_{\mathrm{ferm,SA}}} \tag{9.6}$$

and the overall process yield:

$$Y_{\mathrm{P}} = \frac{\dot{m}_{\mathrm{bio-SA}}}{\dot{m}_{\mathrm{Glu}}} \tag{9.7}$$

Based on the mass flow of succinic acid in the respective process stream. The reference stream for Y_{DSP} is the mass flow of succinic acid in the effluent of the fermentor $\dot{m}_{ferm,SA}$.

Economic assessment The cost of manufacturing (COM) are calculated based on operational expenditure (OPEX) considering costs for raw material, utilities, waste disposal, labor and maintenance, and depreciation. The inventory of prices is listed in appendix H. A nameplate capacity of 30 kT/a is selected. Equipment costs are estimated with the Aspen sizing tool. The bioreactor volume is calculated manually on the basis of the volumetric productivity, respectively residence time, and the desired product mass flow. Capital expenditures (CAPEX) are calculated from the equipment costs scaled by the Lang factor method [298]. The capital costs of the pH swing electrolysis are calculated on the basis of the installed power [31].

9.3. Results and Discussion

9.3.1. Cost of manufacturing analysis

The stream data obtained from the ASPEN flowsheet simulation is used to estimate the COM of bio-SA production fig. 9.8. Of the five different downstream technologies that were investigated, calcium precipitation (1-Ca), thermal acid and base recycling (2-Therm) and flexible electrochemical pH swing extraction with energy (5-eEx-flex) show the potential to produce bio-SA below the current market price of fossil succinic acid [273]. The chemical pH swing extraction process (3-ABEx), the low pH fermentation (4-Ac) and likewise the electrochemical pH swing extraction with natural gas based electricity supply are not competitive.

In line with previous studies, raw material expenses account for 36-68% of the total COM [114, 273]. Maintenance and depreciation costs

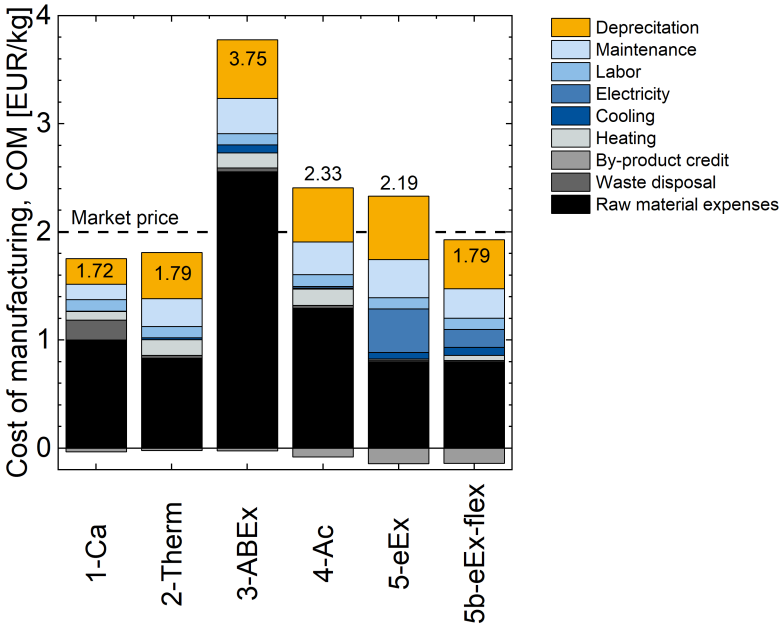

Figure 9.8.: Cost of manufacturing for 1 kg of bio-SA exCO2-tax. Labor costs calculated from 36 FTEs for the operation of two personal engineers and two plant engineers. The maintenance costs are calculated as 6 % of the installed capital and depreciation of the plant equipment is based on a ten years period.

are identified as second and third, indicating a high relevance of total capital costs [92]. The calculated CAPEX ranges from 71 mioEUR (1-Ca) to 179 mioEUR (5-eEx). This range is comparable to the investment reported for the BioAmber plant [265]. The 1-Ca process has the lowest overall CAPEX, as it does not require sophisticated equipment. Low pH 4-Ac fermentation requires larger fermentor volumes compared to the other processes. This is due to the low volumetric productiv-

ity of yeast hosts compared to prokaryotic succinic acid producers table 9.2. Similarly, a volumetric productivity of 6.02 g/L/h was reported for *M. succiniciproducens*[120] while the productivity for *Y. lipolytica* is an order of magnitude lower (0.6 g/L/h)[283]. To compensate for the lack of productivity, yeast fermentation operates with a higher cell density of 24.5 g/L compared to the 7 g/L reported for prokaryotic strains. Electrolyzer costs constitute the largest CAPEX position for the 5-eEx and 5-eEx-flex process. However, an industrialization of the electrolyzer manufacturing and a reduction of the noble metal content in the catalysts have the potential to reduce the required CAPEX. Based on current projections, an expected cost cut of 50 % for the electrolyzer CAPEX would place the 5-eEx-flex process in the same range as the 4-Ac and 2-Therm process.

Raw material expenditures are the most relevant constituent of the bio-SA COM. A detailed division is shown in fig. 9.9. Except for 3-ABEx, glucose costs account for the largest fraction of raw material costs. Second to glucose come the costs of pH control agents. In case of 4-Ac the glucose expenses account for 85 % of the raw material costs, which is a result of the low yield in fermentation. Although the 4-Ac downstream process achieves a recovery of 96 % and a yield of 92 % in the polishing section. The downstream process cannot compensate for the loss of carbon substrate in aerobic fermentation. This finding underlines the previous conclusion and illustrates that optimizing fermentation to facilitate downstream processing must not compromise on the carbon yield of fermentation. The 5-eEx process revealed the highest overall yield with 83 %. This results from closed recycle loops that minimize product losses downstream. However, accumulation of acetate in the mother liquor recycling loop was observed fig. 9.7. This accumulation required a stream of purge of 2 % to maintain constant acetate concentrations in the crude crystallization of bio-SA. A similar trend is expected for other potential side products, especially lactic and formic acid. Optimization of the product spectrum and targeted metabolic engineering to reduce the amount of short-chain carboxylic acids could

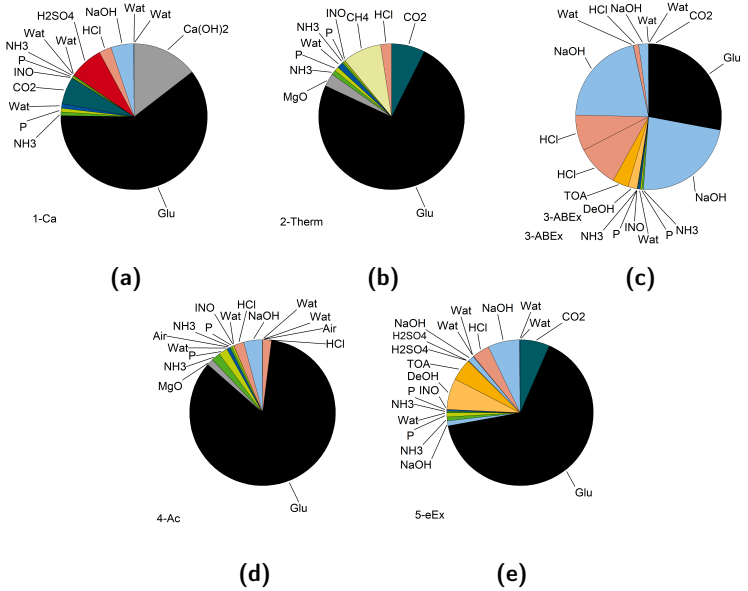

Figure 9.9.: Distribution of raw material expenses for a) 1-Ca, b) 2-Therm, c) 3-ABEx, d) 4-Ac and f) 5-eEx process. Water (Wat), Acids (H_2SO_4, HCl), Base (NaOH, $Ca(OH)_2$, MgO), Inoculum (INO), Nutrients (P, NH_3) and solvents: n-Decanol (DeOH), Tri-n-octylamine (TOA)

reduce the required purge stream and thus reduce the associated loss of product [3].

Product losses in the other separation processes are mainly imposed by solubility limits. In 1-Ca the residual solubility of calcium succinate causes product losses in the recovery step. The product losses in 2-Therm and 3-ABEx are caused by the solubility limit of the co-salt NaCl and MgCl respectively, which prevent complete evaporation. To minimize significant product losses in this step, only acids and bases that form a highly soluble salt are recommended to be used for pH control. The results presented here are based on the available solubility data. It should be noted that salting-out effects could reduce product loss, because high salt concentrations reduce the solubility of succinic acid

[299]. On the other hand, the high salt concentration reduces the purity of the crude bio-SA.

9.3.2. Environmental footprint

Figure 9.10 shows the environmental scope 1 for the process related to CO_2, water, and emissions (off-gas, waste, biogas). Scope 2 emissions of CO_2 for utilities (electricity, heating, and cooling) are inculded, while other scope 2 and scope 3 environmental impacts are beyond the scope of this technology assessment. However, external production of pH control agents may be a significant source of additional CO_2 emissions [278]. Especially in the case of CaO which is often produced by thermal decomposition of carbonate minerals:

$$CaCO_3 \longrightarrow CaO + CO_2 \tag{9.8}$$

Utility consumption was identified as the main contributor to the CO_2 emission of the bio-SA production process fig. 9.10. Taking into account that natural gas was assumed to be the primary energy source for the utilities, this seems a natural consequence. The 1-Ca, 3-ABEx and 5-eEx processes reveal a negative CO_2 footprint which can be attributed to the utilization of CO_2 as a cosubstrate in anaerobic fermentation [119, 292, 267]. In 2-Therm and 4-Ac the combustion of natural gas for thermal recycling of MgO and HCl, respectively, the emission from aerobic fermentation yields a positive CO_2 emission balance for the process. The electrochemical pH swing extraction process has the highest CO_2 when electricity is obtained from natural gas (5-eEx). However, the 5-eEx process has the lowest CO_2 footprint when a low carbon electricity mix is available. An electrical carbon footprint of $30\,\mathrm{g/kWh}$ corresponds to a negative carbon footprint of $-38\,\mathrm{g_{CO2}/kg_P}$. As a consequence, more CO_2 are fixed by this process than produced.

The water footprint fig. 9.10 (b) of all processes is comparable with the exception of 5-eEx. Closed recycling streams reduce the fresh water demand by 80 % compared to the reference process (1-Ca). The

pH swing extraction operated with acid and base addition has a waste water footprint of 27 kg/kg_P with salt concentrations of approximately 99 g/L chloride and 45 g/L sodium ions. The discharge of salt-containing wastewater is a significant environmental challenge and will likely prohibit the implementation of this separation technology.

With regard to direct emissions from the process, the calcium precipitation produces the highest amount of solid waste among the investigated downstream technologies. The 1-Ca process produces 1.2 kg/kg_P gypsum with succinic acid. The disposal of this material is strongly affected by local regulations and market demand. In principle, the construction industry has a demand for gypsum, but the discoloration of the biomass residues often impedes the utilization of gypsum for that purpose [190].

9.3.3. Economic sensitivity

A sensitivity analysis was conducted to evaluate the impact of changes in CO_2 taxation, energy prices, and regulatory emission constraints on bio-SA COM. COMs are calculated as the sum of the individual cost contributions $\mathfrak{c}_i$ calculated from the flowsheet simulation.

$$COM = \sum_{i}^{n} \mathfrak{c}_i \tag{9.9}$$

The COM^* for the new price level $\mathfrak{p}^*$ was calculated by eq. (9.10) from the reference COM and the reference price level $\mathfrak{p}_0$.

$$COM^* = COM + \left(\frac{\mathfrak{p}^*}{\mathfrak{p}_0} - 1\right) \cdot \mathfrak{c}_i \tag{9.10}$$

A carbon tax of 25 EUR/t is assumed, an electricity price of 70 EUR/MWh and a natural gas price of 30 EUR/MWh in the reference scenario.

A change in the carbon tax has only a minor impact on the bio-SA COM for 1-Ca, 2-Therm and 5-eEx-flex operated with renewable electricity fig. 9.11 (a). Acidic fermentation (4-Ac) and downstream

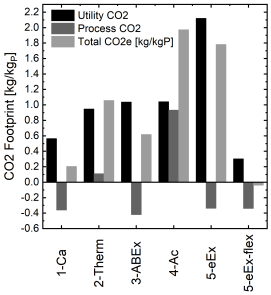

(a) Process carbon footprint

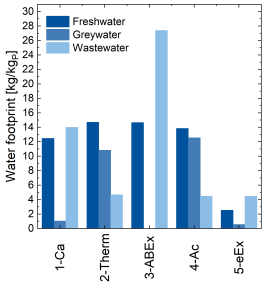

(b) Process water footprint

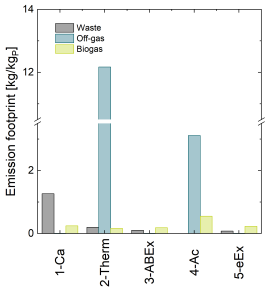

(c) Process emission footprints

Figure 9.10.: Process footprints

electrochemical processing powered by fossil fuel electricity (5-eEx) are significantly affected by the CO_2 taxation and any increase would preempt any theoretical viability of economic competitiveness.

Changes in electricity price are only relevant for electrochemical separation technologies, while the cost impact of electricity with the other downstream technologies appears to be practically irrelevant fig. 9.11 (b). If renewable electricity is available at a low price level, the 5-eEx-flex process becomes the most competitive downstream technology among those investigated. A breakeven with electricity costs in the

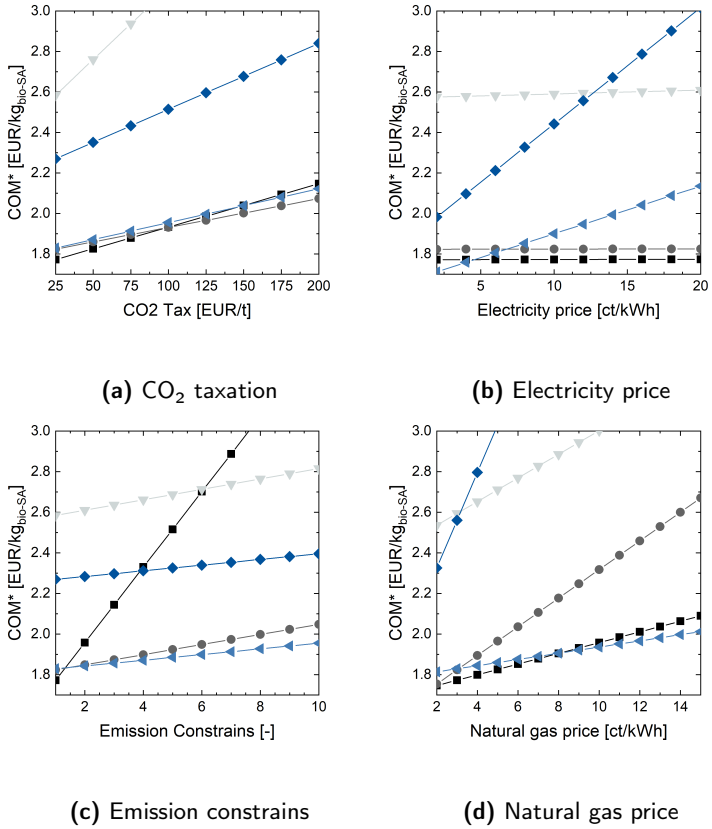

(a) CO_2 taxation **(b)** Electricity price

(c) Emission constrains **(d)** Natural gas price

Figure 9.11.: Sensitivity of bio-SA COM with regard to selected economic bondary conditions: (■) 1-Ca, (●) 2-Therm, (▲) 3-ABEx (non competitive), (▼) 4-Ac, (◆) 5-eEx, (◀) 5b-eEx-flex

range of 40-50 EUR/MWh is expected. This cost range appears to be viable with state-of-the-art renewable energy generation [30].

The 1-Ca process was identified as the most competitive economic downstream technology in the reference scenario. However, this result holds only as long as no regulatory limitations on waste disposal. The economic competitiveness of calcium precipitation is very sensitive with

regard to waste disposal cost. A double in constraints or disposal costs obliterates the cost advantage of this process fig. 9.11 (c).

Natural gas is an important energy source and also a raw material for the thermal regeneration of acid and base in the 2-Therm process. The effect of increasing gas prices was investigated. Gas prices saw a drastic increase due to increasing geopolitical tensions and strategic tightening of natural gas supply to support military actions [300]. the results indicate that 2-Therm is highly affected by changes in natural gas prices. Below 30 EUR/MWh 2-Therm reveals the lowest COM for bio-SA manufacturing. However, an increase in 60 EUR/MWh eliminates the cost advantage and makes the 1-Ca and 5-eEx-flex process more competitive. It is concluded that the sensitivity analysis does not reveal a downstream technology that outperforms the others in all cases. Thus, the "best" downstream technology option for bio-SA manufacturing must be determined considering the local economic background. If there are little or no regulations for waste disposal, calcium precipitation is likely the technology of choice. When waste disposal is limited due to regulations or missing disposal markets, but low-cost natural gas is available, it is recommended to opt for the 2-Therm process. Lastly, electrochemical pH swing extraction has the potential to become an equally competitive separation technology with a highly interesting perspective to enable CO_2 negative bio-SA production. For this to happen, two conditions must be met: First, renewable electricity with a carbon footprint below 30 g/kWh must be available, preferably at costs below 40 EUR/MWh. Second, investment costs for pH swing electrolyzer equipment should be reduced. Additionally, reduction of cell voltage and the development of innovative cell designs for pH swing electrolysis would bring additional benefit to the overall cost competitiveness of electrified bio-SA production.

The results of the techno-economic assessment were used to derive targets for the development of pH swing electrolysis. More precisely, the COM for bio-SA was calculated with regard to improvements in cell voltage and electrolyzer investment costs and determined break-even lines for market price and competing downstream technologies fig. 9.12. To-

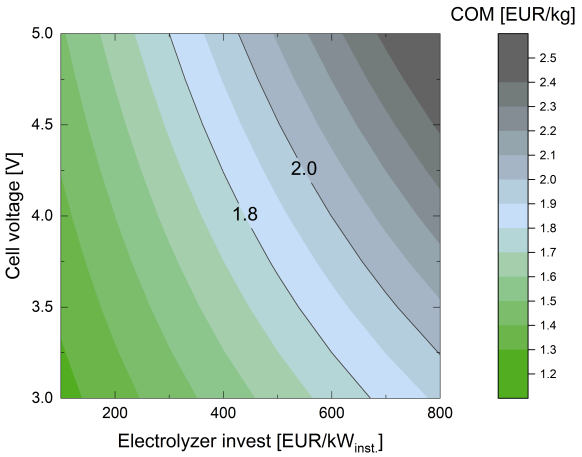

Figure 9.12.: Target setting for cell voltage and pH swing electrolysis investment costs

day, investment costs for electrolyzer equipment are expected to be in the range of 600-800 EUR [31] and a cell voltage of 5 V for technical applications. A cell voltage between 3-4 V would make pH swing electrolysis competitive even with the current available electrolysis equipment price range. Any further reduction of the investment costs would improve the competitive edge of the electrochemical downstream technology.

As discussed in the previous section, investment costs and obviously the revenue generated by the product sales are important for the overall attractiveness of bio-SA production as an investment case. The sensitivity of the net present value (NPV) calculated from investment $\mathfrak{I}$, the annual revenue streams $\mathfrak{z}$ discounted by the discount rate $\mathfrak{i}$ and the revenue from asset liquidation $\mathfrak{L}$ at the end of the life of the plant $\mathfrak{T}$, which was set to 20 years, was analyzed.

$$NPV = \sum_{i=1}^{\mathfrak{T}} \frac{\mathfrak{z}}{(1+\mathfrak{i})^t} + \mathfrak{L}(1+\mathfrak{i})^{-T} \tag{9.11}$$

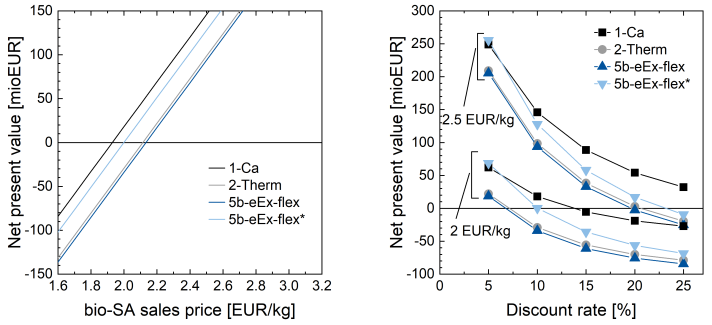

Figure 9.13.: Sensitivity of net present value with regard to sales price (a) and discount rate (b)

The results are displayed in fig. 9.13. In (a) the sensitivity of NPV to the bio-SA sales price is shown at a discount rate of 10 %. 1-Ca reaches an NPV break even with sales prices of approximately 1.95 EUR/kg, followed by 5-eEx-flex at around 2 EUR/kg. This indicates that both technologies constitute a profitable investment case. However, downstream electrochemical processing is a rather new technology that is rarely applied on a large scale for the processing of carboxylic acids [42, 43]. Therefore, its implementation is associated with significant development risks [273].

Regarding the risk related to technology, two opportunities were identified to mitigate the risk of investment. First, marketing the sustainability bonus associated with low emissions and potentially carbon-negative bio-SA could improve the willingness of customers to pay higher prices. A bio-SA sales price of 2.5 EUR/kg would generate sufficient revenue to achieve a positive NPV even with a 20 % discount rate. The higher discount rate would compensate for the higher risk the investor places by investing in a novel process technology. In the past, strong price competition from fossil sources of succinic acid made it difficult to actually

monetize the sustainability bonus. A potential avenue of escape from this dilemma is to integrate the value chain for end products derived from bio-SA, such as sustainable and perhaps carbon negative plastics or fibers[301, 302, 303] instead of providing a drop-in chemical that is not differentiable from its petrochemical alternative and thus provides little added value to the customer.

The second option to improve the investment case is the diversification of revenue streams. As discussed earlier, the flexibilization of the 5-eEx process by incorporation of catch-up capacity and storage tanks enables demand side management and provides dispatchable load capacities that can be used to stabilize the electricity grid [249]. In addition, hydrogen is produced in the cathodic reaction of pH swing electrolysis, which will likely become a valuable energy resource in the future. The effect of this potential revenue diversification is displayed in fig. 9.14. The added revenue from the dispatchable load sales is expected to be in the order of 20 % of the electricity costs and a higher sales price for hydrogen of 4.9 EUR/kg. This hydrogen price reflects the use of hydrogen as a fuel for long-distance transport and corresponds to a diesel price of 1.5 EUR/L. The added revenue makes electrochemical pH swing extraction more profitable than the 1-Ca process in the long run.

In summary, the following recommendations can be derived.

a) The carbon atom efficiency, respectively, and product yield, are crucial performance indicators for bio-SA production. Microbial engineering efforts should prioritize the maximization of the yield first and then seek to improve titer and pH.

b) Low pH succinic acid fermentation eases the product separation but in order to achieve an overall competitive process, microbial energy demand for product export must be balanced against the gain in the downstream process.

c) *In situ* product separation shows a promising potential to reduce

the waste and water footprint of bio-SA production and can potentially overcome the limitations encountered with the cellular product export. The combination of low pH tolerant strains with *in situ* product removal should be tested.

d) The profitability of sustainable downstream technologies is largely affected by the primary energy costs. Policy makers should consider implementing the steering power of primary energy costs in future legislation. They should also be aware that taxes and transmission fees which increase energy prices may compromise the intended effect of CO_2-taxation and prevent the implementation of sustainable production processes.

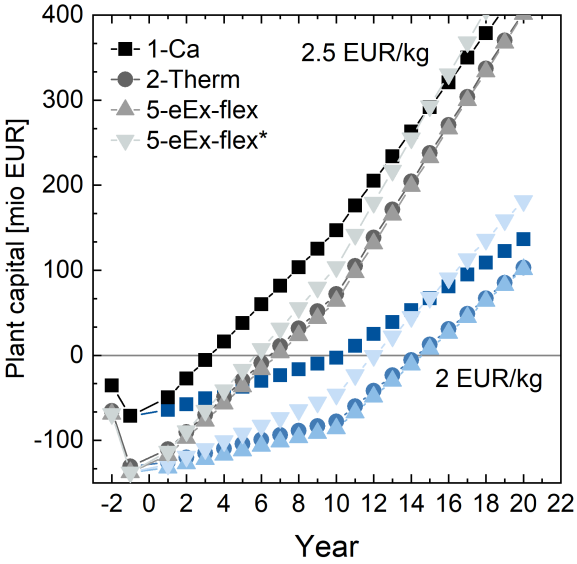

Figure 9.14.: Development of plant capital. *Including added revenue from dispatchable load and hydrogen sales.

9.4. Conclusion

In this chapter different downstream technologies for the recovery and purification of bio-SA were analyzed. The technological limits and the economic limits that determine the competitiveness of the respective process were identified. The recycling of additives, namely, acid and base used in the downstream, is crucial for the development of sustainable processes. The development of acid-tolerant strains for bio-SA production can alleviate additive consumption, but must consider the trade-off between the carbon efficiency of fermentation and the environmental and energy footprint of the downstream. The thermodynamic

limits of the known cellular export mechanisms suggest that, without additional metabolic energy sources, bio-SA fermentation at low pH and high yields seems not feasible. The conjunction of acid-tolerant strains with *in situ* extraction should be investigated for bio-SA production. Regulatory or market-associated emission restrictions and energy prices were identified as a relevant factor that determines the most competitive downstream technology. With little or no emission constraints in place, the established calcium precipitation is probably the most attractive investment case for bio-SA production. However, downstream technologies that feature acid and base recycling by thermal salt cracking or electrochemical pH swing electrolysis appear to be the most sustainable technology option with regard to direct emissions from bio-SA production. The economic preference between both technologies is determined by the prices of natural gas and electricity. With the increase in the supply of renewable energy resources with a low carbon footprint, downstream electrochemical technologies showed an interesting perspective for CO_2-negative production of bio-SA [304]. Given the expected improvements in electrolysis technology, bio-SA has the potential to become a platform for biobased, biodegradable and CO_2 negative polymers [302, 303]. In conclusion, this study highlights the importance of balancing development efforts between upstream and downstream, and the relevance of energy costs that appear to have a strong steering power for the investment decision in the respective downstream technology. For that reason, a successful electrification of bio-SA production requires the availability of low-cost electricity, but comes with the advantage of reduced environmental footprints.

10. Reflection and Outlook

Electrification of separation technologies is a viable route to establish sustainable chemical processes. The increasing supply from renewable energy resources, accompanied by efforts to reduce the utilization of fossil feedstock and energy resources in the process industry, creates an environment well-fitted for the industrialization of electricity-driven separation processes. However, the realization of new process technologies is a long journey and requires joint development and execution efforts. Achievements in microbial engineering must be matched with energy-efficient and resource-efficient process technologies to form a competitive technology for carboxylic acid production.

The objective of this work was to investigate the viability of an electrochemically driven pH swing extraction process that overcomes the salt waste production that currently limits the large-scale application of biobased production routes for carboxylic acids. For this purpose chapter 2 introduces the fundamental principles of electrochemical pH swing extraction followed by an experimental essay on the electrochemical stability of important bioproducts. Although most of the fundamental investigations were carried out on the example of succinic acid, the application notes in the later chapters demonstrate that those conclusions are to some extent transferable to other carboxylic acids as well. The long-chain carboxylic acids revealed a sufficient electrochemical stability to withstand a degradation during the electrochemical pH swing electrolysis.

chapter 3 presents a DoE supported identification of operational parameters with a significant effect and practical relevance for efficient reactive extraction of succinic acid. The results highlighted the extraordinary importance of the aqueous pH value that dominates the effects

of all other parameters with regard to extraction yield. The competing extraction of anions was observed and mass balance-based extraction mechanisms were proposed. This hypothesis follows the state of the current literature, but it should be validated by future investigations to determine the best operating point for the reactive extraction of succinic and other carboxylic acids.

In chapter 4 the viability of the electrochemical pH swing separation of succinic acid was demonstrated. Electrochemical extraction, back-extraction, and crystallization of succinic acid was demonstrated without the production of salt waste inevitable in previous processes.

In order to analyze the first principles of electrochemical pH swing extraction and to identify potential bottlenecks, a dynamic simulation model is developed and presented in chapter 5. The model employs the numerical calculation of complex aqueous pH and extraction equilibria. Although the nonideal effect induced by the electrolyte chemistry of real solutions is neglected in this work, the modeling results are in satisfactory agreement with validation experiments. A sensitivity analysis showed that the kinetic of electrolysis is probably the rate-limiting step of an electrochemical pH swing extraction. The model was extended to account for the competitive extraction of inorganic anion, exemplary sulfate. The extended model was likewise in good agreement with the experimental results in the operational region of interest. Deviations were observed at low pH values, which could be an indication that the true extraction mechanisms deviate from the implemented mechanisms at acidic pH values. As already suggested for chapter 3 resolving the underlying extraction mechanism of competitive anion extraction would improve the ability to achieve high extraction yields and selectivity. The results of this work give an indication that hydrogen sulfate ions are extracted sulfate species instead of the previously assumed sulfate extraction. However, this hypothesis has to be proven or falsified.

A spatially resolved model for the electrolysis cell is presented in chapter 6. This model reveled in the mechanisms causing known bottlenecks in the scale-up and operation of electrochemical pH swing electrolysis. The "proton poisoning" effect could be replicated *in-silico*. It results

from the depletion of the aqueous buffer capacity occurring near the end of the pH swing electrolysis. As it reduces faradaic efficiency, such conditions need to be avoided. The second important result is that electrolyte entrainment is likely to occur when cells with small electrolyte gap sizes are operated at high current density. The results of the simplified cell model suggest that gaps of 4-6 mm are a reasonable lower limit for the electrolyte gap, resulting in a minimal electrode distance of 8-12 mm. Pressurized operation or improved spacer or cell designs that foster gas and liquid separation inside the electrolysis cell should be tested to overcome the entrainment of the electrolyte. The results showed a high sensitivity with regard to the fluid dynamics of the gas bubbles in the electrolyte gap. However, the knowledge in the literature on the true size distribution and flow behavior of the gas bubble dispersion inside an electrolysis cell is limited and requires more fundamental research.

The application notes in chapters 7 and 8 demonstrated the transfer and applicability of the electrochemical pH swing extraction concept to itaconic and lactic acid, respectively. The application of the developed process and methodology to a realistic solution like itaconic acid fermentation broth from acid-tolerant strains demonstrated how sophisticated microbial engineering and advanced separation technologies enable a waste-free production of an important intermediate chemical.

Finally, the economic and ecological competitiveness of different succinic acid downstream technologies, including electrochemical pH swing extraction, was evaluated in chapter 9. With fossil-based electricity supply, other separation technologies are more competitive than electrochemical pH swing extraction. Although that picture changes as soon as renewable electricity becomes available and emission regulations restrict the discharge of salt waste or fossil energy resources, a significant price increase is expected. In light of the recent geopolitical tensions, such conditions may be constituted earlier than expected. The key findings of this thesis are:

- The electrochemical stability of (di)carboxylic acids enables direct

pH swing electrolysis to shift the pH value of a carboxylate solution to recover the carboxylic acid in its protonated form.

- A combination of both electrode reactions enables closed-loop pH swing separation that overcomes the waste-generating use of acid and base for the pH adjustment in the downstream processing of bioproducts.
- The presented modeling approaches revealed the mechanisms that cause inefficiencies and compromise the competitiveness of electrochemical separation technologies.
- The success of industrial biotechnology is the result of high-performance microbes that live in synergy with a sustainable downstream technology.
- Electrification of succinic acid processing potentially enables CO_2 negative production of succinic acid.

Despite the promising perspective, some aspects benefit from a critical reflection. In the experiments presented in chapter 4 the solvent is in direct contact with the membrane. This caused swelling of the membrane and reduced the mechanical stability of the cation-exchange membrane. In principle, no ion-selective membrane is required, as the electron migration directs the cations and anions in the right direction. However, the use of cation-exchange membranes eases the control of the hydrodynamic pressure. Regarding membrane stability, it is questionable if an integrated electrolysis/extraction setup has more advantages compared with a sequential setup like chapters 7 and 8. Furthermore, the success of electrified separation processes is largely dependent on the availability of renewable energy sources that generate electricity at competitive prices. But once the transition provides the right market framework, electrochemical pH swing separation could become a key enabling technology for price-competitive and sustainable industrial biotechnology.

A. Historic oil prices

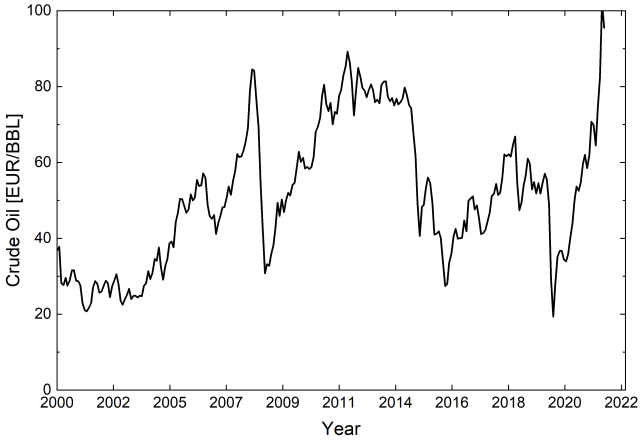

Figure A.1.: Historic data for crude oil price. Adapted from `https://www.indexmundi.com/commodities/?commodity=crude-oil`

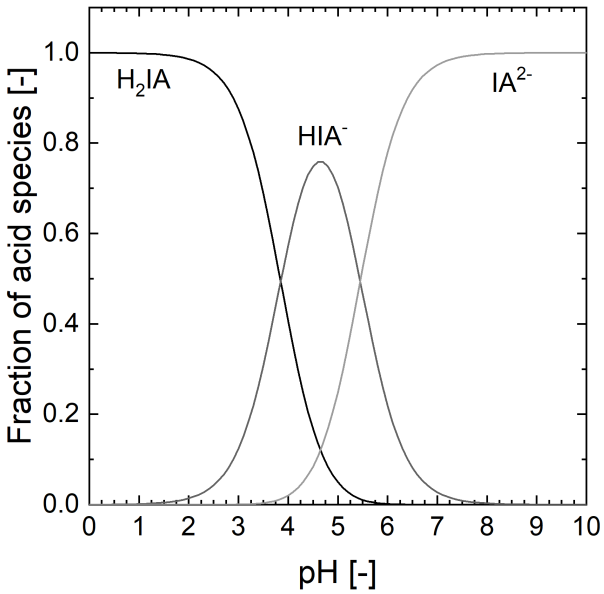

Figure A.2.: Fraction of itaconic acid species calculated for a pKa_1=3.85 and pKa_2=5.45 [2]

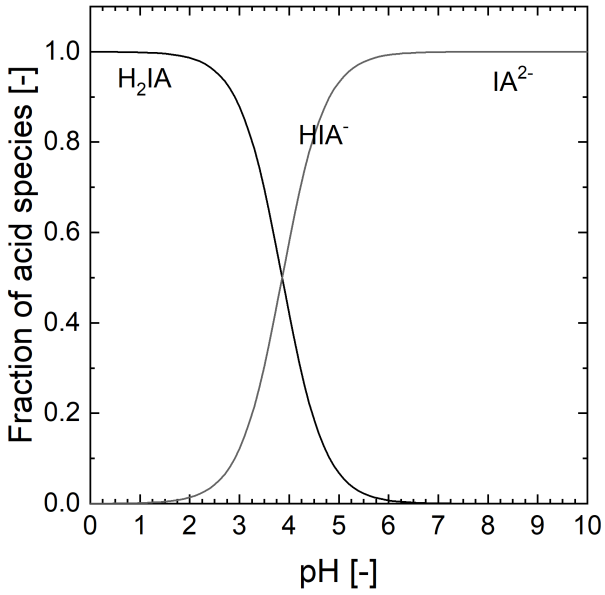

Figure A.3.: Fraction of lactic acid species calculated for a pKa_1=3.86 [2]

B. Cyclic Voltammetrie Experiments

B.1. Materials

Table B.1.: List of chemicals used in CV experiments

Compound	**Supplier**	**Purity**
Adipic acid	Alfa Aesar	99%
Itaconic acid	Alfa Aesar	99%
Succinic acid	Alfa Aesar	99%
Lactic acid	VWR	85 – 90%
Acetic acid	VWR	98%
Formic acid	Merck	99%
Ethanol	VWR	99.98%
Glycerol	VWR	100%
Glucose	Alfa Aesar	99%
Fructose	Carl Roth	99.5%
L-Alanine	Merck	99%
Hexanediamine	Alfa Aesar	98%
Sodium hydroxide	Carl Roth	98%
Sodium sulfate	VWR	98%

Table B.2.: Concentration and initial pH value of compound solution for CV experiments

Compound	Concentration [gL^{-1}]	low pH	high pH
Adipic acid	15	2.95	5.92
Itaconic acid	40	2.36	6.26
Succinic acid	40	2.52	6.85
Lactic acid	50	2.12	6.5
Acetic acid	50	2.61	6.31
Formic acid	50	1.96	5.09
Ethanol	50		6.27
Glycerol	50		5.97
Glucose	50		5.94
Fructose	50		5.88
L-Alanine	50		6.28
Hexanediamine	50		12.5

B.2. CV Results

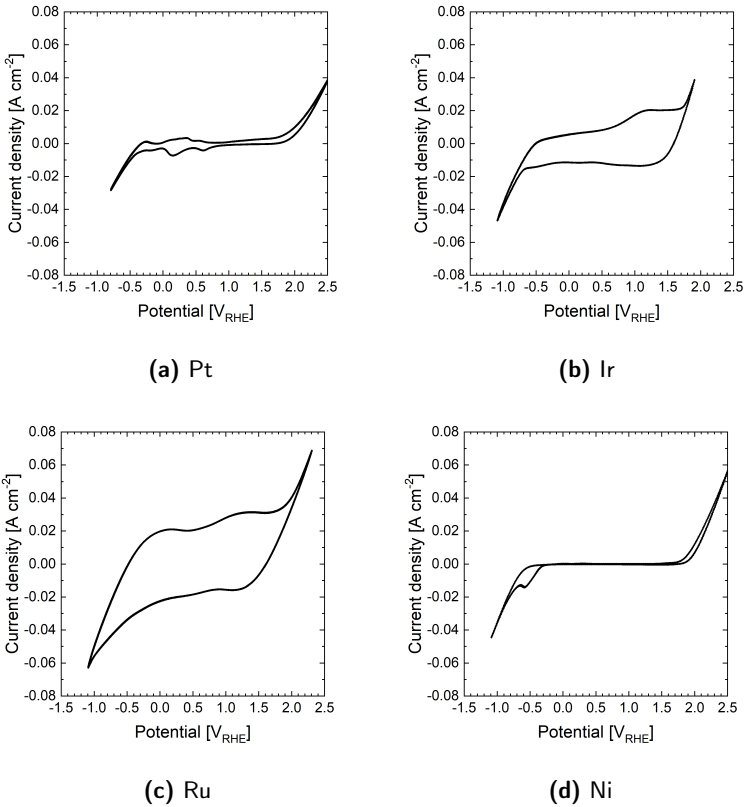

(a) Pt **(b)** Ir

(c) Ru **(d)** Ni

Figure B.1.: CV scan of adipic acid at pH 5.92. Potential recorded vs. Hg/HgE and corrected for RHE

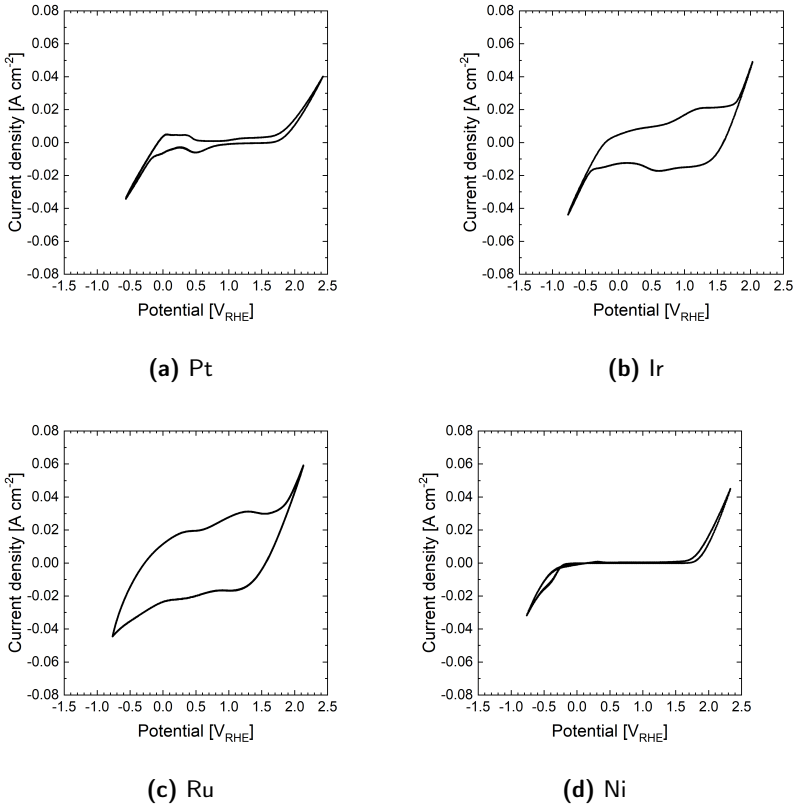

(a) Pt **(b)** Ir

(c) Ru **(d)** Ni

Figure B.2.: CV scan of adipic acid at pH 2.95. Potential recorded vs. Hg/HgE and corrected for RHE

The most obvious feature is the shift of the beginning of the anodic tafel region at Pt fig. B.13a to potentials exceeding 2 V. A minor shift is visible in the curve recorded for alanine fig. B.12a. The genesis of this shift is unclear since the conversion to RHE should subtract the anodic potential increase caused by the alkaline pH values of the electrolyte. The influence of local buffer effects that are not considered in the conversion of the potential could induce a deviation of the recorded

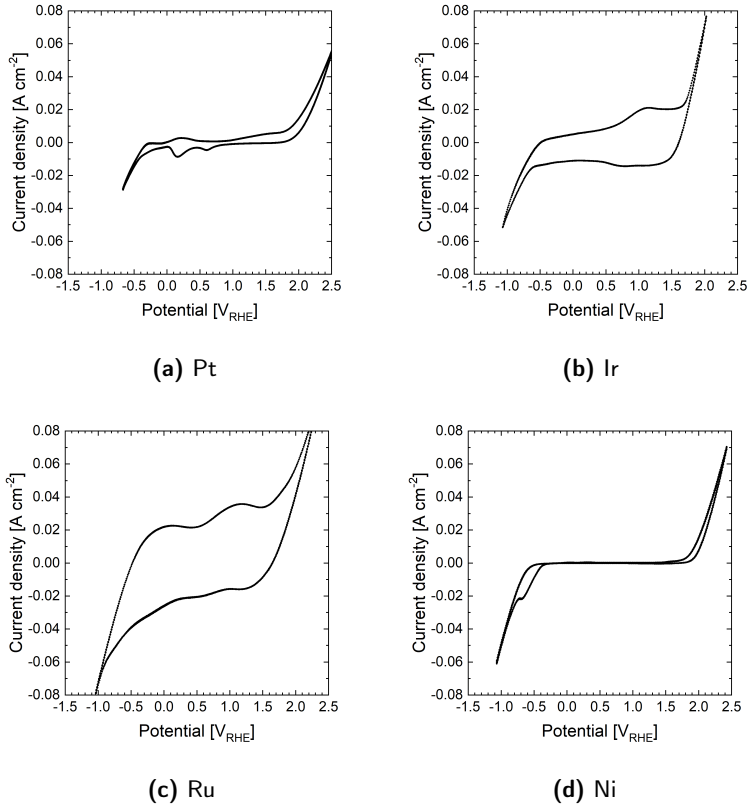

(a) Pt **(b)** Ir

(c) Ru **(d)** Ni

Figure B.3.: CV scan of itaconic acid at pH 6.26. Potential recorded vs. Hg/HgE and corrected for RHE

potential [305]. This hypothesis could be validated with a more detailed analysis of the anodic potential regions at different pH values and solute concentrations, which is outside the scope of this thesis.

Likewise to Pt, Ni shows clear signs for the electrochemical reaction of alanine and hexane diamine (HDA). The observed reactions agree with the fact that Ni-based catalysts are employed for the production or conversion of HDA to hexanedinitrile [306, 307]. Again, the indications

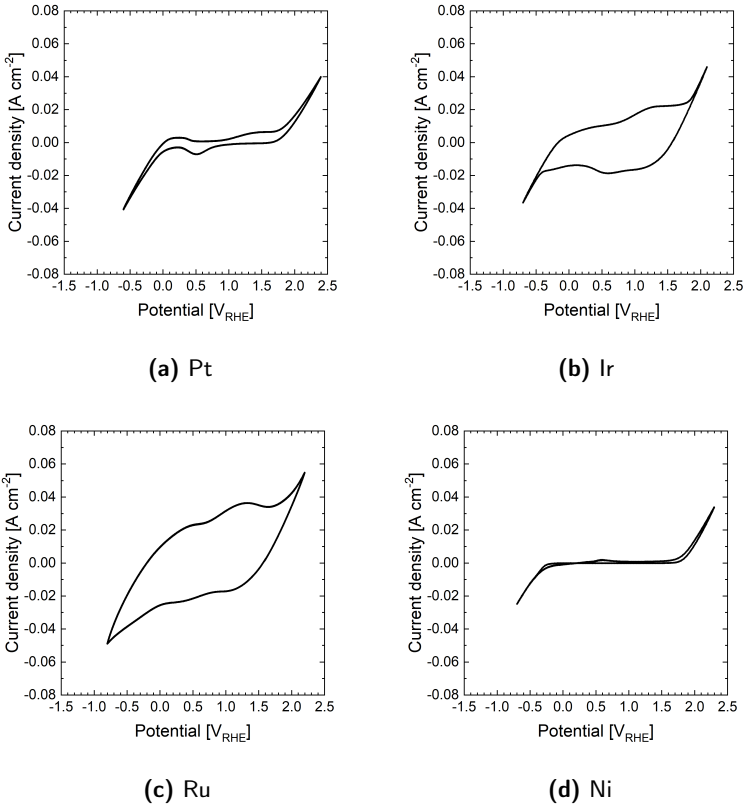

(a) Pt **(b)** Ir

(c) Ru **(d)** Ni

Figure B.4.: CV scan of itaconic acid at pH 2.36. Potential recorded vs. Hg/HgE and corrected for RHE

for a reaction at Ir and Ru are not as clear as they are with Ni or Pt. These electrode materials potentially provide suitable catalysts to be used in the electrochemical pH swing extraction of amino acids or amines but based on the herein presented results, more rigorous validation of the electrochemical stability is recommended.

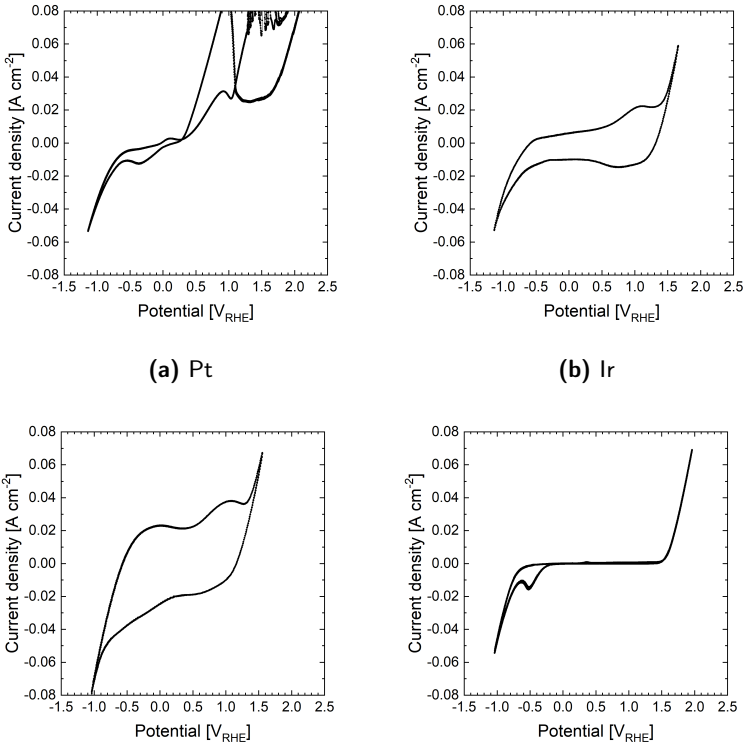

(a) Pt **(b)** Ir

(c) Ru **(d)** Ni

Figure B.5.: CV scan of formic acid at pH 5.09. Potential recorded vs. Hg/HgE and corrected for RHE

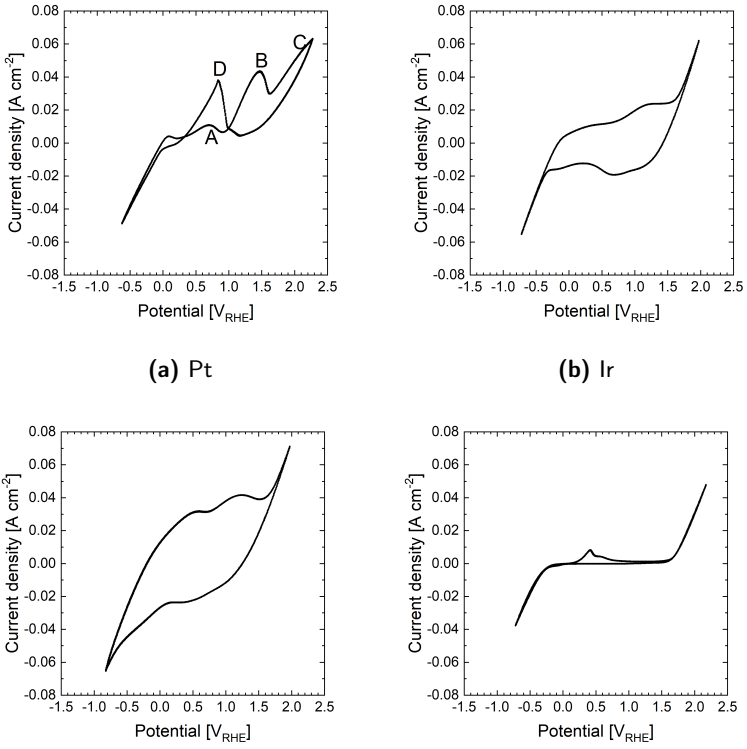

(a) Pt **(b)** Ir

(c) Ru **(d)** Ni

Figure B.6.: CV scan of formic acid at pH 1.96. Potential recorded vs. Hg/HgE and corrected for RHE

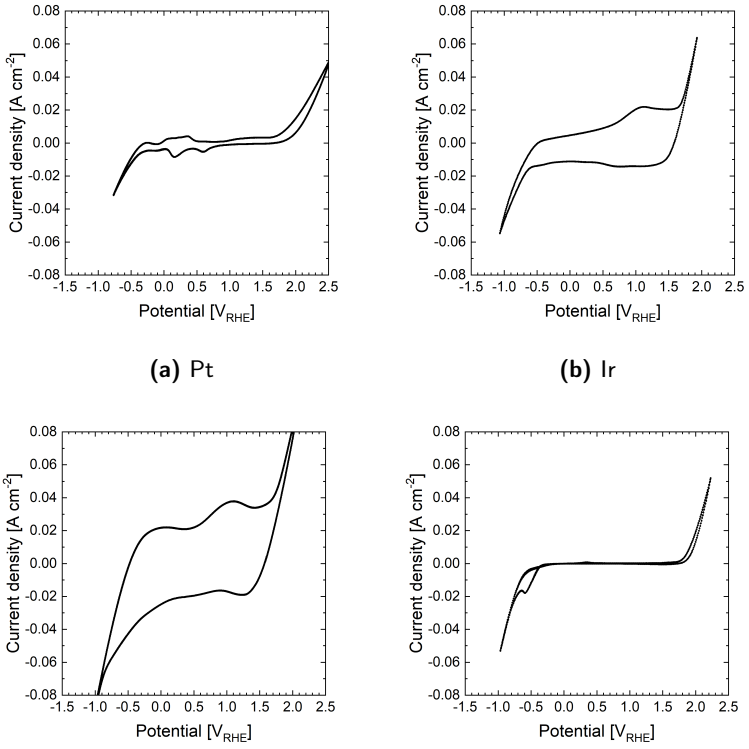

(a) Pt **(b)** Ir

(c) Ru **(d)** Ni

Figure B.7.: CV scan of acetic acid at pH 6.31. Potential recorded vs. Hg/HgE and corrected for RHE

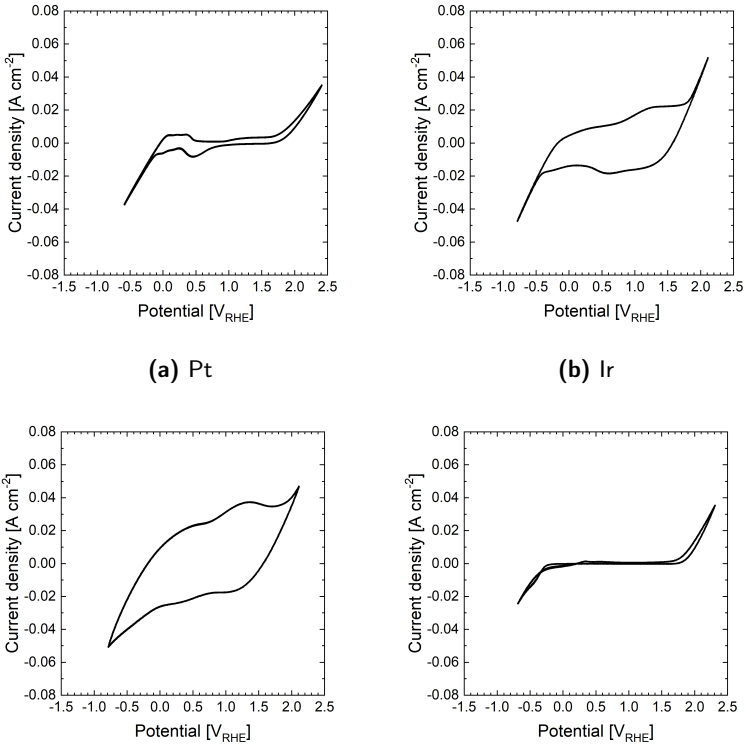

(a) Pt **(b)** Ir

(c) Ru **(d)** Ni

Figure B.8.: CV scan of acetic acid at pH 2.61. Potential recorded vs. Hg/HgE and corrected for RHE

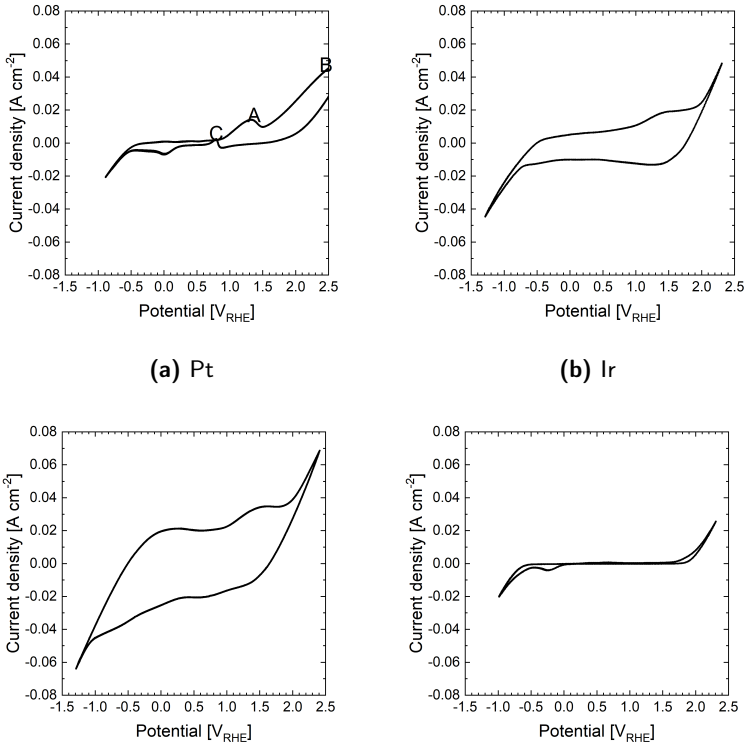

(a) Pt **(b)** Ir

(c) Ru **(d)** Ni

Figure B.9.: CV scan of glycerol at pH 5.97. Potential recorded vs. Hg/HgE and corrected for RHE

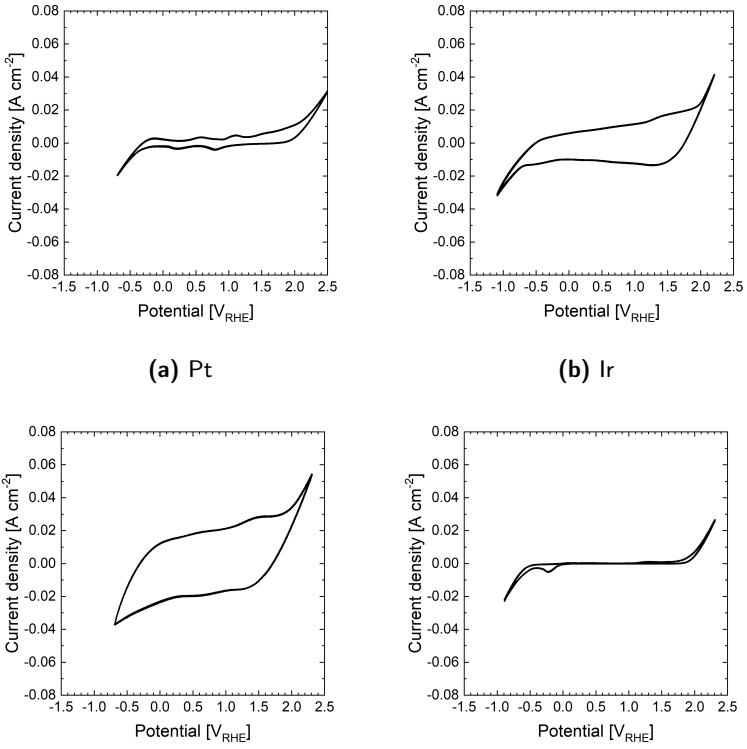

(a) Pt **(b)** Ir

(c) Ru **(d)** Ni

Figure B.10.: CV scan of glucose at pH 5.94. Potential recorded vs. Hg/HgE and corrected for RHE

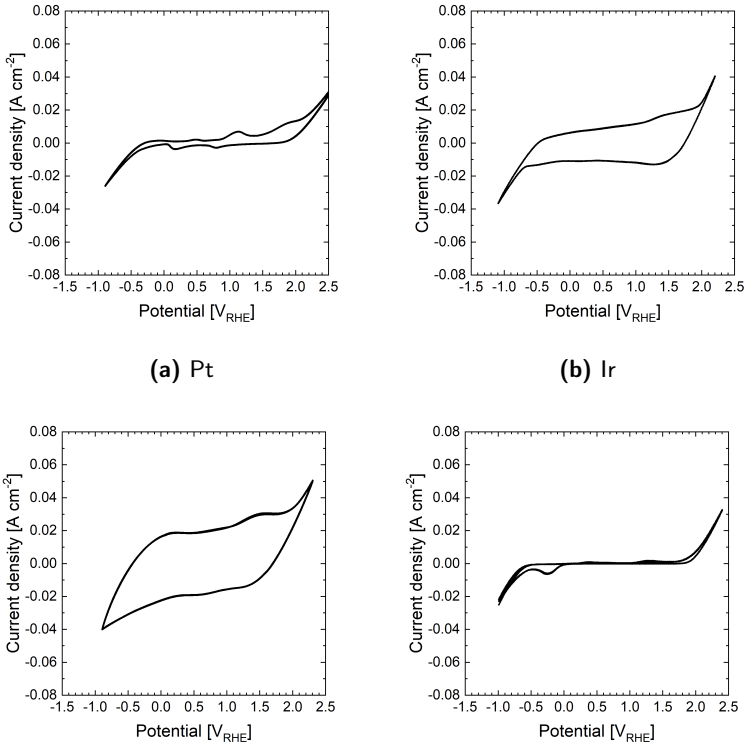

(a) Pt **(b)** Ir

(c) Ru **(d)** Ni

Figure B.11.: CV scan of fructose at pH 5.88. Potential recorded vs. Hg/HgE and corrected for RHE

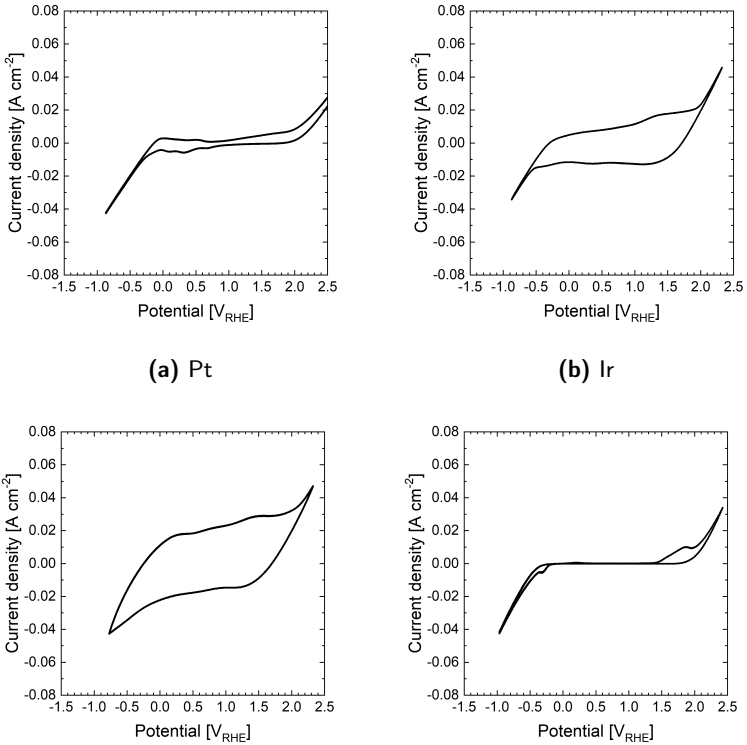

(a) Pt **(b)** Ir

(c) Ru **(d)** Ni

Figure B.12.: CV scan of alanine at pH 6.8. Potential recorded vs. Hg/HgE and corrected for RHE

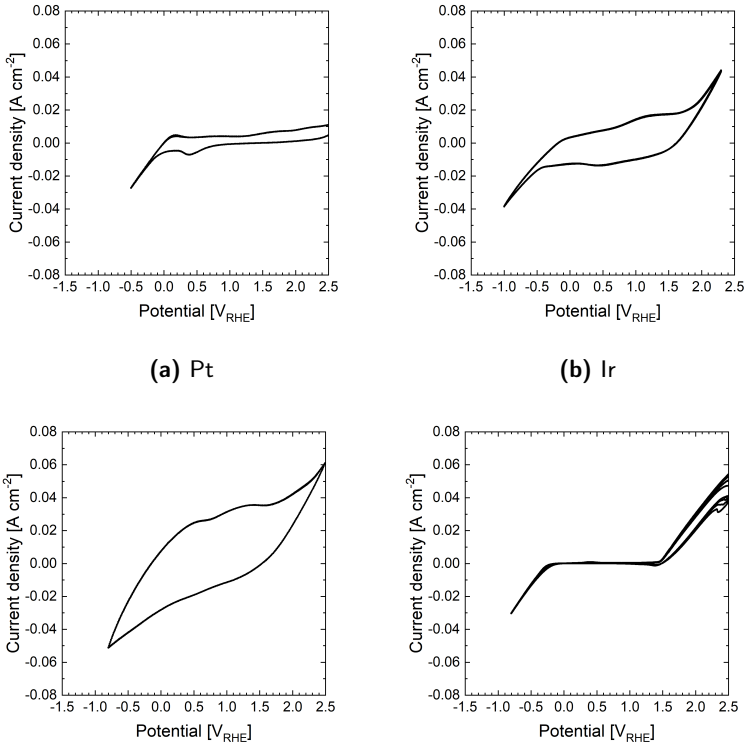

(a) Pt **(b)** Ir

(c) Ru **(d)** Ni

Figure B.13.: CV scan of hexadiamine at pH 12.5. Potential recorded vs. Hg/HgE and corrected for RHE

C. 2 Experimental data for DoE

† The values given for SO_4 and PO_4 represent the total concentration of the respective anion species.

Table C.1.: Screening Experiments

	T [°C]	c_{SA} [g L_{aq}^{-1}]	Extractant	c_{ex} [mol L_{org}^{-1}]	Diluent	pH [-]	Anion †	c_{ion} [mol L_{aq}^{-1}]	E_{SA} [%]	E_{Anion} [%]	S_{SA} [%]	S_{Anion} [%]
1	80	20	THA	0.5	MIBK	3	SO4	0.5	39 ± 05	6 ±3	65.5 ±10.5	33.5 ±10.5
2	80	20	THA	1	nHex	5	CL	0	0.5 ±0.5	-	-	-
3	25	20	THA	1	MIBK	3	PO4	0	76 ±0	-	-	-
4	25	20	THA	1	Dodec	3	PO4	0	51 ±2	-	-	-
5	25	20	TEHA	1	nHex	3	PO4	0.5	4 ±1	8.5 ±0.5	12 ±1	88 ±1
6	25	20	TEHA	0.5	Oct	5	SO4	1	1 ±1	3.5 ±0.5	3 ±3	97 ±3
7	80	60	THA	0.5	Oct	5	PO4	0	10.5 ±0.5	-	-	-
8	25	60	TOA	0.5	nHex	5	SO4	0	5.5 ±0.5	-	-	-
9	25	20	TOA	1	Oct	5	CL	0.5	3.5 ±0.5	14 ±0	13.5 ±1.5	86.5 ±1.5
10	25	60	THA	1	nHex	5	SO4	0.5	1 ±0	1 ±0	42 ±4	58 ±4
11	25	20	TEHA	0.5	Dodec	3	CL	0	8 ±0	-	-	-
12	25	20	TEHA	0.5	nHex	5	SO4	1	2.5 ±0.5	3.5 ±1.5	10 ±6	90 ±6
13	80	20	TEHA	1	nHex	5	CL	0	1 ±0	-	-	-
14	80	20	TOA	0.5	nHex	3	PO4	1	4 ±1	5 ±1	11.5 ±1.5	88.5 ±1.5
15	80	60	TOA	0.5	Oct	3	PO4	1	36 ±1	9.5 ±0.5	63.5 ±1.5	36.5 ±1.5
16	80	20	TEHA	1	Oct	5	CL	0	1 ±0	-	-	-
17	80	60	TOA	0.5	Dodec	3	CL	0.5	11 ±0	21.5 ±0.5	50.5 ±0.5	49.5 ±0.5
18	80	20	TOA	1	MIBK	3	SO4	0	34.5 ±1.5	-	-	-
19	80	60	THA	1	Oct	3	SO4	0.5	47 ±0	15 ±0	72 ±0	28 ±0
20	80	60	TEHA	1	Oct	5	CL	0	1.5 ±0.5	-	-	-
21	25	60	THA	0.5	MIBK	3	CL	1	30 ±1	33 ±1	48 ±0	52 ±0
22	25	60	TOA	1	Dodec	5	SO4	0	4 ±0	-	-	-
23	80	20	TOA	0.5	Oct	3	SO4	0	58.5 ±4.5	-	-	-
24	80	20	TOA	1	nHex	5	PO4	1	1.5 ±0.5	0.5 ±0.5	29 ±1	71 ±1
25	80	60	TEHA	1	nHex	5	PO4	0.5	2 ±1	2 ±1	52 ±2	48 ±2
26	80	20	TOA	0.5	Oct	5	CL	0.5	4 ±0	9 ±0	21.5 ±0.5	78.5 ±0.5
27	80	20	THA	0.5	Dodec	5	CL	1	3 ±0	6.5 ±0.5	13.5 ±0.5	86.5 ±0.5
28	25	60	THA	0.5	Oct	5	PO4	0	15 ±0	-	-	-
29	25	60	THA	1	Oct	3	CL	1	18.5 ±2.5	28 ±3	41.5 ±3.5	58.5 ±3.5
30	80	20	TOA	0.5	Oct	3	PO4	1	51.5 ±1.5	11 ±0	41.5 ±0.5	58.5 ±0.5
31	80	60	TEHA	1	Dodec	3	PO4	0.5	6 ±1	3 ±1	65.5 ±4.5	33.5 ±5.5
32	25	20	TOA	0.5	MIBK	5	SO4	0	14.5 ±0.5	-	-	-
33	80	60	TOA	1	nHex	3	SO4	0	3.5 ±0.5	-	-	-
34	80	60	TOA	1	Dodec	5	SO4	0	9 ±0	-	-	-
35	80	20	TOA	1	MIBK	3	CL	0.5	18.5 ±1.5	15.5 ±1.5	46 ±0	54 ±0
36	80	20	TEHA	1	Oct	3	PO4	0.5	8 ±0	1.5 ±0.5	60.5 ±3.5	39.5 ±3.5
37	25	60	TOA	1	Dodec	3	CL	0.5	6.5 ±0.5	15 ±1	47 ±0	53 ±0
38	80	60	TEHA	0.5	MIBK	5	PO4	0.5	3 ±2	4 ±2	37 ±3	63 ±3
39	25	20	THA	0.5	Dodec	5	SO4	0.5	2.5 ±2.5	3.5 ±2.5	18.5 ±2.5	81.5 ±2.5

40	25	20	THA	0.5	nHex	3	PO4	0	2 ±0	-	-	-
41	25	20	TOA	1	Dodec	5	PO4	1	11.5 ±5.5	10 ±0	14 ±6	86 ±6
42	25	60	TEHA	0.5	Dodec	5	CL	0	2.5 ±0.5	-	-	-
43	25	20	TOA	0.5	Oct	3	SO4	0	44 ±3	-	-	-
44	25	20	THA	1	MIBK	5	SO4	0.5	14 ±0	1 ±0	76.5 ±1.5	23.5 ±1.5
45	25	60	THA	1	Oct	3	SO4	0.5	30 ±1	9 ±1	73 ±2	27 ±2
46	80	60	THA	0.5	nHex	5	PO4	0	5.5 ±4.5	-	-	-
47	80	60	THA	0.5	MIBK	5	CL	1	2 ±0	3 ±0	38.5 ±0.5	61.5 ±0.5
48	25	60	TOA	0.5	nHex	5	CL	0.5	1.5 ±0.5	1.5 ±0.5	73 ±4	27 ±4
49	80	20	THA	1	Dodec	3	PO4	0	60.5 ±3.5	-	-	-
50	25	20	TOA	1	nHex	3	CL	0.5	8 ±0	6.5 ±0.5	44 ±2	56 ±2
51	25	60	TEHA	0.5	nHex	3	CL	0	4 ±1	-	-	-
52	25	60	TOA	0.5	MIBK	3	PO4	1	54.5 ±4.5	7 ±3	87.5 ±3.5	22.5 ±6.5
53	80	60	THA	1	Oct	3	CL	1	27.5 ±0.5	38 ±0	42.5 ±0.5	57.5 ±0.5
54	25	60	TEHA	0.5	Dodec	5	PO4	0.5	2.5 ±0.5	2 ±0	49.5 ±0.5	50.5 ±0.5
55	25	20	TEHA	1	MIBK	5	SO4	1	1 ±0	4 ±0	2.5 ±0.5	97.5 ±0.5
56	80	60	TEHA	0.5	nHex	3	SO4	1	1 ±1	1 ±1	26.5 ±2.5	73.5 ±2.5
57	80	60	TEHA	1	Dodec	3	SO4	1	8.5 ±3.5	4.5 ±3.5	52.5 ±12.5	47.5 ±12.5
58	25	20	TEHA	0.5	MIBK	3	PO4	0.5	8.5 ±0.5	4 ±0	37.5 ±1.5	62.5 ±1.5
59	80	60	TOA	0.5	MIBK	5	CL	0.5	1.5 ±0.5	1 ±0	76.5 ±2.5	23.5 ±2.5
60	25	20	THA	1	nHex	3	CL	1	12.5 ±0.5	7.5 ±0.5	34.5 ±0.5	65.5 ±0.5
61	25	60	TOA	1	Dodec	5	PO4	1	8 ±0	3.5 ±0.5	54.5 ±2.5	45.5 ±2.5
62	25	60	TOA	1	MIBK	5	PO4	1	15 ±0	3.5 ±0.5	68.5 ±3.5	31.5 ±3.5
63	25	20	TEHA	0.5	Oct	5	PO4	0.5	1.5 ±0.5	2 ±1	19.5 ±2.5	80 ±3
64	80	60	TEHA	1	MIBK	3	SO4	1	3 ±0	2.5 ±0.5	31.5 ±0.5	68.5 ±0.5
65	80	60	THA	0.5	nHex	3	SO4	0.5	3 ±2	1.5 ±1.5	54 ±16	46 ±16
66	80	20	THA	0.5	Dodec	5	SO4	0.5	6.5 ±0.5	5 ±0	26 ±1	74 ±1
67	25	60	TEHA	1	Oct	5	SO4	1	3.5 ±2.5	2.5 ±2.5	50 ±18	50 ±18
68	80	20	TEHA	1	MIBK	5	CL	0	1 ±0	-	-	-
69	25	60	TEHA	0.5	MIBK	3	CL	0	9 ±1	-	-	-
70	25	20	THA	0.5	Dodec	5	CL	1	4 ±3	5.5 ±2.5	15.5 ±6.5	84.5 ±6.5
71	80	60	THA	1	MIBK	5	PO4	0	4.5 ±0.5	-	-	-
72	80	20	TEHA	0.5	Dodec	3	SO4	1	7 ±0	1.5 ±0.5	44.5 ±8.5	55.5 ±11

D. 2 Biotechnological Calculations

Table D.1.: Degree of reduction (DoR)

Element	DoR
C	+4
H	+1
O	-2
N	-3
S	+6
P	+5

Table D.2.: Degree of reduction of components

Molecule	Formula	DoR	DoR C
	CO_2	0	0
Ethanol	C_2H_6O	12	6
Glucose	$C_6H_{12}O_6$	24	4
Succinic acid	$C_4H_6O_2$	14	3.5
Glycerol	$C_3H_8O_3$	14	4.67
Acetate	$C_2H_4O_2$	8	4

E. 3 Experimental data for succinic acid analysis

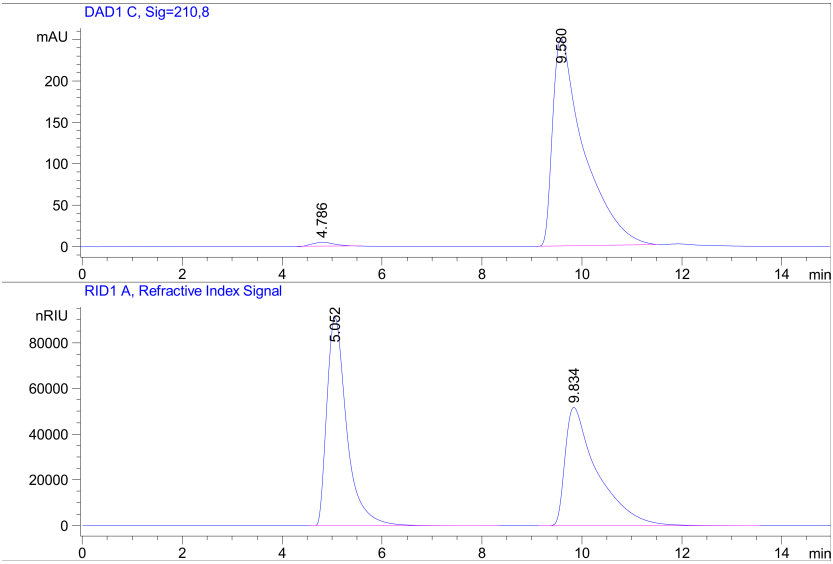

(a) Initial

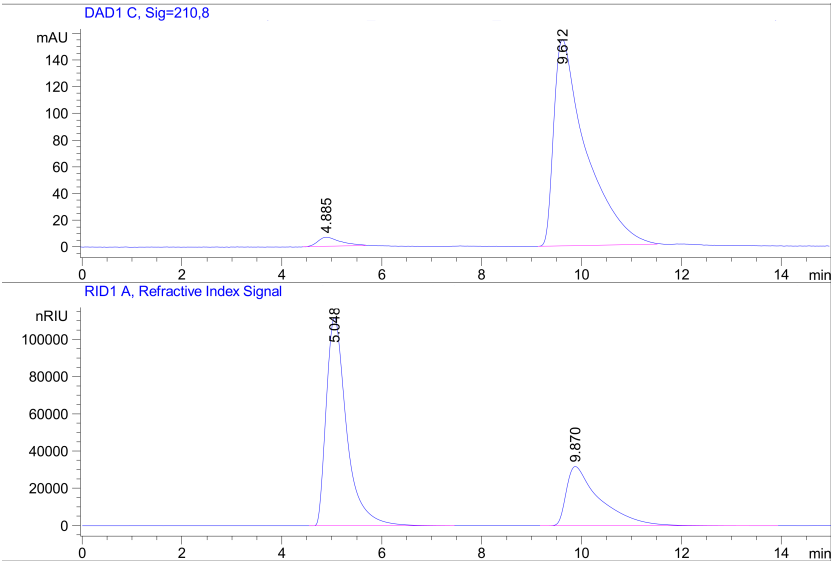

(b) End

Figure E.1.: HPLC chromatogram of initial and end state in exp. 2. (Anode)

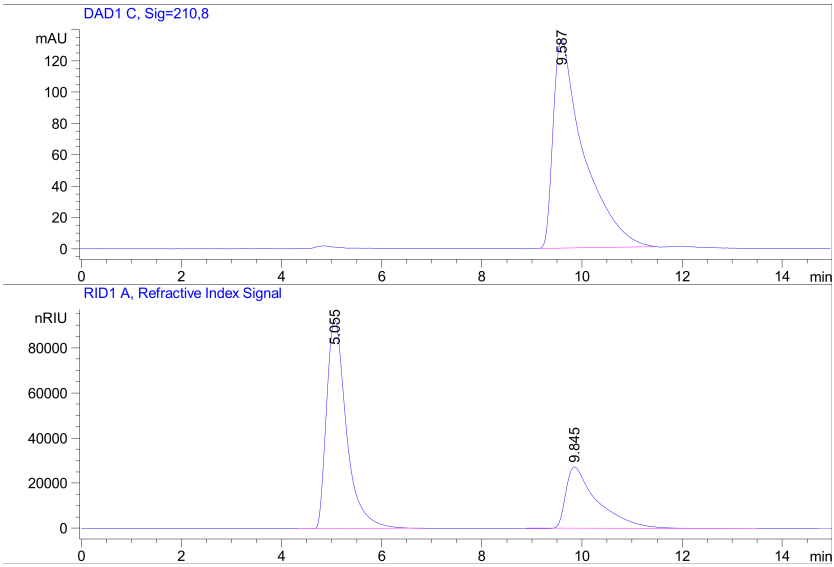

(a) Initial

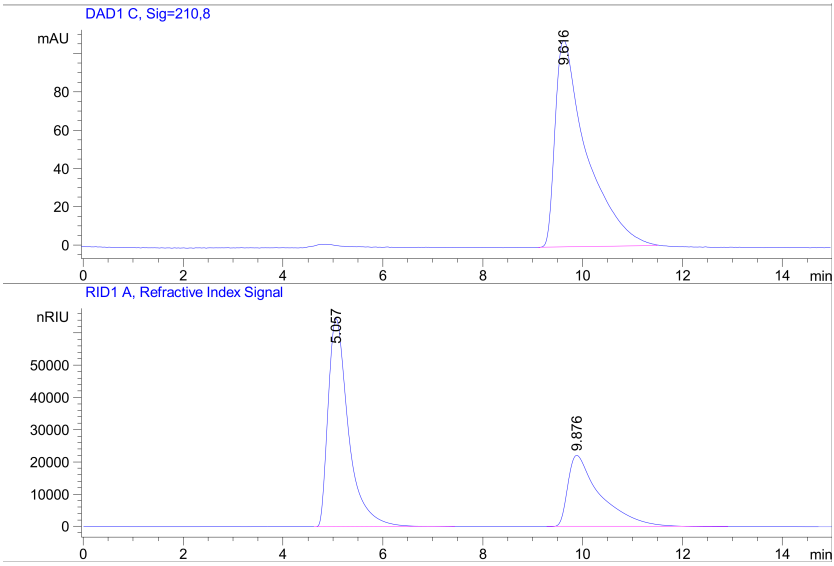

(b) End

Figure E.2.: HPLC chromatogram of initial and end state in exp. 2. (Cathode)

F. 4 Electrolytic Conductance

Table F.1.: Limiting conductances of relevant ionic species [2]

Species	$\lambda_i^0 \left[\frac{Scm^2}{mol}\right]$
H^+	349.65
OH^-	198.00
Na^+	50.08
HCO_3^-	44.50
$1/2CO_3^{2-}$	69.30
$HSuc^-$	47.00
$1/2Suc^{2-}$	58.80
Ace^-	40.90
For^-	54.60
HSO_4^-	52.00
$1/2SO_4^{2-}$	80.00

F.0.1. Determination of the electrolyte concentration

The electrolyte concentration characteristic for fermentation broth is determined as follows. The concentrations of all nutrient salts contained in the fermentation broth are related to Na_2SO_4 with the aim of finding an equivalent sulfate concentration.

The idea is to combine the different nutrient salts in an electrolyte through their ionic strength. The ionic strength $I_{c,i}$ for any electrolyte yields to:

$$I_{c,i} = 0.5 \cdot ((z_i^+)^2 \cdot C_i^+ + (z_i^-)^2 \cdot C_i^-) \tag{F.1}$$

z_i^+ and z_i^- are the valencies of the ions contained in the electrolyte. C_i^+ are C_i^- are the molar concentration of the ions.

The ionic strength of a solution containing multiple electrolytes, the combined ionic strength is the sum of all participating ionic strengths:

$$I_{c,total} = \sum_{i=1} I_{c,i} \tag{F.2}$$

The combined ionic strength of all electrolytes in the fermentation broth must be equal to the ionic strength of the equivalent Na_2SO_4-solution:

$$I_{c,total} = I_{c,Na_2SO_4} \tag{F.3}$$

$$I_{c,Na_2SO_4} = 0.5 \cdot ((z^+_{Na^+})^2 \cdot C^+_{Na^+} + (z^-_{SO_4^{2-}})^2 \cdot C^-_{SO_4^{2-}}) \tag{F.4}$$

$$I_{c,Na_2SO_4} = 0.5 \cdot (1^2 \cdot C^+_{Na^+} + (-2)^2 \cdot C^-_{SO_4^{2-}}) \tag{F.5}$$

$$I_{c,Na_2SO_4} = 0.5 \cdot (1 \cdot 2 \cdot C_{Na_2SO_4} + 4 \cdot C_{Na_2SO_4}) \tag{F.6}$$

$$I_{c,Na_2SO_4} = 3 \cdot C_{Na_2SO_4}) \tag{F.7}$$

Rearranging yields:

$$C_{Na_2SO_4} = \frac{1}{3} \cdot I_{c,Na_2SO_4} = \frac{1}{3} \cdot I_{c,total} \tag{F.8}$$

Inserting the concentrations of all nutrient salts used in [282], [**?**] and [120] yields equivalent Na_2SO_4-concentrations of 0.0807 M [282], 0.1043 M [**?**] and 0.1067 M [**?**]. For the continuous experiments conducted in this work, Na_2SO_4-concentration was set to 0.1 M.

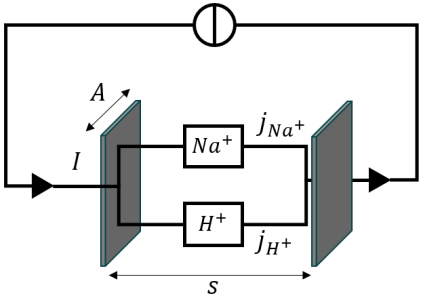

Figure F.1.: Caption

The electric current in an aqueous electrolyte is carried by the migration of ions. In the case of complex electrolyte solutions with more than one charged-ion species which can participate in the electric charge transfer, the total electric current is partitioned among the single-ion charge transfer. In the bulk phase where cations and anions are present, modeling the local charge transfer is a complex endeavor but at an ion selective membrane the complex electrolytic ion transfer is reduced to the migration of either anions or cations. In this work, the ion flux at the cations exchange membrane is modeled as two resistors constituted by the conductivity of Na^+ and H^+ ions F.1.

With the ion-specific conductivity κ [cm^{-1}] and the geometric properties of the electrolyte A/s the ohmic resistance R [Ω] of the electrolyte is calculated with F.10.

$$R = \frac{1}{L} \tag{F.9}$$

$$L = \frac{A}{s}\kappa \tag{F.10}$$

In a parallel circuit, the total conductivity is the sum of the individual conductivity of each current-carrying element F.11.

$$L_{tot} = \sum_i L_i \tag{F.11}$$

Which is equivalent with the more commonly known rule for resistors in parallel F.12.

$$\frac{1}{R_{tot}} = \sum_i \frac{1}{R_i} \tag{F.12}$$

For the current I in a parallel circuit applies F.13.

$$I = \sum_i j_i \ , \quad j = z_{\pm} \cdot \dot{n}_{\pm} \cdot F \tag{F.13}$$

If we take into account the relation of current, voltage and conductivity

$$I = L \cdot U, \tag{F.14}$$

the distribution of the electric current to the individual ion fluxes follows:

$$U = \frac{I}{L_{tot}} \tag{F.15}$$

$$= \frac{j_{\mathrm{H}^+} + j_{\mathrm{Na}^+}}{L_{\mathrm{H}^+} + L_{\mathrm{Na}^+}} \tag{F.16}$$

$$\frac{I}{L_{tot}} = \frac{j_{\mathrm{H}^+} + j_{\mathrm{Na}^+}}{L_{\mathrm{Na}^+} + L_{\mathrm{H}^+}} \tag{F.17}$$

$$\frac{j_{\mathrm{Na}^+}}{I} + \frac{j_{\mathrm{H}^+}}{I} = \frac{L_{\mathrm{Na}^+}}{L_{\mathrm{Na}^+} + L_{\mathrm{H}^+}} + \frac{L_{\mathrm{H}^+}}{L_{\mathrm{Na}^+} + L_{\mathrm{H}^+}} \tag{F.18}$$

$$\underbrace{\frac{L_{\mathrm{Na}^+}}{L_{\mathrm{Na}^+} + L_{\mathrm{H}^+}} I}_{j_{\mathrm{Na}^+}} + \underbrace{\frac{L_{\mathrm{H}^+}}{L_{\mathrm{Na}^+} + L_{\mathrm{H}^+}} I}_{j_{\mathrm{H}^+}} = j_{\mathrm{Na}^+} + j_{\mathrm{H}^+} \tag{F.19}$$

Taking into account that in the electrolyte element the geometric element for the both ion species are equals the overall conductivity corre-

sponds directly with the ion specific conductivity.

$$\frac{\kappa_{\mathrm{Na^+}}}{\kappa_{\mathrm{Na^+}} + \kappa_{\mathrm{H^+}}} I = j_{\mathrm{Na^+}} = z_{\mathrm{Na^+}} \cdot F \cdot \dot{n}_{\mathrm{Na^+}} \tag{F.20}$$

$$\frac{\kappa_{\mathrm{H^+}}}{\kappa_{\mathrm{Na^+}} + \kappa_{\mathrm{H^+}}} I = j_{\mathrm{H^+}} = z_{\mathrm{H^+}} \cdot F \cdot \dot{n}_{\mathrm{H^+}} \tag{F.21}$$

This has the implication that in an electrolyte solution the fraction of the current carried by one ion species directly depends on the contribution of this ion species to the overall electrolyte conductivity, which depends on the ion specific conductivity and its concentration. As a consequence, the ion species with the highest contribution to the electrolyte conductivity will be the main species responsible for the charge transfer by ion migration.

G. 5 pH Calculation of Initial States

$$\begin{bmatrix} H_M^+ & 0 & -H_M^+ & -2H_M^+ & 0 & -H_M^+ & -2H_M^+ \\ 0 & K_{S,H_2Suc} & -H_M^+ & 0 & 0 & 0 & 0 \\ 0 & 0 & K_{S,HSuc} & -H_M^+ & 0 & 0 & 0 \\ 0 & 1 & 1 & 1 & 0 & 0 & 0 \\ 0 & 0 & 0 & 0 & K_{S,H_2SO4} & -H_M^+ & 0 \\ 0 & 0 & 0 & 0 & 0 & K_{S,HSO4} & -H_M^+ \\ 0 & 0 & 0 & 0 & 1 & 1 & 1 \end{bmatrix} \begin{bmatrix} Na^+ \\ H2Suc \\ HSuc \\ Suc \\ H2SO4 \\ HSO4 \\ SO4 \end{bmatrix} = \begin{bmatrix} K_W - (H_M^+)^2 \\ 0 \\ 0 \\ H2Suc_{tot,M} \\ 0 \\ 0 \\ SO4_{tot,M} \end{bmatrix} \tag{G.1}$$

$$\begin{bmatrix} 1 & 0 & 0 & 0 & 0 & 0 & 0 & 0 \\ 0 & K_{S,H_2Suc} & -H_M^+ & 0 & 0 & 0 & 0 & 0 \\ 0 & 0 & K_{S,HSuc} & -H_M^+ & 0 & 0 & 0 & 0 \\ 0 & 1 & 1 & 1 & 0 & 0 & 0 & 0 \\ 0 & 0 & 0 & 0 & K_{S,H_2SO4} & -H_M^+ & 0 & 0 \\ 0 & 0 & 0 & 0 & 0 & K_{S,HSO4} & -H_M^+ & 0 \\ 0 & 0 & 0 & 0 & 1 & 1 & 1 & \\ H_M^+ & 0 & -H_M^+ & -2H_M^+ & 0 & -H_M^+ & -2H_M^+ & H_M^+ \end{bmatrix} \begin{bmatrix} Na^+ \\ H2Suc \\ HSuc \\ Suc \\ H2SO4 \\ HSO4 \\ SO4 \\ h \end{bmatrix} = \begin{bmatrix} NaOH_{tot,M} \\ 0 \\ 0 \\ H2Suc_{tot,M} \\ 0 \\ 0 \\ SO4_{tot,M} \\ K_W \end{bmatrix} \tag{G.2}$$

Table G.1.: Diffusivities and kinematic viscosities for mass transfer coefficient estimation [10]

Species system	D_j $[\frac{m^2}{s}]$	γ $[\frac{m^2}{s}]$	$k_{j,org/aq}$ $[\frac{m}{s}]$
Iodine/water	$1.549 \cdot 10^{-9}$	-	$9.34 \cdot 10^{-5}$
Iodine/kerosene	$3.000 \cdot 10^{-9}$	-	$4.90 \cdot 10^{-5}$
Succinic acid/water	$9.583 \cdot 10^{-10}$	-	-
TOA/1-octanol	$1.456 \cdot 10^{-10}$	-	-
Complex/1-octanol	$1.338 \cdot 10^{-10}$	-	-
Kerosene	-	$1.520 \cdot 10^{-6}$	-
1-octanol	-	$7.360 \cdot 10^{-6}$	-

G.1. List of Materials and Devices

The tables in this section give an overview over all materials and devices used for the experiments.

Table G.2.: Materials

Name	Molecular formula	Purity	Producer	LOT-No.
Succinic acid	$C_4O_6H_4$	99+%	Alfa Aesar	10211054
Sodium sulfate	Na_2SO_4	technical; min. 98%	VWR Chemicals	19H274103
		GPR RECTAPUR	VWR Chemicals	20H044126
di-Sodium succinate	$C_4H_4Na_2O_4$	anhydrous for synthesis	Merck KGaA	S7277901 912
		anhydrous for synthesis	Merck KGaA	S8017901 038
		anhydrous for synthesis	Merck KGaA	S7277901 950
Sodium hydroxide	NaOH	>=98% pa; Iso;	Carl Roth	
Tri-n-octylamine	$C_{24}H_{51}N$	95%	Alfa Aesar	10214764
		for synthesis	Merck KGaA	S7297549 004
1-Octanol	$C_8H_{17}OH$	99%	Alfa Aesar	10198618
		99%	Alfa Aesar	10216490
sulfuric acid	H_2SO_4	95-97%, for analysis	Merck KGaA	K50804031 846

Table G.3.: Devices

Device	Producer	Specifications	Location
Density meter	Anton Paar GmbH	density & sound analyzer DA 48	Graz, Austria
Current supply	EA Elektro-Automatik GmbH & Co. KG	EA-PSI 9040-120 2U	Viersen, Germany
Pump	Cole-Parmer GmbH	Masterflex L/S	Wertheim, Germany
Pump head	Cole-Parmer GmbH	Masterflex L/S easy-load II	Wertheim, Germany
Pump tube	Cole-Parmer GmbH	Masterflex L/S 14	Wertheim, Germany
Pulsation pump	ProMinent GmbH	ProMinent-Dulcometer PHD	Heidelberg, Germany
pH meter	KOBOLD Messring GmbH	HND-R106	Hofheim a.T., Germany
pH meter	KOBOLD Messring GmbH	KOBO-pH APM-X	Hofheim a.T., Germany
pH electrode	VWR International GmbH	pH electrode pHenomenal	Darmstadt, Germany
HPLC	AGILENT TECHNOLOGIES, INC.	Agilent 1100 HPLC	Santa Clara, CA, USA
Infrared camera	RS Components GmbH	Smart thermal camera	Frankfurt a.M., Germany

Table G.4.: Information on HPLC analytics

Parameter	**Value**	**[Unit]**	**Additional information**
Eluent	10	mM	H_2SO_4
Calibration Date			May, 25th 2020
Column size	8 x 250	mm x mm	Organic Acid Resin, CS Chromatographie
Column temperature	40	°C	
Flow Rate	1.0	$mL \cdot min^{-1}$	
Injected volume	5	μL	
Runtime	17.5	min	
RID signal	35	°C	
DAD signal	210	nm	

G.2. Derivation of Design Equations for Membrane Contactors with Dissociating Solutes

† The design framework for the calculation of the membrane area of a membrane-assisted extraction is based on the approach suggested by Melin and Rautenbach [209]. The original approach does not consider the dissociation of the extracted solute. To cover the important effect of the aqueous pH for the extraction of lactic acid, the original model is extended to account for the influence of the aqueous pH equilibrium on the extraction. The mass balances around a differential volume of the

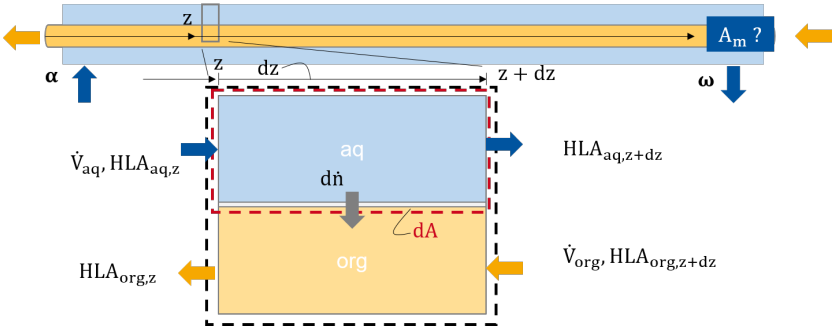

Figure G.1.: Differential volume of the membrane contactor, the balance boundary around the aqueous phase is indicated in red and the overall mass balance boundary in black.

membrane contactor in counter current operation fig. G.1,

$$K_{\mathrm{LA}} = \frac{[LA^-][H^+]}{[HLA]} \tag{G.3}$$

†Parts of this chapter have been published in the ESI with "Gausmann & Gössi et al. "Electrochemical membrane-assisted pH-swing extraction and back-extraction" 2022, Separation and Purification Technology" Parts of this chapter are also used in the Dissertation of Angelo Gössi, " Membrane supported reactive extraction using membranes with enhanced stability".

$$\begin{aligned} d\dot{n} &= \dot{V}_{\mathrm{aq}}([HLA]|_z - [HLA]|_{z+dz}) \\ &= \dot{V}_{\mathrm{org}}([HLA_{\mathrm{org}}]|_z - [HLA_{\mathrm{org}}]|_{z+dz}) \end{aligned} \tag{G.4}$$

and around a differential element of the aqueous phase:

$$d\dot{n} = k_{\mathrm{m}} dA_{\mathrm{M}} (K_{LA}[TOA][HLA] - [HLA_{\mathrm{org}}]) \tag{G.5}$$

Yield an overall mass balance equation:

$$\dot{V}_{\mathrm{aq}}([HLA]|_z - [HLA]|_{z+dz}) = k_{\mathrm{m}} dA_{\mathrm{M}} (K_{LA}[TOA][HLA] - [HLA_{\mathrm{org}}]) \tag{G.6}$$

The overall mass balance is approximated by a Taylor's series according to:

$$0 = \dot{V}_{\mathrm{aq}} \frac{\partial [HLA]}{\partial z} dz + k_{\mathrm{m}} dA_{\mathrm{M}} (K_{LA}[TOA][HLA] - [HLA_{\mathrm{org}}]) \tag{G.7}$$

Next, a separation of vaiables dA_{M} and dz gives a differential expression of the membrane area:

$$\frac{dA_{\mathrm{M}}}{d[HLA]} = \frac{-\dot{V}_{\mathrm{aq}}/k_{\mathrm{m}}}{\left([HLA]K_{LA}[TOA] + \frac{\dot{V}_{\mathrm{aq}}}{\dot{V}_{\mathrm{org}}}([HLA_{\mathrm{tot}}]_{\alpha} - [HLA_{\mathrm{tot}}]) - [HLA_{\mathrm{org}}]_{\omega}\right)} \tag{G.8}$$

Now we must take into account that only the protonated fraction of the lactic acid is available for the extraction. The concentration of the protonated form and the total concentration of lactic acid are related by the dissociation equilibrium.

$$[HLA] = [HLA_{\mathrm{tot}}] \frac{[H^+]}{[H^+] + K_{\mathrm{LA}}} \tag{G.9}$$

Due to the dissociation equilibrium a change of the integration variable is required.

$$\frac{dA_{\mathrm{M}}}{d[HLA_{\mathrm{tot}}]} = \frac{dA_{\mathrm{M}}}{d[HLA]} \cdot \frac{d[HLA]}{d[HLA_{\mathrm{tot}}]} \tag{G.10}$$

The change of the integration variable introduces a new differential $\frac{d[HLA]}{d[HLA_{\mathrm{tot}}]}$ which describes how the concentration of the protonated lactic acid changes with the removal of lactic acid by extraction. In addition, the change of the TOA concentration with the extraction of lactic acid is assumed to be one.

$$\frac{d[TOA]}{d[HLA_{\mathrm{tot}}]} = 1 \tag{G.11}$$

This assumption holds as long as 1:1 complexes are formed, which is the case except for overloading conditions [64]. The mass balance for the lactic acid dissociation is:

$$[HLA_{tot}] = [HLA] + [LA^{-}] \tag{G.12}$$

and with the insertion of eq. (G.3) becomes:

$$[HLA] = [HLA_{\mathrm{tot}}]\frac{[H^{+}]}{[H^{+}] + K_{\mathrm{LA}}} \tag{G.13}$$

Differentiation of eq. (G.12) with respect to $[HLA_{\mathrm{tot}}]$ yields the required differential expression introduced with the change of integration variables:

$$\frac{d[HLA]}{d[HLA_{\mathrm{tot}}]} = \frac{[H^{+}]}{[H^{+}] + K_{\mathrm{LA}}} + [HLA_{\mathrm{tot}}]\frac{d[H^{+}]}{d[HLA_{\mathrm{tot}}]}\left[\frac{K_{\mathrm{LA}}}{([H^{+}] + K_{\mathrm{LA}})^{2}}\right] \tag{G.14}$$

An expression for the last unknown differential is obtained by inserting eq. (G.3) in eq. (G.12), solving the resulting quadratic equation for $[H^{+}]$, followed by differentiation with respect to $[HLA_{\mathrm{tot}}]$. This leads to the

searched differential:

$$\frac{d[H^+]}{d[HLA_{\mathrm{tot}}]} = \frac{K_{\mathrm{LA}}}{2\sqrt{\frac{K_{\mathrm{LA}}^2}{4} + [HLA_{\mathrm{tot}}]K_{\mathrm{LA}}}} \tag{G.15}$$

The resulting set of differential expressions eqs. (G.8), (G.10), (G.11), (G.14) and (G.15) is solved numerically for the required membrane area using the MATLAB ode15s solver.

H. 9 Techno-economic assessment

Table H.1.: Price inventory products

Revenue	***Unit***	***Price range***	***€ per unit***
Succinic acid 99,99%	kg	1,5-2	2
Biogas	$t_C H4$		375
Hydrogen	3	2000-3000	2500
Oxygen	t		40

Table H.2.: Price inventory raw materials

Raw Material	***Unit***	***Price range***	***€ per unit***
Fresh water	t		0,85
Glucose	t	400-500	450
Ammoniumphosphate	t		550
Ammonia	t		530
CO2	t		150
CDW	t		1150

Table H.3.: Price inventory auxiliary chemicals

Additives	***0,2***	***Price range***	***€ per unit***
Hydrochloric acid 32w%	t	85-130	90
Sodium Hydroxide 99w%	t	380-630	510
CaOH	t	100-320	170
MgOH	t	350-650	430
Sulfuric acid 98w%	t	60-150	80
Phosphoric acid 85w%	t	600-900	700
Trioctylamine	t	600-1600	1100
Decanol	t	1300-1800	1500
Octanol	t	1000-1300	1200
MgCl2	t	100-300	250

Table H.4.: Price inventory utilities and waste treatment

Utilities and Waste treatment	***Unit***	***Price range***	***€ per unit***
Natural gas	kWh	2,2-3,6	0,03
	t	275-450	375
Electricity	kWh	4,5-8,5	0,07
Cooling water (20°C 25°C)	t		0,015
LP Steam (125°C 124°C)	t		20
MP Steam (175°C 174°C)	t		22
HP Steam (250°C 249°C)	t		25
Refrigerant (-25°C -24°C)	MJ		0,002329
Wastewater hydraulic	t		
Solid waste disposal	t		110
Off-gas treatment	t		0
Solid waste incineration	t		0,25

Bibliography

[1] T. Werpy and G. Petersen. Top value added chemicals from biomass: Volume i–results of screening for potential candidates from sugars and synthesis gas.

[2] Haynes and William M. Lide2014 - book - crc handbook of chemistry and physics. 2015.

[3] Wubliker Dessie, Fengxue Xin, Wenming Zhang, Youming Jiang, Hao Wu, Jiangfeng Ma, and Min Jiang. Opportunities, challenges, and future perspectives of succinic acid production by actinobacillus succinogenes. *Applied microbiology and biotechnology*, 102(23):9893–9910, 2018.

[4] Michael Binns, Anestis Vlysidis, Colin Webb, Constantinos Theodoropoulos, Pedro de Atauri, and Marta Cascante. Glycerol metabolic conversion to succinic acid using actinobacillus succinogenes. In Michael Binns, Anestis Vlysidis, Colin Webb, Constantinos, editor, *Glycerol metabolic conversion to succinic acid using Actinobacillus succinogenes: a metabolic network-based analysis*, volume 29 of *21st European Symposium on Computer Aided Process Engineering – ESCAPE 21*, pages 1421–1425. Elsevier, 2011.

[5] Antonius J. A. van Maris, Wil N. Konings, Johannes P. van Dijken, and Jack T. Pronk. Microbial export of lactic and 3-hydroxypropanoic acid: implications for industrial fermentation processes. *Metabolic engineering*, 6(4):245–255, 2004.

[6] Velayudham Ramadoss, Yue Zheng, Xiaoqing Shao, Lifang Tian, and Yahui Wang. Advances in electrochemical decarboxyla-

tive transformation reactions. *Chemistry (Weinheim an der Bergstrasse, Germany)*, 27(10):3213–3228, 2021.

[7] K. ALDAS, N. PEHLIVANOGLU, and M. MAT. Numerical and experimental investigation of two-phase flow in an electrochemical cell. *International Journal of Hydrogen Energy*, 33(14):3668–3675, 2008.

[8] Marcel Gausmann, Angelo Gössi, Franziska Bertram, Wolfgang Riedl, Boelo Schuur, and Andreas Jupke. Electrochemical membrane-assisted ph-swing extraction and back-extraction of lactic acid. *Separation and Purification Technology*, page 120702, 2022.

[9] Carl H. Hamann and Wolf Vielstich. *Elektrochemie*. Wiley-VCH Verlag GmbH & Co. KGaA, Weinheim, 2005.

[10] Young-Si Jun, Yun Suk Huh, Won Hi Hong, and Yeon Ki Hong. Kinetics of the extraction of succinic acid with tri-n-octylamine in 1-octanol solution. *Biotechnology progress*, 21(6):1673–1679, 2005.

[11] Arnold L. Demain. The business of biotechnology. *Industrial Biotechnology*, 2007.

[12] IEA. Technology roadmap energy and ghg reductions in the chemical industry via catalytic processes. 2013.

[13] Arne Kätelhön, Raoul Meys, Sarah Deutz, Sangwon Suh, and André Bardow. Climate change mitigation potential of carbon capture and utilization in the chemical industry. *Proceedings of the National Academy of Sciences of the United States of America*, 116(23):11187–11194, 2019.

[14] James H. Clark, Rafael Luque, and Avtar S. Matharu. Green chemistry, biofuels, and biorefinery. *Annual Review of Chemical and Biomolecular Engineering*, 3(1):183–207, 2012.

[15] Hassan I. Moussa, Ali Elkamel, and Steven B. Young. Assessing energy performance of bio-based succinic acid production using lca. *Journal of Cleaner Production*, 139:761–769, 2016.

[16] Sudeep Vaswani. Bio-based succinic acid.

[17] Jeong Wook Lee, Hyun Uk Kim, Sol Choi, Jongho Yi, and Sang Yup Lee. Microbial production of building block chemicals and polymers. *Current Opinion in Biotechnology*, 22(6):758–767, 2011.

[18] Judith Becker and Christoph Wittmann. Bio-based production of chemicals, materials and fuels -corynebacterium glutamicum as versatile cell factory. *Current Opinion in Biotechnology*, 23(4):631–640, 2012.

[19] Rathin Datta and David A. Glassner. Fermentation and purification process for succinic acid: Us, 1992.

[20] Anton A. Kiss, Jean-Paul Lange, Boelo Schuur, D.W.F. Brilman, A.G.J. van der Ham, and Sascha R.A. Kersten. Separation technology–making a difference in biorefineries. *Biomass and Bioenergy*, 95:296–309, 2016.

[21] Qiang Li, Dan Wang, Yong Wu, Wangliang Li, Yunjian Zhang, Jianmin Xing, and Zhiguo Su. One step recovery of succinic acid from fermentation broths by crystallization. *Separation and Purification Technology*, 72(3):294–300, 2010.

[22] Ke-Ke Cheng, Xue-Bing Zhao, Jing Zeng, Ru-Chun Wu, Yun-Zhen Xu, De-Hua Liu, and Jian-An Zhang. Downstream processing of biotechnological produced succinic acid. *Applied microbiology and biotechnology*, 95(4):841–850, 2012.

[23] Camilo S. López-Garzón and Adrie J.J. Straathof. Recovery of carboxylic acids produced by fermentation. *Biotechnology advances*, 32(5):873–904, 2014.

[24] Eric M. Karp, Robin M. Cywar, Lorenz P. Manker, Patrick O. Saboe, Claire T. Nimlos, Davinia Salvachúa, Xiaoqing Wang, Brenna A. Black, Michelle L. Reed, William E. Michener, Nicholas A. Rorrer, and Gregg T. Beckham. Post-fermentation recovery of biobased carboxylic acids. *ACS Sustainable Chemistry & Engineering*, 6(11):15273–15283, 2018.

[25] K. Prochaska, J. Antczak, M. Regel-Rosocka, and M. Szczygiełda. Removal of succinic acid from fermentation broth by multistage process (membrane separation and reactive extraction). *Separation and Purification Technology*, 192:360–368, 2018.

[26] Kris A.Berglund, Ponnampalam Elankovan, and David A. Glassner. Carboxylic acid purification and crystallization process, 1991.

[27] Alberto Vertova, Gabriele Aricci, Sandra Rondinini, Roberta Miglio, Lino Carnelli, and Paolo D'Olimpio. Electrodialytic recovery of light carboxylic acids from industrial aqueous wastes. *Journal of Applied Electrochemistry*, 39(11):2051–2059, 2009.

[28] Chuanhui Huang, Tongwen Xu, Yaping Zhang, Yanhong Xue, and Guangwen Chen. Application of electrodialysis to the production of organic acids: State-of-the-art and recent developments. *Journal of Membrane Science*, 288(1-2):1–12, 2007.

[29] Sai Bhavaraju and Kean Duffy. Method and device for carboxylic acid production, 2012.

[30] Christoph Kost, Shivenes Shammugam, Verena Fluri, Dominik Peper, Aschkan Davoodi Memar, and Thomas Schlegl. Stromgestehungskosten erneuerbare energien.

[31] Sayed M. Saba, Martin Müller, Martin Robinius, and Detlef Stolten. The investment costs of electrolysis – a comparison of cost studies from the past 30 years. *International Journal of Hydrogen Energy*, 43(3):1209–1223, 2018.

[32] Tahmineh Nasrollahnejad, Johan Urbanus, Joop H. ter Horst, Dirk Verdoes, and Cornelis P.M. Roelands. Electrochemically induced crystallization as a sustainable method for product recovery of building block chemicals: Techno-economic evaluation of fumaric acid separation. *Industrial Biotechnology*, 8(3):133–151, 2012.

[33] Korneel Rabay and Christian Merlebeke. Electrochemical processes to separate products derived from biological conversions, 2013.

[34] Jiajie Xu, Juan J. L. Guzman, Stephen J. Andersen, Korneel Rabaey, and Largus T. Angenent. In-line and selective phase separation of medium-chain carboxylic acids using membrane electrolysis. *Chemical communications (Cambridge, England)*, 51(31):6847–6850, 2015.

[35] Joachim Desloover, Andualem Abate Woldeyohannis, Willy Verstraete, Nico Boon, and Korneel Rabaey. Electrochemical resource recovery from digestate to prevent ammonia toxicity during anaerobic digestion. *Environmental science & technology*, 46(21):12209–12216, 2012.

[36] Stephen J. Andersen, Ilje Pikaar, Stefano Freguia, Brian C. Lovell, Korneel Rabaey, and René A. Rozendal. Dynamically adaptive control system for bioanodes in serially stacked bioelectrochemical systems. *Environmental science & technology*, 47(10):5488–5494, 2013.

[37] Stephen J. Andersen, Tom Hennebel, Sylvia Gildemyn, Marta Coma, Joachim Desloover, Jan Berton, Junko Tsukamoto, Christian Stevens, and Korneel Rabaey. Electrolytic membrane extraction enables production of fine chemicals from biorefinery sidestreams. *Environmental science & technology*, 48(12):7135–7142, 2014.

[38] Stephen J. Andersen, Pieter Candry, Thais Basadre, Way Cern Khor, Hugo Roume, Emma Hernandez-Sanabria, Marta Coma,

and Korneel Rabaey. Electrolytic extraction drives volatile fatty acid chain elongation through lactic acid and replaces chemical ph control in thin stillage fermentation. *Biotechnology for biofuels*, 8:221, 2015.

[39] Way Cern Khor, Stephen Andersen, Han Vervaeren, and Korneel Rabaey. Electricity-assisted production of caproic acid from grass. *Biotechnology for biofuels*, 10:180, 2017.

[40] Chrysanthi Pateraki, Stephen J. Andersen, Dimitrios Ladakis, Apostolis Koutinas, and Korneel Rabaey. Direct electrochemical extraction increases microbial succinic acid production from spent sulphite liquor. *Green Chemistry*, 21(9):2401–2411, 2019.

[41] S. S. Yi, Y. C. Lu, and G. S. Luo. Separation and concentration of lactic acid by electro-electrodialysis. *Separation and Purification Technology*, 60(3):308–314, 2008.

[42] L. Handojo, A. K. Wardani, D. Regina, C. Bella, M. T. A. P. Kresnowati, and I. G. Wenten. Electro-membrane processes for organic acid recovery. *RSC Advances*, 9(14):7854–7869, 2019.

[43] Nayeong Kim, Jemin Jeon, Raylin Chen, and Xiao Su. Electrochemical separation of organic acids and proteins for food and biomanufacturing. *Chemical Engineering Research and Design*, 178:267–288, 2022.

[44] Tanja Kurzrock and Dirk Weuster-Botz. New reactive extraction systems for separation of bio-succinic acid. *Bioprocess and biosystems engineering*, 34(7):779–787, 2011.

[45] Emmanuel Zoulias, Elli Varkaraki, Nicolaos Lymberopoulos, Christodoulos N. Christodoulou, and George N. Karagiorgis. A review on water electrolysis. *Tcjst*, (4.2):41–71, 2004.

[46] Walther Nernst. Die elektromotorische wirksamkeit der jonen. *Zeitschrift für Physikalische Chemie*, 4U(1), 1889.

[47] H . Taymaz-Nikerel, E . Jamalzadeh, A . Espah Borujeni, P .J .T . Verheijen, W . M . van Gulik, and J .J . Heijnen. A thermodynamic analysis of dicarboxylic acid production in microorganisms. 2013.

[48] Isabelle Meynial-Salles, Sophie Dorotyn, and Philippe Soucaille. A new process for the continuous production of succinic acid from glucose at high yield, titer, and productivity. *Biotechnology and bioengineering*, 99(1):129–135, 2008.

[49] Zhongxue Dai, Feng Guo, Shangjie Zhang, Wenming Zhang, Qiao Yang, Weiliang Dong, Min Jiang, Jiangfeng Ma, and Fengxue Xin. Bio-based succinic acid: an overview of strain development, substrate utilization, and downstream purification. *Biofuels, Bioproducts and Biorefining*, 2:505, 2019.

[50] S. Aljoscha Wahl, Cristina Bernal Martinez, Zheng Zhao, Walter M. van Gulik, and Mickel L. A. Jansen. Intracellular product recycling in high succinic acid producing yeast at low ph. *Microbial cell factories*, 16(1):90, 2017.

[51] Matteo Gabba, Jacopo Frallicciardi, Joury van 't Klooster, Ryan Henderson, Łukasz Syga, Robert Mans, Antonius J. A. van Maris, and Bert Poolman. Weak acid permeation in synthetic lipid vesicles and across the yeast plasma membrane. *Biophysical journal*, 118(2):422–434, 2020.

[52] Riki Canari and Aharon M. Eyal. Extraction of carboxylic acids by amine-based extractants: Apparent extractant basicity according to the ph of half-neutralization. *Industrial & Engineering Chemistry Research*, 42(7):1285–1292, 2003.

[53] Dipaloy Datta, Sushil Kumar, and Hasan Uslu. Status of the reactive extraction as a method of separation. *Journal of Chemistry*, 2015(2):1–16, 2015.

[54] Tanja Kurzrock and Dirk Weuster-Botz. Recovery of succinic acid

from fermentation broth. *Biotechnology letters*, 32(3):331–339, 2010.

[55] Yeon Ki Hong, Won Hi Hong, and Dong Hoon Han. Application of reactive extraction to recovery of carboxylic acids. *Biotechnology and Bioprocess Engineering*, 6(6):386–394, 2001.

[56] Anil Kumar and Avinash Thakur. Parametric optimization of green synergistic reactive extraction of lactic acid using trioctylamine, aliquat336, and butan-2-ol in sunflower oil by response surface methodology. *Chemical Engineering Communications*, 206(8):1072–1086, 2019.

[57] Guneet Kaur and Kathy Elst. Development of reactive extraction systems for itaconic acid: A step towards in situ product recovery for itaconic acid fermentation. *RSC Adv*, 4(85):45029–45039, 2014.

[58] Maria Marinova, George Kyuchoukov, Joël Albet, Jacques Molinier, and Guy Malmary. Separation of tartaric and lactic acids by means of solvent extraction. *Separation and Purification Technology*, 37(3):199–207, 2004.

[59] Areli Flores Morales, Joël Albet, George Kyuchoukov, Guy Malmary, and Jacques Molinier. Influence of extractant (tbp and toa), diluent, and modifier on extraction equilibrium of monocarboxylic acids. *Journal of Chemical & Engineering Data*, 48(4):874–886, 2003.

[60] Kunio Kawamura, Keiji Takahashi, and Akitsugu Okuwaki. Influence of ph and diluent on the ion–pair solvent extraction of aromatic carboxylic acids using quaternary ammonium salts. *Separation Science and Technology*, 41(12):2795–2806, 2006.

[61] L.M.J. Sprakel and B. Schuur. Solvent developments for liquid-liquid extraction of carboxylic acids in perspective. *Separation and Purification Technology*, 211:935–957, 2019.

[62] Janet A. Tamada and C. Judson King. Extraction of carboxylic acids with amine extractants. 2. chemical interactions and interpretation of data. *Industrial & engineering chemistry research*, (29):1327–1333, 1990.

[63] Armin Eggert, Tim Maßmann, Dirk Kreyenschulte, Moritz Becker, Benedikt Heyman, Jochen Büchs, and Andreas Jupke. Integrated in-situ product removal process concept for itaconic acid by reactive extraction, ph-shift back extraction and purification by ph-shift crystallization. *Separation and Purification Technology*, 215:463–472, 2019.

[64] Zhiyong Zhou, Zhenyu Li, and Wei Qin. Reactive extraction of saturated aliphatic dicarboxylic acids with trioctylamine in 1-octanol: Equilibria, model, and correlation of apparent reactive equilibrium constants. *Industrial & Engineering Chemistry Research*, 52(31):10795–10801, 2013.

[65] Aharon M. Eyal and Riki Canari. ph dependence of carboxylic and mineral acid extraction by amine-based extractants: Effects of pka, amine basicity, and diluent properties. *Industrial & Engineering Chemistry Research*, (34):1789–1798, 1995.

[66] Marcelo Carmo, David L. Fritz, Jürgen Mergel, and Detlef Stolten. A comprehensive review on pem water electrolysis. *International Journal of Hydrogen Energy*, 38(12):4901–4934, 2013.

[67] Jingang Yao, Michael Kraussler, Florian Benedikt, and Hermann Hofbauer. Techno-economic assessment of hydrogen production based on dual fluidized bed biomass steam gasification, biogas steam reforming, and alkaline water electrolysis processes. *Energy Conversion and Management*, 145:278–292, 2017.

[68] José Luz Silveira. *Sustainable Hydrogen Production Processes*. Springer International Publishing, Cham, 2017.

[69] Davide Di Marino, Tim Jestel, Caroline Marks, Jörn Viell, Malte Blindert, Stefanie M. A. Kriescher, Antje C. Spiess, and Matthias Wessling. Carboxylic acids production via electrochemical depolymerization of lignin. *ChemElectroChem*, 6(5):1434–1442, 2019.

[70] Shi-Hui Shi, Yujie Liang, and Ning Jiao. Electrochemical oxidation induced selective c-c bond cleavage. *Chemical reviews*, 121(1):485–505, 2021.

[71] Stefan Palkovits and Regina Palkovits. The role of electrochemistry in future dynamic bio–refineries: A focus on (non–)kolbe electrolysis. *Chemie Ingenieur Technik*, 91(6):699–706, 2019.

[72] F. Joschka Holzhäuser, Jens Artz, Stefan Palkovits, Dirk Kreyenschulte, Jochen Büchs, and Regina Palkovits. Electrocatalytic upgrading of itaconic acid to methylsuccinic acid using fermentation broth as a substrate solution. *Green Chem*, 19(10):2390–2397, 2017.

[73] André Bardow and Matthias Wessling. Converting two wastes to value. *Nature Energy*, 4(6):440–441, 2019.

[74] Allen J. Bard and Larry R. Faulkner. *ELECTROCHEMICAL METHODS*. John Wiley & Sons, Inc, 2001.

[75] Carl H. Hamman and Wolf Vielstich. *Elektrochemie*. Wiley-VCH, 2015.

[76] B. E. Conway, H. Angerstein-Kozlowska, and F. C. Ho. Electrochemical study of multiple states of chemisorption of atoms at metal surfaces. *Journal of Vacuum Science and Technology*, 14(1):351–364, 1977.

[77] Rudolf Holze. *Experimental Electrochemistry*. Wiley-VCH, Weinheim, 2019.

[78] Serhiy Cherevko, Simon Geiger, Olga Kasian, Andrea Mingers, and Karl J.J. Mayrhofer. Oxygen evolution activity and stability

of iridium in acidic media. part 1. – metallic iridium. *Journal of Electroanalytical Chemistry*, 773(1):69–78, 2016.

[79] Igor Povar and Oxana Spinu. Ruthenium redox equilibria: 3. pourbaix diagrams for the systems ru-h2o and ru-cl–h2o. *Journal of Electrochemical Science and Engineering*, 6(1):145, 2016.

[80] Marcel Pourbaix. *Atlas of Electrochemical Equilibria in Aqueous Solutions*. 1974.

[81] A. Seghiouer, J. Chevalet, A. Barhoun, and F. Lantelme. Electrochemical oxidation of nickel in alkaline solutions: a voltammetric study and modelling. *Journal of Electroanalytical Chemistry*, (442):119–123, 1998.

[82] V. S. Bagotsky. *Fundamentals of electrochemistry*. The Electrochemical Society series. Wiley-Interscience, Hoboken N.J., 2nd ed. edition, 2006.

[83] Lars Ostervold, Sergio I. Perez Bakovic, Jamie Hestekin, and Lauren F. Greenlee. Electrochemical biomass upgrading: degradation of glucose to lactic acid on a copper(ii) electrode. *RSC Advances*, 11(50):31208–31218, 2021.

[84] Mahinder Ramdin, Andrew R. T. Morrison, Mariette de Groen, Rien van Haperen, Robert de Kler, Erdem Irtem, Antero T. Laitinen, Leo J. P. van den Broeke, Tom Breugelmans, J. P. Martin Trusler, Wiebren de Jong, and Thijs J. H. Vlugt. High-pressure electrochemical reduction of co 2 to formic acid/formate: Effect of ph on the downstream separation process and economics. *Industrial & Engineering Chemistry Research*, 58(51):22718–22740, 2019.

[85] Guo-Qiang Lu, Alechia Crown, and Andrzej Wieckowski. Formic acid decomposition on polycrystalline platinum and palladized platinum electrodes. *The Journal of Physical Chemistry B*, 103(44):9700–9711, 1999.

[86] Yanan Chen, Felipe Mojica, Guangfu Li, and Po-Ya Abel Chuang. Experimental study and analytical modeling of an alkaline water electrolysis cell. *International Journal of Energy Research*, 41(14):2365–2373, 2017.

[87] Youngkook Kwon, Stanley C. S. Lai, Paramaconi Rodriguez, and Marc T. M. Koper. Electrocatalytic oxidation of alcohols on gold in alkaline media: base or gold catalysis? *Journal of the American Chemical Society*, 133(18):6914–6917, 2011.

[88] Constantinos G. Vayenas, editor. *Interfacial phenomena in electrocatalysis*. Springer, 2011.

[89] Jiaojiao Jin, Gangying Zheng, Yangyang Ge, Shanggui Deng, Wei Liu, and Guohua Hui. A non-enzyme electrochemical qualitative and quantitative analyzing method for glucose, d-fructose, and sucrose utilizing cu foam material. *Electrochimica Acta*, 153:594–601, 2015.

[90] Sejin Park, Hankil Boo, and Taek Dong Chung. Electrochemical non-enzymatic glucose sensors. *Analytica chimica acta*, 556(1):46–57, 2006.

[91] Eiichi Shoji and Michael S. Freund. Potentiometric saccharide detection based on the pk(a) changes of poly(aniline boronic acid). *Journal of the American Chemical Society*, 124(42):12486–12493, 2002.

[92] Arun Shaji, Yogendra Shastri, Vinod Kumar, Vivek V. Ranade, and Neil Hindle. Economic and environmental assessment of succinic acid production from sugarcane bagasse. *ACS Sustainable Chemistry & Engineering*, 9(38):12738–12746, 2021.

[93] Andreas Bednarz, Antje C. Spieß, and Andreas Pfennig. Reactive and physical extraction of bio-based diamines from fermentation media. *Journal of Chemical Technology & Biotechnology*, 92(7):1817–1824, 2017.

[94] Florian Buchbender and Martin Wiese. Efficient concentration of an amino acid using reactive extraction coupled with bipolar electrodialysis. *Chemical Engineering & Technology*, 41(12):2298–2305, 2018.

[95] Moritz Doeker, Vincent Hüttche, and Andreas Jupke. Reactive extraction for the recovery of primary amines from aqueous streams. *Separation and Purification Technology*, 277(4):118229, 2021.

[96] Stefania Marini, Paolo Salvi, Paolo Nelli, Rachele Pesenti, Marco Villa, Mario Berrettoni, Giovanni Zangari, and Yohannes Kiros. Advanced alkaline water electrolysis. *Electrochimica Acta*, 82:384–391, 2012.

[97] Hainan Sun and WooChul Jung. Recent advances in doped ruthenium oxides as high-efficiency electrocatalysts for the oxygen evolution reaction. *Journal of Materials Chemistry A*, 9(28):15506–15521, 2021.

[98] Ting Zhu, Shangheng Liu, Bin Huang, Qi Shao, Man Wang, Fan Li, Xinyue Tan, Yecan Pi, Shih-Chang Weng, Bolong Huang, Zhiwei Hu, Jianbo Wu, Yong Qian, and Xiaoqing Huang. High-performance diluted nickel nanoclusters decorating ruthenium nanowires for ph-universal overall water splitting. *Energy & Environmental Science*, 14(5):3194–3202, 2021.

[99] A. S. Kertes and C. J. King. Extraction chemistry of fermentation product carboxylic acids. *Biotechnology and bioengineering*, 28(2):269–282, 1986.

[100] Janet A. Tamada and C. Judson King. Extraction of carboxylic acids with amine extractants. 3. effect of temperature, water coextraction, and process considerations. *Industrial & Engineering Chemistry Research*, 1990.

[101] Janet A. Tamada, A. Steven Kertes, and C. Judson King. Extraction of carboxylic acids with amine extractants. 1. equilibria and

law of mass action modeling. *Industrial & Engineering Chemistry Research*, 1990.

[102] Young-Si Jun, Eun Zoo Lee, Yun Suk Huh, Yeon Ki Hong, Won Hi Hong, and Sang Yup Lee. Kinetic study for the extraction of succinic acid with toa in fermentation broth; effects of ph, salt and contaminated acid. *Biochemical Engineering Journal*, 36(1):8–13, 2007.

[103] Y. K. Hong and W. H. Hong. Reactive extraction of succinic acid with tripropylamine (tpa) in various diluents. *Bioprocess Engineering*, 2000.

[104] Karl Siebertz, David van Bebber, and Thomas Hochkirchen, editors. *Statistische Versuchsplanung: Design of Experiments (DoE)*. Springer, 2010.

[105] Hyohak Song and Sang Yup Lee. Production of succinic acid by bacterial fermentation. *Enzyme and Microbial Technology*, 39(3):352–361, 2006.

[106] Boelo Schuur, Thomas Brouwer, Dion Smink, and Lisette M.J. Sprakel. Green solvents for sustainable separation processes. *Current Opinion in Green and Sustainable Chemistry*, 18:57–65, 2019.

[107] Hans-Jörg Bart. *Reactive Extraction*. Springer, Heidelberg, 2001.

[108] Maria Alexandri, Anestis Vlysidis, Harris Papapostolou, Olga Tverezovskaya, Viacheslav Tverezovskiy, Ioannis K. Kookos, and Apostolis Koutinas. Downstream separation and purification of succinic acid from fermentation broths using spent sulphite liquor as feedstock. *Separation and Purification Technology*, 209:666–675, 2019.

[109] N. Thakre. Reactive extraction of citric acid using different extractants: Equilibrium, kinetics and modeling. *Chemical and Biochemical Engineering Quarterly*, 31(4):437–446, 2018.

[110] Kailas L. Wasewar, Archis A. Yawalkar, Jacob A. Moulijn, and Vishwas G. Pangarkar. Fermentation of glucose to lactic acid coupled with reactive extraction: A review. *Industrial & Engineering Chemistry Research*, 43(19):5969–5982, 2004.

[111] Wei Qin, Zhenyu Li, and Youyuan Dai. Extraction of monocarboxylic acids with trioctylamine: Equilibria and correlation of apparent reactive equilibrium constant. *Industrial & Engineering Chemistry Research*, 42(24):6196–6204, 2003.

[112] Dharm Pal, Ayush Tripathi, Arushi Shukla, Kush R. Gupta, and Amit Keshav. Reactive extraction of pyruvic acid using tri- n - octylamine diluted in decanol/kerosene: Equilibrium and effect of temperature. *Journal of Chemical & Engineering Data*, 60(3):860–869, 2015.

[113] Hans Kiefer. Verfahren zur gewinnung von bernsteinsaeure aus fermentationsbrühen, 2013.

[114] Merten Morales, Meriç Ataman, Sara Badr, Sven Linster, Ioannis Kourlimpinis, Stavros Papadokonstantakis, Vassily Hatzimanikatis, and Konrad Hungerbühler. Sustainability assessment of succinic acid production technologies from biomass using metabolic engineering. *Energy & Environmental Science*, 9(9):2794–2805, 2016.

[115] Michael O. Daramola and Augustine O. Ayeni, editors. *Valorization of Biomass to Value-Added Commodities*. Springer, 2020.

[116] Rajaram A. Pai, Michael F. Doherty, and Michael F. Malone. Design of reactive extraction systems for bioproduct recovery. *AIChE Journal*, (48), 2002.

[117] Agnieszka Krzyżkowska and Magdalena Regel-Rosocka. The effect of fermentation broth composition on removal of carboxylic acids by reactive extraction with cyanex 923. *Separation and Purification Technology*, 236:116289, 2020.

[118] Bong Seock Kim and Yeon Ki Hong, Won Hi Hong. Effect of salts on the extraction characteristics of succinic acid by predispersed solvent extraction. *Biotechnology and Bioprocess Engineering*, (9):207–211, 2004.

[119] Hyohak Song, Jeong Wook Lee, Sol Choi, Jong Kyun You, Won Hi Hong, and Sang Yup Lee. Effects of dissolved co2 levels on the growth of mannheimia succiniciproducens and succinic acid production. *Biotechnology and bioengineering*, 98(6):1296–1304, 2007.

[120] Jeong Wook Lee, Jongho Yi, Tae Yong Kim, Sol Choi, Jung Ho Ahn, Hyohak Song, Moon-Hee Lee, and Sang Yup Lee. Homosuccinic acid production by metabolically engineered mannheimia succiniciproducens. *Metabolic engineering*, 38:409–417, 2016.

[121] Jeng Yih Law, Abdul Wahab Mohammad, Zhao Kang Tee, Nadiah Khairul Zaman, Jamaliah Md Jahim, Jude Santanaraj, and Mohd Shaiful Sajab. Recovery of succinic acid from fermentation broth by forward osmosis-assisted crystallization process. *Journal of Membrane Science*, 583:139–151, 2019.

[122] Thomas Brouwer, Marek Blahusiak, Katarina Babic, and Boelo Schuur. Reactive extraction and recovery of levulinic acid, formic acid and furfural from aqueous solutions containing sulphuric acid. *Separation and Purification Technology*, 185:186–195, 2017.

[123] I. S. Udachan and A. K. Sahoo. A study of parameters affecting the solvent extraction of lactic acid from fermentation broth. *Brazilian Journal of Chemical Engineering*, 31(3):821–827, 2014.

[124] Eun Zoo Lee, Yun Suk Huh, Yong-Si Jun, Hyo Jin Won, Yeon Ki Hong, and Won Hi Hong. Effect of operating variables on back-extraction characteristics of succinic acid from organic phase. *Biotechnology and Bioprocess Engineering*, 13(3):342–346, 2008.

[125] Amit Keshav, Kailas L. Wasewar, and Shri Chand. Extraction of

propionic acid from model solutions: Effect of ph, salts, substrate, and temperature. *AIChE Journal*, 55(7):1705–1711, 2009.

[126] A. Thakur, P. S. Panesar, and M. S. Saini. Response surface modeling of lactic acid extraction by emulsion liquid membrane: Box-behnken experimental design. *International Journal of Biological, Biomolecular, Agricultural, Food and Biotechnological Engineering*, 2014.

[127] Victoria M. Inyang and David Lokhat. Reactive extraction of propionic acid using trioctylamine in 1–decanol by response surface methodology optimization technique. *International Journal of Low-Carbon Technologies*, 15(2):171–179, 2020.

[128] Victoria Inyang and David Lokhat. Butyric acid reactive extraction using trioctylamine in 1-decanol: Response surface methodology parametric optimization technique. *Arabian Journal for Science and Engineering*, 16(5):1019, 2021.

[129] Anil Kumar and Avinash Thakur. Statistical optimization of lactic acid extraction using green solvent and mixed extractants (toa and tomac). *Chemical Engineering Research Bulletin*, 21(1):20–35, 2020.

[130] K. Rewatkar. Reactive separation of gallic acid: Experimentation and optimization using response surface methodology and artificial neural network. *Chemical and Biochemical Engineering Quarterly*, 31(1):33–46, 2017.

[131] Dirk Kreyenschulte, Benedikt Heyman, Armin Eggert, Tim Maßmann, Christina Kalvelage, Ronja Kossack, Lars Regestein, Andreas Jupke, and Jochen Büchs. In situ reactive extraction of itaconic acid during fermentation of aspergillus terreus. *Biochemical Engineering Journal*, 135:133–141, 2018.

[132] Patrick O. Saboe, Lorenz P. Manker, William E. Michener, Darren J. Peterson, David G. Brandner, Stephen P. Deutch, Manish

Kumar, Robin M. Cywar, Gregg T. Beckham, and Eric M. Karp. In situ recovery of bio-based carboxylic acids. *Green Chemistry*, 20(8):1791–1804, 2018.

[133] Ulrike Grömping. *Tutorial for designing experiments using the R package RcmdrPlugin.DoE*. Berichte aus der Mathematik, Physik und Chemie. 2011.

[134] Lisette M.J. Sprakel and Boelo Schuur. Improving understanding of solvent effects on intermolecular interactions in reactive liquid–liquid extraction with isothermal titration calorimetry and molecular modeling. *Journal of Industrial and Engineering Chemistry*, 72:364–373, 2019.

[135] F. Chemarin, M. Moussa, M. Chadni, B. Pollet, P. Lieben, F. Allais, I. C. Trelea, and V. Athès. New insights in reactive extraction mechanisms of organic acids: An experimental approach for 3-hydroxypropionic acid extraction with tri-n-octylamine. *Separation and Purification Technology*, 179:523–532, 2017.

[136] Mariateresa Ferone, Francesca Raganati, Giuseppe Olivieri, and Antonio Marzocchella. Bioreactors for succinic acid production processes. *Critical Reviews in Biotechnology*, 39(4):571–586, 2019.

[137] David Dupont, Daphne Depuydt, and Koen Binnemans. Overview of the effect of salts on biphasic ionic liquid/water solvent extraction systems: Anion exchange, mutual solubility, and thermomorphic properties. *The journal of physical chemistry. B*, 119(22):6747–6757, 2015.

[138] Lisette M.J. Sprakel, A.F.M. Holtkamp, R. Bassa, and B. Schuur. Swing processes for solvent regeneration in liquid-liquid extraction of succinic acid. *Chemical Engineering and Processing - Process Intensification*, 143:107600, 2019.

[139] Tanja Kurzrock, Stefan Schallinger, and Dirk Weuster-Botz. Integrated separation process for isolation and purification of biosuccinic acid. *Biotechnology Progress*, 27(6):1623–1628, 2011.

[140] Marcel Gausmann, Christian Kocks, Moritz Doeker, Armin Eggert, Tim Maßmann, and Andreas Jupke. Recovery of succinic acid by integrated multi-phase electrochemical ph-shift extraction and crystallization. *Separation and Purification Technology*, 240(240):116489, 2020.

[141] Sushil Kumara, B.V. Babua, and K.L. Wasewar. Recovery of propionic acid using reactive extraction. *International Symposium & 59th Annual Session of IIChE*, 2006.

[142] Yeon Ki Hong and Won Hi Hong. Equilibrium studies on reactive extraction of succinic acid from aqueous solutions with tertiary amines. *Bioprocess Engineering*, 2000.

[143] Jung Ho Ahn, Yu-Sin Jang, and Sang Yup Lee. Production of succinic acid by metabolically engineered microorganisms. *Current Opinion in Biotechnology*, 42:54–66, 2016.

[144] Andrea Schievano, Tommy Pepé Sciarria, Karolien Vanbroekhoven, Heleen de Wever, Sebastià Puig, Stephen J. Andersen, Korneel Rabaey, and Deepak Pant. Electro-fermentation - merging electrochemistry with fermentation in industrial applications. *Trends in biotechnology*, 34(11):866–878, 2016.

[145] Arno Behr, David W. Agar, and Jakob Jörissen. *Einführung in die Technische Chemie*. Spektrum Akademischer Verlag, Heidelberg, 2010.

[146] Christian Kocks, Jonas Görtz, Arne Holtz, Marcel Gausmann, and Andreas Jupke. Electrochemical crystallization concept for succinic acid reduces waste salt production. *Chemie Ingenieur Technik*, 92(3):221–228, 2020.

[147] Tobias Reier, Mehtap Oezaslan, and Peter Strasser. Electrocatalytic oxygen evolution reaction (oer) on ru, ir, and pt catalysts: A comparative study of nanoparticles and bulk materials. *ACS Catalysis*, 2(8):1765–1772, 2012.

[148] Tomoya Suzuki, Takeshi Ogata, Mikiya Tanaka, Tohru Kobayashi, Hideaki Shiwaku, Tsuyoshi Yaita, and Hirokazu Narita. Speciation of ruthenium(iii) chloro complexes in hydrochloric acid solutions and their extraction characteristics with an amide-containing amine compound. *Metals*, 8(7):558, 2018.

[149] Bong Seock Kim, Yeon KJ Hong, and Won Hi Hong. Effect of ph on the extraction characteristics of succinic acid and the stability of colloidal liquid aphrons. *Korean Journal of Chemical Engineering*, 2002.

[150] Tanja Kurzrock. *Integrierte Reaktivextraktion zur Gewinnung von biotechnologisch hergestellter Bernsteinsäure*. 2010.

[151] David Hasson, Georgiy Sidorenko, and Raphael Semiat. Calcium carbonate hardness removal by a novel electrochemical seeds system. *Desalination*, 263(1-3):285–289, 2010.

[152] Largus T. Angenent, Joseph G. Usack, Jiajie Xu, Doris Hafenbradl, Roy Posmanik, and Jefferson W. Tester. Integrating electrochemical, biological, physical, and thermochemical process units to expand the applicability of anaerobic digestion. *Bioresource technology*, 247:1085–1094, 2018.

[153] Marcel Gausmann, Armin Eggert, Tim Maßmann, and Andreas Jupke. Verfahren zur übertragung eines zielstoffs zwischen zwei flüssigen phasen: Anmeldung, 29.1.2018.

[154] Georgy Givirovskiy, Vesa Ruuskanen, Leo S. Ojala, Michael Lienemann, Petteri Kokkonen, and Jero Ahola. Electrode material studies and cell voltage characteristics of the in situ water electrolysis

performed in a ph-neutral electrolyte in bioelectrochemical systems. *Heliyon*, 5(5):e01690, 2019.

[155] James E. Kipp. Phcalc: A computer program for acid/base equilibrium calculations. *computer series*, (158), 1994.

[156] James E. Kipp and David F. Schuck. Computer simulation of the effect of temperature on ph. *Journal of Pharmaceutical Sciences*, 84(11):1347–1352, 1995.

[157] Tore K. Gustafsson, Bengt O. Skrifvars, Katarina V. Sandstroem, and Kurt V. Waller. Modeling of ph for control. *Industrial & Engineering Chemistry Research*, 1995.

[158] Marcel Gausmann and Andreas Jupke. Dynamic modeling of electrochemical ph-swing extraction. *Chemie Ingenieur Technik*, 2020.

[159] Juan José Baeza-Baeza and María Celia García-Álvarez-Coque. Systematic approach to calculate the concentration of chemical species in multi-equilibrium problems. *Journal of Chemical Education*, 88(2):169–173, 2011.

[160] Juan J. Baeza-Baeza and M. Celia García-Álvarez-Coque. Systematic approach for calculating the concentrations of chemical species in multiequilibrium problems: Inclusion of the ionic strength effects. *Journal of Chemical Education*, 89(7):900–904, 2012.

[161] Rainer E. Glaser, Marco A. Delarosa, Ahmed Olasunkanmi Salau, and Carmen Chicone. Dynamical approach to multiequilibria problems for mixtures of acids and their conjugated bases. *Journal of Chemical Education*, 91(7):1009–1016, 2014.

[162] Jaroslaw Milewski, Giulio Guandalini, and Stefano Campanari. Modeling an alkaline electrolysis cell through reduced-order and loss-estimate approaches. *Journal of Power Sources*, 269(4):203–211, 2014.

[163] Lin Liu and Qing Cheng. Mass transfer characteristic research on electrodialysis for desalination and regeneration of solution: A comprehensive review. *Renewable and Sustainable Energy Reviews*, 134(3):110115, 2020.

[164] Allen J. Brad and Larry R. Faulkner. *ELECTROCHEMICAL METHODS Fundamentals and Application*. John Wiley & Sons, Inc, 2001.

[165] John Newman and Karen E. Thomas-Alyea. *Electrochemical Systems*. Wiley-Interscience, 2004.

[166] John Owen. *Ionic Conductivity: Comprehensive Polymer Science and Supplements*. 1989.

[167] W. K. Lewis and W. G. Whitman. Principles of gas absorption. *Industrial & engineering chemistry research*, (16):1215–1220, 1924.

[168] Paul Delahay and Wolf Vielstich. Kinetics of the dissociation of weak acids and bases—application of polarography and voltammetry at constant current. *Journal of the American Chemical Society*, (77):4955–4958, 1955.

[169] D. Huppert, E. Kolodney, M. Gutman, and E. Nachliel. Effect of water activity on the rate of proton dissociation, 1982.

[170] Ethan Zars, Joseph Schell, Marco A. Delarosa, Carmen Chicone, and Rainer Glaser. Dynamical approach to multi-equilibria problems considering the debye–hückel theory of electrolyte solutions: Concentration quotients as a function of ionic strength. *Journal of Solution Chemistry*, 46(3):643–662, 2017.

[171] Werner Stumm. *Aquatic Chemistry*. John Wiley & Sons, Inc, 1996.

[172] Dirk Henkensmeier, Malikah Najibah, Corinna Harms, Jan Žitka, Jaromír Hnát, and Karel Bouzek. Overview: State-of-the art commercial membranes for anion exchange membrane water electrol-

ysis. *Journal of Electrochemical Energy Conversion and Storage*, 2021.

[173] Takashi Kojima and Hiroshi Fukutomi. Extraction equilibria of hydrochloric acid by trioctylamine in low-polar organic solvents. *The Chemical Society of Japan*, 1987.

[174] Jesús Rodríguez and Ernesto Amores. Cfd modeling and experimental validation of an alkaline water electrolysis cell for hydrogen production. *Processes*, 8(12):1634, 2020.

[175] Octave Levenspiel. *Chemical Reaction Engineering*. John Wiley & Sons, Inc, 1999.

[176] Andreas Jupke, Achim Epping, and Henner Schmitdt-Traub. Optimal design of batch and simulated moving bed chromatographic separation processes. *Journal of Chromatography*, 2002.

[177] W. S. WU, G. P. RANGAIAH, and M. FLEISCHMANN. Effect of gas evolution on dispersion in an electrochemical reactor. *JOURNAL OF APPLIED ELECTROCHEMISTRY*, (23):113–119, 1993.

[178] F. Moukalled, F. Moukalled L. Mangani, and M. Darwish, editors. *The Finite Volume Method in Computational Fluid Dynamics*. Springer, 2016.

[179] Stefan Rönsch. *Anlagenbilanzierung in der Energietechnik: Grundlagen, Gleichungen und Modelle für die Ingenieurpraxis*. Springer Vieweg, Wiesbaden, 2015.

[180] J. P. Glas and J.W. Westwater. Measurements of the growth of electrolytic bubbles. *International Journal of Heat Mass Transfer*, 1964(7):1427–1443, 1964.

[181] P. BOISSONNEAU and P. BYRNE. An experimental investigation of bubble-induced free convection in a small electrochemical cell. *JOURNAL OF APPLIED ELECTROCHEMISTRY*, (30):767–775, 2000.

[182] Helmut Vogt and Karl Stephan. Local microprocesses at gas-evolving electrodes and their influence on mass transfer. *Electrochimica Acta*, 155:348–356, 2015.

[183] Valois Parisien, Alixia Farrell, Dominic Pjontek, Craig A. McKnight, Jason Wiens, and Arturo Macchi. Bubble swarm characteristics in a bubble column under high gas holdup conditions. *Chemical Engineering Science*, 157:88–98, 2017.

[184] J. M. Bisang. Theoretical and experimental studies of current distribution in gas-evolving electrochemical reactors with parallel-plate electrodes. *JOURNAL OF APPLIED ELECTROCHEMISTRY*, (21):760–766, 1991.

[185] A. Kuznetsov, A. Beloded, A. Derunets, V. Grosheva, L. Vakar, R. Kozlovskiy, and V. Shvets. Biosynthesis of lactic acid in a membrane bioreactor for cleaner technology of polylactide production. *Clean Technologies and Environmental Policy*, 19(3):869–882, 2017.

[186] J. Vijayakumar, R. Aravindan, and T. Viruthagiri. Recent trends in the production, purification and application of lactic acid. *Chemical and Biochemical Engineering Quarterly*, 22(2):245–264, 2008.

[187] Nanditha Murali, Keerthi Srinivas, and Birgitte K. Ahring. Biochemical production and separation of carboxylic acids for biorefinery applications. *Fermentation*, 3(2):22, 2017.

[188] Majdiah Othman, Arbakariya B. Ariff, Leonardo Rios-Solis, and Murni Halim. Extractive fermentation of lactic acid in lactic acid bacteria cultivation: A review. *Frontiers in Microbiology*, 0:2285, 2017.

[189] D. Yankov, J. Molinier, J. Albet, G. Malmary, and G. Kyuchoukov. Lactic acid extraction from aqueous solutions with tri-

n-octylamine dissolved in decanol and dodecane. *Biochemical Engineering Journal*, 21(1):63–71, 2004.

[190] H. G. Joglekar, Imran Rahman, Suresh Babu, B. D. Kulkarni, and Ajit Joshi. Comparative assessment of downstream processing options for lactic acid. *Separation and Purification Technology*, 52(1):1–17, 2006.

[191] Filipe S. Oliveira, João M. M. Araújo, Rui Ferreira, Luís Paulo N. Rebelo, and Isabel M. Marrucho. Extraction of l-lactic, l-malic, and succinic acids using phosphonium-based ionic liquids. *Separation and Purification Technology*, 85:137–146, 2012.

[192] Konstantza Tonova, Ivan Svinyarov, and Milen G. Bogdanov. Hydrophobic 3-alkyl-1-methylimidazolium saccharinates as extractants for l-lactic acid recovery. *Separation and Purification Technology*, 125:239–246, 2014.

[193] Ján Marták and Štefan Schlosser. Extraction of lactic acid by phosphonium ionic liquids. *Separation and Purification Technology*, 57(3):483–494, 2007.

[194] Ehsan Reyhanitash, Egor Fufachev, Kaspar D. van Munster, Michael B. M. van Beek, Lisette M. J. Sprakel, Carmen N. Edelijn, Bert M. Weckhuysen, Sascha R. A. Kersten, Pieter C. A. Bruijnincx, and Boelo Schuur. Recovery and conversion of acetic acid from a phosphonium phosphinate ionic liquid to enable valorization of fermented wastewater. *Green Chemistry*, 21(8):2023–2034, 2019.

[195] Angelo Gössi, Florian Burgener, David Kohler, Alessandro Urso, Boris A. Kolvenbach, Wolfgang Riedl, and Boelo Schuur. In-situ recovery of carboxylic acids from fermentation broths through membrane supported reactive extraction using membrane modules with improved stability. *Separation and Purification Technology*, 241:116694, 2020.

[196] B. Choudhury and T. Swaminathan. Lactic acid extraction with trioctyl amine. *Bioprocess Engineering*, 19(4):317–320, 1998.

[197] D. Yankov, J. Molinier, G. Kyuchoukov, J. Albet, and G. Malmary. *Improvement of the lactic acid extraction. Extraction from aqueous solutions and simulated fermentation broth by means of mixed extractant and TOA, partially ...*. 2005.

[198] Agnieszka Krzyzaniak, Boelo Schuur, Murali Sukumaran, Han Zuilhof, and André B. de Haan. *Extractant screening for liquid-liquid extraction in environmentally benign production routes*. 2011.

[199] Shang Tian Yang, Scott A. White, and Sheng Tsiung Hsu. Extraction of carboxylic acids with tertiary and quaternary amines: effect of ph. *Industrial & Engineering Chemistry Research*, 30(6):1335–1342, 1991.

[200] Pratibha Baral, Anushka Pundir, Akhilesh Kurmi, Raghuvir Singh, Vinod Kumar, and Deepti Agrawal. Salting-out assisted solvent extraction of l (+) lactic acid obtained after fermentation of sugarcane bagasse hydrolysate. *Separation and Purification Technology*, 269:118788, 2021.

[201] Falk Harnisch and Carolin Urban. Electrobiorefineries: Unlocking the synergy of electrochemical and microbial conversions. *Angewandte Chemie (International ed. in English)*, 57(32):10016–10023, 2018.

[202] Jin Soo Kang, Seoni Kim, and T. Alan Hatton. Redox-responsive sorbents and mediators for electrochemically based co2 capture. *Current Opinion in Green and Sustainable Chemistry*, 31:100504, 2021.

[203] Salma Aathika Abdur Rawoof, P. Senthil Kumar, Dai-Viet N. Vo, Kubendran Devaraj, Yuvarani Mani, Thiruselvi Devaraj, and Sivanesan Subramanian. Production of optically pure lactic acid

by microbial fermentation: a review. *Environmental Chemistry Letters*, 19(1):539–556, 2021.

[204] Kexin Meng, Guangyu Zhang, Chuanqin Ding, Tongyang Zhang, Hui Yan, Dongpei Zhang, Tianqi Fang, Mengyuan Liu, Zhenchao You, Chaohe Yang, Jian Shen, and Xin Jin. Recent advances on purification of lactic acid. *Chemical record (New York, N.Y.)*, 20(11):1236–1256, 2020.

[205] Agnieszka Krzyżaniak, Michel Leeman, Frank Vossebeld, Ton J. Visser, Boelo Schuur, and André B. de Haan. Novel extractants for the recovery of fermentation derived lactic acid. *Separation and Purification Technology*, 111:82–89, 2013.

[206] Boelo Schuur, Jozef G. M. Winkelman, and Hero J. Heere. Equilibrium studies on enantioselective liquid−liquid amino acid extraction using a cinchona alkaloid extractant. (47):10027–10033, 2008.

[207] Angelo Gössi, Wolfgang Riedl, and Boelo Schuur. Mass transfer analysis and kinetic modeling for process design of countercurrent membrane supported reactive extraction of carboxylic acids. *Chemical Engineering Science: X*, 13(18):100119, 2022.

[208] Joseph Schell, Ethan Zars, Carmen Chicone, and Rainer Glaser. Simultaneous determination of all species concentrations in multiequilibria for aqueous solutions of dihydrogen phosphate considering debye–hückel theory. *Journal of Chemical & Engineering Data*, 63(6):2151–2161, 2018.

[209] Thomas Melin and Robert Rautenbach. *Membranverfahren*. Springer, 2007.

[210] Kailas L. Wasewar. Reactive extraction: An intensifying approach for carboxylic acid separation. *International Journal of Chemical Engineering and Applications*, pages 249–255, 2012.

[211] Mamata Singhvi, Takeshi Zendo, and Kenji Sonomoto. Free lactic acid production under acidic conditions by lactic acid bacteria strains: challenges and future prospects. *Applied microbiology and biotechnology*, 102(14):5911–5924, 2018.

[212] Dae Sung Park, Omar A. Abdelrahman, Katherine P. Vinter, Patrick M. Howe, Jesse Q. Bond, Theresa M. Reineke, Kechun Zhang, and Paul J. Dauenhauer. Multifunctional cascade catalysis of itaconic acid hydrodeoxygenation to 3-methyl-tetrahydrofuran. *ACS Sustainable Chemistry & Engineering*, 6(7):9394–9402, 2018.

[213] Andressa Neves Marchesan, ean Felipe Leal Silva, Rubens Maciel Filho, and Maria Regina Wolf Maciel. Techno-economic analysis of alternative designs for low-ph lactic acid production. *ACS Sustainable Chemistry & Engineering*, (9):12120–12131, 2021.

[214] Nurcan Tik, Emine Bayraktar, and Ülkü Mehmetoglu. In situ reactive extraction of lactic acid from fermentation media. *Journal of Chemical Technology & Biotechnology*, 76(7):764–768, 2001.

[215] Mallika Boonmee, Onanong Cotano, Sittipong Amnuaypanich, and Nurak Grisadanurak. Improved lactic acid production by in situ removal of lactic acid during fermentation and a proposed scheme for its recovery. *Arabian Journal for Science and Engineering*, 41(6):2067–2075, 2016.

[216] Bong Seock Kim, Yeon Ki Hong, and Won Hi Hong. Effect of salts on the extraction characteristics of succinic acid by predispersed solvent extraction. *Biotechnology and Bioprocess Engineering*, 9(3):207–211, 2004.

[217] Agnieszka Krzyzaniak, Boelo Schuur, and André B. de Haan. Equilibrium studies on lactic acid extraction with n,n-didodecylpyridin-4-amine (ddap) extractant. *Chemical Engineering Science*, 109:236–243, 2014.

[218] Antonio Irineudo Magalhães, Júlio Cesar de Carvalho, Jesus David Coral Medina, and Carlos Ricardo Soccol. Downstream process development in biotechnological itaconic acid manufacturing. *Applied microbiology and biotechnology*, 101(1):1–12, 2017.

[219] Antonio Irineudo Magalhães, Júlio Cesar de Carvalho, Juliano Feliz Thoms, Jesus David Coral Medina, and Carlos Ricardo Soccol. Techno-economic analysis of downstream processes in itaconic acid production from fermentation broth. *Journal of Cleaner Production*, 206:336–348, 2019.

[220] Levente Karaffa and Christian P. Kubicek. Citric acid and itaconic acid accumulation: variations of the same story? *Applied microbiology and biotechnology*, 103(7):2889–2902, 2019.

[221] Oscar Rosales-Calderon and Valdeir Arantes. A review on commercial-scale high-value products that can be produced alongside cellulosic ethanol. *Biotechnology for biofuels*, 12:240, 2019.

[222] Susan Krull, Antje Hevekerl, Anja Kuenz, and Ulf Prüße. Process development of itaconic acid production by a natural wild type strain of aspergillus terreus to reach industrially relevant final titers. *Applied microbiology and biotechnology*, 101(10):4063–4072, 2017.

[223] Mickel L. A. Jansen and Walter M. van Gulik. Towards large scale fermentative production of succinic acid. *Current Opinion in Biotechnology*, 30:190–197, 2014.

[224] Adrie J. J. Straathof, S. Aljoscha Wahl, Kirsten R. Benjamin, Ralf Takors, Nick Wierckx, and Henk J. Noorman. Grand research challenges for sustainable industrial biotechnology. *Trends in biotechnology*, 37(10):1042–1050, 2019.

[225] Guneet Kaur, Miranda Maesen, Linsey Garcia-Gonzalez, Heleen de Wever, and Kathy Elst. Novel intensified back extraction process for itaconic acid: Toward in situ product recovery for itaconic

acid fermentation. *ACS Sustainable Chemistry & Engineering*, 6(6):7403–7411, 2018.

[226] Antje Hevekerl, Anja Kuenz, and Klaus-Dieter Vorlop. Influence of the ph on the itaconic acid production with aspergillus terreus. *Applied microbiology and biotechnology*, 98(24):10005–10012, 2014.

[227] Tobias Klement, Sofia Milker, Gernot Jäger, Philipp M. Grande, Pablo Domínguez de María, and Jochen Büchs. Biomass pretreatment affects ustilago maydis in producing itaconic acid. *Microbial cell factories*, 11(43):43, 2012.

[228] Anja Kuenz and Susan Krull. Biotechnological production of itaconic acid-things you have to know. *Applied microbiology and biotechnology*, 102(9):3901–3914, 2018.

[229] Nick Wierckx, Gennaro Agrimi, Peter Stephensen Lübeck, Matthias G. Steiger, Nuno Pereira Mira, and Peter J. Punt. Metabolic specialization in itaconic acid production: a tale of two fungi. *Current Opinion in Biotechnology*, 62:153–159, 2020.

[230] Lars Regestein, Tobias Klement, Philipp Grande, Dirk Kreyenschulte, Benedikt Heyman, Tim Maßmann, Armin Eggert, Robert Sengpiel, Yumei Wang, Nick Wierckx, Lars M. Blank, Antje Spiess, Walter Leitner, Carsten Bolm, Matthias Wessling, Andreas Jupke, Miriam Rosenbaum, and Jochen Büchs. From beech wood to itaconic acid: Case study on biorefinery process integration. *Biotechnology for biofuels*, 11:279, 2018.

[231] Elena Geiser, Sandra K. Przybilla, Meike Engel, Wiebke Kleineberg, Linda Büttner, Eda Sarikaya, Tim den Hartog, Jürgen Klankermayer, Walter Leitner, Michael Bölker, Lars M. Blank, and Nick Wierckx. Genetic and biochemical insights into the itaconate pathway of ustilago maydis enable enhanced production. *Metabolic engineering*, 38:427–435, 2016.

[232] Thiemo Zambanini, Sandra K. Hartmann, Lisa M. Schmitz, Linda Büttner, Hamed Hosseinpour Tehrani, Elena Geiser, Melanie Beudels, Dominik Venc, Georg Wandrey, Jochen Büchs, Markus Schwarzländer, Lars M. Blank, and Nick Wierckx. Promoters from the itaconate cluster of ustilago maydis are induced by nitrogen depletion. *Fungal biology and biotechnology*, 4:11, 2017.

[233] Anna Voll and Wolfgang Marquardt. Benchmarking of next-generation biofuels from a process perspective. *Biofuels, Bioproducts and Biorefining*, 2012.

[234] Tobias Klement. *Itaconic Acid Fermentation with Ustilago maydis and its Integration into a Next Generation Bio-based Process.* Ph.d., Aachen, RWTH Aachen University, 2013.

[235] Hamed Hosseinpour Tehrani, Katharina Saur, Apilaasha Tharmasothirajan, Lars M. Blank, and Nick Wierckx. Process engineering of ph tolerant ustilago cynodontis for efficient itaconic acid production. *Microbial cell factories*, 18(1):213, 2019.

[236] Hamed Hosseinpour Tehrani, Apilaasha Tharmasothirajan, Elia Track, Lars M. Blank, and Nick Wierckx. Engineering the morphology and metabolism of ph tolerant ustilago cynodontis for efficient itaconic acid production. *Metabolic engineering*, 54:293–300, 2019.

[237] Jannick Gorden, Elena Geiser, Nick Wierckx, Lars M. Blank, Tim Zeiner, and Christoph Brandenbusch. Integrated process development of a reactive extraction concept for itaconic acid and application to a real fermentation broth. *Engineering in life sciences*, 17(7):809–816, 2017.

[238] Yang Hoon Kim and Seung-Hyeon Moon. Lactic acid recovery from fermentation broth using one-stage electrodialysis. *Journal of Chemical Technology & Biotechnology*, 76(2):169–178, 2001.

[239] Věra Hábová, Karel Melzoch, Mojmír Rychtera, and Barbora Sekavová. Electrodialysis as a useful technique for lactic acid separation from a model solution and a fermentation broth. *Desalination*, 162:361–372, 2004.

[240] D. Arslan, Y. Zhang, K.J.J. Steinbusch, L. Diels, H.V.M. Hamelers, C.J.N. Buisman, and H. de Wever. In-situ carboxylate recovery and simultaneous ph control with tailor-configured bipolar membrane electrodialysis during continuous mixed culture fermentation. *Separation and Purification Technology*, 175:27–35, 2017.

[241] J. Urbanus, R.J.M. Bisselink, K. Nijkamp, J. H. ter Horst, D. Verdoes, and C.P.M. Roelands. Integrated product removal of slightly water-soluble carboxylates from fermentation by electrochemically induced crystallization. *Journal of Membrane Science*, 363(1-2):36–47, 2010.

[242] Lili Fu, Xueli Gao, Yang Yang, Fan Aiyong, Huawei Hao, and Congjie Gao. Preparation of succinic acid using bipolar membrane electrodialysis. *Separation and Purification Technology*, 127:212–218, 2014.

[243] Xiaohu Xu, Tao Wang, Lijuan Dong, Wenbo Lu, and Xiangyang Miao. Energy-efficient hydrogen evolution reactions via hydrazine oxidation over facile synthesis of cobalt tetraoxide electrodes. *ACS Sustainable Chemistry & Engineering*, 8(21):7973–7980, 2020.

[244] Shenglin Lu, Bin Zhao, Mingxing Chen, Lei Wang, Xian-Zhu Fu, and Jing-Li Luo. Electrolysis of waste water containing aniline to produce polyaniline and hydrogen with low energy consumption. *International Journal of Hydrogen Energy*, 45(43):22419–22426, 2020.

[245] Marcel Gausmann, Christian Kocks, Johannes Pastoors, Jochen Büchs, Nick Wierckx, and Andreas Jupke. Electrochemical ph-t-swing separation of itaconic acid for zero salt waste biorefineries. *in submission*, 2021.

[246] John Owen. *Ionic Conductivity*. Pergamon Press, Oxford, 2, chap. 21 edition, 1989.

[247] Katharina Grave, Mandana Hazrat, Sil Boeve, Felix von Blücher, Charles Bourgault, Barbara Breitschopf, Nele Friedrichsen, Marlene Arens, Ali Aydemir, Martin Pudlik, Christian Lutz, Anett Großmann, and Markus Flaute. Electricity costs of energy intensive industries.

[248] Steve Hanley. La & 8 minute solar ink lowest cost solar-plus-storage deal in us history, 2019.

[249] Joachim Bertsch, Helena Schwerter, and Amelie Sitzmann. *Ausgangsbedingungen für die Vermarktung von Nachfrageflexibilität*. 2017.

[250] J. Gregory Zeikus, M. K. Jain, and P. Elankovan. Biotechnology of succinic acid production and markets for derived products. *Applied microbiology and biotechnology*, 1991.

[251] T. Werpy and G. Petersen. Top value added chemicals from biomass: Volume i–results of screening for potential candidates from sugars and synthesis gas.

[252] Tae Yong Kim, Hyun Uk Kim, Jong Myoung Park, Hyohak Song, Jin Sik Kim, and Sang Yup Lee. Genome-scale analysis of mannheimia succiniciproducens metabolism. *Biotechnology and bioengineering*, 97(4):657–671, 2007.

[253] Sang Yup Lee, Ji Mahn Kim, Hyohak Song, Jeong Wook Lee, Tae Yong Kim, and Yu-Sin Jang. From genome sequence to integrated bioprocess for succinic acid production by mannheimia succiniciproducens. *Applied microbiology and biotechnology*, 79(1):11–22, 2008.

[254] Shohei Okino, Ryoji Noburyu, Masako Suda, Toru Jojima, Masayuki Inui, and Hideaki Yukawa. An efficient succinic

acid production process in a metabolically engineered corynebacterium glutamicum strain. *Applied microbiology and biotechnology*, 81(3):459–464, 2008.

[255] Derek A. Abbott, Rintze M. Zelle, Jack T. Pronk, and Antonius J. A. van Maris. Metabolic engineering of saccharomyces cerevisiae for production of carboxylic acids: current status and challenges. *FEMS yeast research*, 9(8):1123–1136, 2009.

[256] James B. McKinlay, C. Vieille, and J. Gregory Zeikus. Prospects for a bio-based succinate industry. *Applied microbiology and biotechnology*, 76(4):727–740, 2007.

[257] Joseph J. Bozell and Gene R. Petersen. Technology development for the production of biobased products from biorefinery carbohydrates—the us department of energy's "top 10" revisited. *Green Chemistry*, 12(4):539, 2010.

[258] Judith Becker, Anna Lange, Jonathan Fabarius, and Christoph Wittmann. Top value platform chemicals: Bio-based production of organic acids. *Current Opinion in Biotechnology*, 36:168–175, 2015.

[259] Nhuan Nghiem, Susanne Kleff, and Stefan Schwegmann. Succinic acid: Technology development and commercialization. *Fermentation*, 3(2):26, 2017.

[260] Viera Liebe. Determination of market potential for selected platform chemicals, itaconic acid, succinic acid: Bioconsept market research report weastra.

[261] Pieter C. A. Bruijnincx and Bert M. Weckhuysen. Shale gas revolution: an opportunity for the production of biobased chemicals? *Angewandte Chemie (International ed. in English)*, 52(46):11980–11987, 2013.

[262] Ioannis Tsiropoulos Benjamin Cok, Alexander L. Roes, and Martin K. Patel. Succinic acid production derived from carbohydrates:

An energy and greenhouse gas assessment of a platform chemical toward a bio-based economy. *Biofuels, Bioproducts and Biorefining*, (8):16–29, 2013.

[263] Jim Lane. The doe's 12 top biobased molecules – what became of them?

[264] Michael McCoy. Succinic acid maker bioamber is bankrupt, 2018.

[265] Xue Li and Edmund Mupondwa. Empirical analysis of large-scale bio-succinic acid commercialization from a technoeconomic and innovation value chain perspective: Bioamber biorefinery case study in canada. *Renewable and Sustainable Energy Reviews*, 137:110587, 2021.

[266] Ke-Ke Cheng, Xue-Bing Zhao, Jing Zeng, and Jian-An Zhang. Biotechnological production of succinic acid: current state and perspectives. *Biofuels, Bioproducts & Biorefining*, 2012.

[267] Jolandi Herselman, Michael F.A. Bradfield, Uma Vijayan, and Willie Nicol. The effect of carbon dioxide availability on succinic acid production with biofilms of actinobacillus succinogenes. *Biochemical Engineering Journal*, 117:218–225, 2017.

[268] Raffaella Desirè Di Lorenzo, Immacolata Serra, Danilo Porro, and Paola Branduardi. State of the art on the microbial production of industrially relevant organic acids. *Catalysts*, 12(2):234, 2022.

[269] Siddharth Gadkari, Deepak Kumar, Zi-Hao Qin, Carol Sze Ki Lin, and Vinod Kumar. Life cycle analysis of fermentative production of succinic acid from bread waste. *Waste management (New York, N.Y.)*, 126:861–871, 2021.

[270] Dan Wang, Qiang Li, Ziyu Song, Wei Zhou, Zhiguo Su, and Jianmin Xing. High cell density fermentation via a metabolically engineered escherichia coli for the enhanced production of succinic acid. *Journal of Chemical Technology & Biotechnology*, 86(4):512–518, 2011.

[271] Andreas M. Raab, Gabi Gebhardt, Natalia Bolotina, Dirk Weuster-Botz, and Christine Lang. Metabolic engineering of saccharomyces cerevisiae for the biotechnological production of succinic acid. *Metabolic engineering*, 12(6):518–525, 2010.

[272] Zhennan Jiang, Zhiyong Cui, Ziwei Zhu, Yinghang Liu, Ya-Jie Tang, Jin Hou, and Qingsheng Qi. Engineering of yarrowia lipolytica transporters for high-efficient production of biobased succinic acid from glucose. *Biotechnology for biofuels*, 14(1):145, 2021.

[273] Enrico Mancini, Rofice Dickson, Serena Fabbri, Isuru A. Udugama, Humzaa Imtiaz Ullah, Srikanth Vishwanath, Krist V. Gernaey, Jianquan Luo, Manuel Pinelo, and Seyed Soheil Mansouri. Economic and environmental analysis of bio-succinic acid production: From established processes to a new continuous fermentation approach with in-situ electrolytic extraction. *Chemical Engineering Research and Design*, 179:401–414, 2022.

[274] Qiao Yang, Min Wu, Zhongxue Dai, Fengxue Xin, Jie Zhou, Weiliang Dong, Jiangfeng Ma, Min Jiang, and Wenming Zhang. Comprehensive investigation of succinic acid production by actinobacillus succinogenes : a promising native succinic acid producer. *Biofuels, Bioproducts and Biorefining*, 179:151, 2019.

[275] David A. Glassner and Rathin Datta. Process for the production and purification of succinic acid, 1992.

[276] Lili Fu, Xueli Gao, Yang Yang, Fan Aiyong, Huawei Hao, and Congjie Gao. Preparation of succinic acid using bipolar membrane electrodialysis. *Separation and Purification Technology*, 127:212–218, 2014.

[277] Paula Andrea Hernandez, Miaomiao Zhou, Igor Vassilev, Stefano Freguia, Yang Zhang, Jürg Keller, Pablo Ledezma, and Bernardino Virdis. Selective extraction of medium-chain carboxylic acids by electrodialysis and phase separation. *ACS omega*, 6(11):7841–7850, 2021.

[278] Rofice Dickson, Enrico Mancini, Nipun Garg, John M. Woodley, Krist V. Gernaey, Manuel Pinelo, Jay Liu, and Seyed Soheil Mansouri. Sustainable bio-succinic acid production: superstructure optimization, techno-economic, and lifecycle assessment. *Energy & Environmental Science*, 14(6):3542–3558, 2021.

[279] Andre Banier de HAAN, Jan van BREUGEL, VAN DER WEIDE, Paulus Loduvicus Johannes, Peter Paul JANSEN, Jose VIDAL LANCIS, and Agustin CERDA BARO. Recovery of carboxylic acid from their magnesium salts by precipitation using hydrochloric acid, useful for fermentation broth work-up, 2012.

[280] Zhiyong Cui, Cuijuan Gao, Jiaojiao Li, Jin Hou, Carol Sze Ki Lin, and Qingsheng Qi. Engineering of unconventional yeast yarrowia lipolytica for efficient succinic acid production from glycerol at low ph. *Metabolic engineering*, 42:126–133, 2017.

[281] Marcel Gausmann, Christian Kocks, Johannes Pastoors, Jochen Büchs, Nick Wierckx, and Andreas Jupke. Electrochemical pht-swing separation of itaconic acid for zero salt waste downstream processing. *ACS Sustainable Chemistry & Engineering*, 9(28):9336–9347, 2021.

[282] Judith Becker, Jasper Reinefeld, René Stellmacher, Rudolf Schäfer, Anna Lange, Hanna Meyer, Michael Lalk, Oskar Zelder, Gregory von Abendroth, Hartwig Schröder, Stefan Haefner, and Christoph Wittmann. Systems-wide analysis and engineering of metabolic pathway fluxes in bio-succinate producing basfia succiniciproducens. *Biotechnology and bioengineering*, 110(11):3013–3023, 2013.

[283] Chong Li, Khai Lun Ong, Xiaofeng Yang, and Carol Sze Ki Lin. Bio-refinery of waste streams for green and efficient succinic acid production by engineered yarrowia lipolytica without ph control. *Chemical Engineering Journal*, 371:804–812, 2019.

[284] Joeline Xiberras, Mathias Klein, Erik de Hulster, Robert Mans, and Elke Nevoigt. Engineering saccharomyces cerevisiae for succinic acid production from glycerol and carbon dioxide. *Frontiers in bioengineering and biotechnology*, 8:566, 2020.

[285] Chrysanthi Pateraki, Henrik Almqvist, Dimitris Ladakis, Gunnar Lidén, Apostolis A. Koutinas, and Anestis Vlysidis. Modelling succinic acid fermentation using a xylose based substrate. *Biochemical Engineering Journal*, 114:26–41, 2016.

[286] Chrysanthi Pateraki, Maria Patsalou, Anestis Vlysidis, Nikolaos Kopsahelis, Colin Webb, Apostolis A. Koutinas, and Michalis Koutinas. Actinobacillus succinogenes : Advances on succinic acid production and prospects for development of integrated biorefineries. *Biochemical Engineering Journal*, 112:285–303, 2016.

[287] Hartwig Schroder, Stefan Haefner, Gregory, von Abendroth, Rajan Hollmann, Raddatz, Aline, Ernst Hansgeorg, and Hans Gurski. Microbial succinic acid producers andpurification of succinic acid, 2010.

[288] Anna Lange, Judith Becker, Dennis Schulze, Edern Cahoreau, Jean-Charles Portais, Stefan Haefner, Hartwig Schröder, Joanna Krawczyk, Oskar Zelder, and Christoph Wittmann. Bio-based succinate from sucrose: High-resolution 13c metabolic flux analysis and metabolic engineering of the rumen bacterium basfia succiniciproducens. *Metabolic engineering*, 44:198–212, 2017.

[289] G. N. Vemuri, M. A. Eiteman, and E. Altman. Succinate production in dual-phase escherichia coli fermentations depends on the time of transition from aerobic to anaerobic conditions. *Journal of industrial microbiology & biotechnology*, 28(6):325–332, 2002.

[290] Boris Litsanov, Melanie Brocker, and Michael Bott. Toward homosuccinate fermentation: metabolic engineering of corynebacterium glutamicum for anaerobic production of succinate from glucose

and formate. *Applied and environmental microbiology*, 78(9):3325–3337, 2012.

[291] Hongtao Xu, Zhihui Zhou, Chen Wang, Zhongjun Chen, and Heng Cai. Enhanced succinic acid production in corynebacterium glutamicum with increasing the available nadh supply and glucose consumption rate by decreasing h(+)-atpase activity. *Biotechnology letters*, 38(7):1181–1186, 2016.

[292] Wei Zou, Li-Wen Zhu, Hong-Mei Li, and Ya-Jie Tang. Significance of co2 donor on the production of succinic acid by actinobacillus succinogenes atcc 55618. *Microbial cell factories*, 10:87, 2011.

[293] Yun-jian Zhang, Qiang Li, Yu-xiu Zhang, Dan Wang, and Jianmin Xing. Optimization of succinic acid fermentation with actinobacillus succinogenes by response surface methodology (rsm). *Journal of Zhejiang University. Science. B*, 13(2):103–110, 2012.

[294] Victoria Inyang and David Lokhat. Reactive extraction of malic acid using trioctylamine in 1–decanol: Equilibrium studies by response surface methodology using box behnken optimization technique. *Scientific Reports*, 10(1):1–10, 2020.

[295] S. Eda, T. Prathap Kumar, B. Satyavathi, P. Sudhakar, and R. Parthasarathy. Recovery of succinic acid by reactive extraction using tri-n-octylamine in1-decanol: Equilibrium optimization using response surface method and kinetic studies. *International Journal of Chemical Separation Technology*, 2016.

[296] Mickel Leonardus August Jansen, Van de Graaf, Maarten Job, and René Verwaal. Dcarboxylic acid production process, 2012.

[297] Chong Li, Khai Lun Ong, Zhiyong Cui, Zhenyu Sang, Xiaotong Li, Raffel Dharma Patria, Qingsheng Qi, Patrick Fickers, Jianbin Yan, and Carol Sze Ki Lin. Promising advancement in fermentative succinic acid production by yeast hosts. *Journal of hazardous materials*, 401:123414, 2020.

[298] Richard Turton, Richard C. Bailie, Wallace B. Whiting, and Joseph A. Shaeiwitz, editors. *Analysis, Synthesis and Design of Chemical Processes, Third Edition.* Pearson Education, 2009.

[299] Christian Kocks, Christina Maria Krekel, Marcel Gausmann, and Andreas Jupke. Determination of the metastable zone width and nucleation parameters of succinic acid for electrochemically induced crystallization. *Crystals*, 11(9):1090, 2021.

[300] Jeff D. Makholm. The 2021-2022 european natural gas disaster: Was reagan right and thatcher wrong? *Climate and Energy*, (10), 2022.

[301] Venkateshwaran Venkatachalam, Sebastian Spierling, Rafael Horn, and Hans-Josef Endres. Lca and eco-design: Consequential and attributional approaches for bio-based plastics. *Procedia CIRP*, 69(3):579–584, 2018.

[302] Martin K. Patel, Aude Bechu, Juan David Villegas, Manon Bergez-Lacoste, Kenny Yeung, Richard Murphy, Jeremy Woods, Onesmus N. Mwabonje, Yuanzhi Ni, Akshay D. Patel, Joe Gallagher, and David Bryant. Second–generation bio–based plastics are becoming a reality – non–renewable energy and greenhouse gas (ghg) balance of succinic acid–based plastic end products made from lignocellulosic biomass. *Biofuels, Bioproducts and Biorefining*, 2018.

[303] Kai-Hung Hsu, Chin-Wen Chen, Li-Yuan Wang, Hao-Wei Chan, Cyuan-Lun He, Chia-Jung Cho, Syang-Peng Rwei, and Chi-Ching Kuo. Bio-based thermoplastic poly(butylene succinate-co-propylene succinate) copolyesters: effect of glycerol on thermal and mechanical properties. *Soft matter*, 15(47):9710–9720, 2019.

[304] Sara Bello, Dimitris Ladakis, Sara González-García, Gumersindo Feijoo, Apostolis Koutinas, and Maria Teresa Moreira. Renewable carbon opportunities in the production of succinic acid applying

attributional and consequential modelling. *Chemical Engineering Journal*, 428(3):132011, 2022.

[305] Adriaan W. Jeremiasse, Hubertus V. M. Hamelers, J. Mieke Kleijn, and Cees J. N. Buisman. Use of biocompatible buffers to reduce the concentration overpotential for hydrogen evolution. *Environmental Science & Technology*, 43(17):6882–6887, 2009.

[306] Shigekazu Yamazaki and Yasuyuki Ymazaki. Nickel-catalyzed dehydrogenation of amines to nitriles. *Bulletin of the Chemical Society of Japan*, (63):301–303, 1990.

[307] Marc Serra, Pilar Salagre, Yolanda Cesteros, Francisco Medina, and Jesús E. Sueiras. Nickel–magnesia catalysts: An alternative for the hydrogenation of 1,6-hexanedinitrile. *Journal of Catalysis*, 209(1):202–209, 2002.